

Modelling and model based control of turbomachinery

Citation for published version (APA):

Essen, van, H. A. (1998). *Modelling and model based control of turbomachinery*. [Phd Thesis 1 (Research TU/e / Graduation TU/e), Mechanical Engineering]. Technische Universiteit Eindhoven.
<https://doi.org/10.6100/IR515952>

DOI:

[10.6100/IR515952](https://doi.org/10.6100/IR515952)

Document status and date:

Published: 01/01/1998

Document Version:

Publisher's PDF, also known as Version of Record (includes final page, issue and volume numbers)

Please check the document version of this publication:

- A submitted manuscript is the version of the article upon submission and before peer-review. There can be important differences between the submitted version and the official published version of record. People interested in the research are advised to contact the author for the final version of the publication, or visit the DOI to the publisher's website.
- The final author version and the galley proof are versions of the publication after peer review.
- The final published version features the final layout of the paper including the volume, issue and page numbers.

[Link to publication](#)

General rights

Copyright and moral rights for the publications made accessible in the public portal are retained by the authors and/or other copyright owners and it is a condition of accessing publications that users recognise and abide by the legal requirements associated with these rights.

- Users may download and print one copy of any publication from the public portal for the purpose of private study or research.
- You may not further distribute the material or use it for any profit-making activity or commercial gain
- You may freely distribute the URL identifying the publication in the public portal.

If the publication is distributed under the terms of Article 25fa of the Dutch Copyright Act, indicated by the "Taverne" license above, please follow below link for the End User Agreement:

www.tue.nl/taverne

Take down policy

If you believe that this document breaches copyright please contact us at:

openaccess@tue.nl

providing details and we will investigate your claim.

Modelling and Model Based Control of Turbomachinery

Harm van Essen

Modelling and Model Based Control of Turbomachinery

CIP-DATA LIBRARY TECHNISCHE UNIVERSITEIT EINDHOVEN

Essen, Harm, A. van

Modelling and model based control of turbomachinery / by Harm A. van
Essen. - Eindhoven : Technische Universiteit Eindhoven, 1998. -

Proefschrift. - ISBN 90-386-0830-6

NUGI 841

Trefwoorden: turbomachines / gasturbines / compressoren / model
predictive control / regelsystemen / dynamische simulatie

Subject headings: turbomachinery / gas turbines / compressors / model
predictive control / control systems / dynamic simulation

Druk: Universiteitsdrukkerij TU Eindhoven

Modelling and Model Based Control of Turbomachinery

PROEFSCHRIFT

ter verkrijging van de graad van doctor
aan de Technische Universiteit Eindhoven,
op gezag van de Rector Magnificus,
prof.dr. M. Rem, voor een commissie
aangewezen door het College voor Promoties
in het openbaar te verdedigen op
donderdag 12 november 1998 om 16.00 uur

door

Harm Alberts van Essen

geboren te Tiel

Dit proefschrift is goedgekeurd door de promotoren:

prof.dr.ir. A.A. van Steenhoven

en

prof.dr.ir. J.J. Kok

Copromotor:

dr.ir. H.C. de Lange

This research was supported by TNO-TPD.

Contents

Contents	i
Symbols	v
1 Introduction.....	1
1.1 Turbomachinery	1
1.2 Modelling and control of turbomachinery	2
1.3 Statement of the problem and methodology of this study.....	3
1.4 Scope of the thesis	5
2 Experimental Set-up	7
2.1 Laboratory gas turbine installation.....	7
2.2 Measurement instrumentation.....	12
2.3 Data-acquisition and automatic control	14
2.4 Operation and control	14
2.4.1 Operating points of the installation.....	14
2.4.2 Opportunities for influencing the operating point of the installation.....	15
2.5 Discussion.....	17
3 Model Development	19
3.1 Modelling approach	19
3.2 Compressible fluid flow.....	21
3.2.1 Discretised equations for a pipe element	21
3.2.2 Discretised equations for a volume element	24
3.3 Components modelling	25
3.3.1 Compressor and expander.....	25
3.3.2 Control valves and piping appendages.....	27
3.3.3 Combustion chamber	28
3.3.4 Volume.....	29
3.3.5 Pipe junction	29
3.4 Laboratory gas turbine installation.....	30
3.4.1 Physical flow model.....	31
3.4.2 Lumped parameter model	31
3.5 Discussion	32

4 Model Validation.....	37
4.1 Available data from experiments	37
4.2 Parameter validation on the laboratory installation	39
4.2.1 Mass flows	39
4.2.2 Compressor and expander polytropic efficiencies	41
4.2.3 Combustion efficiency	43
4.2.4 Pressure drop over the installation	45
4.3 Model performance: stationary operating points	47
4.4 Inertia parameters.....	48
4.5 Model performance: transient response	49
4.6 Frequency response analysis	50
4.7 Discussion	52
5 Model Predictive Control.....	55
5.1 Introduction.....	55
5.2 Principles of MPC and Primacs implementation	56
5.2.1 MPC Concept.....	56
5.2.2 Tuning parameters in MPC.....	58
5.2.3 Implementation of MPC in Primacs	58
5.2.4 Linear optimisation	60
5.2.5 Successive linearisation	62
5.2.6 Filter and reconstruction	63
5.3 Discussion.....	65
6 MPC on the gas turbine installation.....	69
6.1 Gas turbine control.....	69
6.1.1 Control objectives	69
6.1.2 Constraints	70
6.1.3 Outputs and filter	71
6.1.4 Real-time implementation.....	72
6.1.5 Resolution of valves and minimal input move	73
6.2 Computation times and tuning parameters	74
6.3 Control of the operating point.....	75
6.3.1 New set point within the operation area	76
6.3.2 Constraints and operation area.....	78
6.3.3 Unreachable set point.....	80
6.4 Transient response	81
6.4.1 Transients during set point change.....	81
6.4.2 Influence of the input weightings.....	83
6.4.3 Influence of temperature constraint	84
6.4.4 Trajectory control: sine response	86
6.5 Robust performance	87
6.5.1 Different model combinations	88
6.5.2 Model combinations and throttle valve disturbance	89
6.5.3 Compressed air disturbances.....	91

6.6 Anticipation.....	92
6.6.1 Set point change with and without anticipation.....	92
6.6.2 Anticipative behaviour for different sizes of the control horizon.....	93
6.7 Discussion and conclusions	95
7 Compressor station control.....	97
7.1 Industrial compressor control and opportunities for MPC.....	97
7.1.1 Configuration and control	97
7.1.2 Conventional control of multiple compressors	99
7.1.3 Opportunities for Model Predictive control	99
7.2 Compressor station control case	100
7.2.1 System configuration	100
7.2.2 Model assumptions	101
7.2.3 Control objectives	102
7.3 MPC implementation	102
7.4 MPC simulation results.....	104
7.4.1 Reference load pattern with anticipation	104
7.4.2 Reference load pattern without anticipation	106
7.4.3 Reference load pattern and ideal power load balancing.....	108
7.4.4 Actual load pattern with and without set point on header pressure	111
7.4.5 Actual load pattern and ideal power load balancing	113
7.4.6 Reference load pattern and model mismatches.....	115
7.5 Discussion and conclusions	116
8 Conclusions and recommendations	119
8.1 Model development	119
8.2 Model based control.....	120
8.3 Application of MPC on turbomachinery.....	121
8.4 Consequences for industrial systems	122
8.5 Recommendations.....	123
References.....	125
A Component Characteristics.....	129
A.1 Gas turbine preliminaries	129
A.2 Compressor characteristic	130
A.3 Scaling compressor characteristic	132
A.4 Expander characteristic	134
A.5 Mass flow corrections compressor and expander	135
A.6 Compressor and expander polytropic efficiencies	137
A.7 Matching of compressor and expander	139
A.8 Control valve characteristics.....	140
A.9 Orifice characteristic	141
A.10 Fuel supply characteristic.....	143

B Expander Cooling Modelling	145
B.1 Geometry of the turbine cooling system.....	145
B.2 Determination of the heat exchanger coefficient.....	146
B.3 Temperature after cooling and cooled power	147
B.4 Thermodynamic data	148
B.5 Parameter heatfact and temperature profile.....	149
C Model Equations	151
C.1 Conservation equations for a homogeneous volume.....	151
C.2 Lumped parameter gas turbine model	153
C.3 Lumped parameter compressor station model.....	155
C.4 Alternative mass flow equations	157
C.5 Sensitivity analysis	158
D Instrumentation and Control.....	163
D.1 LabVIEW data-acquisition system.....	163
D.2 LabVIEW valve positioning control system	164
D.3 Threshold and Scaling.....	165
D.4 Primacs.....	167
D.5 Linear optimisation algorithms	167
D.6 Controller computation times.....	169
D.7 Resolution of valves and minimal input move.....	171
D.8 Filter gain	172
E Visualisation of Anticipative Behaviour.....	175
F Controller Settings in Experiments and Simulations.....	179
Summary.....	191
Samenvatting.....	193
Nawoord.....	195
Curriculum Vitae.....	197

Symbols

Symbol	Description	Dimension
a	velocity of sound	m s^{-1}
A	area	m^2
A, B, C	polynomial coefficients	-
c	constant	-
C_p	specific heat capacity	$\text{J kg}^{-1} \text{K}^{-1}$
C_v	specific heat capacity	$\text{J kg}^{-1} \text{K}^{-1}$
d, D	diameter	m
F	force	N
g	gravitational constant	m s^{-2}
h	heat transfer coefficient	$\text{W m}^{-2} \text{K}^{-1}$
H	specific enthalpy	kJ kg^{-1}
H_0	combustion energy	MJ kg^{-1}
I	shaft inertia	kg m^2
k	thermal conductivity	$\text{W m}^{-1} \text{K}^{-1}$
k	(reference) discrete sample	-
K_v	valve flow coefficient	$\text{m}^3 \text{hr}^{-1}$
L	length	m
m	(length of) control horizon	-
\dot{m}	mass flow	kg s^{-1}
M	mass	kg
N	rotational speed	rev min^{-1} or rev s^{-1}
Nu	Nusselt number	-
p	(length of) prediction horizon	-
p	pressure	N m^{-2}
Pr	Prandtl number	-
$Prat$	pressure ratio	-
q	heat	J
Q	power	W
R	gas constant	$\text{J kg}^{-1} \text{K}^{-1}$
Re	Reynolds number	-
S	valve seat opening factor	-
Sr	Strouhal number	-
t	time	s
T	temperature	K
U	overall heat transfer coefficient	$\text{W m}^{-2} \text{K}^{-1}$
u	input	-
v	velocity	m s^{-1}
V	volume	m^3
\dot{V}	volume flow	$\text{m}^3 \text{s}^{-1}$
x	x co-ordinate	-
x	length	m
x	state vector or state variable	-
y	output	-

Greek symbols	Description	Dimension
α	flow coefficient	-
Δ	difference	-
Γ	weighting factor	-
γ	ratio of heat capacities	-
η	efficiency	-
κ	steady state friction factor	-
ρ	density	kg m^{-3}
τ	friction factor	-
τ	time constant	s
ν	kinematic viscosity	$\text{m}^2 \text{s}^{-1}$
ω	rotational speed	rev s^{-1}
ξ	pressure drop factor	-
Subscripts	Description	
0	total or stagnation property	
1	compressor inlet	
2	compressor outlet	
3	expander inlet	
4	expander outlet	
<i>a</i>	compressor a	
<i>a</i>	annulus	
<i>air</i>	air	
<i>amb</i>	ambient conditions	
<i>b</i>	compressor b	
<i>bl</i>	blow-off (valve)	
<i>c</i>	compressor	
<i>cc</i>	combustion chamber	
<i>comp</i>	compressor duct	
<i>cool</i>	cooled	
<i>cor</i>	corrected or updated value	
<i>fuel</i>	fuel (valve)	
<i>i</i>	discretisation index	
<i>in</i>	inlet or input	
<i>isen</i>	isentropic	
<i>lumped</i>	lumped parameter model	
<i>m</i>	model	
<i>n</i>	normalised	
<i>org</i>	original	
<i>out</i>	outlet or output	
<i>p</i>	process	
<i>physical</i>	physical flow model	
<i>pl</i>	plenum	
<i>q</i>	cooling	
<i>recl</i>	recycle (valve)	
<i>ref</i>	reference	
<i>ss</i>	steady state	
<i>t</i>	expander (turbine)	
<i>th</i>	throttle (valve)	

1 Introduction

This thesis is about modelling and control of turbomachinery. In this introduction, first an explanation on the notion of turbomachinery and its applications is presented, followed by a brief review on modelling and control of turbomachinery installations. After that, we formulate a statement of the problem that is investigated in this study and discuss the methodology to follow. The chapter closes with a presentation of the scope of the thesis.

1.1 Turbomachinery

The generic term turbomachinery refers to devices like rotary compressors and expanders. The main component of these devices is a bladed rotor. In a turbo compressor, work is being done on the working fluid to raise its pressure. The rotor is driven by an external torque. The velocity of the fluid increases when it passes the rotor, i.e. flows between the rotor blades. After this passage, the fluid slows down with an accompanying rise of pressure while flowing through a ring of fixed diffuser blades and a volute. In a turbo expander, this series of events is reversed. A pressurised fluid enters the expander and acquires increased velocity as it expands to a lower pressure while flowing through a volute and a ring of fixed nozzle blades. This kinetic energy is transformed into output torque of the shaft when the fluid passes the rotor of the expander. An expander is a net producer of power, while a compressor is a net power consumer. There are two main types of rotary compressors and expanders, distinguished by whether the flow is in the axial or in the radial direction.

A compressor and an expander can be combined to a *gas turbine*. A gas turbine produces mechanical (shaft) power by expansion of compressed gas through an expander. A compressor provides the required pressure ratio. Compressor and expander are mounted on the same shaft and the expander powers the compressor. To overcome losses and develop useful power, energy has to be added by raising the temperature of the compressed air before expansion. This is accomplished in a combustion chamber positioned between compressor and expander. Figure 1.1 shows the gas turbine configuration. The cycle is called the *simple gas turbine* or *Joule-Brayton* cycle. This cycle is schematically represented by the ideal (isentropic) temperature-entropy (T-s) diagram of figure 1.2.

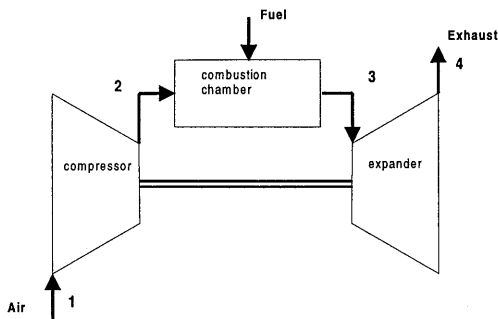


figure 1.1 : Schematic drawing of a gas turbine.

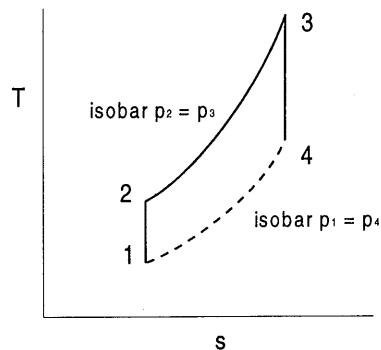


figure 1.2 : Isentropic T-s diagram of a simple gas turbine cycle.

Usually the inlet conditions of the compressor (index 1) are equal to the ambient temperature and pressure. Likewise, the outlet pressure of the expander (index 4) is usually equal to ambient pressure. Appendix A.1 presents a more elaborate analysis of the simple gas turbine cycle, including component losses, power and efficiencies. In [Cohen, 1987], [Cumpsty, 1989] and [Rogers, 1992] detailed information on design, performance and application of turbomachinery can be found.

Turbo compressors and gas turbines are widespread used. Separate turbo compressors are used for fluid transportation and pressure built-up. A typical application is a *compressor station* in a natural gas grid or in a compressed air utility network. A compressor station often consists of multiple compressors, that are connected in series or in parallel.

Typical applications of gas turbines can be found in aero engines and in power generation. In power generation, a gas turbine drives an electrical generator. When the exhaust heat of the gas turbine is usefully applied we speak of co-generation of power and heat. An example can be found in so-called *steam and gas* power stations where a gas turbine drives an electrical generator and the steam, that is generated from the exhaust gasses, powers a steam turbine and another electrical generator. Another example is the so-called *steam-injected gas turbine*. In these co-generation plants, the steam produced from the exhaust gasses of the gas turbine is normally used in production processes like drying or heating. When during production interruptions the steam is temporarily not used, the excess can be injected into the expander of the gas turbine. This principle realises a flexible trade-off between power and heat generation.

1.2 Modelling and control of turbomachinery

In the design process of turbomachinery, simulation models are used more and more. Nowadays, sophisticated three-dimensional CFD (computational fluid dynamics) methods are capable to predict accurately the flow conditions and the performance at the design point of compressor and expander stages. Advances in the design of turbomachinery result in performance improvements that lead to design points where components operate near their aerodynamic (surge), thermal, and mechanical load limits. Under these circumstances dynamic operation may cause excessive stresses on components that affect the safety, reliability and operation of the whole installation. An accurate prediction of these phenomena and their causes is critical in design of both components and overall installations like power plants. CFD methods, however, are not the appropriate tools for simulation of the dynamic operation of a whole installation because of the extensive problem definition and computation times. Straightforward dynamic simulation models with a relative low number of degrees of freedom are used for this purpose.

Control plays a major role in modern operation of advanced turbomachinery. Examples can be found in minimising fuel demand, power output and rotational speed control, noise and disturbance rejection, avoidance of instabilities like compressor surge and stall, and minimising combustion emissions. Dynamic operation plays an important role in the design of control systems. During transients, caused by changing load conditions or set point changes, the interaction between turbomachinery (and other) components becomes increasingly important for the overall system behaviour that is to be controlled. Dynamic models of both components and complete installations may be integrated in the control system, leading to model based control systems.

With regard to model development and the design of control systems for turbomachinery, most research effort is put into the dynamic simulation of modern aero engines since these are the most critical and valuable applications [Badmus, 1995a, 1995b, 1996], [Garrard, 1996]. This is expensive and often confidential research sponsored by NASA or US Airforce, leading to detailed component descriptions. Emphasis is often put on surge avoidance and the enlargement of the operation area by means of (active) surge and stall control [Simon, 1993].

Besides aero engines, also the simulation of modern power generation systems has become increasingly important since high efficiency and more flexible operation may be achieved [Schobeiri, 1994, 1996]. In these cases, emphasis is often put on complete installations rather than on turbomachinery components only. The overall system includes buffer tanks, piping geometry and capacity, recycle and relief systems, control valves etc. Also in compressor stations the interactions between individual compressors play a major role in the design of the system configuration and its control system. Recycle systems, for instance, are very important in the operation of compressor stations. Recycling is essential during start-up operation, for surge protection and for emergency shut-down. These operations are inherently dynamic where complex interactions between equipment, control and gas flow occur with the associated risk of compressor surge [Botros, 1991, 1994a].

1.3 Statement of the problem and methodology of this study

The aim of this study is to investigate the dynamic behaviour and control of compressor and expander installations. This is done by means of

1. The development of general purpose dynamic simulation models. This development includes experimental validation and an analysis of simulation and experimental results.
2. The development of model-based control configurations. A special control concept has been selected: *Model Predictive Control (MPC)*. A derived aim of the study is therefore to investigate the feasibility of MPC for use on turbomachinery.
3. The application of MPC to representative configurations of compressor/expander systems. This part includes simulations and real-time implementation.

Model development The first step in our methodology is to obtain a physical model of relevant phenomena in a generalised system configuration. The physical basis is expected to ensure the applicability of the model for a large class of compressor/expander systems. The model will have a generic, modular, component-wise structure. Components are compressor, turbine or expander, control valves, combustion chamber, flow-restrictions and piping. The resulting model is based on general conservation laws for compressible fluid flow through pipes, on well-known empirical relations for flow restrictions and for heat transfer and on (vendor supplied) stationary component characteristics.

It is very important to determine the model validity. Therefore, experiments must be performed on a representative installation. For this purpose a small, custom built, laboratory gas turbine set-up at Eindhoven University of Technology has been realised. A model for the laboratory gas turbine installation is composed from the generic model components. To obtain all model parameters, stationary as well as transient measurements are required. Parameter values are determined from a comparison between model simulation results and experimental data.

Several orders of model complexity are taken into account. Besides a full order (one dimensional) physical flow model, we also develop low order lumped-parameter and linear models that fulfil the requirements determined by the controller and the control objectives. To evaluate and compare the different model types, straightforward model simulations are performed and discussed.

Model based control The second step in our methodology is to develop a model predictive control configuration. Especially the well constraint and interactions handling of MPC form the basis for selecting this particular controller concept for turbomachinery systems as they are characterised by (highly) non-linear behaviour, fast dynamics, constraints and multi-variable control with a large degree of interaction.

Necessary elements of the development of an MPC configuration are:

- the formulation of control objectives, inputs, outputs, and constraints,
- the selection of an internal model used for prediction and optimisation,
- the implementation of MPC algorithms,
- selection, design, and implementation of a filter,
- the tuning of the MPC controller.

An essential element of the controller development is the internal model. This control oriented model should be able to predict the phenomena and time scales that are to be controlled with satisfying accuracy but should also meet the limited (sample) time available for the MPC algorithms. For this reason, in standard MPC, the internal model is linear so the optimisation problem can be solved with efficient algorithms. Strong non-linearities, displayed by the gas turbine installation, cannot always be handled adequately by standard linear MPC. Therefore, we develop non-linear methods, based on successive linearisation and non-linear prediction.

Application of MPC on turbomachinery Representative configurations of compressor/expander systems are selected. Besides the laboratory gas turbine installation, also a generalised compressor station has been considered. Both systems are schematically shown in figure 1.3 en figure 1.4 respectively. The design and the properties of the laboratory gas turbine set-up are extensively discussed in Chapter 2. The generalised compressor station configuration is comprised of two parallel connected compressors and a common header. In this thesis, the generic compressor station is related to the properties (i.e., geometry, components, and time scales etc.) of the laboratory gas turbine.

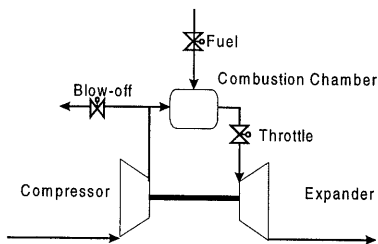


figure 1.3 : Schematic view of the laboratory gas turbine installation.

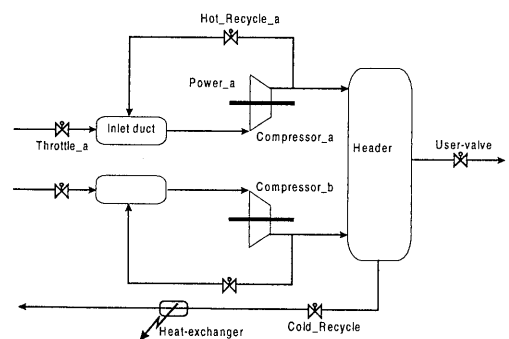


figure 1.4 : Generic compressor station configuration.

For the gas turbine set-up the emphasis is put on real-time implementation. The target is to meet rather straightforward objectives as set point and trajectory control, concerning constraints, interactions, disturbances, and measurement noise. Simulation techniques are used to gain insight in the application of MPC before real-time application. In a real-time environment, a strictly limited computation time for each sample is available.

The development of MPC for the compressor station is restricted to simulations since no real-life compressor station is available for measurement and testing. Although essentially the same types of dynamics, constraints, and interactions hold for the compressor station and the gas turbine, some of the elements of the MPC specification are quite complementary. The emphasis is on the optimisation of the surplus of degrees of freedom that parallel connected compressors possess.

Simulations and experiments of MPC for both configurations are analysed and discussed. Subjects of our feasibility study are closed-loop control performance, robustness for disturbances and for model mismatches, and the required computation times. Emphasis is put on the supposed advantages of MPC: anticipation and constraint handling.

1.4 Scope of the thesis

The first part of the thesis is about model development. We begin, in Chapter 2, with the presentation of the laboratory set-up of the gas turbine which will be used to validate the models and to test a real-time implementation of Model Predictive Control. Chapter 3 discusses the model development. The models are validated in Chapter 4, where results from experiments and simulation are compared and some values of model parameters are determined.

The second part of this thesis is about MPC on turbomachinery installations. Chapter 5 discusses the properties of MPC and presents the algorithms and implementations used in this study. In two subsequent chapters the application of MPC to the laboratory gas turbine and the parallel compressor station are treated. Chapter 6 presents the real-time control configuration of the gas turbine and discusses results of experiments. Chapter 7 presents the control configuration of the compressor station and discusses simulation results.

Finally, Chapter 8 presents general conclusions and recommendations for further studies to both model development and the application of Model Predictive Control on turbomachinery.

2 Experimental Set-up

The main goal of our research is to study the dynamic behaviour and control of turbomachinery. A gas turbine set-up has been realised in the laboratory. This laboratory installation offers the opportunity to influence and to monitor the dynamical operation of a gas turbine in more detail than an existing industrial installation. Since components such as a heat recovery steam generator and electrical generators, that may be present in an industrial (co-generation) installation, are less relevant for the dynamical behaviour of the gas turbine itself and since these components are not easily scaleable, they are not included in this research project.

2.1 Laboratory gas turbine installation

The laboratory-scale gas turbine has been designed around a turbocharger. Figure 2.1 presents a schematic view of the set-up. The main flow of air is sucked into the compressor, where it is compressed. Part of the air may be blown-off to the ambient while the remaining air passes a return or check-valve and reaches the buffer tank. Through the throttle valve, the air flows into the combustion chamber, where natural gas is injected and burnt. The heated compressed air then flows through the expander, where it expands and exhausts to the environment through the flue duct.

Three electrically powered control valves are installed: the compressor blow-off valve, the expander throttle valve, and the fuel supply valve. These appendages provide opportunities for affecting the operation point of the installation. Electrically powered control valves provide opportunities for automatic control.

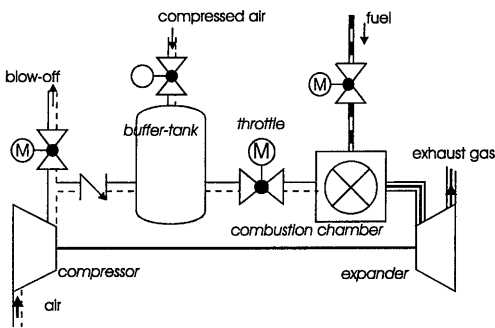


figure 2.1 : Schematic view of the laboratory gas turbine installation

In figure 2.2 a photograph of the laboratory set-up is presented. Stainless steel pipes connect the components of the installation. To intercept thermal expansion and corresponding stresses, compensators have been constructed into the installation. Technical details and design criteria of the installation are gathered in a separate design report [Van Essen, 1995]. In this thesis we focus on the main characteristics of the components.

Turbocharger An industrial sized turbocharger has been selected as the heart of the gas turbine. The turbocharger (type VTR160L) is manufactured by Brown Boveri Company (BBC). It consists of a single-stage radial compressor and a single-stage axial expander mounted on a single axis. This turbocharger is designed for diesel engines in ships or in emergency generators. In the laboratory installation, a combustion chamber replaces the diesel engine. In the photograph of figure 2.2 the relatively small turbocharger can hardly be recognised in the left side, right under the flue gas duct.

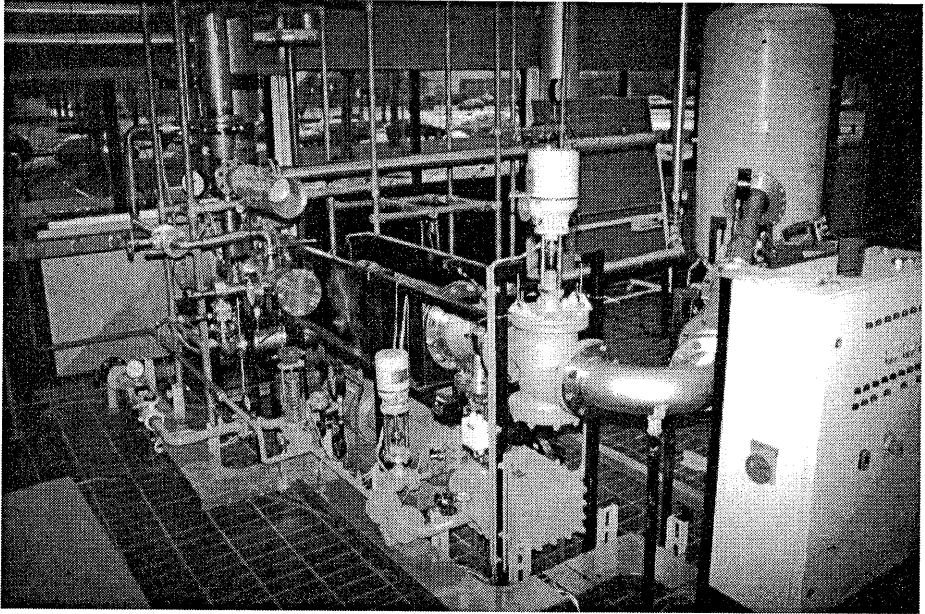


figure 2.2 : Photograph of the laboratory gas turbine installation.

The performance characteristics of the individual components (compressor and expander) are known on basis of specifications from the manufacturer. They consist of a graphical representation of the whole operation area. Figure 2.3 and figure 2.4 present the supplied characteristics for the BBC turbocharger.

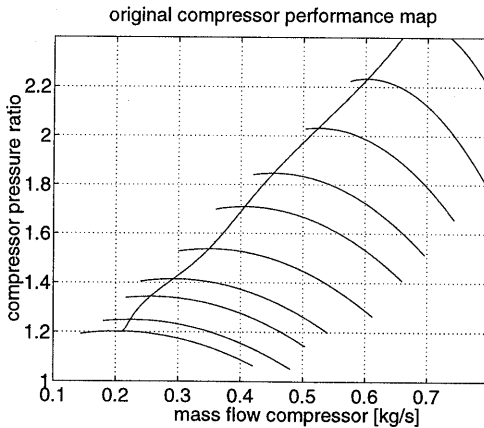


figure 2.3 : Compressor performance map for reference inlet conditions.
($p_{amb}=1.02 \text{ bar}$, $T_{amb}=298 \text{ K}$)

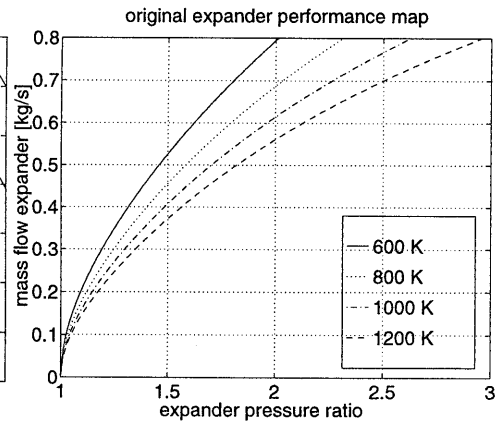


figure 2.4 : Expander performance map as a function of expander inlet temperature.
($p_{out}=1.02 * p_{amb}$)

In the compressor characteristic, curved lines represent the relationship between pressure ratio over, and mass flow through the compressor for various rotational speeds. Note that these lines are a function of the ambient conditions (see Appendix A.3) because the compressor map is related to the volume flow. The so-called *surge-line* connects the extremes of the speed lines. Surge denotes the phenomenon associated with violent limit cycle oscillations of mass

flow and pressure rise, which originate in the compressor and are transmitted throughout the gas turbine. Surge is likely to happen when the mass flow through the compressor decreases enough to enter the part of the compressor characteristic where a decrease in mass flow is accompanied by a fall of delivery pressure, i.e., where the lines of constant speed exhibit a positive slope. In the compressor characteristic this corresponds to passing the surge-line, which approximately separates the stable zone from the unstable zone. Unless the compressor is somehow forced to operate in the stable zone again, the surge instability is bound to persist, repeating the cycle of events at high frequency. This can get highly destructive, which is why surge must always be prevented. For detailed information about surge we refer to [Greitzer, 1976, 1986] and [Moore, 1986] and references therein.

The expander characteristic of figure 2.4 presents the relationship between pressure ratio over, and mass flow through the expander for various inlet temperatures. Indeed the (semi) dimensionless mass flow $\dot{m}\sqrt{T}/p$ reduces to a single curve. In this manufacturer's specification, the expander map does not depend on the rotational speed of the gas turbine. In general, however, a small dependency with the rotational speed is present.

Appendix A presents information about the turbocharger, including a detailed discussion on the performance maps of compressor and expander. Summarising, the maximum number of revolutions per second is 585 rev/s, the maximum expander inlet temperature is 925 K, the maximum compressor pressure ratio is 2.35 and the corresponding maximum mass flow amounts 0.8 kg/s.

The turbocharger needs cooling water, lubricating oil, and a flue gas duct. Within the turbocharger a double cooling water circuit is present to avoid too high casing and bearing temperatures. The cooling water circuitry is connected to an already operating cooling system in the laboratory. The internal lubricating circuit is filled with suitable engine oil. A flue gas duct for the exhaust gases has been realised on location. Figure 2.5 shows a cross-section of the turbocharger. In this drawing, the radial compressor (left) and the axial expander (right) as well as the lubricating and cooling circuitry can be recognised.

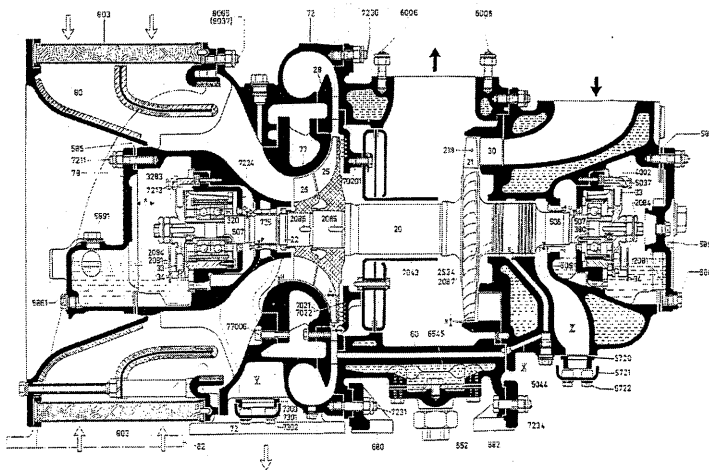


figure 2.5 : Cross-section BBC-VTR 160.

Buffer tank A large buffer tank, with a volume of 2.5 m^3 , is positioned between the compressor outlet and the inlet of the combustion chamber. The main function of the tank is to decouple flow oscillations, with order of frequency higher than 1 Hz, out of the compressor and into the expander. Although the buffer tank is a passive piece of equipment, its influence on the operating points of the installation is worth noting here. The decoupling of the outlet of the compressor from the inlet of the expander has a special meaning for measurements of transients. An example is the sudden injection of fuel into the combustion chamber; the expander inlet temperature increases instantaneously. From that the power developed by the expander increases and the gas turbine axis accelerates. The compressor, however, reacts on the available power and the mass flow and pressure ratio over the compressor will also rise. These effects are, during a short time, buffered in the tank before they influence the phenomena at the expander and establish a new equilibrium operating point.

Fuel supply line Natural gas from the public main has been selected as the most appropriate fuel. Figure 2.6 shows the gas supply line including the required safety devices.

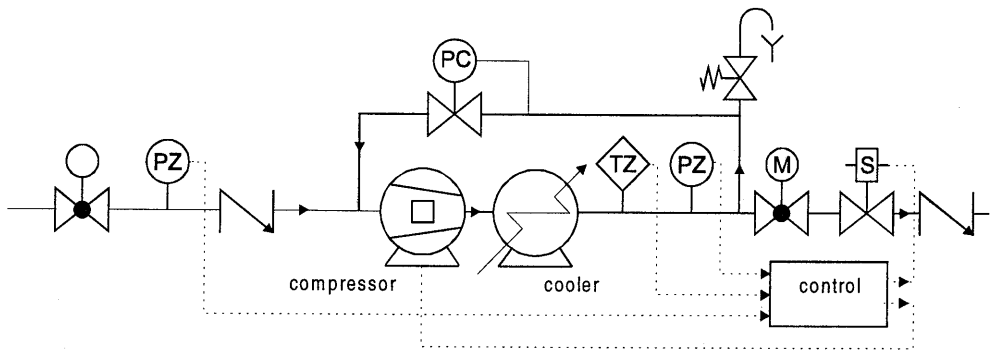


figure 2.6 : Schematic view of the gas supply line and safety devices.

A gas compressor raises the pressure before injection into the combustion chamber. A by-pass control configuration is applied; the capacity of the compressor is constant at its nominal value and the (motor powered) fuel valve (M) controls the fuel flow into the combustion chamber. The over capacity returns to the compressor suction side through an over-flow valve (PC). This over-flow valve is a mechanically controlled pressure regulator, which keeps the pressure upstream at an adjusted value. The downstream pressure equals the pressure in the gas main. Because compression raises the temperature of the gas, a cooler must be installed within the by-pass.

The safety devices are according to [GAVO, 1987] and consist (among other things) of electronic controlled pressure (PZ) and temperature (TZ) switches, return valves and an electronic controlled solenoid valve (S) at the end of the line. The electronic safety devices are controlled by a PLC installed in an electrical switch-board. The functions of the switch-board also include the control of the gas compressor and the automatic burner control. Apart from the prescribed safety devices in the gas line, an electronic temperature switch has been added to prevent the existence of a too high temperature after the combustion chamber (i.e. expander inlet temperature).

Combustion chamber A tubular combustion chamber comprises a cylindrical liner mounted concentrically inside a cylindrical casing. The tubular combustion chamber is the

basic geometry of conventional gas turbine combustion chambers. The tubular design is mechanically robust and has easily matched fuel-flow and air-flow patterns. In figure 2.7 the following components can be recognised: the air main, the air casing, the liner, the fuel injector, the primary air swirler, and the secondary and tertiary liner holes.

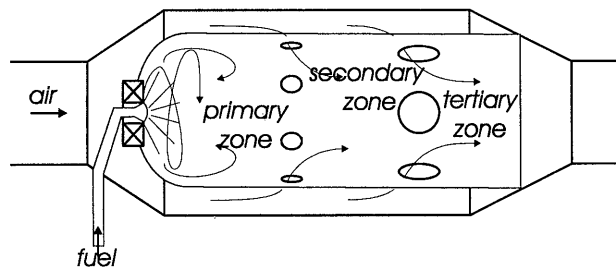


figure 2.7 : Combustion chamber.

The combustion process is divided into three zones: the primary zone, the secondary or intermediate zone and the tertiary or dilution zone. The functions of the primary zone are to provide a combustible mixture of air and fuel, to anchor the flame and to provide sufficient residence time, temperature and turbulence to achieve a complete combustion. This is realised by the swirler which induces a flow reversal in the primary zone. Hot combustion products flow upstream to meet and merge with incoming fuel and air. The secondary or intermediate zone provides sufficient residence time and temperature for complete recovering of dissociated combustion products. Dissociation losses are a result of the chemical instability of the main combustion products CO_2 and H_2O at the high temperatures (2200 K) that occur in the primary zone. Dropping the temperature to an intermediate level (1800 K) by the addition of a small amount of air allows the combustion to proceed to completion. Finally, in the tertiary or dilution zone, the remaining air is mixed with the combustion gasses to meet the required temperature (distribution) that is acceptable for the expander inlet.

The design of the combustion chamber involves the determination of the geometry of the combustion chamber and the specification of additional parts such as swirler, gas nozzle, ignition and flame control. The geometry of the combustion chamber involves the diameter of casing and liner, the length of the separate zones in the combustion chamber, and the area (distribution) of the swirler and the liner holes. All (empirical) design considerations are from [Lefebvre, 1983]. The main design problem is the determination of the total area of holes in the liner and the distribution of this area over the swirler opening and the secondary and tertiary holes in the liner. For any operation point, the optimal area (distribution) can be determined. Such an operation point is determined by a mass flow, a required temperature rise, and an optimal pressure drop over the liner that guarantees good mixing properties. Unfortunately, this optimal area distribution differs from operating point to operating point. Only one geometry can be implemented, therefore the area distribution must be a compromise between the overall requirements and specific influences of the operating points. The final design of the combustion chamber is presented in [Van Essen, 1995].

Additional parts of the combustion chamber The swirler consists of two concentric rings connected by flat vanes. Natural gas is injected into the combustion chamber through a nozzle. This nozzle fits within the swirl generator. Two pairs of electrodes are mounted on the nozzle. One pair of ignition electrodes and one pair of flame-control or ionisation electrodes.

The electrodes are connected to an automatic burner control. This device rules ignition and flame control. At burner start, the ignition transformer is powered and the ignition electrodes are sparking. During a short time gas is released by powering the solenoid of the fuel-line. If no flame signal is detected, the automatic burner control generates a failure alarm and fuel supply is disrupted.

2.2 Measurement instrumentation

Useful measurement data, proper monitoring of the installation, and process control require accurate measurements at several positions in the installation. The positions include compressor inlet, compressor outlet, combustion chamber, natural gas supply line, expander inlet, and expander outlet. Besides some analogue instruments such as thermometers and manometers, electronic sensors and transducers are used to be able to process measurement data at high sample rates in a data-acquisition system. In figure 2.8 a schematic view of the measurement positions and applied instrumentation in the laboratory set-up is presented. The following physical quantities are measured.

Pressures General purpose pressure transducers are located at five positions to measure relative pressure. In these transducers, semiconductor pressure sensitive resistors are coupled to a stainless steel diaphragm. A bridge circuit measures and converts the change in impedance to an analogue DC signal. Due to internal signal conditioning electronics, the output signal is linear over a full span and the accuracy is very good: less than 0.5% error. Piezo-resistive pressure transducers have very high bandwidths (typically >1 kHz).

Temperatures Thermocouples measure temperature at five positions in the set-up. Type K, 0.5 mm and 1.0 mm diameter thermocouples are applied. Output signals vary between 0 and 30 millivolt corresponding to ± 4 mV/ 100°C. A custom built thermocouple amplifier is used to amplify this low signal and to provide cold-junction compensation. The inaccuracy of the applied calibrated thermocouples including the amplifier is about 1%. Uncalibrated thermocouples and couples that are directly coupled to the A/D converter inhibit larger error levels of 2%. The response time of shielded 0.5 mm couples is approximately 1 second [Parr, 1985].

The output signals of the applied temperature safety devices are also available for measurement. For safety and robustness, these devices are much thicker resulting in slower response times (up to 5 seconds) than the thin thermocouples.

Rotational speed An inductive approach switch, mounted into the casing of the turbo-charger, measures the number of revolutions per second (rev/s). An inductive counter is an inexpensive, accurate, and reliable solution. The output is a frequency pulse of 2 pulses per revolution because two grooves are cut into the circular sheet placed on the axis. To process the signal along with the other DC voltages, a custom built frequency-to-voltage converter is applied. The basic accuracy of the rotational speed is in the order of a single revolution. The transformation to DC voltage, however, displays some non-linearity and is susceptible to electronic disturbances. The error level is approximately 1%.

Mass flow An orifice meter, built into the pipe between the buffer tank and the combustion chamber, measures the mass flow (kg/s) through the installation. The pressure difference is measured by means of a differential pressure transducer. Temperature and pressure measurements of air flow through the orifice are necessary to determine the density of the volume

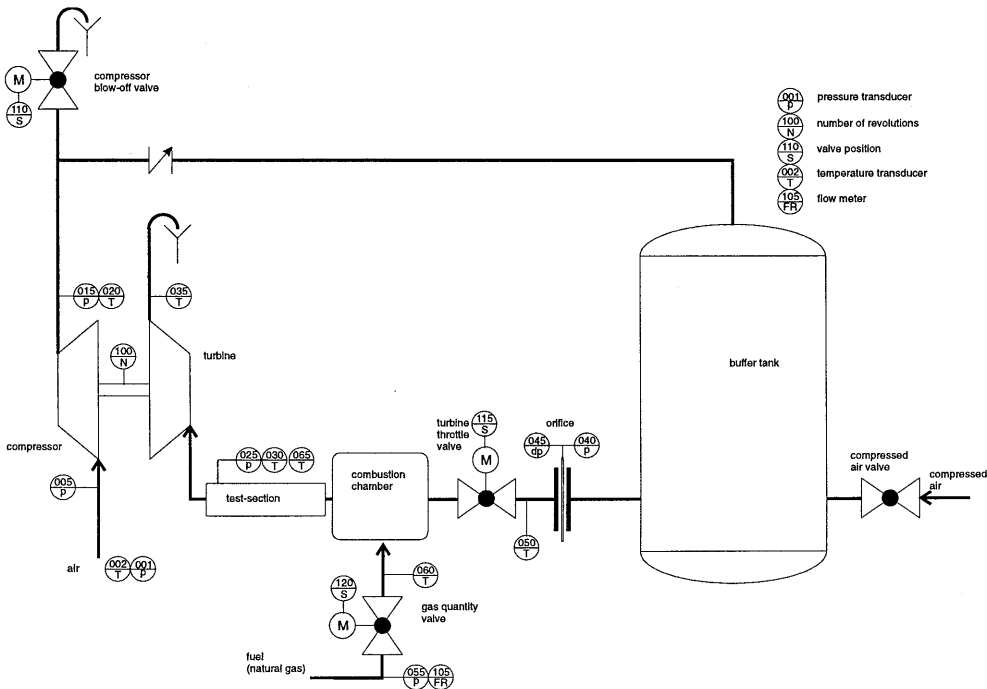


figure 2.8 : Instrumentation scheme, indicating all instruments including type of measurement, identification number and the location of the instrument.

flow. The orifice meter is designed according to NEN 3005 and requires a lead-in length of at least 3 metres. Important draw backs of the orifice meter are the poor accuracy in between 5 - 10% (since no appropriate calibration can be performed) and the relatively large response time of approximately 5 seconds. Especially the measurement of the pressure difference is highly influenced by the turbulence level of the upstream combustion process. Detailed information on the mass flow/pressure drop relation and accuracy is given in Appendix A.9.

The natural gas supply rate (m^3/s) is measured with a turbine flow-meter located in the low pressure gas main. The output of this instrument is a pulse per $1/250 \text{ m}^3$. This frequency is too low to convert to a DC voltage. The measurement is used to compute the fuel-flow off-line. A turbine flow meter is preferable for the relatively low flow rate of natural gas. The turbine flow meter is placed in the suction line of the gas compressor, where the density of the natural gas is assumed to be constant. Therefore not only the volume flow but also the mass flow of fuel can be determined. This position excludes transient measurements.

Valve positions The positions of the three valves are measured by potentiometers, built into the electric motor of the valve drives. The accuracy of the valve position equals the resolution of the mechanical transmission which is typically less than 0.5% but displays some hysteresis and backlash.

2.3 Data-acquisition and automatic control

A LabVIEW based data-acquisition system has been designed and realised. This system provides opportunities to measure, monitor and store all the available measurement signals.

All transducer signals are connected to a National Instruments data-acquisition plug-in board in the measurement PC. Continuous measurement of all signals is hardware timed and may proceed at extremely high sample frequencies up to 100 kHz. The resulting data flow, however, is continuously processed to be real-time monitored on the computer screen and stored to hard disk by a LabVIEW program. This program requires software based timers. Due to the limited properties of these software timers, the maximum measurement frequency is limited to 10 Hz.

The same LabVIEW program is also able to control the positions of the electrically powered control valves. The measured position of the valves is compared to the set point or desired position. This set point may be provided by an (external) controller or may be manually set in the LabVIEW program itself. When the position error is larger than the pre-set maximum error bound, LabVIEW generates a digital signal that switches a relay and powers the electric drive of the corresponding valve. The position of the valve is on/off controlled and its resolution is determined by the LabVIEW measurement frequency but even more by the mechanical properties of the transmission.

More information and specifications of the data-acquisition and control software and hardware are discussed in Appendix D.

2.4 Operation and control

Inherent to the working principle of a gas turbine the installation must be equipped with an effective start-up facility. This facility provides a sufficient high rotational speed of the gas turbine axis, where pressure ratios and mass flows are able to drive the gas turbine. Since the turbocharger does not have external access to its axis the only method is to blow the expander with compressed air from an external compressor. A connection to the compressed air utility is available at the buffer tank (see figure 2.8). The start-up procedure is treated in detail in Appendix A.11. When the installation runs 'on its own air', stationary operating points can be established. Opportunities to reach and to influence stationary operating points are made available.

2.4.1 Operating points of the installation

In section 2.1 the compressor and expander characteristic were presented. This range of possible operating points of individual components reduces considerably when the components are linked together. The problem is to find corresponding points in the characteristics of each component when the gas turbine runs at steady speed. This point is called an equilibrium point. An equilibrium point fulfils the following conditions:

1. A power balance holds between the expander and the compressor. This implies that the power developed by the expander exactly equals the amount of power required by the compressor plus losses. If the power balance does not hold, the turbine axis either accelerates or decelerates.

2. The mass flow through the compressor equals to the mass flow through the expander (including the mass flow of fuel that often may be neglected).
3. The pressure ratio over the expander equals to the pressure ratio over the compressor minus pressure losses. Losses occur over all appendages present between compressor outlet and expander inlet, including the combustion chamber and the throttle valve.

Stable operating points of the turbocharger in the laboratory installation can be found from a matching procedure of the characteristics. Appendix A.7 summarises this procedure. The resulting operating point of the overall gas turbine is usually presented in the compressor characteristic by the compressor pressure ratio, the mass flow and the rotational speed. All equilibrium points together form the operation area of the installation.

An estimate of the maximum power demand of the laboratory installation can be determined by computing the amount of heat that the temperature rise at a certain operating point requires. For a maximum mass flow of 0.80 kg/s and a maximum expander inlet temperature of 925 K this results in 550 kW. Only a fraction of approximately 10% of this thermal input power is used to drive the gas turbine. The remaining power is lost to the environment in the exhaust, the cooling water and heat losses through the piping.

2.4.2 Opportunities for influencing the operating point of the installation

The compressor is directly coupled to the expander. There is no external load or brake that influences the gas turbine. Therefore, other opportunities to affect the operating point of the installation are made available: three control valves and external air. The three control valves are the fuel valve, the compressor blow-off valve and the throttle valve. The fuel supply valve is the most important parameter to adjust the operating point of the gas turbine. When the other valve positions are unchanged, fuel supply variations result in a line of stationary operating points in the compressor characteristic. When the blow-off valve is completely closed and the throttle valve is fully opened, this line is called the standard equilibrium load line. The effect of the other two control valves is a shift of the position of the entire load line.

Figure 2.9 illustrates the influence of variations in valve positions to the operation point of the gas turbine in the compressor characteristic. Results are from straightforward simulations that will be discussed in Chapter 4. From the indicated starting point, in four separate simulations, the fuel valve is opened and closed, the blow-off valve is opened, and the throttle valve is closed.

Fuel supply valve An increase in fuel supply immediately raises the expander inlet temperature. The higher temperature provides more power to the expander resulting in a temporary power difference between compressor and expander and an acceleration of the axis. Due to this increased power and higher rotational speed the compressor delivers more mass flow and a higher pressure ratio until the power balance holds again. With a small delay the extra mass flow reaches the combustion chamber and the expander inlet temperature decreases again. Therefore not the expander inlet temperature but rather the power input is controlled by the fuel supply valve.

From the starting point in the centre of the characteristic in figure 2.9 variations of +5% and -5% indicate the location of the equilibrium load line. In practical operations the fuel valve position varies between 0.20 and 0.50, this is over 30% of its full span. Any equilibrium load

line is characterised by a constant temperature: although the amount of supplied fuel and the pressures and rotational speed differ significantly, the temperature over these three points only varies 5 Kelvin from 852 to 857 K.

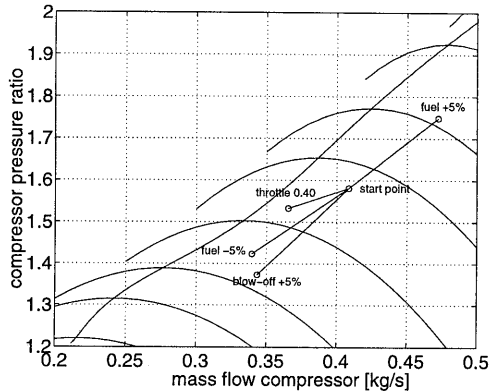


figure 2.9: Simulated influences of variations in valve positions to the operating point of the gas turbine installation indicated in the compressor characteristic .

Compressor blow-off valve Blow-off directly influences the ratio of mass flows through compressor and expander. When this valve is (slightly) opened, the delivery pressure of the compressor decreases. Although the mass flow through the compressor increases slightly, the expander mass flow decreases. The pressure ratio over the expander decreases along with the compressor delivery pressure. This results in a decrease of power developed in the expander. The rotational speed decreases until a power balance is reached again in a stable operating point on another equilibrium load line. The corresponding expander inlet temperatures are significantly higher.

The variation in figure 2.9 due to blow-off of 5% opening leads to an operation point on a slightly shifted (to a larger mass flow) equilibrium line parallel to the original one. The corresponding expander inlet temperature is extremely high (953 K), considerably exceeding the maximum allowed temperature level. For this reason, it is hardly possible to open the blow-off valve for more than 4%. In fact, the capacity of the blow-off valve is too large for control purposes; the resulting resolution within the 4% range is too low. Its main use is start-up.

Throttle valve Throttling influences the ratio of compressor delivery- and expander inlet pressure. When this valve is closed, the pressure losses between compressor and expander increase. The power developed in the expander decreases. A new operating point is reached on a new equilibrium load line that is positioned at lower mass flows and lower pressure ratios in the compressor characteristic. The corresponding expander inlet temperatures are higher on the new equilibrium line. Adjusting the fuel supply allows to impose other operating points on this new equilibrium load line.

In figure 2.9 the throttle valve is closed by 60% from 1.0 to 0.4. The disproportionate change is caused by the large capacity of the throttle valve: a clear effect of additional pressure drop is only seen at valve position below 50%. It can be seen that the new equilibrium line shifts towards the surge line. The corresponding temperature of this line is 893 K (in the simulated

operating point). The location of the surge line corresponds to the equilibrium line at a throttle valve position of approximately 30%.

Additional mass flow When additional mass flow through the expander can be realised, the mass flow and the pressure ratio over the expander are (artificially) increased. A new operating point will be reached on a new equilibrium load line that is, relative to the original, positioned at higher mass flows and higher pressure ratios in the compressor characteristic. Extra mass flow through the expander can be realised with compressed air. The connection to the compressed air, however, is in the buffer tank, *before* the throttle valve. This complicates the injection of air because then not only the expander pressure ratio but also the compressor pressure ratio is affected. Because the compressed air supply is not regulated by an electrically powered control valve its use for control is limited and therefore scarcely applied in this thesis. For the same reason, its influence is not indicated in figure 2.9.

2.5 Discussion

In this closing section, we discuss the relevant time scales of the laboratory set-up that hold for modelling and control. We also indicate the relation between the laboratory gas turbine set-up and industrial scaled gas turbine installations. Finally, we present an extension to the design of the set-up that will be used in future research: steam injection.

Time scales In the laboratory gas turbine different time scales are present. A characteristic time scale for overall transient set point changes is in the order of 10 seconds. This time scale is determined by the total system inertia (acceleration of the turbocharger, pipe length, buffer tank). The time scale is related to the residence time of fluid in the buffer tank.

Individual components react faster than the overall system. The corresponding time scales are in the order of 1.0 second, mainly determined by the acceleration of the turbocharger and the fluid flow through pipes. Smaller time scales can be found in dynamic instabilities like surge or the propagation of pressure waves in the pipelines. The corresponding time scales of these phenomena are in the order of 0.01 second, determined by the velocity of sound.

In this thesis we do not seek to control the small time scales that correspond to pressure wave propagation or dynamic instabilities. The main target is an overall system approach in which we want to control transient changes of the operating point. The model to be developed should fit to an application of a model-based control configuration. This puts strong demands on real-time simulation properties and therefore to the complexity of the model.

Comparison to industrial installations Indeed, the laboratory installation aims to be a fair representation of a gas turbine installation. To be able, however, to compare or to translate results obtained from the laboratory set-up to industrial sized installations, the components of the laboratory installation should be geometrically similar to industrial scale turbines and the same values or ratios for the appropriate dimensionless groups should hold. These numbers describe the dynamic similarity. Relevant dimensionless groups for turbomachinery are gathered in table 2.1 (in which D is a characteristic dimension (m) and R the gas constant).

	compressor	expander
flow number	$\frac{\dot{m}\sqrt{RT_1}}{D^2 p_1}$	$\frac{\dot{m}\sqrt{RT_3}}{D^2 p_3}$
speed number	$\frac{ND}{\sqrt{RT_1}}$	$\frac{ND}{\sqrt{RT_3}}$
pressure ratio	p_2 / p_1	p_3 / p_4

table 2.1 : Dimensionless numbers for turbomachinery.

The turbocharger within the laboratory set-up combines a single stage radial compressor and a single stage axial expander, a combination that is rarely met in industrial practice. Industrial installations can therefore hardly be considered geometrically similar. Therefore, we can not upscale (flow) results directly to industrial installations.

On the other hand, the laboratory set-up is a typical turbomachinery installation. This means that the non-linearities of the gas turbine system, the properties and characteristics of both turbomachinery components and control valves, and the dynamics of the laboratory installation show close correspondence to realistic systems. Therefore, we will be able to touch on interesting (dynamic) problems in turbomachinery. In this thesis we focus our modelling and control efforts on the properties and time scales encountered in the laboratory set-up. We rather investigate the feasibility of models and control strategies than presenting ready-made industrial solutions.

Steam injection The installation has been extended with a steam injection facility. A suitable steam-boiler is available in the laboratory and a custom designed injection piston allows step like mass flow injection. The position of the steam piston is just after the combustion chamber. Stationary as well as pulsating mass flow injections should be considered. Steam injection provides interesting opportunities to influence the operation point of the installation and to perturbate dynamic responses. In this thesis, however, steam injection is not considered yet since it is not fully operational. Future research will focus on the particular dynamic problems encountered in steam-injected co-generation installations.

3 Model Development

In this chapter a physical model for turbomachinery installations will be developed. The model has a generic, modular, component-wise structure. Components are compressor, expander, control valves, combustion chamber, flow-restrictions and piping. The physical basis and the modular approach are expected to ensure the applicability of the model for a large class of compressor/expander systems. The resulting model is based on general conservation laws, on well-known empirical relations for flow restrictions and on (vendor supplied) stationary component characteristics. Only little detailed geometric information is required.

The first section explains and justifies our modelling approach. Two subsequent sections treat basic model parts in detail. The first presents a discussion of general conservation laws applied to describe compressible fluid flow through pipe and volume elements. The second considers the component modelling approach including a discussion of all applicable components.

From all this, two different sets of model equations for the laboratory gas turbine installation are derived. The first type we refer to as the *physical flow model*, since it includes physical equations for compressible fluid flow through pipelines. The second type is the *lumped parameter model*, in which flow through pipelines is neglected and the corresponding inertia is lumped into a single volume. Note, however, that both models are based on first principles and only the extent of lumping differs.

Our first interest is the application of the models to describe and control the laboratory gas turbine installation. Especially for real-time control of transient operating point changes the model ought to be simulated fast enough. Most likely, only the lumped parameter model can satisfy this restriction. The much more involved physical flow model is introduced as an independent reference for the lumped parameter model. It provides opportunities for research to faster phenomena like steam injection, dynamic oscillations in pipes, and turbocharged diesel engines.

In the concluding section of this chapter we discuss the differences between the two types of models as well as the applicability to control the laboratory gas turbine installation. This discussion includes the modelling of instationary and dynamic phenomena in some detail. Also the application towards other turbomachinery installations like industrial co-generation systems and compressor stations are proposed.

3.1 Modelling approach

A generic, modular, one-dimensional approach is applied to model turbomachinery. The basic model comprises several modules representing actual components of the installation such as the compressor, valves, combustion chamber, and expander. Modules are coupled by pipelines or by volumes.

Components are modelled by a coupled static and two dynamic parts. Figure 3.1 presents this approach schematically. The static part is the component characteristic: a set of (non-linear) quasi steady algebraic equations determining the mass flow through the component. In this

way the component characteristics are used as static momentum balances. The characteristics of the components are often available from the manufacturer. Component maps include not only full compressor and expander performance maps but also flow- Δp relationships that hold for control valves or flow restrictions like orifices and pipe bows. Necessary conditions for satisfactory simulation results are that the performance maps are available in an accessible (mathematical) format and are sufficiently accurate.

The dynamic behaviour of the component (i.e., accumulation of mass, momentum, and energy), is modelled by plenum volumes, immediately connected before and after the component. Inside each plenum the conservation equations for mass, momentum and energy are solved. The plenum also provides the dynamic interaction between successive components. The volume of the plenum reflects the partial volumes of two successive components, i.e., half of each. In case two components are directly coupled, like in figure 3.2, the connecting volume consists of the volume of the outlet plenum of the first components added to the volume of the inlet plenum of the second component.

The dynamic coupling modules are pipelines and/or volumes. For overall system simulation, a one dimensional approximation of the flow equations is expected to give sufficient accurate results. A two or even three dimensional solution for the entire system simulation would require computational means not available yet. Moreover, this problem will require complex geometry and system information, resulting in a less generic model.

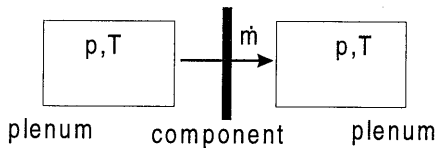


figure 3.1: Sketch of the component modelling approach.

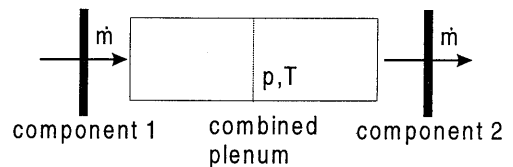


figure 3.2 : Sketch of the approach of two successive components.

System simulation by the performance maps of the components extended by dynamic coupling equations is particularly useful when complete installations are simulated within the operating range defined by the component maps. The modular approach allows easy adjustments to the system configuration and geometry.

This type of modelling of turbomachinery is widely accepted in the literature. First approaches date from the early seventies when NASA started steady state simulations with the overall component characteristics. Simulation of transient dynamics by coupling static components through connecting plenum volumes is, among others, presented by [Schobeiri, 1994] and [Garrard, 1996] with regard to aero engines and [Botros, 1991, 1994a] with regard to compressor stations.

Based on the component modelling approach we distinguish two types of models. The first we refer to as the *physical flow model*, to the second as the *lumped parameter model*. The most important difference between both types of models is the coupling of two successive components. The physical flow model assumes compressible fluid flow through connecting pipe lines and solves the corresponding flow equations, while components in the lumped model are coupled by a volume and flow inertia is completely lumped into a few volumes.

Physical flow model In the physical flow model, a pipeline connects two successive components. Figure 3.3 shows this situation schematically. As can be seen in the figure, the coupling includes the plenum of the component. A pipeline is divided into a number of elements for each of which the full set of conservation laws is solved. Therefore, only in pipelines the instantaneous momentum equation is solved. The algebraic relationships that describe the components are used as boundary conditions to solve the resulting set of equations.

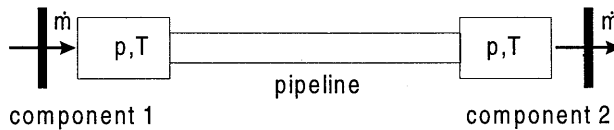


figure 3.3 : Component "Pipeline" in between two successive components in the physical flow model.

Lumped parameter model The lumped parameter model neglects the connecting pipelines as separate components. Figure 3.4 sketches two successive components in the lumped configuration. Although this configuration looks exactly like the basic model type of figure 3.2, the meaning of the connecting volume is different. The volume does no longer represent the (internal) volume of the component itself, but rather the total volume *between* the two components. The total or *effective* volume is *lumped* into this single volume.

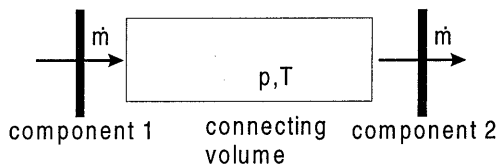


figure 3.4 : Sketch of two successive components in the lumped parameter model.

3.2 Compressible fluid flow

Starting from general one-dimensional conservation laws, this section describes compressible fluid flow in pipelines and volume elements. Two sets of equations are derived. First, we discuss the discretised equations applicable to solve compressible fluid flow through a pipe line which is divided in elements. This set is used in the physical flow model only. Next, we derive the second set of discretised equations which is especially applicable to a single volume element. These equations are used to model the coupling plenums of components as well as the lumped volumes in the lumped model.

3.2.1 Discretised equations for a pipe element

Consider a pipeline with a constant diameter D and a flow surface $A = (\pi/4)D^2$. Assume an infinitesimal element of such a pipe. The one-dimensional momentum equation applied to this element, expressed in terms of mass flow may be written as [Bird, 1960]:

$$\frac{\partial \dot{m}}{\partial t} + \frac{\partial \dot{m}v}{\partial x} + A \frac{\partial p}{\partial x} + \tau \pi D = 0 \quad (3.1)$$

In which $\dot{m} = \rho v A$ and in which the last term refers to friction as the net surface force caused by the shear stress τ . This stress is expressed by the constant steady state friction factor κ according to Darcy-Weisbach [Streeter, 1985]:

$$\tau = \frac{\kappa \dot{m}^2}{8\rho A^2} \quad (3.2)$$

Unless a frequency dependable value of the dissipation factor κ is known, it can not describe any instationary effect of friction forces. A constant value of κ describes a stationary pressure drop as a result of a friction force due to steady flow. Such a pressure drop in the pipe flow may be necessary when long pipelines are modelled. The empirical value of the parameter κ depends on the surface roughness of the pipe and the Reynolds number and may be altered to fit experimental data.

Integrated over the control volume V as indicated in figure 3.5, this formulation (still under the assumption of a constant pipe diameter D and surface A , and $V/A = \delta x$) leads to the following discretised expression of the momentum equation:

$$\frac{d\dot{m}_i}{dt} = - \left[\frac{v_{i+1}\dot{m}_i - v_i\dot{m}_{i-1}}{\delta x} \right] - A \left[\frac{p_{i+1} - p_i}{\delta x} \right] - \frac{\kappa \dot{m}_i^2}{2\rho A D} \quad (3.3)$$

$$\text{with } v_i = \frac{\dot{m}_{i-1} + \dot{m}_i}{2A} \frac{RT_i}{p_i} \text{ and } \rho = \frac{p_i + p_{i+1}}{T_i + T_{i+1}} \frac{1}{R}.$$

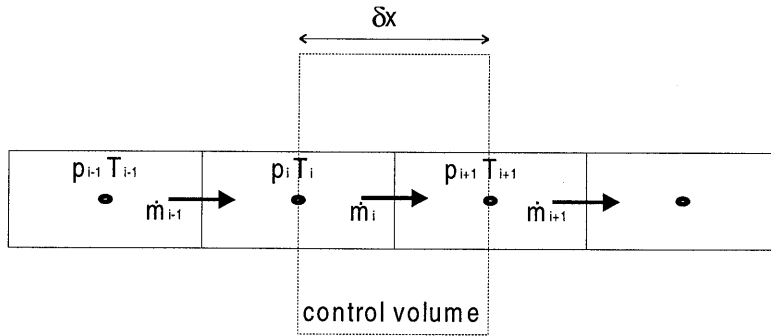


figure 3.5 : Discretisation scheme for the momentum equation.

When gravitation is neglected, no external heat is added or distracted (which includes the heat conduction terms) and viscous dissipation is neglected, the one dimensional energy conservation equation equals [Bird, 1960]:

$$\frac{\partial \rho C_v T}{\partial t} + \frac{\partial \frac{1}{2} \rho v^2}{\partial t} = - \frac{\partial \rho C_v T v}{\partial x} - \frac{\partial \frac{1}{2} \rho v^2 v}{\partial x} - \frac{\partial p v}{\partial x} \quad (3.4)$$

When the continuity and momentum equations are substituted, the kinetic energy part

$$\frac{\partial \frac{1}{2} \rho v^2}{\partial t} = - \frac{\partial \frac{1}{2} \rho v^2 v}{\partial x} - v \frac{\partial p}{\partial x} \quad (3.5)$$

vanishes, while the thermal part

$$\frac{\partial \rho C_v T}{\partial t} = -\frac{\partial \rho v C_v T}{\partial x} - p \frac{\partial v}{\partial x} \quad (3.6)$$

can be simplified to

$$\frac{\partial T}{\partial t} = -v \frac{\partial T}{\partial x} - (\gamma - 1) T \frac{\partial v}{\partial x} \quad (3.7)$$

For which the ideal gas law is applied as an equation of state: $p = \rho RT$. When we assume that the ideal gas law holds for the control volume with a fixed volume V , the equation $pV = MRT$ (with M the total mass within the volume) can be differentiated to

$$\frac{\partial p}{\partial t} = \frac{RT}{V} \frac{\partial M}{\partial t} + \frac{p}{T} \frac{\partial T}{\partial t} \quad (3.8)$$

So, the energy conservation equation can be written as the coupled set of differential equations (3.7) and (3.8). Applied to the control volume defined in figure 3.6, integrating over the control volume, with

$$\frac{\partial M}{\partial t} = \dot{m}_{i-1} - \dot{m}_i \quad \frac{\partial v}{\partial x} = \frac{v_i - v_{i-1}}{\delta x} \quad \frac{\partial T}{\partial x} = \frac{T_i - T_{i-1}}{\delta x} \quad (3.9)$$

gives two discretised equations for an element of a pipe.

$$\frac{dp_i}{dt} = \frac{RT_i}{V} (\dot{m}_{i-1} - \dot{m}_i) + \frac{p_i}{T_i} \frac{dT_i}{dt} \quad (3.10)$$

$$\frac{dT_i}{dt} = -v_{i-1} \left(\frac{T_i - T_{i-1}}{\delta x} \right) - (\gamma - 1) T_i \left(\frac{v_i - v_{i-1}}{\delta x} \right) \quad (3.11)$$

$$\text{in which } v_i = \dot{m}_i \frac{R}{A} \frac{T_i + T_{i+1}}{p_i + p_{i+1}}.$$

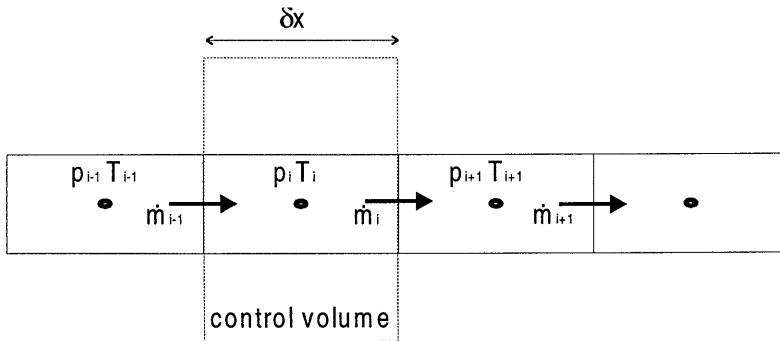


figure 3.6 : Discretisation scheme for the energy equation.

Note that for the determination of the discretised mass flows and velocities in both the momentum and the energy equations the upwind principle has been adapted. The cut-off error of the discretisation is of the order δx .

The control volumes for the momentum and the energy equations are chosen not to coincide. The staggered grid principle of [Patankar, 1980] shifts the control volumes half an element to avoid singularity problems or alternate solutions in the velocities and or densities that are computed at the control volume faces.

A small problem in this discretisation scheme is the choice of v_{i-1} in the integration over the control volume (the first right hand side term of (3.11)). The following section discusses an alternative that is especially applicable to one volume element.

3.2.2 Discretised equations for a volume element

Assume an ideally stirred volume as schematically drawn in figure 3.7. Heat can be supplied to this volume. The ideally stirred assumption implies that the pressure and temperature and, if relevant, the composition and heat capacity of the fluid, are homogeneous within the volume. The outlet values of pressure and temperature are equal to those within the volume, while the input temperature, pressure or composition may vary. The input pressure, however, is accounted for in the incoming mass flow. Therefore, the term $\partial p / \partial x$ is neglected over the volume. A pressure drop over the actual volume must be lumped into the component characteristics or should be described by an additional component.

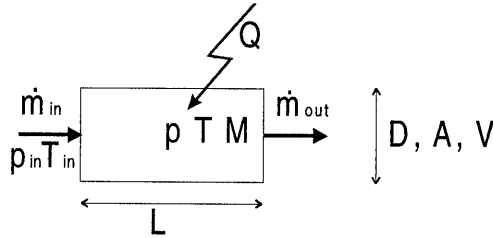


figure 3.7 : Homogeneous volume.

Starting from the ideal gas law and the momentum and mass conservation laws, the general energy equation for this fixed volume

$$\frac{\partial \rho C_p T}{\partial t} = - \frac{\partial \rho C_p T v}{\partial x} - \frac{\partial q}{\partial x} + \frac{D p}{D t} \quad (3.12)$$

can be written as a coupled set of differential equations:

$$\frac{\partial T}{\partial t} = \frac{RT}{pV} \left[\gamma \left(\dot{m}_{in} \frac{C_{p,in}}{C_p} T_{in} - \dot{m}_{out} T + \frac{Q}{C_p} \right) - T (\dot{m}_{in} - \dot{m}_{out}) \right] \quad (3.13)$$

$$\frac{\partial p}{\partial t} = \frac{\gamma R}{V} \left(\dot{m}_{in} \frac{C_{p,in}}{C_p} T_{in} - \dot{m}_{out} T + \frac{Q}{C_p} \right) \quad (3.14)$$

These equations are derived in Appendix C.1. A power term Q (W) represents a heat flux q (W/m^2) over the boundary of the volume or an internal heat source or sink. Such an internal source may be a combustion or cooling process within the volume. In case of large power addition or extraction, differences in values between input and output heat capacity $C_{p,in}$ and C_p should be taken into account. In (3.13) and (3.14) the heat capacity value of the incoming flow is denoted $C_{p,in}$, while C_p , R , and γ correspond to the thermodynamic state T and p within the volume.

In case of fuel addition, the mass of the injected fuel should be taken into account. Additional mass can be described by adding an input: two mass flows in and only one out. Both mass flows may have different temperatures and heat capacities. The mass flow fuel is often negligible compared to the main mass flow of air.

Since only in the combustion chamber and in the expander cooling system significant amounts of heat are added or extracted, the power terms can be omitted for the other components. In the special case of an adiabatic volume in which no heat exchange to or from the volume takes place, the set of equations reduces to:

$$\frac{\partial T}{\partial t} = \frac{RT}{pV} [\gamma(\dot{m}_{in}T_{in} - \dot{m}_{out}T) - T(\dot{m}_{in} - \dot{m}_{out})] \quad (3.15)$$

$$\frac{\partial p}{\partial t} = \frac{\gamma R}{V} (\dot{m}_{in}T_{in} - \dot{m}_{out}T) \quad (3.16)$$

3.3 Components modelling

This section discusses the theoretical foundations of the several model modules. All components are built around dynamic one dimensional conservation laws and static momentum balances from component characteristics. For all components that are used in this thesis, a schematic view, the appropriate equations, and possible remarks and assumptions are discussed. Components under consideration are: compressor, expander and cooling system, control valves and piping appendages (such as flow restrictions, splitting, connections, bows, change in diameter), combustion chamber, buffer tank or volume, and pipe junction. The special coupling "component" pipeline is not discussed since it has already been treated before.

3.3.1 Compressor and expander

The compressor and expander are essential components in turbomachinery systems. Figure 3.8 presents the compressor schematically. Basically, it consists of a pressure rising device, like an actuator disk or a rotor, combined with two representative volumes before and after this rotor.

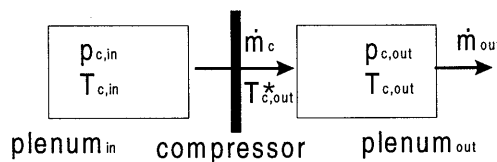


figure 3.8 : Component "Compressor".

Mass flow through the compressor is computed according to the component characteristic from pressure ratio, rotational speed, and inlet conditions. The temperature rise due to compression is computed according to the polytropic component efficiency η_c :

$$T_{c,out}^* = T_{c,in} \left(\frac{P_{c,out}}{P_{c,in}} \right)^{\frac{\gamma-1}{\gamma \eta_c}} \quad (3.17)$$

Pressure and temperature in the plenum in front of the compressor are assumed constant and equal to the ambient pressure and temperature. Possible effects of for instance an air-filter are taken into account by the compressor characteristic which depends on the inlet pressure and temperature. Of course, a filter, or any other device before the actual compressor, may also be modelled as a separate component.

The following set of differential equations (based on (3.15) (3.16)) computes the properties in the plenum after the component according to the quantities in figure 3.8 with V is the volume of this plenum, reflecting the volume of the compressor after the rotor

$$\frac{\partial T_{c,out}}{\partial t} = \frac{RT_{c,out}}{P_{c,out}V} \left[\gamma (\dot{m}_c T_{c,out}^* - \dot{m}_{out} T_{c,out}) - T_{c,out} (\dot{m}_c - \dot{m}_{out}) \right] \quad (3.18)$$

$$\frac{\partial P_{c,out}}{\partial t} = \frac{\gamma R}{V} (\dot{m}_c T_{c,out}^* - \dot{m}_{out} T_{c,out}) \quad (3.19)$$

For the expander component analogous relations can be derived. The presence of a cooling system within the expander, however, complicates the modelling. Figure 3.9 presents the expander schematically.

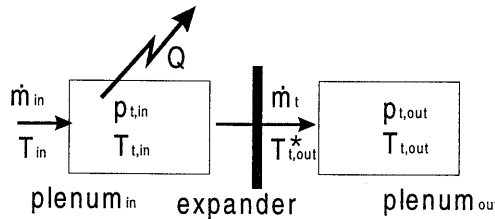


figure 3.9 : Component "Expander".

Pressure and temperature in the plenum before the component are computed from the set of differential equations (3.20) and (3.21), stated according to the quantities in figure 3.9 with \dot{m}_{in} the inlet mass flow of temperature T_{in} , determined by the component preceding the expander and Q the cooled power (negative value) [W].

$$\frac{\partial T_{t,in}}{\partial t} = \frac{R_t T_{t,in}}{P_{t,in} V} \left[\gamma_t \left(\dot{m}_{in} T_{in} - \dot{m}_t T_{t,in} + \frac{Q}{C_{p,t}} \right) - T_{t,in} (\dot{m}_{in} - \dot{m}_t) \right] \quad (3.20)$$

$$\frac{\partial P_{t,in}}{\partial t} = \frac{\gamma_t R_t}{V} \left(\dot{m}_{in} T_{in} - \dot{m}_t T_{t,in} + \frac{Q}{C_{p,t}} \right) \quad (3.21)$$

The mass flow \dot{m}_t through the expander is computed according to the expander characteristic as a function of pressure ratio and inlet temperature.

The same approach holds for the outlet plenum of the expander. The temperature drop due to expansion is computed according to the polytropic component efficiency η_t :

$$T_{t,in} - T_{t,out}^* = T_{t,out}^* \left(\left(\frac{P_{t,in}}{P_{t,out}} \right)^{\frac{\eta_t(\gamma_t-1)}{\gamma_t}} - 1 \right) \quad (3.22)$$

This temperature drop determines the power delivered by the expander. The star marked temperature is the inlet temperature for the plenum after the expander. Since we are only interested in this temperature that determines the power balance, it is not necessary to include an outlet plenum to the expander component. It is sufficient to include the polytropic efficiency in the component description. The required expander outlet pressure is assumed to equal the ambient pressure multiplied with an exhaust channel pressure drop correction. Note that when a following component is involved, a plenum after the expander is required.

In the above formulation, the cooling power Q is subtracted from the inlet plenum of the component. In this way the plenum volume provides for some inertia in the cooling system. It is, however, possible to determine the cooled temperature directly by an algebraic equation. An option to introduce cooling and to add some inertia to this cooling model is to include a first order lag according to

$$\frac{dT_{t,in}^*}{dt} = \frac{1}{\tau_q} (T_{cool} - T_{t,in}^*) \quad (3.23)$$

This (extra) differential equation replaces the Q terms in (3.20) and (3.21) and introduces the new state $T_{t,in}^*$. The modelling of the cooling system is treated in appendix B. T_{cool} is the static solution from the algebraic equation

$$T_{cool} = f(\dot{m}_t, T_{t,in}, P_{t,in}) \quad (3.24)$$

3.3.2 Control valves and piping appendages

The mass flow through a control valve is determined by an industrial, empirical relationship between flow through and pressure difference over the valve according to [Econosto, 1992]

$$\dot{m} = \frac{Kv}{7.0 \cdot 10^5} \sqrt{\frac{\rho_n P_{out}}{T_{in}}} (p_{in} - p_{out}) \quad \text{for subcritical flow, i.e., } \left(\frac{P_{out}}{P_{in}} \right) \geq 0.5 \quad (3.25)$$

$$\dot{m} = \frac{Kv}{14.0 \cdot 10^5} p_{in} \sqrt{\frac{\rho_n}{T_{in}}} \quad \text{for supercritical flow, i.e. } \left(\frac{P_{out}}{P_{in}} \right) < 0.5 \quad (3.26)$$

In which ρ_n is the normalised density of fluid (kg/m^3), Kv is the valve coefficient (m^3/hr) and p is pressure (Pa). The valve coefficient Kv is a function of the valve position. The valve position is defined from 0 (fully closed) to 1 (fully opened). The Kv function is called the valve

control characteristic. Industrial valves apply mostly linear or logarithmic control characteristics. Appendix A.8 presents the control characteristics of valves in detail.

A Bernoulli relation describes piping appendages and flow restrictions in pipelines such as bows, changes in area and orifices. Figure 3.10 shows a schematic view of such a component. The Bernoulli equation can be formulated as:

$$\Delta p = p_{in} - p_{out} = \xi \frac{1}{2} \rho v^2 = \xi \frac{1}{2} \frac{\dot{m}^2}{\rho A^2} \quad (3.27)$$

In which the dimensionless pressure drop coefficient ξ depends on the geometry of the flow restriction. Explicitly rewritten to the mass flow, the static component relation is derived as:

$$\dot{m} = \sqrt{\frac{2 p_{in}}{\xi R T_{in}} A^2 (p_{in} - p_{out})} \quad (3.28)$$

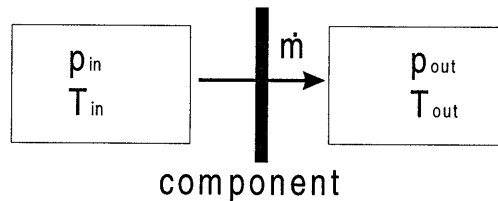


figure 3.10 : Component "Orifice" or "Control valve".

The corresponding differential equations for the plenums at inlet and outlet are the set (3.15) and (3.16). Since we assume an adiabatic expansion over the orifice or restriction, the outlet temperature of the first plenum equals the inlet temperature of the second and no further temperature information is required.

3.3.3 Combustion chamber

The actual geometry of a combustion chamber has been simplified to a hot and a cold volume. The volume within the liner is the hot volume, while the annulus between liner and casing is the cold volume. Both volumes are assumed to be ideally stirred and the mass flow through the combustion chamber has been lumped to a single flow as a function of a single pressure drop. This approach is shown in figure 3.11 and figure 3.12.

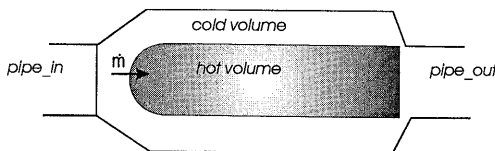


figure 3.11 : Schematic view of combustion chamber geometry.

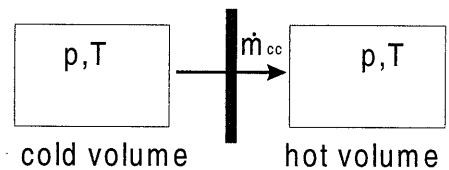


figure 3.12 : Component "Combustion chamber".

In a good approximation, the pressure drop over the combustion chamber is built from a pressure drop over the diffuser due to the area enlargement from A_{pipe} to A_{casing} with a pressure drop factor λ (0.45) and a pressure drop over the liner due to the flow restriction $A_{effective}$. This

effective area in the liner is the sum of the actual hole area in the liner multiplied with a discharge coefficient (0.56) [Lefebvre, 1983].

$$\Delta p = \Delta p_{diffuser} + \Delta p_{liner} = \lambda \frac{1}{2} \rho v^2 \left(1 - \frac{A_{pipe}}{A_{casing}} \right)^2 + \frac{1}{2} \rho v^2 \left(\frac{A_{casing}}{A_{effective}} \right)^2 \quad (3.29)$$

The mass flow relation for the combustion chamber component then becomes:

$$\dot{m}_{cc} = \sqrt{\frac{2p_{in}(p_{in} - p_{out})}{RT_{in}} \frac{A_{casing}^2}{\left(\frac{A_{casing}^2}{A_{effective}^2} + \lambda \left(1 - \frac{A_{pipe}}{A_{casing}} \right)^2 \right)}} \quad (3.30)$$

3.3.4 Volume

Compressor / expander systems often include large volumes as a buffer or storage tank. Figure 3.13 presents a schematic view of such a volume component, including the connecting pipelines. For use in the physical flow model, the total volume of the tank is divided in two or more elements. For each of these elements an energy conservation equation (3.10)-(3.11), is solved to determine the pressure and temperature. The momentum equation (3.3) determines the mass flow from one element to the next. In this sense, the flow *within* the buffer tank is treated the same way as the flow through a pipeline, though with different geometry parameters.

The inlet and the outlet mass flows of the volume, \dot{m}_{in} and \dot{m}_{out} respectively in the figure, are determined by a stationary Bernoulli equation that considers the pressure drop due to area changes and (possible) secondary flows in the volume. The same equations as for flow restrictions (3.27) and (3.28) may be applied, though with an adapted pressure drop factor ξ .

For use in the lumped parameter model, the same Bernoulli equations are used but the pressure and temperature within the volume are solved by the single set (3.15)(3.16), since no instationary momentum balance is taken into account.

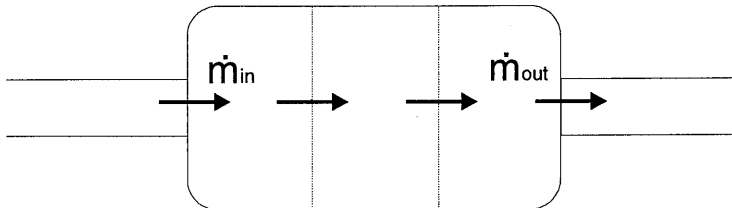


figure 3.13 : Component "Buffer tank".

3.3.5 Pipe junction

In a one dimensional view, a pipe junction indicates either a flow splitting or a joining of flows. When the junction is treated as a separate component, we assume all mass flows in and

out of the junction to be determined by static equations, like in the lumped parameter model. The component junction is schematically introduced in figure 3.14.

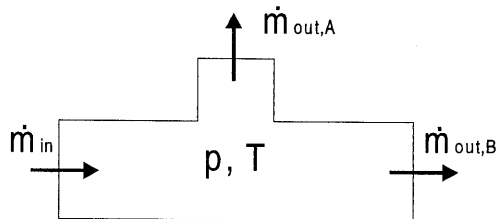


figure 3.14 : Component "Pipe junction" for use in the lumped parameter model.

The standard energy equation (3.15) (3.16) is extended to describe multiple inputs or outputs. According to the homogeneous volume principle, all outputs will have the same temperature as the junction, while each input mass flow can have a different temperature.

It is also possible to include a junction into the pipe modelling of the physical flow model. Instead of algebraic mass flow equations now the instationary momentum equation (3.3) can be used to determine the mass flows. This is accomplished by a proper choice of the fluid velocities at the control volume faces used for the momentum equation. Figure 3.15 shows this principle for the inlet and outlet flow of a pipe junction. The mass flow \dot{m}_{out} is determined by a closed coupled component like a control valve. (When this mass flow is also determined by an instationary momentum equation, strong demands are put on the discretisation in order to include a proper description of wave reflections.)

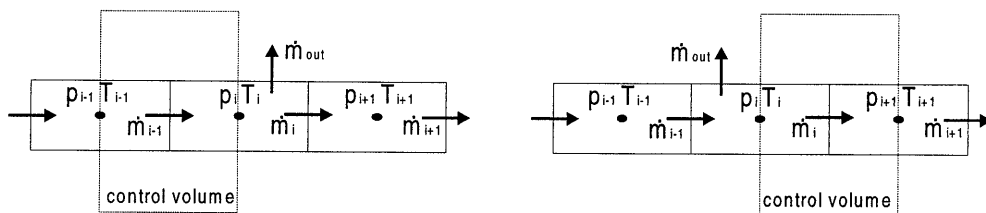


figure 3.15 : Control volume shift for the instationary momentum equations in a pipe junction.

3.4 Laboratory gas turbine installation

A combination of model components treated in the previous section leads to a model of the laboratory gas turbine installation. Doing so requires detailed information on the actual component characteristics, dimensions, and the system configuration. For pipelines and volumes the actual diameters and lengths are used. For components, we apply the vendor supplied characteristics. For the compressor and expander this implies that they are fitted from the originally supplied graphical characteristics (Appendix A). Appropriate values of efficiencies and pressure losses need to be determined.

Two different model structures are derived. Subsequent sections discuss the properties and the intended use of these two model types. The first type is the *physical flow model*, which includes compressible flow through pipelines, and is implemented in FORTRAN. The second

type is the *non-linear lumped parameter model*, in which flow through pipelines is neglected and components are connected by volumes. This model is implemented in Matlab.

3.4.1 Physical flow model

The intended use of the physical flow model is to obtain, within the prescribed boundaries of a one dimensional modular approach and static component characteristics, an as good as possible model of the gas turbine set-up that includes the inertia of fluid flow through pipelines. The physical flow model serves as a reference model.

The implemented model configuration completely describes the laboratory installation. Components are coupled in the order of figure 3.16: compressor, pipeline, blow-off, pipeline, buffer tank, pipeline, throttle valve, combustion chamber, pipeline, steam injection module, pipeline, expander. A power balance couples expander and compressor and closes the loop.

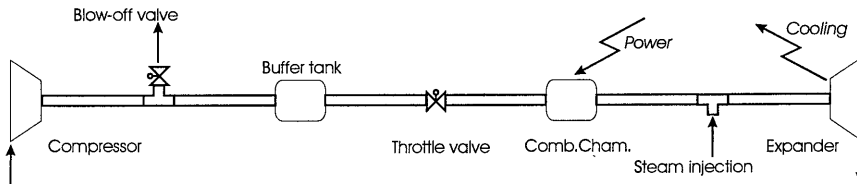


figure 3.16 : Physical flow model configuration.

All the pipelines together are approximately 15 meters long and divided into elements of 1.0 meter. Each pipe element carries three differential equations while each component plenum requires two ode's. Therefore, the model has over 100 ode's combined with about 25 algebraic relations describing mass flows, static temperatures and efficiencies. In order to solve the set of equations, an efficient numerical integration routine according to Bulirsch-Stoer [Press, 1992] has been implemented. It is a multi-step algorithm with Richardson extrapolation and adaptive step size. This routine decreases simulation times compared to the previously used Euler-forward method. Still, real-time simulation is not possible: it takes about 10 seconds (and even more during fast transients) to simulate 1 second of system behaviour.

The physical flow model includes proper modelling of changing thermodynamic properties of air and combustion mixtures. The model uses temperature and composition dependent fits of heat capacity according to [Gasunie, 1987].

3.4.2 Lumped parameter model

The purpose of the non-linear lumped-parameter model is to obtain a simple though accurate model that allows fast simulation. The lumped parameter model is designed for model based control purposes.

Control oriented modelling implies that only actual inputs and controlled or measured outputs are considered and that the model is able to predict the phenomena and time scales which are to be controlled with satisfying accuracy. The number of state variables (i.e., the number of first order differential equations) should be carefully selected. For real-time (control) applications the time required to simulate the model over a future horizon is very important.

Pipelines are omitted in the lumped parameter model. This largely reduces the number of differential equations describing the whole installation. The same component description as in the physical flow model is used, though without any internal volumes. Instead, three connecting volumes are added in which the dynamic behaviour is lumped: the compressor duct, the buffer tank and the combustion chamber volume. The configuration of the lumped parameter model is schematically shown in figure 3.17. The following components are included in the model and can be recognised in the scheme: compressor, compressor duct, blow-off valve, plenum (buffer tank), throttle valve, combustion chamber, cooling system, and expander.

The compressor duct represents the volume just behind the compressor. The plenum volume represents the large size of the buffer tank and connected piping. The last volume represents the combustion chamber. In this combustion chamber an additional power input term gives the added energy of combustion. In the volumes, mass and energy conservation equations are solved. For each volume two ordinary differential equations for pressure and temperature are required. For the compressor duct and the buffer tank these are the set (3.15), (3.16), and for the combustion chamber (3.13), (3.14). The state variables of temperature and pressure are included in the drawing. Two additional differential equations sum up the total number of

first order ode's to eight. First, a power balance couples the required power of the compressor to the delivered power of the expander and determines the rotational speed (N) of the gas turbine axis. Second, the expander cooling system is included by means of equation (3.23), representing a first order lag (with a time constant τ_q) between the actual expander inlet temperature ($T_{t,in}$) and the static cooled temperature. Appendix C.2 contains the complete set of equations of the lumped model.

In sense of a lumped parameter model it is not strictly required to treat the compressor duct as a separate volume. It may, however, be useful to do so since then the compressor outlet pressure is not fixed to the plenum pressure but to the pressure in the much smaller duct volume. This will improve the compressor response time and enables the determination of a physical meaningful mass flow through the blow-off valve.

The value of the heat capacities in the lumped model is fixed at two levels: the low temperature or compressor value of 1010 J/kgK and the high temperature combustion mixture or expander value of 1060 J/kgK. Other variations over temperature or composition are not taken into account.

3.5 Discussion

In this closing section we discuss some aspects of the two types of models derived in this chapter. We start with a discussion on the application area of the models and indicate the expected performance differences between the physical flow and the lumped model. Then we discuss the influence of neglected instationary effects and indicate possible alternatives and

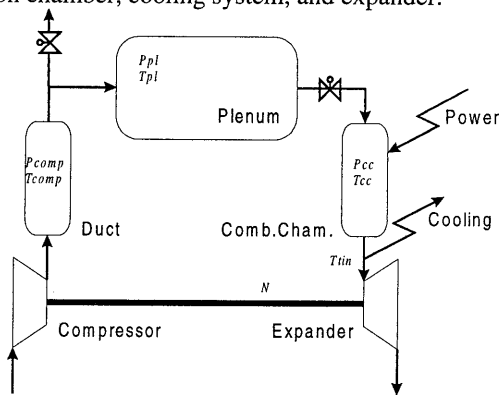


figure 3.17 : Lumped parameter model configuration including the state variables.

model extensions to include them. Finally, some remarks are made with respect to the modelling of dynamic instabilities like surge and stall.

Application of the models Modelling in this thesis is restricted to a single shaft, single stage gas turbine components. Extensions to multi stage compressors or expanders can be made rather straightforward by using the overall component characteristic and the appropriate polytropic efficiency. The simulation can be improved when the more accurate *stage* characteristics are available. In that case the compressor (or expander) is modelled by multiple *internal* components (stages), coupled by volumes which reflect the effective volume between blade rows.

Modelling with static overall component performance maps fails for simulations outside the area presented in the (overall) characteristics. Also for (blade) design of turbomachinery this type of modelling can not be applied. It is also not viable for control system design where local (i.e., within the compressor) aero- and thermodynamic quantities are used. An example is active surge control which uses aero feedback or air injection, variable compressor stator blades, or dynamic volumes [Ffows Williams, 1993], [Gysling, 1995], [Simon, 1993], and [Pinsley, 1991].

Differences between physical flow and lumped model A question that rises is the expected performance difference between the physical flow and the lumped model. The essential difference between the two types of models is the presence of flow equations (including the instationary momentum equation) for fluid flow through pipes in the physical flow model. These equations cause expected differences in the smallest time scale that is included in the model and in the corresponding phenomena that the model describes properly.

A cut-off frequency for the lumped model can be estimated by the reciprocal residence time τ of the largest buffer tank of the model. This residence time is defined by the volume capacity (2.5 m^3) and the characteristic volume flow. As a reference condition, consider a mass flow \dot{m} of 0.5 kg/s of a density ρ of 1.0 kg/m^3 through a pipe with an area A of 0.025 m^2 . The corresponding volume flow F is $\dot{m}/\rho = 0.5 \text{ m}^3/\text{s}$ and the characteristic velocity U is $F/A = 20 \text{ m/s}$. An estimate of the cut-off frequency is therefore

$$f_{0,lumped} = \frac{1}{\tau} = \frac{F}{V} = \frac{[\text{m}^3/\text{s}]}{[\text{m}^3]} = \frac{\dot{m}/\rho}{V} \approx \frac{0.5/1.0}{2.5} = 0.2 \text{ Hz} \quad (3.31)$$

The first time scale that is *not* included in the lumped model corresponds to the convective fluid velocity through the pipe lines and the corresponding propagation time. This frequency is estimated by the characteristic velocity U and the characteristic length L of a pipe (10 m):

$$f_0 \cong \frac{U}{L} \approx \frac{20 \text{ m/s}}{10 \text{ m}} = 2 \text{ Hz} \quad (3.32)$$

This time scale, however, *is* included in the physical flow model. An estimate of the cut-off frequency of the physical flow model is determined by the same characteristic velocity U and the characteristic length L of one pipe element (1.0 m), or equivalently, by the residence time of a dynamic couple plenum ($V=0.025 \text{ m}^3$):

$$\begin{aligned}
 f_{0, \text{physical flow}} &\equiv \frac{U}{L} \approx \frac{20 \text{ m/s}}{1.0 \text{ m}} \\
 &\equiv \frac{F}{V} \approx \frac{0.5 \text{ m}^3/\text{s}}{0.025 \text{ m}^3} = 20 \text{ Hz}
 \end{aligned} \tag{3.33}$$

The first time scale that is *not* included in the physical flow model deals with the wave propagation (i.e., the velocity of sound a) over a single pipe element or coupling volume. The corresponding frequency is roughly estimated by

$$f_0 \equiv \frac{a}{L} \approx \frac{300 \text{ m/s}}{1.0 \text{ m}} = 300 \text{ Hz} \tag{3.34}$$

Although the estimates of cut-off frequencies for both models are only rough estimates, a preliminary conclusion may be that both models should generate the same response to phenomena up to 0.1 Hz. This corresponds to the time scale of transient changes of the operating point we aimed at for the laboratory gas turbine installation. When phenomena at higher frequencies are investigated, only the physical flow model is appropriate. Note that in any case a thorough model validation will be required. Such a model validation is the subject of Chapter 4.

The influences of the static component characteristics are not considered in the previous estimates. The influence of neglected instationary effects is discussed in the following subsection.

Instationary effects The use of steady state component characteristics leads to the question to what extent instationary effects are neglected in the static momentum balances in compressor, expander and pressure drop relations of valves and pipe-connections. An estimate of the influence of the instationary terms in the momentum equation can be made. Starting from the general equation

$$\frac{\partial v}{\partial t} = -v \frac{\partial v}{\partial x} - \frac{1}{\rho} \frac{\partial p}{\partial x} \tag{3.35}$$

In a dimensionless form, with $\hat{t} = tf_0$, $\hat{v} = \frac{v}{U}$, $\hat{x} = \frac{x}{L}$, $\hat{p} = \frac{p}{\rho U^2}$ and $Sr = \frac{f_0 L}{U}$, this equals

$$Sr \frac{\partial \hat{v}}{\partial \hat{t}} = -\hat{v} \frac{\partial \hat{v}}{\partial \hat{x}} - \frac{\partial \hat{p}}{\partial \hat{x}} \tag{3.36}$$

The first term in the right hand side represents the unsteady convection term. The dimensionless Strouhal number (Sr) indicates the relative importance of this term to the left hand side time derivative term. When the Strouhal number is $\ll 1$, the phenomena in “place” are relatively slow with regard to “time” and the process may be assumed quasi-stationary. An estimate of the Strouhal number for the compressor indicates:

$$Sr_{\text{comp}} = \left(\frac{f_0 L}{U} \right)_{\text{comp}} \approx \frac{20 [\text{Hz}] \cdot 0.05 [\text{m}]}{70 [\text{m/s}]} = 0.01 \tag{3.37}$$

With f_0 the cut-of frequency (3.33) estimated for the physical flow model, L the characteristic length over the rotor passage and U the corresponding velocity. The Strouhal number applied to the lumped parameter cut-of frequency (3.31) is a factor 100 lower. On this result

one may, indeed, decide to neglect the instationary effects and apply the static characteristics, especially for the lumped model.

The second right hand side term, the dimensionless pressure term, is assumed of the same order. Indeed, for turbomachinery like compressor and expander, but also for flow through control valves, the quasi steady assumption is justified because of the small characteristic length: a relative large pressure change occurs over a relatively short distance (the rotor).

For control and transient-simulation purposes it is sometimes useful *not* to neglect the instationary effects completely, but only to neglect the convection term, i.e. the first right hand side term of the momentum equation (3.35). In that case, the equation can be transformed into the first order ordinary differential equation:

$$\frac{dm}{dt} = -\frac{A}{L} (\Delta p - \Delta p_{ss}) \quad (3.38)$$

in which Δp is the actual and Δp_{ss} the steady state pressure drop. This equation is derived and discussed in Appendix C.4. It appears, however, that the numerical condition of the problem decreases dramatically because the resulting set of equations turns out to be stiff. For this reason, equation (3.38) is not used in the simulation models of this thesis.

To introduce instationary modelling in turbomachinery, in literature some other approaches are encountered, generally leading to more complex modelling that requires detailed geometrical data. A first approach is to model the instationary momentum equation in which turbomachinery source terms are incorporated like effective axial force, shaft work and heat release rate all per unit length [Garrard, 1996]. The source terms are provided by the steady state compressor characteristic. In a second alternative approach it is possible to model compression and expansion processes without steady state (stage) characteristics using a row-by-row calculation method [Schobeiri, 1994]. Also the instationary modelling of flow through valves is a challenging problem. Besides the dynamic interaction of the changing valve position to the fluid flow, also the dynamics of the valve itself should be introduced in the model. In [Botros, 1996] a more elaborate analysis of this problem is discussed.

Modelling of dynamic instabilities Dynamic instabilities like surge and stall may occur in the compressor. To a certain extent, it is possible to include these phenomena in our simulation models when an appropriate extension to the compressor characteristic is provided. Surge can be described by a steady state characteristic which is extended with a part left from the surge line with a positive slope (which is *unstable*) and a part with a negative slope for negative mass flows (or reversed flow). Figure 3.18 shows this extension of the compressor map for a single constant speed curve and indicates the resulting limit cycle of surge.

The essentially two-dimensional phenomena of rotating stall cannot be described by the one-dimensional steady state characteristic. In the post stall region the characteristic is unstable (positive slope) and globally steady characteristics are no longer applicable. A "stalled" characteristic has to be added to the system as shown in figure 3.19. Also a (periodic) perturbation and a first order lag have to be prescribed to the one-dimensional flow through the compressor to activate the "stalled" characteristic.

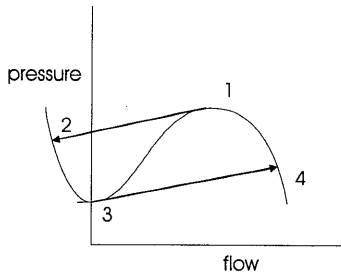


figure 3.18 : Compressor map with deep surge cycle.

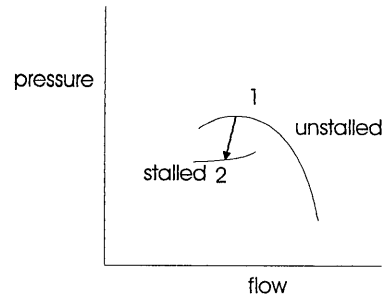


figure 3.19 : Compressor map with stalled flow characteristic.

The applicability of the indicated model extensions strongly depends on the (often unknown) characteristics of surge and stall. Detailed information on the modelling and simulation of dynamic instabilities can be found in [Greitzer, 1976,1986], [Moore, 1986], and [Fink, 1992].

4 Model Validation

The correct values of the parameters in the model equations of the previous chapter can be determined by experiments. The aim of this chapter is to obtain a (close) correspondence between experimental data and results from model simulation. In this chapter a short review of model parameters is given, after which the available experimental data, obtained on the laboratory gas turbine, are presented. These data are compared with simulation results, yielding a systematic determination of model parameters. In the remainder of the chapter, both stationary and transient performance of the different model types are presented and analysed.

Two types of parameters can be distinguished. The first type influences the stationary operating points of the installation: pressure drop factors and efficiencies. *Pressure drop factors* determine the mass flow through components. They include the component characteristics and prescribed pressure drop relations. *Efficiencies* determine power production or consumption of the components. Efficiency parameters include the combustion efficiency and the (polytropic) efficiencies of compressor and expander. Also the parameters of the expander cooling system are considered as efficiencies since the cooling influences the power balance directly.

The second type of parameters influences the transient and dynamic operation of the installation. These parameters are generally referred to as *inertia* parameters and include the effective pipe lengths and plenum volumes, the inertia of the gas turbine shaft, and the maximum move rates of control valves. Inertia parameters can be determined from transient measurement data.

Parameters concerned with components that are provided with vendor-supplied characteristics are equal for the physical flow and the lumped parameter model since both model types include the same static component descriptions. For other components (like piping and volumes) pressure drop relations are prescribed in the model equations. Parameters include pressure losses (per unit length) and Bernoulli pressure drop factors. These parameters differ between the lumped and the physical flow model. Emphasis is on the non-linear lumped model.

4.1 Available data from experiments

Experimental data obtained on the laboratory installation consist of the measurements of stationary operating points and of transients between operating points due to valve variations. We will start the analysis of experimental data with an overview of available experimental data that determine measured stationary operating points. For a vivid presentation, a set of operating points is selected for which only the fuel valve position is adjusted while the blow-off valve is fully closed and the throttle valve is fully opened. The resulting stationary operating points are on a load line in the compressor map.

Eight operating points on this load line are presented in figure 4.1. From a selected starting point we chose to increase the amount of supplied fuel for four operation points and then to decrease the fuel supply again for the last three points. All data points are plotted versus the position of the fuel supply valve. Presented data are the rotational speed of the gas turbine shaft (N , rev/s), the pressure (p_2 , Pa) and the temperature (T_2 , K) measured at the compressor outlet, and the pressure (p_3) and temperature (T_3) measured at the expander inlet. The meas-

ured temperature in the exhaust channel is indicated as T_4 . The ambient reference for these measurements is $p_{amb} = 1.02 \text{ bar}$ and $T_{amb} = 295 \text{ K}$.

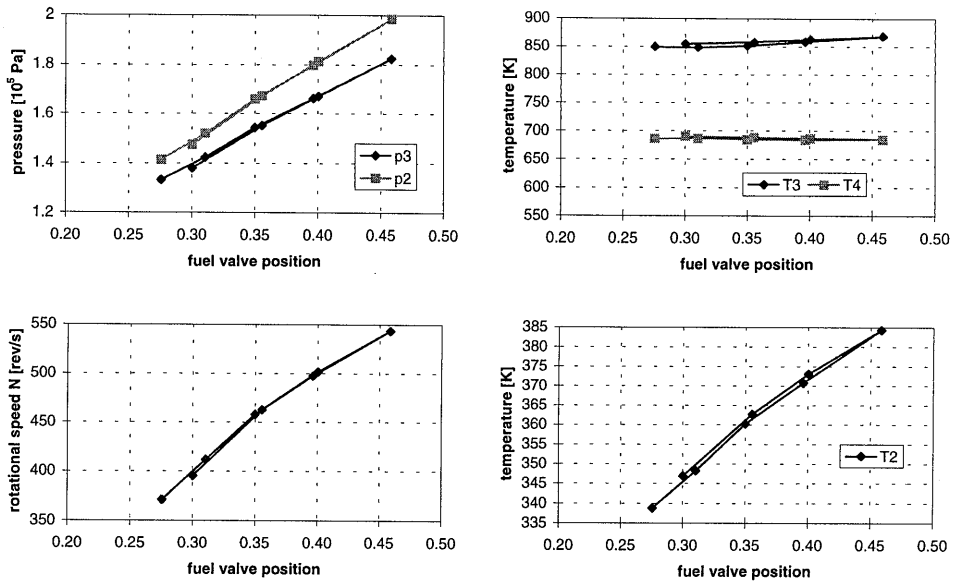


figure 4.1 : Eight stationary operating points on the basic load line.

The measured mass flow of fuel is presented in figure 4.2. In the measured fuel flow a small difference between the rising and the falling curve can be recognised. This is probably due to the inaccuracy in the determination of this mass flow from frequency pulses at low flow rates. The computation of the fuel flow is treated in Appendix A.10. Measurements that are available at the orifice (the pressure difference over the orifice, the pressure before, and the temperature behind the orifice) are not shown separately. Instead, the corresponding mass flow (kg/s) through the orifice is computed and presented in figure 4.3. The determination of the orifice mass flow is discussed in Appendix A.9.

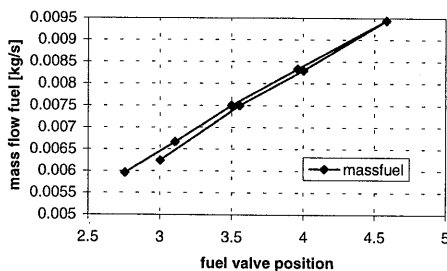


figure 4.2 : Measured mass flow of fuel.

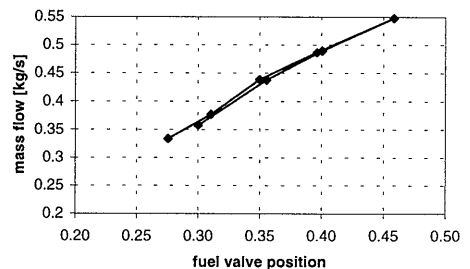


figure 4.3 : Measured mass flow through the orifice.

Not only the position of the fuel valve, but the position of the throttle valve and of the blow-off valve determine the operating point. For validation purposes in this chapter, the data set presented in figure 4.4 will be used. Both fuel valve and throttle valve positions have been varied to the indicated positions, resulting in distinct “load lines” for different positions of the throttle valve. The shift of the load line is caused by the larger pressure drop between compressor and expander that the closing throttle valve brings about. Since the input power is determined by the (constant) fuel valve position, the increasing load causes a decrease in mass flow and pressure ratio. For the same reason, the corresponding expander inlet temperature T_3 on these new load lines is significantly higher. This is indicated in figure 4.5. Blow-off valve variations are not included in this selection: the blow-off valve is closed.

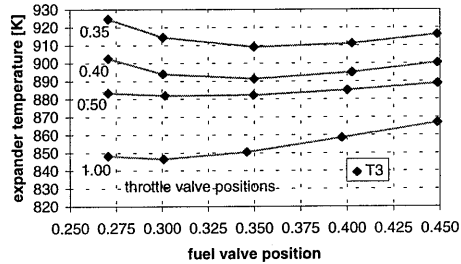
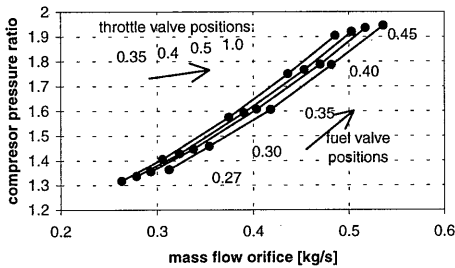


figure 4.4 : Distinct load lines in the compressor characteristic for various operating points. figure 4.5 : Increasing expander inlet temperatures over the distinct load lines.

4.2 Parameter validation on the laboratory installation

For stationary operating points, a mass and a power balance hold for all components of the installation. The mass flows through compressor and expander are equal and the power delivered by the expander equals the power required by the compressor. By a comparison between experimental and simulation data, the unknown parameters are determined from the data set presented in figure 4.4. Subsequently, mass flow correction factors, polytropic and combustion efficiencies and pressure drop factors are discussed in separate subsections.

4.2.1 Mass flows

The mass flow through the orifice is measured, the mass flows through compressor and expander can only be reconstructed by the component characteristics. In figure 4.6 and figure 4.7 the measured stationary operating points are reconstructed in the compressor characteristic and the expander characteristic, respectively. The mass flow through the compressor is reconstructed by the measured pressure ratio and the measured rotational speed (Appendix A.3). The expander mass flow is reconstructed by the measured pressure ratio and measured inlet temperature. In both figures, the mass flows are compared to the measured mass flow at the orifice. In figure 4.7, the dotted line indicates the expander characteristic for the mean inlet temperature.

Clearly, both reconstructed mass flows do not match. In a simulation this leads to unacceptable deviations of the equilibrium points. So although completely described, it appears that the

original (vendor supplied) characteristics do not reflect the real behaviour encountered in the installation.

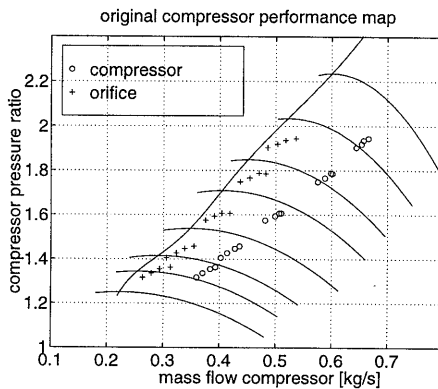


figure 4.6 : Measured stationary operating points reconstructed in the compressor characteristic.

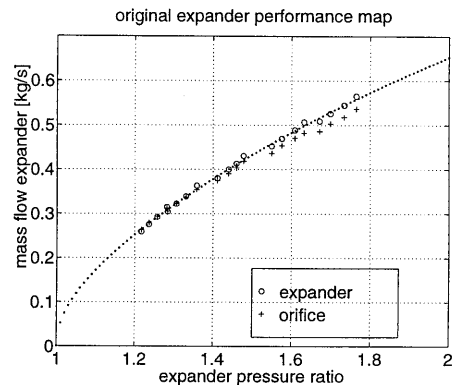


figure 4.7 : Measured stationary operating points reconstructed in the expander characteristic.

For corresponding points, the compressor mass flow is larger than both the orifice and the expander mass flow. The expander mass flow shows a close correspondence to the orifice flow, except for higher pressure ratios. In the expander mass flow also different load lines for different throttle valve positions are recognised, just like in the orifice mass flow of figure 4.4. This information has almost perished in the compressor map: all load lines seem to be located in a very narrow area.

We consider the measured mass flow through the orifice as a good reference for the mass flows in the gas turbine installation. Although an appropriate mass flow calibration is not available, the accuracy of the orifice mass flow is acceptable (5-10% error, see Appendix A.9). This means that the results of figure 4.6 can not be explained by wrong measurements at the orifice. Moreover, the location of the surge line in the compressor map is approximately confirmed in (surge) experiments at measured orifice mass flows. The small deviations with the expander mass flow at higher pressure ratios (figure 4.7), may be explained by the independence of the original expander map with rotational speed.

Because for all stationary operating points the mass flows through compressor and expander must be equal, we decided to adapt both the compressor and the expander map, such that their mass flows correspond to the orifice mass flow. The corrections are derived in Appendix A.5, using the experimental data set of figure 4.4. The resulting compressor characteristic is plotted (and compared with the original one) in figure 4.8. The correction keeps the original surge line, but adapts the location of the top and the steepness of the parabolic constant rotational speed curves. Note that the new characteristic is only valid in the very narrow range (of the used data-set) near the surge line.

Figure 4.9 presents the corrected expander characteristic. Since the correction is a function of both rotational speed and expander inlet temperature, the performance map is now also a function of both. For convenience, only one temperature level (800 K) is plotted in this figure. In this way the (new) influence of the rotational speed is clearly presented.

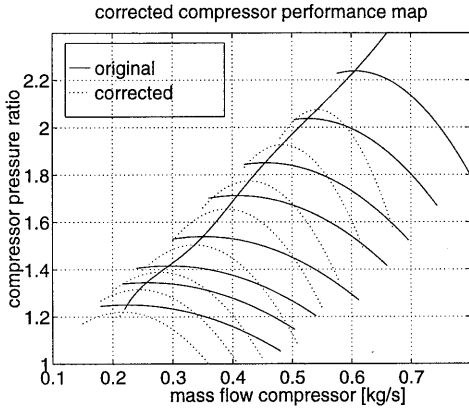


figure 4.8 : Corrected compressor performance map compared with the original one.

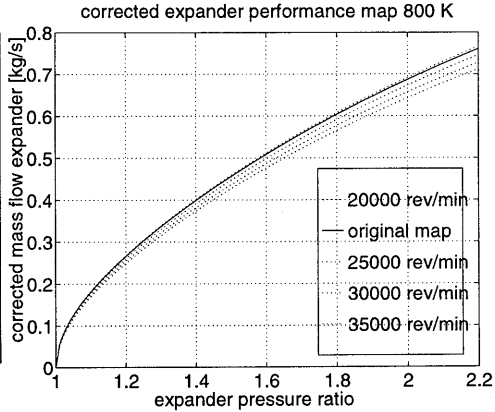


figure 4.9 : Corrected expander performance map as a function of rotational speed compared with original one.

4.2.2 Compressor and expander polytropic efficiencies

We assume that the compressor efficiency can be reconstructed from the measured compressor outlet temperature according to

$$\eta_{c_measured} = \frac{\gamma - 1}{\gamma} \ln\left(\frac{p_2}{p_1}\right) / \ln\left(\frac{T_2}{T_1}\right). \quad (4.1)$$

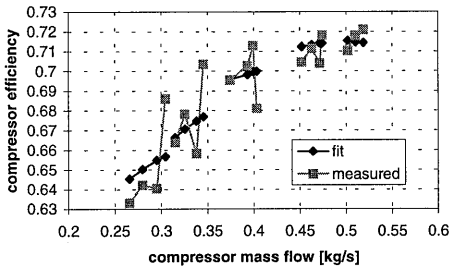


figure 4.10 : Measured compressor efficiency and resulting fit.

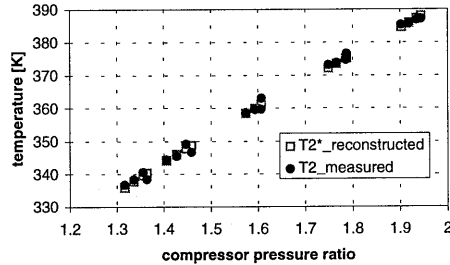


figure 4.11 : Measured and reconstructed compressor outlet temperature.

From the stationary data set a mathematical fit of the compressor efficiency has been derived in Appendix A.6. Figure 4.10 presents the resulting fit, compared to the measured efficiency of each individual data point. For the compressor this indicates a relatively large scattering of measurements and fit. Figure 4.11 plots the very small difference between the measured temperature T_2 and the fictive compressor outlet temperature T_2^* that is reconstructed by the efficiency fit according to

$$T_2^* = T_1 \left(\frac{p_2}{p_1}\right)^{\left(\frac{\gamma - 1}{\gamma \eta_{c_fit}}\right)} \quad (4.2)$$

that causes this scattering. This shows the sensitivity of the efficiency: it can hardly be reconstructed from a single temperature measurement.

The compressor efficiency being fixed, leaves the expander efficiency and the cooling system to match the power balance. For the expander it turns out to be impossible to reconstruct the efficiency from the measured temperatures T_3 and T_4 since infeasible values above 1.0 arise. This is shown in figure 4.12. Instead, we determine the expander efficiency from an optimisation of the *specific* power balance between compressor and expander:

$$C_{p,c}(T_2 - T_1) = C_{p,t}(T_3^* - T_4^*) \quad (4.3)$$

Wherein the temperatures marked by a * are defined by the expander cooling system and by the polytropic efficiency of the expander respectively according to

$$T_3^* = f(\dot{m}_t, T_3, p_3, \text{heatfact}) \quad \text{and} \quad \frac{1}{T_4^*} = \frac{1}{T_3^*} \left(\frac{p_3}{p_4} \right)^{\left(\frac{\eta_{t_fit}(\gamma_t - 1)}{\gamma_t} \right)} \quad (4.4)$$

The reconstructed temperature T_3^* represents the cooled expander inlet temperature. The parameter *heatfact* is an additional correction factor to the heat exchanging surface in the cooling model. Such a correction factor to the expander cooling model is well acceptable since the geometry of the cooler is only roughly estimated (Appendix B). Also the reconstructed temperature T_4^* , that follows from the polytropic expander efficiency fit (that is to be determined) does not compare to the measured expander outlet temperature T_4 because also the outlet flow is affected by the cooling system. Moreover, the star marked temperatures can not be measured at all, since they are only fictive temperatures just before or just behind the rotor, determining the power over the rotor and the efficiency of the component. At these positions it is not possible to measure temperature because of the high fluid velocities and inhomogeneous temperature distribution over the area of the rotor. The star-marked temperatures are a weighted average temperature, determining the power balance of the gas turbine.

By optimising the specific power balance (4.3), we determine a constant value for the factor *heatfact*, and a mathematical fit for the expander efficiency η_{t_fit} . Results are captured in figure 4.12. Apart from the significant difference in y-axis scaling, the correspondence between measured efficiency and the fit is striking, indicating the significant change in efficiency over the operating area. This is remarkable since the original efficiency that is specified by the

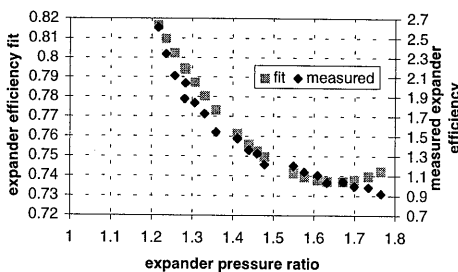


figure 4.12 : Measured expander efficiency compared to optimal fit.

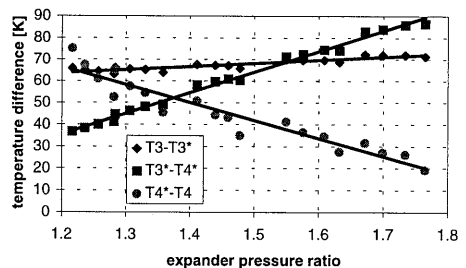


figure 4.13 : Resulting temperature profiles over the expander.

characteristic is rather flat (Appendix A.6). These original values, however, can not be matched to agree with the power balance. The resulting temperature profiles over the expander are shown in figure 4.13 by temperature differences.

From the temperature differences $T_3 - T_3^*$ follow that the cooling has a significant influence. It is approximately constant over the whole operation area of the gas turbine since the difference $T_3 - T_3^*$ increases only slightly with the pressure ratio. The differences $T_3^* - T_4^*$ reflect the power delivered by the expander and increase with the pressure ratio. This difference is fixed by the compressor operating point according to (4.3). The differences $T_4^* - T_4$, finally, show the most striking result. This difference decreases significantly with pressure ratio, indicating that the reconstructed expander outlet temperature T_4^* , which (together with the cooled inlet temperature and the efficiency) matches the power balance, does not compare to the measured outlet temperature. This reflects the prevailing influence of the expander efficiency.

It is worthwhile trying to understand the $T_4^* - T_4$ behaviour. Indeed a cooling is present in the exhaust, but it can hardly be responsible for the strong decrease of the difference over the operating area. A more likely, though complementary, explanation are the constant values of the heat capacities that are used in the determination of $\eta_{t,fit}$. In the underlying lumped model, the C_p values are fixed at two levels: the low temperature or compressor value of 1010 J/kgK and the high temperature or expander value of 1060 J/kgK. When temperature and composition changes are included in the C_p value, the compressor value does hardly change. The expander value, however, varies considerably with in margin of 2.5% from 1050 to 1100 J/kgK. Since variations in the heat capacity directly influence the power balance, it is likely that these effects have been lumped into the expander efficiency.

Also shaft friction losses are not taken into account in the power balance (4.3). It is possible that increasing losses at higher rotational speeds also have been lumped into the expander efficiency. These two effects may explain the deviation between the fit and the original efficiency curve. Of course it is recommended to include both temperature dependent heat capacities and friction losses in a new evaluation of the expander efficiency. Because of the relative definitions, however, the presented approach does not affect the results of the parameter validation. Note, in this respect, that the temperature T_4 is not used in the model and that all efficiencies are determined relative to the compressor temperature rise.

4.2.3 Combustion efficiency

When the added supply of fuel is known, the added power to the gas turbine is known as the mass flow fuel multiplied with the assumed value of the heat of combustion. Due to incomplete burning and leakage this power may not result in the corresponding temperature rise. We define a physically based efficiency of combustion as

$$\eta_{comb} = \frac{\text{power used}}{\text{power input}} = \frac{\dot{m}_{air}(C_{p,t}T_3 - C_{p,c}T_2)}{\dot{m}_{fuel}H_o} \quad (4.5)$$

in which H_o is the lower value of the combustion energy (38.5 MJ/kg for Dutch natural gas) and \dot{m}_{fuel} is the mathematical fit of the mass flow fuel (Appendix A.10). The *power used* term or actually measured power supply is estimated by the mass flow of air multiplied with the actual temperature rise weighted by fixed values of the heat capacity.

In figure 4.14, the measured combustion efficiency according to (4.5) is plotted over the operating range of the expander. Because of the constant values of the heat capacities and the energy of combustion that are presumed in the model, the efficiency is not equal to 100%. More interesting is the variation in the combustion efficiency, within a margin of approximately 6%, over the operating area. Because of the combustion process and the fixed geometry of the combustion chamber, it is plausible that the combustion efficiency is related to the fuel-air ratio in the combustion chamber. To show this relation, the same figure also indicates the fuel-air ratio, defined as fuel mass flow divided by the mass flow of air. Clearly a negative correlation exists. In figure 4.15 the resulting linear fit of combustion efficiency as a function of fuel-air ratio is shown. Deviations are small (typically less than 0.5%).

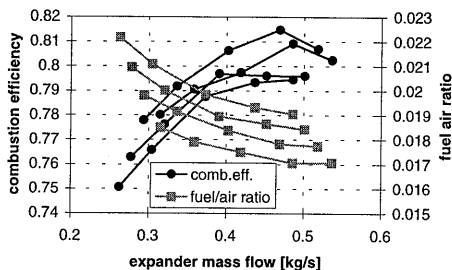


figure 4.14 : Measured combustion efficiency and fuel-air ratio.

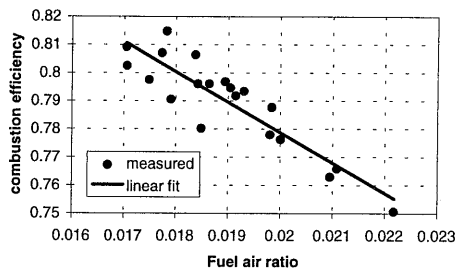


figure 4.15 : Measured combustion efficiency and fit as a function of the fuel-air ratio.

The negative correlation between combustion efficiency and fuel-air ratio may be unexpected because the fuel-air ratio is extremely fuel weak (the stoichiometric ratio is 0.076). It is, however, important to realise that when more fuel is injected, the operation point of the gas turbine shifts towards higher (expander) mass flows. The overall fuel-air ratio *drops* and the corresponding combustion efficiency *rises*.

The fuel-air ratio is defined over the whole combustion chamber. The actual combustion process, however, takes place in the primary zone of the combustion chamber, where 100% fuel is injected into only a fraction of the total air. A possible explanation of the decreasing efficiency is that at lower mass flows of air the combustion mixture within the primary zone can not completely burn with high efficiency. This may be because the mixture is too fuel strong or the axial velocities in the primary zone are too high and the residence time is insufficient to complete combustion.

The fit has been determined from stationary operating points. Since the combustion efficiency is coupled to the fuel-air ratio, especially a *change* in operating point may influence the efficiency. When, for instance, the mass flow of fuel is suddenly raised, the fuel/air ratio in the primary zone of the combustion chamber is immediately increased, only to lower again to its stationary level when the mass flow through the compressor has risen and is transmitted to the combustion chamber. The combustion chamber efficiency therefore plays a major role during transients. This effect is investigated from a transient response to a sinusoid input on the fuel valve. In figure 4.16 the realised input signal is plotted and compared to the original applied sine function with a period of 30 seconds. Figure 4.17 plots the measured combustion efficiency and the corresponding fuel-air ratio as a function of time. During transients the mass

flow through compressor, expander and orifice may temporarily differ from each other. Since the combustion chamber is near to the expander the mass flow through the expander is likely to offer the best phase information. Therefore the expander mass flow is used in the definition of efficiency and fuel-air ratio. It appears that both quantities are approximately in counter-phase. The 'dynamic' combustion efficiency shows a significantly larger margin of approximately 20%, compared to the stationary data (6%).

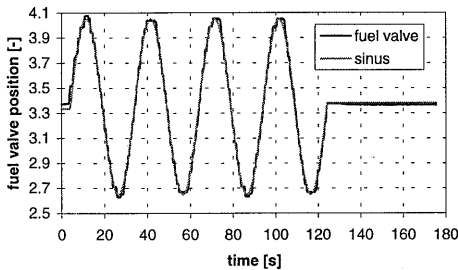


figure 4.16 : Actual realised sine input and prescribed sine function.

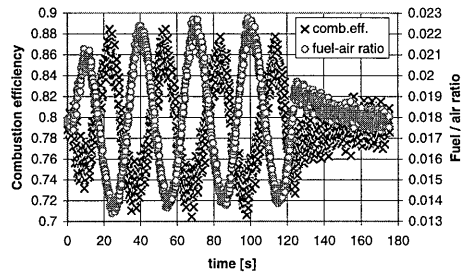


figure 4.17 : Measured combustion efficiency and fuel-air ratio.

In figure 4.18 and figure 4.19 the fit obtained from the stationary data points is compared to the transient measurements. The fit performs well, although it is not able to follow the significant amplitude changes in measured combustion efficiency during the transient. It appears, however, not possible to determine a better fit from this transient data, unless dynamics like the derivative of the fuel-air ratio are taken into account. The period of the prescribed sine function to the fuel valve was 30 seconds. This corresponds to a frequency of approximately 0.03 Hz. Faster transients are not validated because the fuel valve cannot move faster.

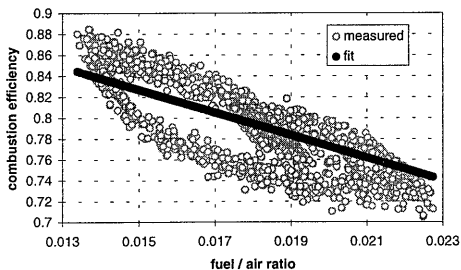


figure 4.18 : Measured combustion efficiency to fuel-air ratio and fit.

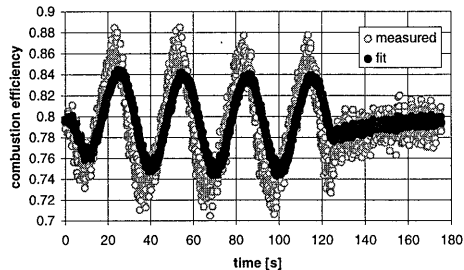


figure 4.19 : Measured combustion efficiency to time and fit.

4.2.4 Pressure drop over the installation

The final parameter that needs to be determined from the analysis of stationary experimental data is the pressure drop between the compressor outlet and the expander inlet. The pressure drop in the lumped parameter model is concentrated in two factors:

- The throttle valve pressure drop which is modelled by a K_v relation as a function of the opening degree (Appendix A.8).

- The overall pressure drop which is modelled by a Bernoulli relation. The overall pressure drop is the lumped equivalence of the pressure drop over the pipelines and the buffer tank.

When we assume a linear throttle valve characteristic, the only two parameters are the constant throttle valve factor Kv_{th} and an overall system pressure drop factor ksi . Since the pressure drop in the model equations is analytically available, a direct correlation between the measured pressure difference and both model parameters can be obtained. The (constant) value of the throttle valve parameter Kv_{th} has been optimised to 430 m^3/hr (vendor specification was 400) along with the determination of the optimal value of the factor ksi for each individual operating point. These optimal values have been correlated to a quadratic fit in the mass flow through the expander, see figure 4.20, in order to compensate for an operating point dependent pressure drop. The large scatter in the optimal ksi values of figure 4.20 is caused by relatively large measurement errors in the pressure drop, especially at low values of this pressure drop. Figure 4.21 compares the results of the overall pressure drop fit to measurements.

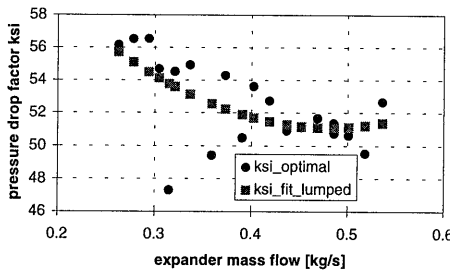


figure 4.20 : Optimal overall pressure drop factor ksi and resulting fit.

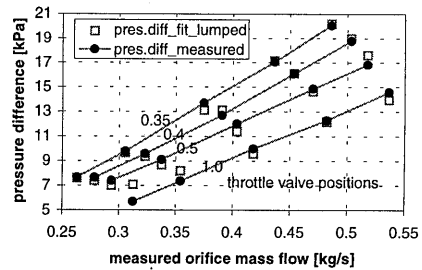


figure 4.21 : Measured and fitted pressure drop (lumped model parameter fits).

In the physical flow model, the pressure drop is not concentrated into one parameter but divided over the pipe length. When the pressure drop over the combustion chamber is fixed by design values, we deal with the (constant) value of the pressure drop parameter over a single pipe element and the (constant) pressure drop factor over the outlet of the buffer tank that includes the orifice pressure drop. Acceptable values of these parameters follow from straightforward simulations. The value of the pressure drop factor κ over a single pipe element is chosen 0.018, while the pressure drop factor over the inlet and outlet of the buffer tank is chosen 2.8. Both values are physically acceptable values for fluid flow through pipes with standard surface roughness and pressure drop values for area changes and orifice restrictions [Streeter, 1985]. Note that the lumped pressure drop factor is considerably higher.

In figure 4.22 the resulting pressure drop is shown over the operation area. Note that this is an overall model simulation that includes the mass flow corrections and the efficiency fits. This figure, therefore, presents not the same as figure 4.21 regarding the lumped parameter model which only compared a fit of the pressure drop to measurements.

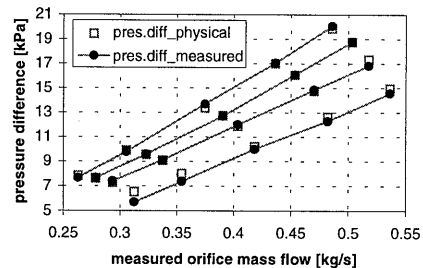


figure 4.22 : Measured and simulated pressure drop (physical flow model).

The physical flow model may deviate from the lumped model and the measurement as the parameters of the physical flow model are not exhaustively validated for the laboratory installation. The correlations for efficiencies that were derived for the lumped parameter model are directly applied to the physical flow model. There is, however, an important difference between both model types. In the physical flow model the pressure drop is divided over the whole installation which means that *locally* other pressures may be present in the physical flow model. When parameter values depend on those pressures, mismatches are likely to occur.

When a proper parameter validation is performed especially for the physical flow model, also the temperature and composition variations of the heat capacity can be included. At this stage, such a validation has not been performed yet.

4.3 Model performance: stationary operating points

When all the fits and corrections that have been derived in the previous section are combined in the models, stationary operating points can be obtained from overall model simulations. To evaluate the model performance, these operating points are compared to the corresponding experimental data points. Figure 4.23 presents the stationary model performance of the lumped parameter model. In four subsequent plots, compressor pressure, rotational speed, expander temperature and pressure losses between compressor and expander are plotted and compared to measured data.

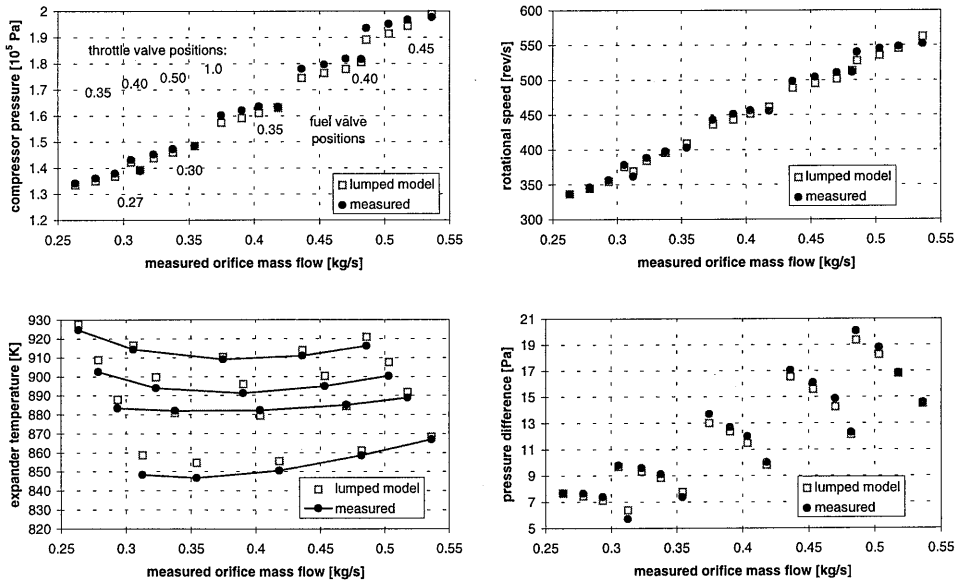


figure 4.23 : Lumped parameter model performance.

Only small deviations between model simulations and measurements are present and the overall performance is well predicted. In figure 4.24 and figure 4.25 the same points are presented in the compressor and expander map to show the cumulated effects of the deviations in all the quantities (pressure, rotational speed, temperatures) in the reconstruction of the mass flows

through compressor and expander. The model performance is good, although the deviations, especially in the compressor map, are significant.

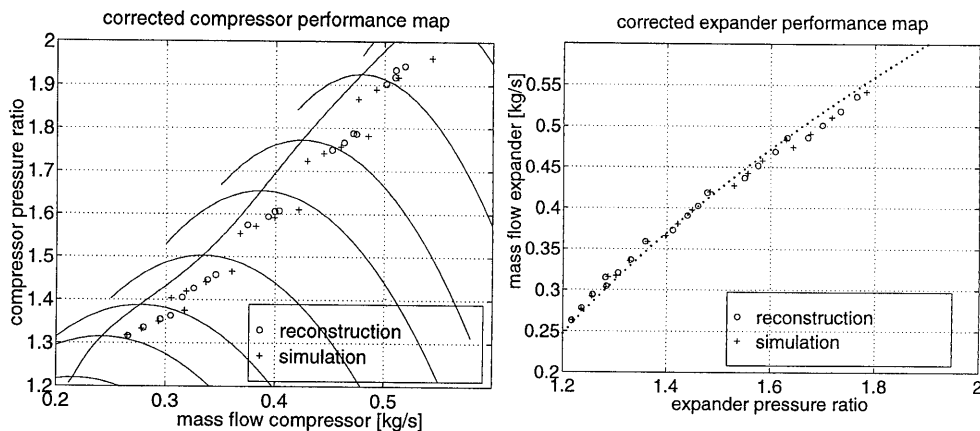


figure 4.24 : Reconstructed (measured) and simulated operating points (lumped model).

figure 4.25 : Reconstructed (measured) and simulated operating points (lumped model).

In figure 4.22 the resulting pressure difference between compressor and expander was shown for the physical flow model. In figure 4.26, the relations are shown for the rotational speed and the expander temperature. Like the lumped model, the response of the physical flow model compares very well to the measured data points. Remind that small deviations between the two types of models are unavoidable since the efficiency correlations are derived for the lumped model.

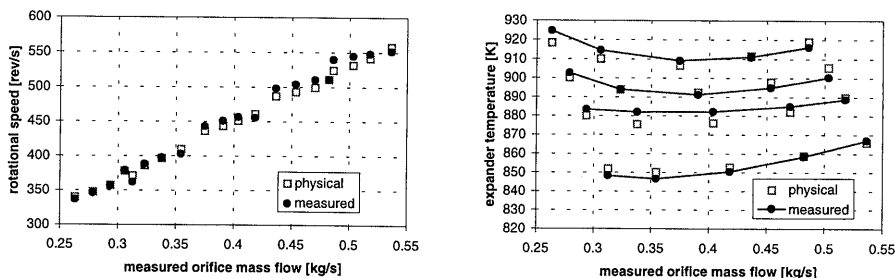


figure 4.26 : Physical flow model performance.

4.4 Inertia parameters

For both model types, the inertia parameters are selected from a comparison between simulations and transient measurement data. Simulation results are presented in the following section.

Lumped model inertia parameters involve the inertia of the turbocharger shaft I and the volume of the three coupling volumes. Shaft inertia I is estimated from the geometry of the turbocharger axis at 0.01 kg m^2 . Appropriate values of the volumes are determined by physical relevant start values, slightly adjusted by simulations.

Physical flow model inertia parameters involve shaft inertia, piping lengths, piping diameters, volume of buffer tank and the volumes of close-coupled component plenums. Determination of these inertia parameters is not unambiguous. Selection has been derived by simulations. A complete validation of physical flow model parameters has not yet been performed.

4.5 Model performance: transient response

To give an impression of the transient properties of the models, a response to a sinusoidal input on the fuel valve (figure 4.16) for both the lumped and the physical flow model are compared to experimental data. The throttle valve is fully open in this experiment.

Figure 4.27 shows the responses of the compressor pressure, the compressor mass flow, the rotational speed and the expander temperature for the lumped model, the physical flow model and the measurements.

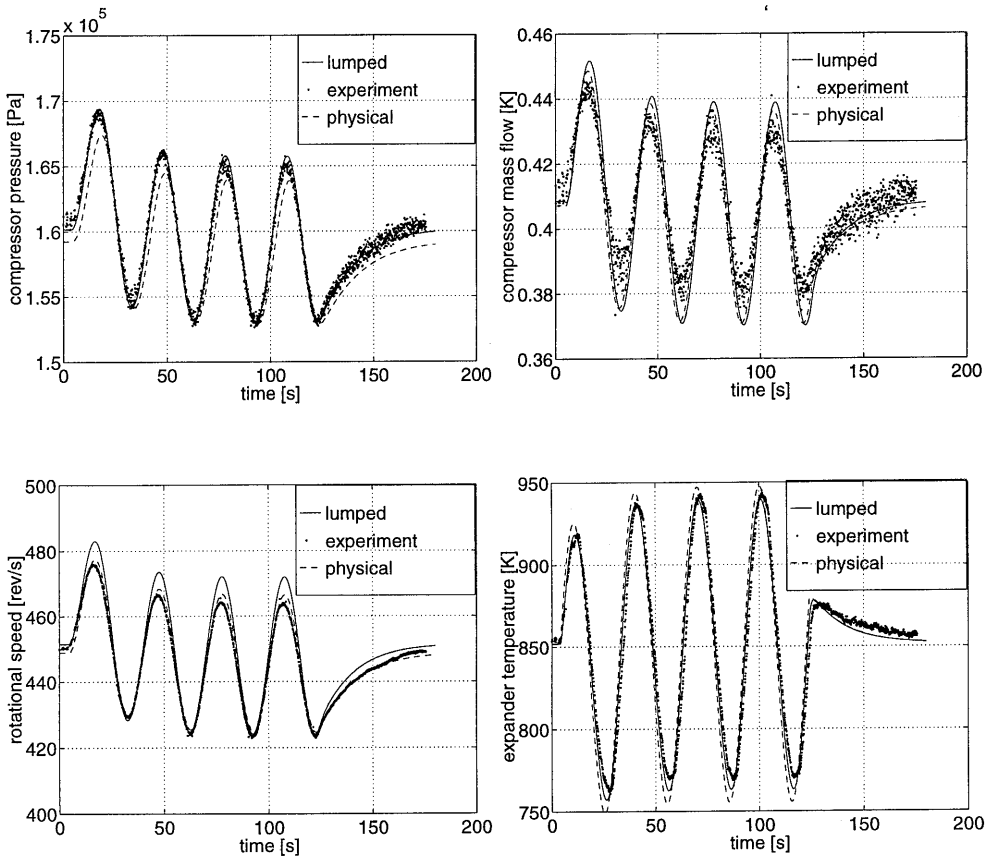


figure 4.27 : Transient response of compressor pressure, compressor mass flow, rotational speed and expander temperature for the lumped model, the physical flow model and experiments.

Both models perform well and show close correspondence to the measurements. Small deviations between both models are visible and are probably caused by differences in stationary

points and differences in inertia. Remind that a complete validation of inertia parameters for the physical flow model has not yet been performed. On the other hand, the measurements, especially the expander temperature, may also suffer from some unmodelled inertia in the instrumentation.

4.6 Frequency response analysis

We conclude this chapter with an analysis of the frequency response behaviour of both model types. When a linear system is subjected to a sinusoidal input, its ultimate response (after some time) is a sustained sinusoidal wave with exactly the same frequency. Frequency response analysis primarily determines how the features of the output sinusoidal wave (changes in amplitude and phase shift) vary with the frequency of the input sinusoid. Amplitude and phase shift are plotted versus input frequency in the so called Bode diagram.

Since the sustained output to a sinusoidal input for a non-linear system is not a pure sine (and also the mean level of the output may be shifted), frequency response analysis is strictly not applicable to non-linear systems. It may provide, however, insight in the usefulness of the model for different frequencies of the inputs.

In the three figures below, the Bode diagrams for compressor pressure, rotational speed, and expander temperature are plotted respectively. Results are generated by simulations with changing input frequencies and an amplitude of 0.03 on the only input: the fuel valve.

The amplitude is determined by the half distance between the maximum and the minimum value of the sustained sine-like output response. The phase shift is determined by comparison of the phase of the input and the sustained output response. Because a long period is required before the output stabilises, the accuracy of the phase shift is difficult to determine, especially for higher frequencies. In simulations the resolution of the phase shift is set to 1/256 period. In experiments, however, the resolution of the phase shift is much worse. Due to the measurement noise and the maximum sample time of 10 Hz it is hard to determine the phase shift. To cover a large range of frequencies we use a logarithmic scale for both frequency and amplitude axis. The phase shift is expressed on a linear scale in degrees.

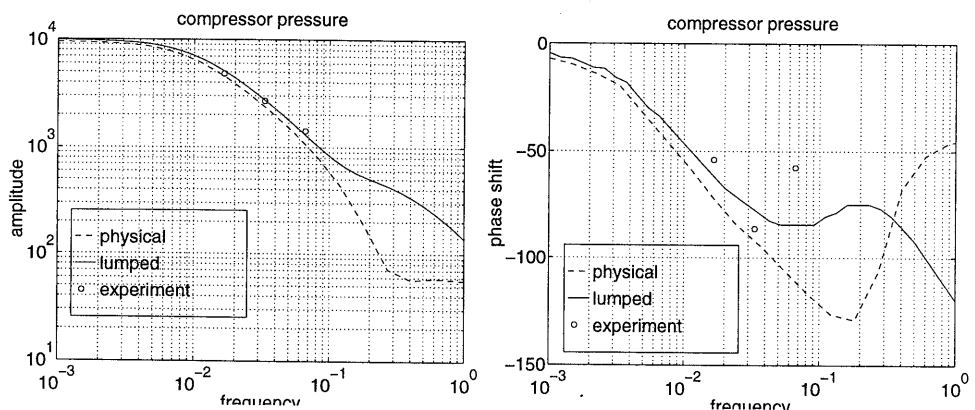


figure 4.28 : Amplitude and phase diagram of the compressor pressure for the lumped model and the physical model, compared to three experimental determined responses.

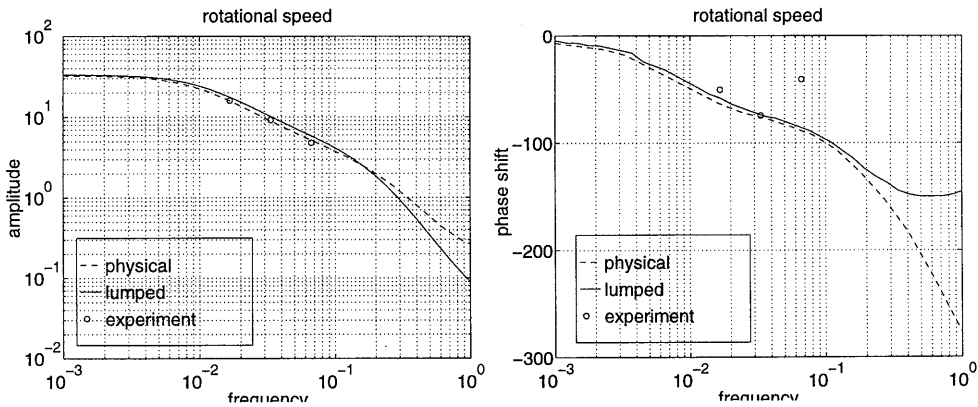


figure 4.29 : Amplitude and phase diagram of the rotational speed for the lumped model and the physical flow model, compared to three experimental determined responses.

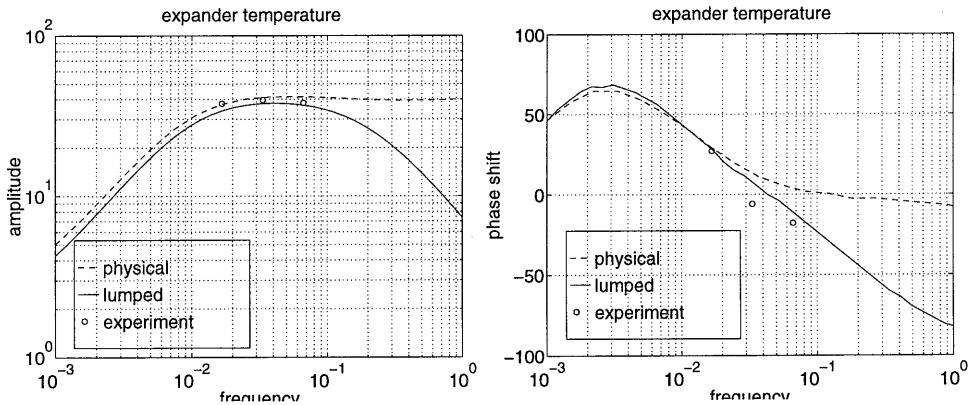


figure 4.30 : Amplitude and phase diagram of the expander temperature for the lumped model and the physical flow model, compared to three experimental determined responses.

From these results we can conclude that both the physical flow and the lumped model show a close correspondence **up to a frequency of approximately 0.1 Hz** (or a period of 10 seconds for sinusoidal input). Within this range, they also correspond to the experimental determined frequency response. The correspondence holds for both the amplitude and the phase shift. This is according to what we expected in Chapter 3. Only the experimentally determined phase shift of the compressor pressure shows a significant deviation for the highest frequency (period of 15 seconds). This seems to be caused by the difficulties in the determination of phase shift from experimental data discussed before.

For **frequencies higher than 0.1 Hz**, we do not have proper means to validate the frequency response in measurements because the fuel valve is not fast enough. Results from both models diverge for frequencies higher than 0.1 Hz. This is caused by the essential difference between the lumped and the physical flow model concerning the smallest time scale that is considered. Also the functions that describe the parameter values (especially the combustion efficiency)

have not been validated for higher frequencies and are likely to cause problems. Since the physical flow model describes smaller time scales, it is likely that it is able to describe the response to higher frequencies. Unfortunately, we can not validate this behaviour at the moment. In future research, pulsated steam injection serves for this purpose. At that time, also the parameter functions should be updated and the validation inertia parameters of the model (the volumes of piping and close-coupled plenums) should be validated for higher frequencies.

For frequencies higher than 0.1 Hz two peculiar phenomena are recognised in the physical flow results. First, in figure 4.28, we see that the phase shift of the compressor pressure decreases at frequencies higher than 0.1 Hz. We do not know why this phenomenon is encountered in the simulations, but it may be caused by some kind of aliasing or by the non-sine shape of the non-linear responses of the simulation. Another phenomenon in this frequency range is the almost flat amplitude curve in figure 4.30 of the expander temperature of the physical flow model. Unfortunately we do not know whether this is actually to be expected or caused by inaccurate values of parameters in question, for instance the static matching of the combustion efficiency.

4.7 Discussion

A main conclusion from the analysis presented in this chapter is that the model performance is good, both for transient and for stationary measurements. We needed, however, extensive fit procedures to match the model parameters to the experimental data. This was required to have the simulated stationary operating points agree with measured operating point. Basically, we had to adjust the characteristics of the components. After that, the transient behaviour did not introduce any problems; the required inertia parameters were easy to select from straightforward (physical) start values. After all, the problem appears to be related to the “inaccurate” vendor supplied component characteristics and not to the type of modelling.

Physical flow model vs. lumped parameter model A comparison between the physical flow model and the lumped parameter model gives expected results. The lumped parameter model can be used to describe phenomena up to 0.1 Hz. When larger frequencies are needed, only the physical flow model can be used. The intended use of the model is the application in a real-time controller that rules changes in operating points of the laboratory installation. Since the overall time constant of the laboratory gas turbine to a step response on the fuel valve is approximately 20 seconds, the lumped model serves excellently for our purposes. The implementation of the model into the controller and the obtained results are subjects of the remaining chapters.

Open-loop experiment In this chapter we applied extensive fit procedures to match the model parameters to the experimental data. This gives rise to the question to what extent the (lumped parameter) model agrees to an arbitrary data set. As an illustration of this ability, figure 4.31 shows a selection from the results of a so called open-loop experiment. In an open-loop experiment the inputs to the installation, i.e. the valve positions, are computed by a controller so that desired *model* outputs are obtained. Completely independent, the same input sequence is used at the actual process and measurements can be compared to the simulation results to evaluate the model performance. In this experiment the set points on the rotational speed and the mass flow through the expander are stepwise and simultaneously increased at sample 60, and back at sample 130. One sample is 1.2 seconds in this experiment. Although

the controller is not to be discussed here we state that the expander temperature is limited by the controller to 925 K.

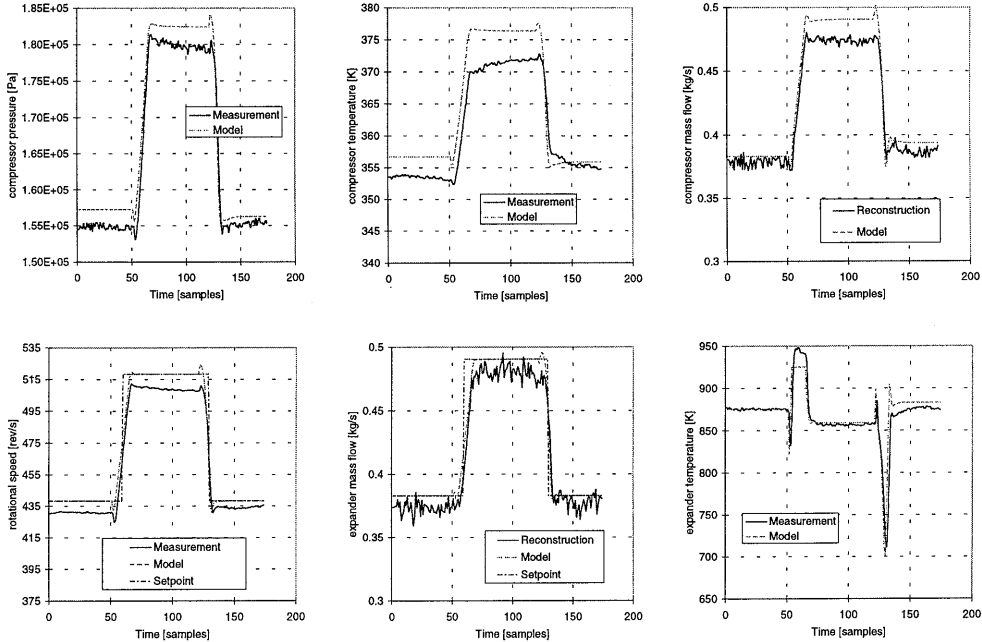


figure 4.31 : Open-loop control experiment.

In the data we clearly recognise static deviations between model and measurements. These deviations are caused by model errors. Especially by accumulation of the errors in the fits of mass flow correction, pressure drops and efficiencies. Moreover, additional errors are likely to be introduced as the fits have been determined from a standard data set of stationary operating points and not on transient experimental data.

Of course, for control we are interested in the actual process variables and not in the model predictions. In a closed loop controller, the mismatches are corrected by a filter. This will be extensively treated in the next chapter.

The dynamic response predicted by the model corresponds closely to the response of the installation. We also see that unmodelled phenomena, like heating up of the piping and cooling water cause the measurements to change even when there are no changes in the inputs and the model variables are already settled. From this experiment we conclude that the lumped model performs well on other data-sets and is suitable for control purposes.

Reconstruction of mass flows In the open-loop results also the mass flows through the compressor and through the expander are presented. Note that these have been reconstructed from other measured data as they cannot be measured directly. It appears that especially the reconstruction of the compressor mass flow is very sensitive for errors. In fact, this sensitivity deals with the observability of the mass flow from the measurements. This problem will be dealt with in the next chapter. In Appendix C.5, a sensitivity analysis shows the condition numbers for the reconstruction of the mass flows.

5 Model Predictive Control

The introductory section of this chapter gives a brief survey on Model Predictive Control, including a discussion of linear versus non-linear MPC. Also the main objective of this thesis with regard to MPC is highlighted. In the body of the chapter we present the concept of MPC and discuss the implementation of the algorithms and the filter used in this thesis. The concluding section discusses some particular problems related to the properties of MPC and the application of MPC to our gas turbine models.

5.1 Introduction

Model Predictive Control (MPC) is a control strategy that uses a model of the process which is to be controlled. MPC is an essentially discrete time controller. At each sample interval, the model provides a prediction of future process outputs. Based on this prediction, an objective function is optimised on-line with regard to the future control inputs of the process. In this optimisation, it is possible to take constraints (limits on the inputs or limits on the outputs) into account. Only the values of the inputs for the next sample are used and the optimisation is repeated at the next sample. This mechanism is known as *moving* or *receding* horizon.

Because of the constraint handling capacity, MPC became known in the late 1970s and early 1980s under a variety of names including Model Algorithmic Control [Mehra, 1982], Model Predictive Heuristic Control [Richalet, 1978] and (Quadratic) Dynamic Matrix Control, (Q)DMC, [Cutler, 1980] and [Garcia, 1984, 1986]. While the details of the various algorithms differ, the main idea is much the same. A review of MPC is in [Garcia, 1989]. Also Generalised Predictive Control, GPC [Clark, 1987], adopts the receding horizon idea, but starts from SISO transfer functions and was initially proposed for adaptive control applications.

MPC is applied successfully in controlling relatively slow processes with complex dynamics and constraints in the process industries. Standard linear MPC incorporates a linear model for both prediction and optimisation. Linear models allow the use of “proven” and fast algorithms in both the unconstrained (Least Squares, LS) and the constrained optimisation problem (Quadratic Programming, QP). A comprehensive treatment on linear MPC is given by [Morari, 1993a, 1993b]. Although linear MPC is successful in controlling linear and mildly non-linear processes, performance degradation and instability often occur in the presence of strong non-linearities.

During the past decade, the number of non-linear model-based control algorithms has increased significantly. A comprehensive review is provided by [Bequette, 1991]. Non-linear predictive control involves the solution of non-linear differential equations for model prediction and non-linear programming techniques for constrained optimisation. Basically, two iterative approaches to this problem exist. First, in a sequential procedure, the model equations are simulated and the objective function is evaluated in an “inner-loop”, while an optimisation code serves as an “outer-loop” [Sistu, 1991]. This first approach can be very time consuming. Second, in a simultaneous procedure, the model equations are discretised (for instance by orthogonal allocation) and formulated as non-linear equality constraints in a non-linear programming problem that solves the optimisation [Patwardhan, 1990], [Eaton, 1992]. This second approach results in large optimisation problems. In spite of successful implementations

and the advances made in developing efficient algorithms [Sistu, 1993], the excessive computational requirements of both non-linear methods remain a serious obstacle for implementation on complex systems or on systems that exhibit fast dynamics. Also, difficulties arise in understanding their stability and performance properties [Gattu, 1992].

A computationally less demanding approach is linear approximation. The non-linear model equations can be linearised around the current operating point to obtain a locally linearised model. This can be done only once, resulting in linear MPC, or successively at each sample. Successively linearised models allow the use of (computationally fast) linear optimisation algorithms to “non-linear” problems. At each sample interval an updated linearised model is used to perform prediction and optimisation over a future horizon. Because of this horizon, it is also possible to repeat the linearisation within each sample of the prediction horizon, something which is done, e.g., by [Bregel, 1989], [Li, 1989], and [Oliveira, 1995]. These methods, however, are expected to increase the computational demands substantially, since they incorporate a sequential (SQP) optimisation problem instead of a single QP problem.

Another extension to (linear) MPC is introduced by [Garcia, 1984]. A (successively) linearised model for optimisation can be combined with (the original) non-linear model for prediction. This approach is refined by [Gattu, 1992] and [Lee, 1993] to include an Extended Kalman Filter. In this case a non-linear prediction and a linear optimisation model are combined. In this thesis we refer to the extended Kalman filter as *augmented* Kalman filter.

The main objective of this thesis is to assess the feasibility and advantages of MPC on systems like turbomachinery installations. For this purpose, we need algorithms which handle non-linearities and constraints adequately, but are guaranteed not to require computation-times larger than allowable for real-time implementation on the laboratory gas turbine installation.

For both real-time implementation and MPC simulations we adopt the *Primacs* package. Primacs is being developed by TNO-TPD at Delft (The Netherlands) as an application for model based process control. First versions, based on linear state-space model formulations, date from 1994. In this thesis we investigate the use of non-linear process models in MPC and the opportunities to implement them in Primacs. We restrict, however, this research to linear optimisation routines since we are developing a time-critical control application. Special attention is paid to successive linearisation, the selection and implementation of filters, and to the feasibility of the optimisation.

5.2 Principles of MPC and Primacs implementation

5.2.1 MPC Concept

Figure 5.1 presents the concept of MPC and its receding horizon schematically. For convenience, in this scheme only one input and one output are considered. At the present time (sample) k , the response of the output y is predicted over the *prediction horizon* with a length of p samples. This prediction is based on past inputs, current model states, latest process measurements, proposed future inputs, and possibly predicted disturbances. The manipulated variables are allowed to vary over the *control horizon* with a length of m samples. The changes Δu are computed such that future deviations between the predicted output and the desired reference r are minimised. Of the computed optimal control moves, only the value for

the first sample is actually implemented and the algorithm repeats the same procedure for the next sample.

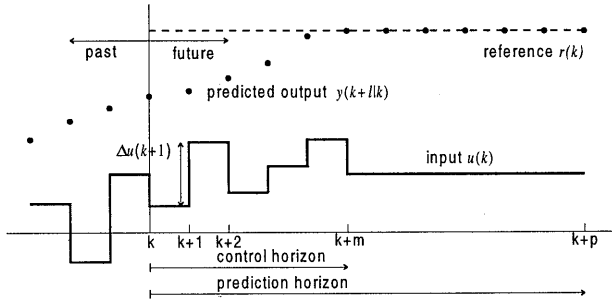


figure 5.1 : Concept of Model Predictive Control.

To minimise future deviations of the controlled variables from their reference values (set points or trajectories), while preventing the inputs from changing inadmissibly fast, the following (common for MPC) quadratic objective function (in $y - r$ and Δu) is used

$$\min_{\Delta u(k+1) \dots \Delta u(k+m)} \sum_{l=2}^p \left[\Gamma^y (y(k+llk) - r(k+l)) \right]^2 + \sum_{l=1}^m \left[\Gamma^u (\Delta u(k+l)) \right]^2 \quad (5.1)$$

where weights are included to express the relative importance of outputs following their reference (Γ^y) compared with the actions of manipulated variables (Γ^u). Furthermore, $y(k+llk)$ denotes the estimate of $y(k+l)$ obtained at sample k , taking into account all (available) information up to and including the current sample k . Note that, at sample k , input moves Δu are optimised starting from sample $k+1$, to minimise predicted output deviations from sample $k+2$ onwards. This way, the computational sample-delay of the discrete implementation is accounted for, with the inherent implication that $y(k+llk)$ can never be influenced at sample k .

A feature that distinguishes MPC from standard feedback control is the explicit use of a finite prediction horizon in the control problem. The prediction horizon allows the MPC controller to take control action at the current time step, in response to a forecast of a future error between the reference and the actual output, even if this error is zero at the current time. This anticipation capacity is one of the advantages of MPC. An even more important advantage is the constraint handling capability of MPC. In contrast to conventional controllers, constraints can be explicitly incorporated in the optimisation criterion. Physical, safety and performance constraints can be taken into account. Another advantage is that, because of the straightforward optimisation, MPC can deal with a high degree of interaction between inputs and outputs. Since the objective function is formulated in the time-domain, the control strategy is intuitively clear to operators.

There are also “disadvantages” associated with MPC. First, MPC is computational demanding and, therefore, useful for “slow” processes only. Second, the performance of MPC strongly depends on the values of tuning parameters including weighting factors, length of horizons, and sample intervals. The selection of the tuning parameters will be discussed in the following section. Last but not least, one needs a model of the process to be controlled. The performance of MPC depends on the accuracy of the available model.

5.2.2 Tuning parameters in MPC

For a proper operation of the controller, the controller must be able to observe the results of its actions in the model predictions. For this reason, a rule of thumb is that the *prediction horizon* must exceed the largest (controlled) time constant of the system, periods of inverse response, and dead time periods. In practice the *control horizon* is chosen to be 1/6 to 1/3 of the prediction horizon. This is a compromise between the speed of the system response on the one hand and robustness of the closed-loop behaviour and computational effort on the other hand [Morari, 1993a].

Increasing the prediction horizon or the control horizon leads to increased computation times, as the system response must be predicted for a larger period, or more input moves need to be computed. When the required control horizon leads to inadmissibly large computation times, these can be reduced by applying *control blocking*. Then, the control horizon is divided into a number of control blocks that consist of more than one sample. The input variables are not allowed to change from one sample to another, but from one control block to another. Control blocking enables the system to manipulate its inputs “further” in the prediction horizon, without extra computational effort. Control blocking slows down system response.

For processes, like most chemical processes, that show responses corresponding to first-order responses, basic guidelines for the tuning are formulated by [Morari, 1993a]. A faster system response and a more aggressive control action are obtained when either the size of the prediction horizon is decreased, the size of the control horizon is increased, or the *set-point weights* are increased relative to the *input weights*. This also results in a less robust closed-loop behaviour, since also the reactions on disturbances and model errors become more aggressive. As the control action gets more aggressive, the system response may become unstable.

The *controller sampling time* or *sample interval* should be chosen with respect to the process dynamics, input, and reference signals. A maximal interval is determined by the required bandwidth of the closed-loop system. When the sample interval is too large, fast transients are not predicted by the controller, yielding a slow “steady state” controller which may result in unstable behaviour. Also, the model accuracy is of importance for the determination of the sample interval. When large (static or dynamic) mismatches occur between process and measurements, the sample interval should be chosen small to allow the model predictions to be updated with measurement information as often as possible. A lower limit for the sample interval is obviously the required computation time per sample. Note that the computation time is a function of the sample interval. When the interval is decreased, more samples are needed in the control and prediction horizon, to cover the same time span. This results in increasing computational effort for the controller and thus a larger computation time per sample.

5.2.3 Implementation of MPC in Primacs

Figure 5.2 presents a schematic view of the controller implemented in Primacs. At sample k , the current values of the state variables $x(k)$ and the inputs $u(k)$ are available. These are the actual state and inputs, measured from the process. (In general, however, only an estimate $x_{cor}(k)$ of the state is available when not all state variables can be measured or when the model states differ from the process measurements.)

The controller computes the value of the inputs for the next sample. This calculation proceeds in two stages, based on the superposition theorem. This theorem states that when the input to a

system is a linear combination of input signals and or initial conditions, the corresponding output is the same linear combination of individual responses. First, the values of the output over the prediction horizon are computed for constant values of the inputs ($\Delta u = 0$). Then, the optimisation problem (5.1) is solved for Δu . To perform these two computation steps, two different models may be used to which we refer as the Internal Prediction Model (IPM) and the Internal Optimisation Model (IOM) respectively. Note, however, that only for two identical linear models the underlying superposition theorem is valid. In most other cases an error is introduced.

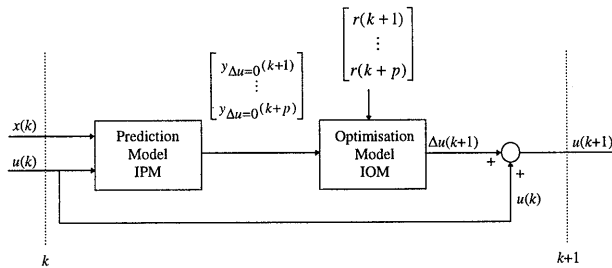


figure 5.2 : Primacs implementation of the *Controller*.

In figure 5.3 the overall MPC configuration is presented schematically. The controller of figure 5.2 is now embedded in the actual process. At each sample k , the measurement system provides the process output y_p . These measurements are fed to the controller by means of a *filter*. The filter “updates” the model predictions with the measurement information by comparing the predicted model outputs y_m with the actual process measurements y_p . The filter provides a “corrected state” x_{cor} to the controller block. The correction involves model mismatches and noise as well as the reconstruction (or estimate) of states that are not directly measured. The filter is extensively discussed in section 5.2.6.

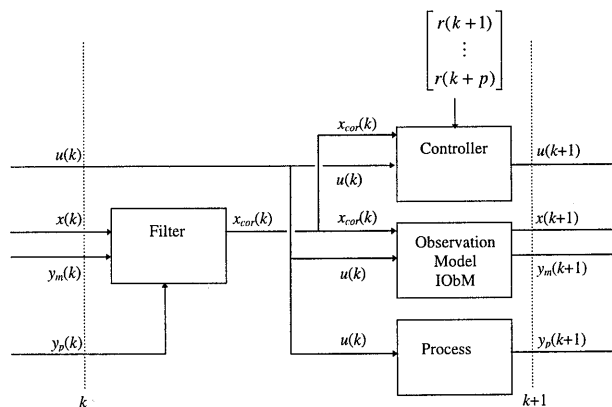


figure 5.3 : Primacs implementation of MPC.

A final component of the Primacs MPC configuration in figure 5.3, is the Internal Observation Model (IObM). Its task is to predict the model outputs $y_m(k+1)$, that is, only one sample ahead. The prediction is based on the most recent values of the input and the corrected state. Obviously, this prediction is also available from the IPM inside the controller, but here is an op-

portunity to select another model for a one-step-ahead prediction. For instance, the IOBM can be a non-linear model since it is not applied to an optimisation and also computation time (over one sample) is not very restrictive. This observation model is the third model type that may be used in MPC.

Primacs thus uses three internal models to perform its computations. In standard linear MPC one and the same model version is used for all the internal models. This is a linear (state space) model, linearised in a prescribed starting point. When the process moves away from the starting point, it may exhibit a different behaviour than the model which was linearised in the starting point, due to non-linearities in the process. In this thesis, three different non-linear approaches are addressed, based on non-linear internal models, which are then compared to linear MPC. Since we do not have the intention to look into the expanding field of non-linear optimisation algorithms, it is assumed that our non-linear approaches still use a linear model for the optimisation (IOM in figure 5.2). We also assume that the non-linear model may be linearised along an arbitrary operating point, so we are able to repeat the linearisation at every sample interval. This approach is referred to as successive linearisation.

In all approaches a non-linear internal observation model (IOBM in figure 5.3) is used. This allows the filter to compensate for actual model mismatches and disturbances and not for inevitable static deviations due to linearisation. Three different combinations for the prediction and the optimisation model are summarised in table 5.1. The first non-linear approach uses a linearisation of the non-linear model, obtained at each sample interval, for prediction as well as optimisation. The second approach uses the non-linear model for prediction and a linearisation of the non-linear model for optimisation, but does *not* repeat the linearisation. The third approach combines a non-linear model for prediction and successive linearisation for optimisation. The use of successive linearisation or non-linear prediction requires extra computational effort, which leads to larger computation times. In table 5.1 the options are put in order of increased computation time per sample.

	Type of Model Predictive Control	Internal Observation Model	Internal Prediction Model	Internal Optimisation Model
1	Linear MPC	linearised once	linearised once	linearised once
2	Successive linearisation	non-linear	linearised successively	linearised successively
3	Non-linear prediction	non-linear	non-linear	linearised once
4	Non-linear prediction and successive linearisation	non-linear	non-linear	linearised successively

table 5.1 : Combinations of models in linear and non-linear MPC.

5.2.4 Linear optimisation

The solution to the linear unconstrained problem can be obtained analytically with relatively little computational effort [Morari, 1993a] and can be expressed in the following control law:

$$\Delta u^m(k+1) = \begin{bmatrix} \Delta u(k+1) \\ \vdots \\ \Delta u(k+m) \end{bmatrix} = \mathbf{K}_{\text{MPC}} \mathbf{E}_{\Delta u=0}^p = \mathbf{K}_{\text{MPC}} \begin{bmatrix} y_{\Delta u=0}(k+1|k) - r(k+1) \\ \vdots \\ y_{\Delta u=0}(k+p-1|k) - r(k+p-1) \end{bmatrix} \quad (5.2)$$

The constant $m \times p$ matrix \mathbf{K}_{MPC} is an off-line computed matrix that reflects the weightings and model dynamics (Appendix D.5). The vector \mathbf{E}^p contains p elements reflecting the predictions of the output deviations from the reference over the whole prediction horizon when the inputs are not changed. These predictions are computed at sample k , using process information up to sample k . The vector \mathbf{E}^p contains time varying elements and needs to be computed every sample.

In general, constraints will always be present at one time or another. Three types of constraints can be distinguished:

- constraints on the output (or states) of the process, for instance a maximum or minimum pressure or temperature level,
- constraints on the input signals u , for instance a maximum or a minimum valve position,
- constraints on the changes in input signals Δu , or move constraints, that is, the maximum move rate of the input signals per sample.

Incorporating these constraints leads to a Quadratic Program (QP) of the following standard form (Appendix D.5):

$$\min_{\Delta u^m(k+1)} \left\{ \frac{1}{2} \Delta u^m(k+1)^T \mathbf{H} \Delta u^m(k+1) - \mathbf{G}^{m-1}(k+2|k) \Delta u^m(k+1) \right\} \quad (5.3)$$

subject to $\mathbf{C} \Delta u^m(k+1) \geq \mathbf{c}^{m-1}(k+2|k)$

where $\Delta u^m(k+1)$ contains the control moves $[\Delta u(k+1) \dots \Delta u(k+m)]^T$, \mathbf{H} and $\mathbf{G}^{m-1}(k+2|k)$ are the Hessian and gradient vector of the QP formulation and \mathbf{C} and $\mathbf{c}^{m-1}(k+2|k)$ formulate the inequality constraints on the inputs and the outputs.

This QP problem may not always have a solution, in that case the problem is called infeasible. A strategy must be specified to handle these infeasibilities. In Primacs, constraint violations are included into the optimisation criterion, once infeasibility occurs. It is implemented by simply adding the absolute value of the (suitably weighted) constraint violations ε ($\varepsilon \geq 0$) to the optimisation criterion, which will then look like [Oliveira, 1994]:

$$J_{\text{modified}} = J + \rho^T \varepsilon \quad (5.4)$$

where J denotes the unmodified optimisation criterion, and ρ the vector with weights on the constraint violations. Due to this modification, the magnitude and the duration of any constraint violation is minimised. The optimisation is still linear and the modified QP problem is guaranteed feasible.

The linear optimisation strategy in Primacs, including constraint handling, can now be summarised as follows:

1. Solve the unconstrained problem (5.2). If constraints are violated, go to step 2. Else, implement the controller moves and return to step 1.
2. Find a solution to the QP (5.3). The solution of step 1 is used as starting value. If infeasible, go to step 3. Else, implement the controller moves and return to step 1.
3. Include constraint violations into the QP, and solve this modified problem (5.4). Implement the controller moves and return to step 1.

5.2.5 Successive linearisation

Our development of non-linear MPC is based on a non-linear model of the process in a state space formulation, expressed by the following set of non-linear ordinary differential equations and algebraic output equations:

$$\begin{aligned}\dot{x}(t) &= f(x(t), u(t)) \\ y(t) &= h(x(t), u(t))\end{aligned}\quad (5.5)$$

in which $x(t)$ represents the model state, $y(t)$ represents the output, and $u(t)$ the input. We assume that this model is sufficiently accurate to describe the process and allows fast enough simulation times to meet MPC sampling limits.

The linear model that MPC requires for its optimisations can be obtained from the non-linear model (5.5) by the first-order Taylor expansion in an arbitrary operating point (x_0, u_0) . This operating point does not need to be a stationary operating point, but we need to assume that it is (at least approximately) a solution of (5.5), that is,

$$\begin{aligned}\dot{x}_0 &\equiv f(x_0, u_0) \\ y_0 &\equiv h(x_0, u_0)\end{aligned}\quad (5.6)$$

The Taylor approximation yields:

$$\begin{aligned}\dot{x}(t) &= \dot{x}_0 + \dot{\tilde{x}}(t) \equiv f(x_0, u_0) + \mathbf{A}\tilde{x}(t) + \mathbf{B}\tilde{u}(t) \\ y(t) &= y_0 + \tilde{y}(t) \equiv h(x_0, u_0) + \mathbf{C}\tilde{x}(t) + \mathbf{D}\tilde{u}(t)\end{aligned}\quad (5.7)$$

With $\tilde{x}(t), \tilde{u}(t), \tilde{y}(t)$ small perturbations from the linearisation point (x_0, u_0, y_0) according to

$$\begin{aligned}\tilde{x}(t) &= x(t) - x_0 \\ \tilde{y}(t) &= y(t) - y_0 \\ \tilde{u}(t) &= u(t) - u_0\end{aligned}\quad (5.8)$$

and $\mathbf{A}, \mathbf{B}, \mathbf{C}, \mathbf{D}$ are Jacobi matrices. These Jacobians can be determined either analytically or numerically according to

$$\begin{aligned}\mathbf{A} &= \left. \frac{\partial f(x, u)}{\partial x} \right|_{x=x_0, u=u_0} & \mathbf{B} &= \left. \frac{\partial f(x, u)}{\partial u} \right|_{x=x_0, u=u_0} \\ \mathbf{C} &= \left. \frac{\partial h(x, u)}{\partial x} \right|_{x=x_0, u=u_0} & \mathbf{D} &= \left. \frac{\partial h(x, u)}{\partial u} \right|_{x=x_0, u=u_0}\end{aligned}\quad (5.9)$$

In Primacs we need the discrete-time version of equation (5.7) which is obtained by discretising the matrices $\mathbf{A}, \mathbf{B}, \mathbf{C}$ and \mathbf{D} , as described in [Kwakernaak, 1972]. The discretisation time can be chosen equal to the MPC sample interval allowing one step computation. With $\mathbf{A}_d, \mathbf{B}_d, \mathbf{C}, \mathbf{D}$ and $f_d(x_0, u_0)$ denoting the discrete versions of $\mathbf{A}, \mathbf{B}, \mathbf{C}, \mathbf{D}$ and $f(x_0, u_0)$, the following equations for the discrete-time representation are obtained:

$$\begin{aligned}x(k+1) &= f_d(x_0, u_0) + \mathbf{A}_d(x(k) - x_0) + \mathbf{B}_d(u(k) - u_0) + x_0 \\ y(k+1) &= h(x_0, u_0) + \mathbf{C}(x(k+1) - x_0) + \mathbf{D}(u(k) - u_0)\end{aligned}\quad (5.10)$$

This formulation allows linearisation in any arbitrary operating point (x_0, u_0) . The term $f_d(x_0, u_0)$ will only have a value not equal to zero when the linearisation point is not a station-

ary point of the non-linear model. In (5.10) the causality of the model is guaranteed by only using available information up to and including sample k to compute the output at sample $k+1$.

5.2.6 Filter and reconstruction

A filter is required to correct the predictions of the internal models towards the actual measurements of the process. Due to model mismatches and unmodelled phenomena, the static and dynamic behaviour of the model may differ from the real process. Also measurement and system noise will affect the difference.

Several kinds of filters exist, and the selection of a filter and its parameters influence the performance of the closed loop control system. Basically, model based and non-model based filters are distinguished. The most straightforward non-model based filter is the first order filter. Such a filter adapts the output of the model until it corresponds to the measured process output. Model based filters use a model of the process to adapt the states of the model in such a way that the output of the model corresponds to the output of the process. Two model-based filters are discussed: a Kalman filter and an augmented Kalman filter.

A *first-order* filter adds a number of extra state elements, equal to the number of model outputs to be corrected, to the original model state x . The additional states d are (each sample) updated by adding a fraction of the corresponding difference between model output and process output. The original state x is left unaltered. The new state elements may be regarded as disturbances on the outputs. Therefore, the first order filter, implemented in this way, is often referred to as an output disturbance filter. Applied to a linear state space model, the system equations become:

$$\begin{aligned}
 x_{cor}(k) &= \begin{bmatrix} x(k) \\ d(k) \end{bmatrix} + \begin{bmatrix} \mathbf{0} \\ \mathbf{K}_f \end{bmatrix} [y_m(k) - y_p(k)] \\
 \begin{bmatrix} x(k+1) \\ d(k+1) \end{bmatrix} &= \begin{bmatrix} \mathbf{A}_d & \mathbf{0} \\ \mathbf{0} & \mathbf{I} \end{bmatrix} x_{cor}(k) + \begin{bmatrix} \mathbf{B}_d \\ \mathbf{0} \end{bmatrix} u(k) \\
 y_m(k+1) &= [\mathbf{C} \quad \mathbf{I}] \begin{bmatrix} x(k+1) \\ d(k+1) \end{bmatrix} + \mathbf{D}u(k)
 \end{aligned} \tag{5.11}$$

in which \mathbf{K}_f is the filter gain matrix and d represents the additional states. The filter gain matrix \mathbf{K}_f is usually taken as a diagonal matrix, that is, one scalar filter gain for every output. The filter gain determines how much of the deviation between model and process output is added to the model output and should be chosen between 0 and 1. The larger the filter gain, the faster deviations are corrected. However, in that case also more measurement noise of the process output will be present in the corrected model output, leading to unnecessary or wrong corrections. When the gain is equal to 1, the extra states are updated such that the model output equals the process output instantaneously, which is useful only if the process measurements are quite accurate. When no additional model information is used, y_m and y_p should correspond, in other words, all model outputs that need to be filtered must also be measured directly from the process. With additional model information it may be possible to reconstruct unmeasured process outputs from other available data.

The advantages of the first order filter are that it can correct for offsets between model and process. It can be used in conjunction with any linear (5.11) or non-linear model. The most

important disadvantage of the first order filter is that only the outputs are corrected, while the states remain unchanged. Large deviations between model and process, could lead to a model which operates in an operating point with totally different dynamics than the process. This may cause the controller to perform wrong control actions. To avoid this, the model should reasonably well describe the static process behaviour and the local dynamics.

A model-based filter that possibly avoids this drawback is the well-known *Kalman* filter. It uses the model and process measurements to update the model *states* in such a way that the model outputs are corrected towards the process outputs. For a linear state space model the Kalman filter is implemented as follows:

$$\begin{aligned}x_{cor}(k) &= x(k) + \mathbf{K}_k (y_m(k) - y_p(k)) \\x(k+1) &= \mathbf{A}_d x_{cor}(k) + \mathbf{B}_d u(k) \\y_m(k+1) &= \mathbf{C}x(k+1) + \mathbf{D}u(k)\end{aligned}\quad (5.12)$$

In conjunction with a linear state space model, the optimal Kalman filter gain \mathbf{K}_k is determined from the discrete algebraic Riccati equation, as a function of the system dynamics and of the covariance matrices of the measurement and system noise [Kwakernaak, 1972]. Under the condition that states are observable, the Kalman filter is able to reconstruct also state variables that cannot be measured directly. A state is said to be observable if it is possible to determine this state from the observation of the available outputs over a finite time interval. The optimal Kalman gain minimises the estimation error.

The main disadvantage of the Kalman filter is that it can only correct for (system and measurement) noise with zero mean (unless detailed information on the offset is available). This implies that it is not capable to correct for offsets between model and process. For this reason, the Kalman filter is not very suitable for MPC. Moreover, a non-linear version of the Kalman filter, that is a Kalman filter applied to a non-linear model (5.5), involves a non-linear state observer and the solution of Hamilton-Jacobi equalities and is very complicated.

A combination of the Kalman filter and the first order filter leads to the *augmented Kalman filter* [Gattu, 1992], [Lee, 1993]. Indeed, the augmented Kalman filter can handle system- and measurement noise as well as offsets between model and process. This is achieved by augmenting the original model states with a number of additional states d that may be regarded as disturbances on the outputs. All states are corrected in a similar way as in the original Kalman filter. For a linear state space model the augmented Kalman filter is implemented as follows (in which the filter gain \mathbf{K}_{ek} may be obtained from the discrete algebraic Riccati equation):

$$\begin{aligned}x_{cor}(k) &= \begin{bmatrix} x(k) \\ d(k) \end{bmatrix} + \mathbf{K}_{ek} (y_m(k) - y_p(k)) \\ \begin{bmatrix} x(k+1) \\ d(k+1) \end{bmatrix} &= \begin{bmatrix} \mathbf{A}_d & \mathbf{0} \\ \mathbf{0} & \mathbf{I} \end{bmatrix} x_{cor}(k) + \begin{bmatrix} \mathbf{B}_d \\ \mathbf{0} \end{bmatrix} u(k) \\ y_m(k+1) &= \begin{bmatrix} \mathbf{C} & \mathbf{I} \end{bmatrix} \begin{bmatrix} x(k+1) \\ d(k+1) \end{bmatrix} + \mathbf{D}u(k)\end{aligned}\quad (5.13)$$

The augmented Kalman filter is suitable for use within MPC. It compensates for model mismatches as well as noise. In general, however, it is not possible to update more states than the number of independent process measurements. Consequently, it may be impossible to update

the state vector in an augmented Kalman filter. A mathematical solution for the filter gain matrix \mathbf{K}_{ek} is therefore often not available. Moreover, the filter design may fail when a strict separation between noise and (steady state) offset cannot be made. Ad-hoc solutions in which the available process information provides the most useful model updates need to be determined. Finally, also the implementation of the augmented Kalman filter on a non-linear model is complicated.

Because only a limited number of measured process outputs are available and because we use the filter in conjunction with a non-linear prediction model (the internal observation model or IOBM, figure 5.3), we selected the first order filter as the most practicable filter. The first order filter is easy to implement whereas the (non-linear) augmented Kalman filter causes implementation problems. The ordinary Kalman filter is not suitable for use in our MPC application.

5.3 Discussion

In this closing section we discuss an important problem that arises in the application of a first order filter: the reconstruction of unmeasured process outputs. We also indicate, very briefly, some theoretical properties of (non-linear) model predictive control.

Filter and reconstruction Because in the first order filter only outputs (and not states) are updated and because, in general, model outputs are static relations of state variables, a problem arises in the reconstruction of unmeasured process outputs. If the applied steady state model equations are only valid for the original values of the states in the model, and if the actual process values are different from these original values because of model mismatches or systematic measurement errors, the unmeasured process outputs may become badly estimated or even undetermined.

For our gas turbine model, this is, for instance, the case for the mass flows through the compressor and the expander. Consider the reconstruction of the compressor mass flow. We have already seen that the computation of the mass flow from measured rotational speed and measured pressure ratio is ill-conditioned by the flat curves of constant rotational speed in the compressor characteristic (Appendix C.5). Not strictly the ill-conditioned reconstruction, however, but also inevitable model mismatches and (systematic) measurement errors influence the reconstruction of the mass flow. Also the non-validated influence of the ambient conditions exerts influence on the reproducibility of the reconstruction of the compressor mass flow. Even small deviations may cause large errors in the reconstructed mass flow when measured or filtered data are substituted into the static equation for the mass flow. The reconstruction may even fail for certain combinations of measured pressure ratio and measured rotational speed. This is, for instance, the case when the measured pressure ratio is too high compared to the measured rotational speed. In simulations, when there are no model mismatches nor measurement noise, it is possible to reconstruct the mass flow properly. This is why the problem is only encountered in the real-time setting. In the next chapter we discuss the control of the laboratory gas turbine and deal with this problem extensively.

A conclusion is that the first order filter cannot solve this reconstruction problem completely. A few remedies for this problem are worth discussing. First, a well implemented *augmented* Kalman filter, that corrects the model states in such a way that the model outputs correspond to the measured process outputs is expected to improve the reconstruction. The implementa-

tion of this augmented Kalman filter has not yet been performed and tested in this thesis. We recommend it for future work. A major problem is whether the augmented Kalman filter can observe the full state, that is, whether the process outputs contain enough information to reconstruct all states (including offsets). Also the inherent ill-conditioning of the compressor map remains a serious obstacle.

Other solutions are based on a different model description. It may, for instance, be useful to reformulate the (mathematical) description of the compressor characteristic. Also, a direct measurement of the mass flow would benefit the problem as reconstruction becomes unnecessary. Finally, we realise that the problem is introduced by the compressor mass flow. It may be useful to reformulate the control problem (and the inherent modelling) such that the compressor mass flow is not used at all. For instance, the compressor may be replaced by the (measurable) orifice mass flow, or the expander mass flow.

Theoretical properties In this study we investigate MPC from a practical point of view. We do not concentrate on theoretical properties of receding horizon control like *stability* and *controllability* analysis. In this concluding section, however, we introduce some results on both properties for reference.

Stability Controllers are designed to stabilise the system and to meet certain performance requirements. For model based controllers like MPC, often a decomposition into *nominal* and *robust* stability and performance is made. The nominal model is assumed to describe the system to be controlled perfectly. This means that the internal model in the MPC controller equals the system or that the same model is used to simulate the system. Then, nominal stability refers to the stabilisation of the nominal model and nominal performance considers the performance of the nominal closed-loop system. Nominal stability is a minimal requirement on the stability of the closed-loop control system and nominal performance is the first step for tuning the controller in the closed-loop.

In general, the internal model is not equal to the system to be controlled. Robust stability refers to the stabilisation of the closed-loop system when the internal model does not describe the system perfectly. All kind of model uncertainties (parametric variations or unmodelled disturbances) can be taken into account. Robust performance, finally, concerns the performance of the controlled system when the internal model does not describe the system perfectly, or in other words, irrespective of changes in the systems dynamics.

Because of the receding horizon and the explicit constraints, it is difficult to guarantee the stability of MPC [Kuznetsov, 1996]. Only in the case of infinite horizons the nominal stability of linear MPC has been proved for both unconstrained [Bitmead, 1990], [Muske, 1993] and constrained MPC [Rawlings, 1993], [Zheng, 1995]. The last only holds under the condition of a feasible QP problem. When the constrained problem is rendered feasible by weighting of the constraints violations (as we implemented in Primacs), in theory the controller can stabilise the system. Of course this is not possible for all types of constraints, especially not for physical or safety constraints like surge.

New controller types provide stability guarantees with finite horizons. The key idea is to use equality constraints at the end of the prediction horizon to force the controlled output to match the set point [Mosca, 1992], [Clark, 1991]. The presence of a terminal equality constraint,

however, places an heavy requirement on the on-line optimisation. The weight of this constraint can be selected equal to the cost incurred by a stabilising linear control law.

With regard to the stability properties of non-linear MPC, the same approaches are followed. Also in this case a terminal constraint can be applied. Assuming linearisability of the linearised system, local exponential stability of the equilibrium is guaranteed. The region of attraction grows with the length of the control horizon. More recently, schemes have been proposed that combine a terminal penalty with a terminal *inequality* constraint. A review of stability of non-linear receding horizon control is presented in [De Nicolao, 1998]. With regard to robust stability, it is possible to formulate the linear, unconstrained controller within the H_∞ theory [Lee, 1994]. Recent developments also concern the non-linear H_∞ control problem [Magni, 1998]. We will not address these items in this thesis any further.

Controllability and observability With respect to controllability and observability the usual analysis for linear systems can be followed for linear unconstrained MPC. The inherently non-linear influence of constraints makes this analysis impossible for constrained MPC. Of course, this holds even more for an analysis of controllability and observability of non-linear predictive control. Again, these items will not be addressed in this thesis.

6 MPC on the gas turbine installation

This chapter describes the application of Model Predictive Control on the laboratory gas turbine installation. First, the control case of the gas turbine is specified including a discussion of the control objectives, the constraints, the inputs and outputs, and a presentation of the real-time implementation in Primacs. Second, the selection of appropriate model combinations and the tuning of the controller are motivated. This section also deals with the question whether MPC is achievable with respect to computation time and stability. In the remainder of the chapter, simulation results and real-time experiments are presented and analysed. Points of attention for the evaluation of the MPC controller are the quality of control (*performance*), the robustness of MPC (*robust performance*), and special *advantages* like constraints handling and anticipation. The settings of all parameters, set points and constraints for all experiments (including simulations) that are presented in this chapter are included in Appendix F.

6.1 Gas turbine control

6.1.1 Control objectives

Two control objectives for the laboratory gas turbine installation are formulated and summarised in table 6.1. The first, and most involved, objective is to control the operating point of the gas turbine. This objective serves as an appropriate tool to investigate set point and trajectory control. The operating point of the installation can be represented in either the compressor characteristic or in the expander characteristic. In the compressor map, the controlled outputs can be the pressure ratio over the compressor, the mass flow through the compressor, and the rotational speed of the gas turbine. Of course not all three variables can be controlled independently since two out of three determine the exact position in the characteristic. This is not a controllability item, since the mass flow through the compressor is not an independent state. It is an algebraic function of the two states pressure and rotational speed. Equivalently, when the operating point is displayed in the expander characteristic, the controlled outputs are the pressure ratio over the expander and the mass flow through the expander. Control of the operating point is a multivariable problem with two inputs and two outputs. Note that although three electrically powered valves serve as inputs to the system, here only the fuel valve and the throttle valve are used for control (see the discussion in Chapter 2).

	Control objective	Controlled process outputs	Manipulated inputs	Disturbances
1	Control of the operating point of the installation	(p_2, N) , or (p_2, \dot{m}_c) , or (N, \dot{m}_c) , or (p_3, \dot{m}_t) , etc.	fuel valve and throttle valve	compressed air supply (feedback only)
2	Speed control	N	fuel valve only	throttle valve (feedforward, feedback)

table 6.1 : Control objectives for the laboratory gas turbine installation.

The second control objective, speed control, is particularly interesting because of the disturbance that may be added: the position of the throttle valve. Varying the throttle valve induces additional (pressure) losses over the gas turbine that simulate changing load conditions. Be-

cause no external connection to the gas turbine axis is available, it is impossible to impose a direct load disturbance to the axis. When, however, an external load can be simulated, the opportunity to investigate more realistic control problems is created. The most common type of load used with a gas turbine is the electric generator which runs at a constant speed with the load varied electrically. The corresponding control problem is then to keep the rotational speed constant over changing loads. Translated to the laboratory set-up, the throttle valve is no longer an input to the system but an external disturbance. This control objective is SISO: The only input is the fuel valve position that controls the only output, the rotational speed. Note that the disturbance (throttle valve position) is measured, and therefore exactly known, which may lead to a feedforward control. This information can also be disregarded, leading to a feedback control.

6.1.2 Constraints

An overview of all the constraints imposed on the controller is presented in table 6.2. We distinguish constraints on the inputs and constraints on the outputs.

Constraints on the inputs:			
Valve	Move Constraint	Low Constraint	High Constraint
Blow-off valve	0.022255	0	1
Throttle valve	0.013636	0	1
Fuel valve	0.034325	0	1

Constraints on the outputs:			
Output	Constraint penalty	Low Constraint	High Constraint
expander temperature (T_{cc})	$\gg 1$ (99)	-	925
rotational speed (N)	$\gg 1$ (99)	325	550
surge ratio (R_{surge})	$\gg 1$ (99)	-	0.97

table 6.2 : Constraints on the laboratory gas turbine.

The move constraints on the inputs reflect the maximum valve speed related to the sample interval (Appendix D.2). The high constraints on the temperature and on the rotational speed are set by the manufacturer's specifications. The low constraint on the speed is selected because of model limitations. Below 325 rev/s most of the fits in the model are extrapolated and the model predictions become inaccurate. The output constraint penalties listed in table 6.2 are only used when one or more constraints are exceeded and the controller weights the constraint violations. A relatively high value of these penalties ensures that the process returns within constraints.

To keep the process on a safe distance from surge, a value of $R_{surge} = 0.97$ has been selected as a high constraint. The surge ratio R_{surge} is an additional model output, a measure of the distance of the actual operating point to the surge line in the compressor characteristic. R_{surge} is defined as the ratio of the mass flow at the surge line on the current constant rotational speed line and the compressor mass flow of the actual operating point. Surge avoidance is not a primary control objective but is always required. It involves a constraint on the location of the operating point in the compressor characteristic: the surge line in the compressor characteristic may never be exceeded. The constraint on the expander temperature is interesting because this temperature is (normally) not a controlled output but significantly influences the (dynamical) behaviour of the installation.

6.1.3 Outputs and filter

All process variables that need to be controlled or that are constrained, are required to be measured directly from the process or to be reconstructed from other measured data. In table 6.3 all five measured outputs of the installation are gathered. Since the compressor temperature is neither controlled nor constrained, it is not used for control. Also the ambient pressure ($p_{amb} = p_1$) and the ambient temperature ($T_{amb} = T_1$) can be measured. As they are reasonably constant, we assumed constant values of $1.013 \cdot 10^5$ Pa and 297.5 K respectively in our simulations and experiments. Therefore, also the pressure ratios of compressor and expander may be considered as measured process outputs.

Description	Process measurement	Corresponding model output	Controlled	Constrained
compressor pressure	p_2	p_{comp}	x	
compressor temperature	T_2	T_{comp}		
expander pressure	p_3	p_{cc}	x	
expander temperature	T_3	T_{cc}		x
rotational speed	N	N	x	x

table 6.3 : Process measurements and corresponding model states (outputs) that may be controlled or constrained.

Table 6.4 summarises the model outputs that may be controlled or constrained, and cannot be measured directly. The corresponding process values should be reconstructed from measured data by the filter. The non-linear observation model can be used for this reconstruction, applying the model equations indicated in the table.

Model output	Symbol	Controlled	Constrained	Reconstruction from measurements
mass flow compressor	\dot{m}_c	x		$\dot{m}_c = f(N, \frac{p_2}{p_1})$
mass flow expander	\dot{m}_t	x		$\dot{m}_t = f(\frac{p_3}{p_4}, T_3)$
compressor power	P_c	x		$P_c = \dot{m}_c C_{p,c} (T_2 - T_1)$
expander power	P_t	x		$P_t = \dot{m}_t C_{p,t} (T_3^* - T_4^*)$
surge ratio	R_{surge}	x	x	$R_{surge} = \frac{\dot{m}_{surge}}{\dot{m}_c}$
cooled expander inlet temperature	T_3^*			$T_3^* = f(\dot{m}_t, T_3, p_3)$
expander outlet temperature	T_4^*			$T_4^* = f(T_3^*, \frac{p_3}{p_4}, \eta_t)$

table 6.4 : Model outputs that may be controlled or constrained, and cannot be measured.

All process outputs that need to be reconstructed from available measurements relate to the mass flows through compressor and expander. From these mass flows, the surge ratio can be determined and the power required by the compressor and the power delivered by the expander can be reconstructed. In doing so, the cooled expander inlet temperature T_3^* and the efficiency η_t of the expander are required.

In this real-time setting, due to model mismatches and measurement noise, the mass flow through the compressor cannot be reconstructed accurately by the first order filter. This has been discussed in section 5.3. It is, therefore, impossible to consider the mass flow through the compressor as a controlled output. It is, however, known as an internal model value and can be controlled in *open-loop*. This means that only the internal model value is being controlled and that this variable is not updated by its reconstructed process counterpart. (This is equivalent to a filter gain of 0.) The same holds for the surge ratio and the compressor power, that are dependent on the mass flow.

On the other hand, due to the much better conditioned reconstruction of the mass flow through the expander, it appears possible to use this mass flow as a controlled variable. Therefore, the most useful combinations of process quantities to control the operating point of the installation do not include the mass flow through the compressor. From all possible combinations, (p_2, \dot{m}_t) , (p_3, \dot{m}_t) , (p_3, N) , or (N, \dot{m}_t) are valid in experiments.

The filter gain determines the fraction of the deviation between model output (y_m) and process output (y_p) that is added to the model output. A qualitative and quantitative analysis of experimental results in Appendix D.8, shows that when the filter gain increases, the contribution (for a particular experiment) of the set point deviations to the total criterion value decreases while the contribution of the inputs increases. This suggests that a minimum total criterion value can be expected at an optimal filter gain. The criterion value, however, depends strongly on scaling and weighting of inputs and set points. We did not attempt to tune the filter, as this would require many experiments. A filter gain of 0.3 performs well and is used in most experiments (See also Appendix D.8).

6.1.4 Real-time implementation

To realise closed-loop control, the gas turbine installation, the data acquisition system, the valve positioning system and the controller are included in a control loop. This control loop is depicted schematically in figure 6.1. The data acquisition and valve positioning systems have been implemented in LabVIEW (see Appendix D). The controller has been implemented in Primacs on a separate computer. Both computers are connected by a LAN network and communicate by means of the Dynamic Data Exchange (DDE) protocol.

During closed-loop control, the LabVIEW data-acquisition system performs measurements on the installation, which are processed and passed through to the controller (via the filter). Primacs computes optimal new valve positions (set points), which are passed through to the valve positioning system. The valve positioning system implements the desired valve positions as accurate as possible.

An important issue is the interaction between the completely independent timing of the controller and of the data acquisition system. Whenever new inputs, computed by the controller, are not implemented fast enough, or when new measurement data is not updated fast enough, dead time problems may cause performance degradation. To prevent these problems, a multi-rate system has been introduced, that is, different sample rates for data-acquisition and the controller. The sample rate of the data acquisition system has been chosen as high as possible. In practice, the controller picks up these measurements only when it needs new data and will always find the most recent data. Also the valve positioning system checks as often as possi-

ble if it needs to implement new valve positions, that is, whether Primacs already has computed new set points. Because of the multirate implementation, the overall timing of the controlled system is determined by the controller and completely independent of the data-acquisition system. For the data acquisition system, a sample interval of 0.1 s has been chosen. The controller uses a sample interval which is more than 10 times higher. Therefore, the maximum time delay between LabVIEW and Primacs is limited to 0.1 seconds.

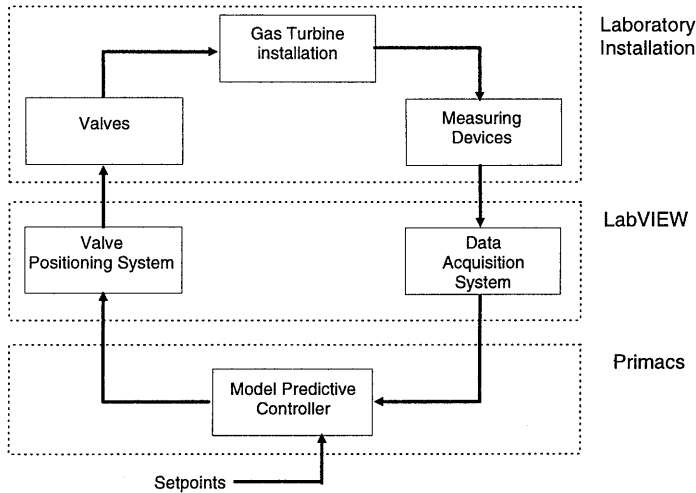


figure 6.1 : Closed-loop control configuration of the gas turbine installation.

6.1.5 Resolution of valves and minimal input move

In appendix D.2, we show that there is a minimal step size which can be implemented by the valve positioning system. This implies that there also must be a minimal set point change which can be realised by the controller. This minimal step size limits the performance of the system, because small set point changes cannot be realised.

Because it is not included in the (linear) models, MPC cannot account for the minimal step size in its optimisations. When the controller eliminates a small set point deviation, it computes a small step in the (fuel) valve. Because the small step cannot be implemented on the installation, MPC observes (through the filter corrections) that its input-change did not have the intended effect and computes another small additional step. This process continues until the successive small steps have accumulated to a step that can be implemented. Most likely, however, this step is too large and the process exceeds its set point. Then, the accumulation of inputs starts all over again at the other side of the set point. The result is that the process keeps moving around its set point with continuous control actions. The same happens when there is measurement noise, or when a control input is not very effective within a certain range (like the almost open throttle valve).

A simple way to solve this problem is to define a threshold range around the set point values. While the process measurement is within this range, the corresponding filter gain is temporarily set to zero. The model predictions are no longer updated by filter corrections, allowing the controller to reach the set point *for the internal model*. The process, however, does not reach its set point completely. The threshold levels of individual signals have been determined from

an analysis of both the measurement-noise level and the sensitivity of minimal valve position changes on the signals. Its main function is to reduce control moves. The threshold is experimentally investigated in Appendix D.7. In most of the experiments and simulations in the remainder of this chapter, the threshold range has been applied.

6.2 Computation times and tuning parameters

In the implementation of MPC we apply four different model combinations, as stated in table 5.1. All cases are based on the non-linear lumped parameter model. This model has been derived in Chapter 3, and validated for the laboratory installation in Chapter 4. The full set of model equations is presented in Appendix C.2. Analytical expressions for the Jacobian matrices have been derived to facilitate fast linearisation in arbitrary operating points.

The most important tuning parameters of the MPC controller are the lengths of the prediction horizon and of the control horizon, and the size of the MPC sample interval. The length of the *prediction horizon* is determined by estimating the (largest) time constant of the system response to changes in the input. These step responses show a close resemblance with a step response of a first order system. A fair estimate of the time constants in the system is the time needed for the response to reach 63% of its stationary end-value. An exception is the response of the expander temperature to a step on the fuel supply. This response is characterised by a large peak. The response of the rotational speed and the expander temperature to a 3% step in the fuel valve are presented in figure 6.2. These results are obtained from a simulation with the non-linear lumped model. From this, a value for the prediction horizon of 20 seconds has been selected. This value is greater than any relevant time constant in the system.

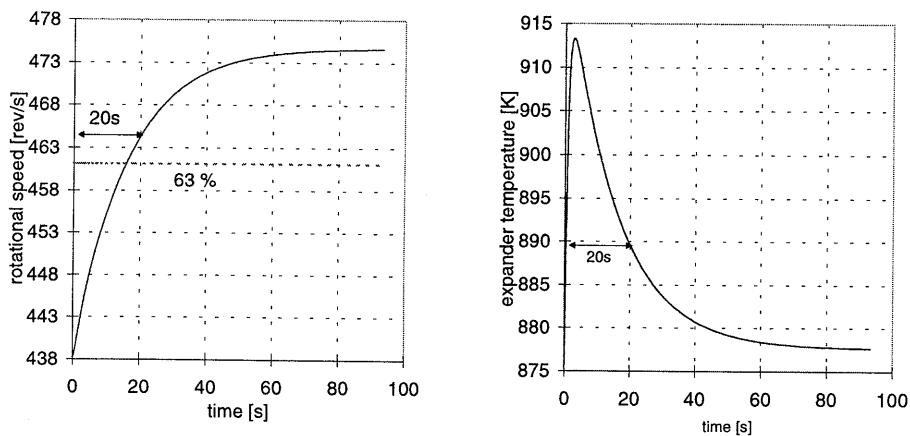


figure 6.2 : Simulation of the responses of rotational speed and expander temperature for a step in the fuel supply. Indication of semi-first order time constant of the system and the selected MPC prediction horizon.

As indicated in section 5.2.2, the *MPC sample interval* should be selected as small as the system requires and computation times allow. When the interval is decreased, more samples are needed in the control and in the prediction horizon to cover the same time span. This results in increased computational effort in a smaller sample interval. Computation time also depends on the type of models which are used and on the constraints the controller encounters. In ap-

pendix D.6 the computation times are determined in open-loop simulations for different sample intervals (and the accompanying sizes of the prediction and control horizon), for different model combinations, and for different constraint situations. The resulting minimal sample intervals (Pentium 200Mhz, Windows NT) are presented in table 6.5:

	Model combination	Minimum sample interval [s]
1	Linear MPC: Linear models for prediction and optimisation.	1.05
2	Non-linear MPC: Non-linear model for observation, successively linearised models for prediction and optimisation.	1.25
3	Non-linear MPC: Non-linear model for observation and prediction, successively linearised model for optimisation.	> 3

table 6.5 : Minimum required MPC sample interval for different internal model combinations of the laboratory gas turbine when one constraint is (permanently) exceeded.

In order to leave sufficient space for other processes on the computer, in all experiments a sample interval of 1.5 seconds has been used. According to the table, this sample interval allows the implementation of successive linearisation. These results also indicate the advantage of successive linearisation. It promises to deliver a significant improvement in controller performance with respect to linear MPC, while computation times are not so high that real-time implementation becomes impossible. Due to the high computation times, non-linear prediction is not used for real-time experiments. Note that the intended prediction horizon of 20 seconds corresponds to 13 samples or 19.5 seconds.

According to the rules of thumb, the *control horizon* should be selected between 1/6 and 1/3 of the prediction horizon. So in this case the control horizon should be between 3.33s and 6.66s, that is, 3 or 4 samples. A control horizon of 4 samples has been selected, as this leads to a faster system response (at least in simulations). Because this selection did not result in computation time problems, no control blocking has been applied.

Summarised, the selections made for the parameter values used in the experiments and simulations of this thesis are as follows:

prediction horizon	p	13 samples	19.5 seconds
control horizon	m	4 samples	6 seconds
MPC sample interval			1.5 seconds

6.3 Control of the operating point

Within the operation area, the controller should be able to reach a certain set point or to follow a prescribed trajectory. In this section, we investigate the performance of the controller by presenting and analysing different real-time experiments and simulations.

6.3.1 New set point within the operation area

In this first experiment we illustrate the controlled response to new set points on the combination of rotational speed (N) and mass flow through the expander (\dot{m}_t). Figure 6.3 shows the closed loop responses for a prescribed step-wise set point change up and down again. The actually realised process values (measured rotational speed and reconstructed expander mass flow) are compared to the internal model value of the controller. This model value is the output of the internal model (IOBM) that has already been corrected by the filter.

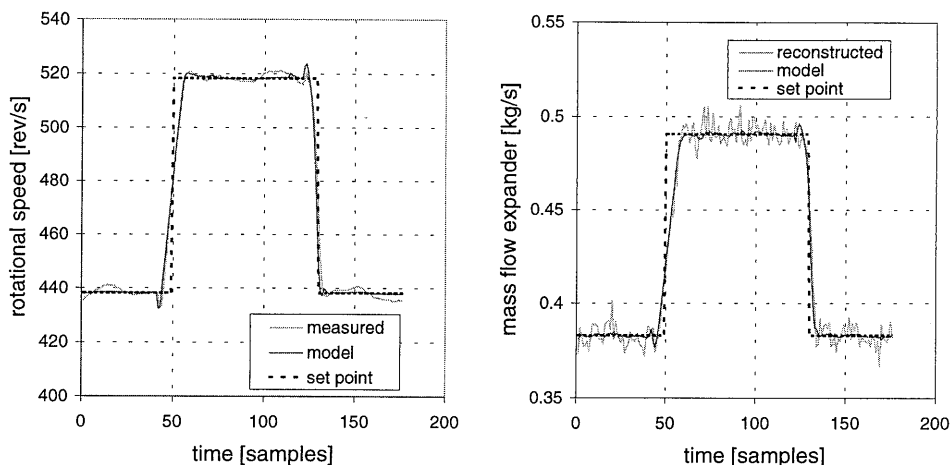


figure 6.3 : Response of rotational speed and expander mass flow to a new set point.

The figures show that the new set points are almost perfectly reached. Apart from some measurement noise, the steady state deviations (offsets) between process and model, that were encountered in the open-loop results of section 4.7, are completely eliminated by the filter.

Note that the controller already reacts 13 samples before the set point change is activated. This is a consequence of the anticipation of MPC, that is, its reaction to future set point changes as soon as they enter the prediction horizon. Also note that the outputs initially move in the “wrong” direction. This should not be confused with an inverse response, which the system does not exhibit. This phenomenon will be often seen in the simulations and experiments of this chapter. It is caused by the anticipation of the MPC controller and discussed in detail in section 6.6.

The input signals that realise these set point changes are presented in figure 6.4. Both the computed inputs (“controller”) and the actually measured valve positions are displayed. A small, one sample, delay can be seen between them. Indeed, the inverse response of the inputs, especially of the fuel valve can be seen.

In this particular experiment also the blow-off valve has been used as a control input. Indeed, the behaviour of the blow-off is unwanted because of the limited mechanical properties of the valve that results in unsatisfactory positioning of the blow-off valve, leading to a relatively large mismatch between the controller value and the actual valve position (figure 6.4). Moreover, the blow-off valve also tends not to come back to its original position

(corresponding to the initial operating point). This is mainly caused by the applied optimisation criterion (5.1) and the fact that two outputs are now controlled by three inputs. In other experiments, the blow-off valve has not been used anymore as a control input. Also the throttle valve does not return to its original position. The throttle valve shows a kind of “unstable” behaviour. This is caused by the relative insensitivity of the throttle valve when it is more than 70% open (see section 6.1.5). This effect is decreased by the application of a threshold on the set point, which is not yet applied in this experiment.

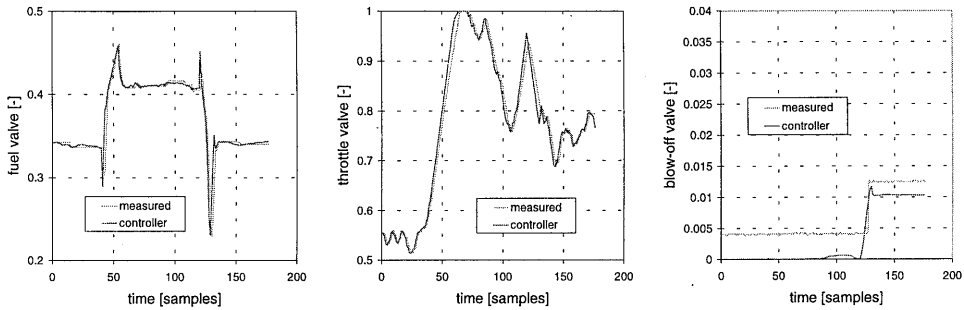


figure 6.4 : Corresponding input signals of three control valves.

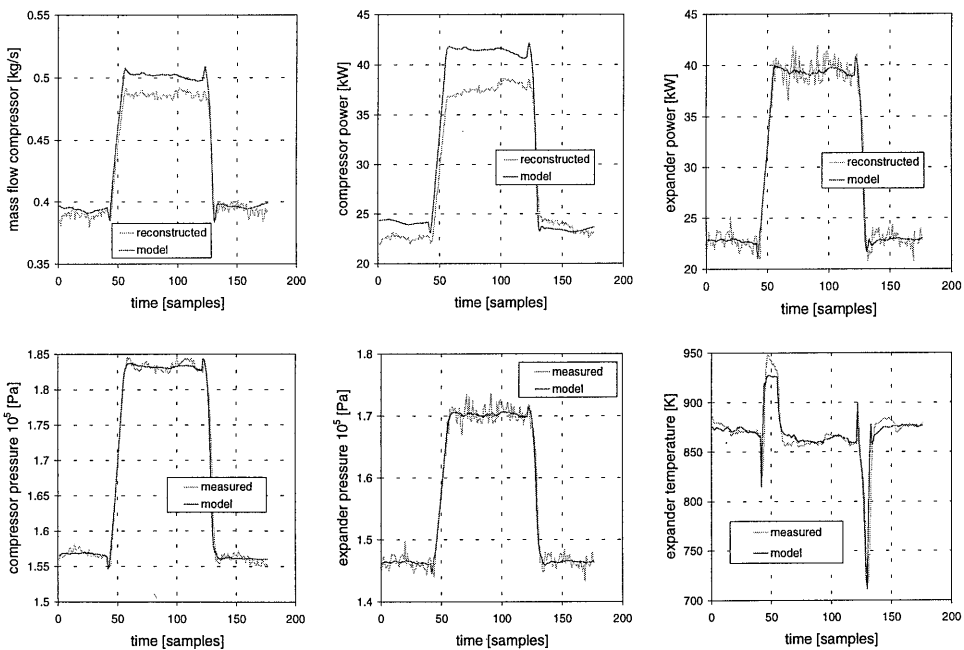


figure 6.5 : Unfiltered (mass flow compressor and compressor power) and filtered model outputs compared to measured (or reconstructed) process outputs.

In the previous explanation, we presumed the filter to compensate for mismatches between model and measurements for the set points. In figure 6.5 several other model outputs of the

same experiment are compared to the measured (or reconstructed) process outputs. In the upper row, the *unfiltered* compressor mass flow and compressor power are presented. In previous chapters we concluded that the compressor mass flow (and its derivatives like power and surge ratio) could not be reconstructed. Indeed, in figure 6.5, we see that large errors are encountered between the (unfiltered) model values and the reconstructed process measurements.

In the other graphs of figure 6.5, *filtered* outputs are gathered: expander power, compressor pressure, expander pressure and expander temperature. Due to the filter corrections, the correspondence between model and process is good. Apart from (high frequency) measurement noise, only in the expander temperature a slight dynamic mismatch can be seen. This is caused by the constraint on the temperature. In fact, the measured (process) temperature temporarily exceeds its constraint of 925 K while the model value does not. This problem will be discussed in section 6.4.3. A preliminary conclusion is that the current filter setting (with a gain of 0.3) is fast enough to prevent too large deviations between process and model and prevents the controller for unnecessary actions on measurement noise.

6.3.2 Constraints and operation area

The constraints, introduced in table 6.2, on the rotational speed, the surge line and the saturation of the throttle valve position (minimum pressure drop between compressor and expander) determine the operating point of the installation. Additional constraints on the maximum allowed expander temperature and the surge ratio, further decrease the area of operation. Figure 6.6 displays the operating area of the gas turbine installation in the compressor characteristic. This result is obtained from simulations with the non-linear lumped model. Although the same operation area can also be displayed in the expander characteristic, this figure is omitted here because the operation area almost reduces to a single line, especially in a dimensionless characteristic.

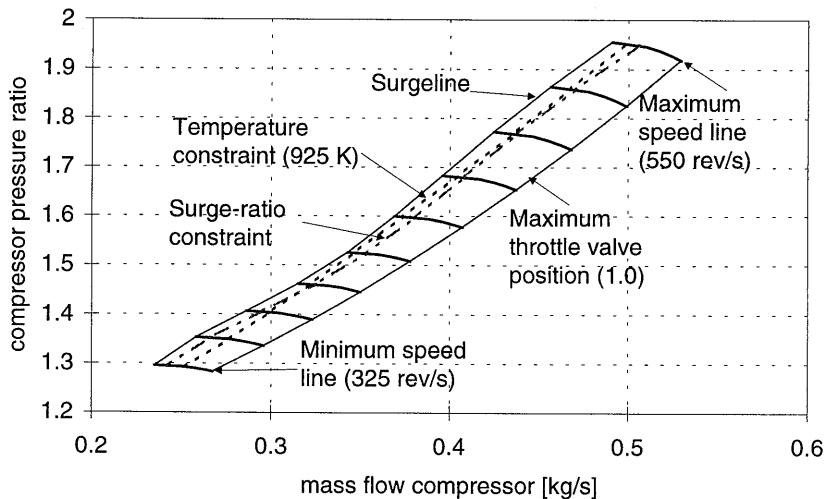


figure 6.6: Operating area of the laboratory gas turbine installation displayed in the compressor characteristic.

Close to the surge line, the (simulated) operating area is restricted by two alternating constraints. Depending on the rotational speed, either the surge ratio constraint or the temperature constraint restricts the operating area. The intersection point of these two constraint lines is at a rotational speed of approximate 400 rev/s. In two experiments, it is examined whether the controller “stops” at the surge ratio constraint or at the temperature constraint for different rotational speeds.

In both experiments, the mass flow through the expander and the rotational speed have been defined as set points and the weighting of the rotational speed set point is set high compared to the mass flow set point. The starting points for the two different experiments are a mean rotational speed of 438 rev/s (corresponding to 0.38 kg/s for the expander mass flow) and a low rotational speed operating point of 350 rev/s and a corresponding mass flow of 0.29 kg/s. In both experiments, starting at sample 70, the mass flow set point is lowered slowly to 0.28 kg/s and 0.19 kg/s respectively, while the set point on the rotational speed is kept constant. These new operating points are unreachable as they are located within the surge area.

For easy comparison, the results of both experiments are combined in the same figures. Figure 6.7 shows that in both experiments the controller manages to keep the rotational speed set point, whereas the trajectory to a lower mass flow set point cannot be followed anymore.

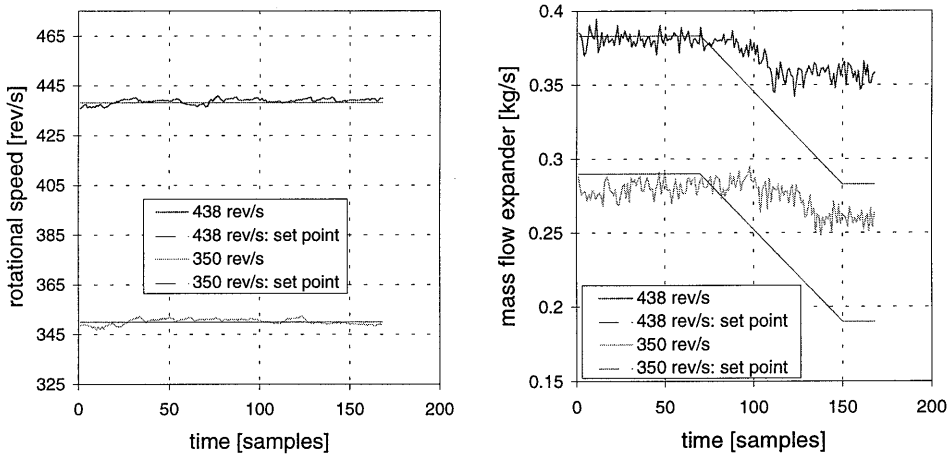


figure 6.7 : Measured rotational speed and corresponding expander mass flow compared to the set points for two different values of the rotational speed set point.

The corresponding constraints are indicated in figure 6.8. This figure shows that at the high rotational speed, the controller stops at the surge ratio constraint, while at the low rotational speed, the controller stops at the temperature constraint. These results completely compare to the expected results from the simulation. Indeed, the operating area is restricted at high rotational speeds by the surge ratio constraint, while at low rotational speeds the operating area is restricted by the temperature constraint. (Note that the surge ratio has been controlled in open-loop, based on the internal model value only).

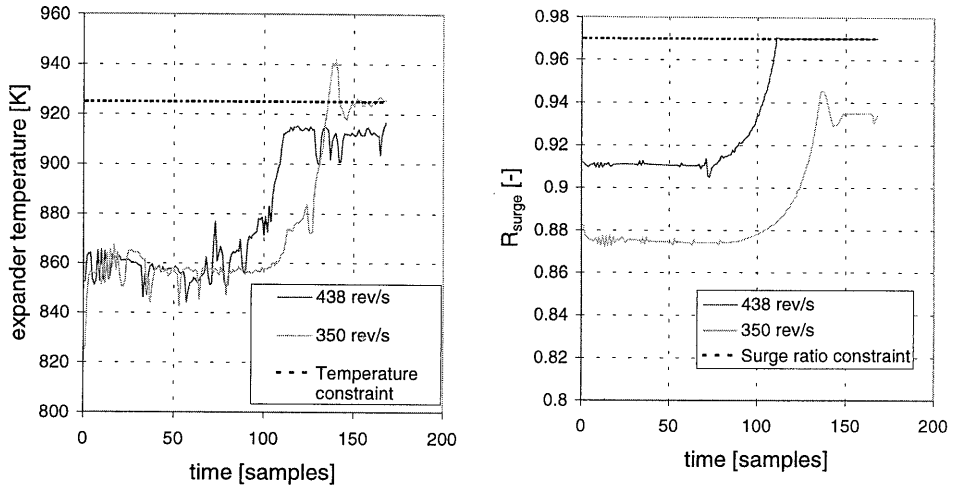


figure 6.8 : Measured expander temperature and surge ratio compared to the constraint levels for two different values of the rotational speed set point.

6.3.3 Unreachable set point

In the previous section we saw that the new operation point cannot be reached when new set points are prescribed that lay outside the operating area of the gas turbine. The remaining deviations are determined by the output weightings on the controlled variables. In this section the influence of the output weightings is examined in two experiments. For these experiments, an identical set point trajectory to an unreachable set point in the expander characteristic has been specified. The set point on the expander pressure is constant at 1.46 bar, while at sample

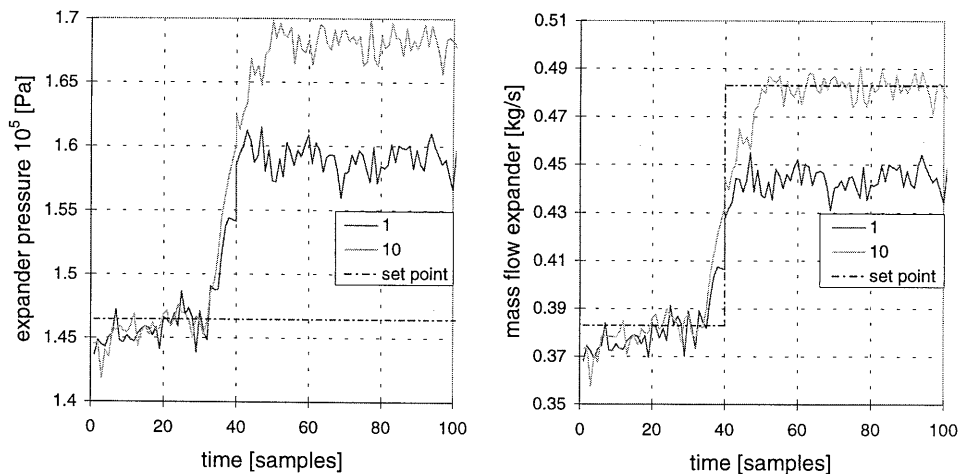


figure 6.9 : Measured expander pressure and mass flow through the expander compared to the corresponding set points for different values of the set point weighting of the mass flow.

40 a step in the expander mass flow has been specified from 0.38 kg/s to 0.48 kg/s. The experiments have different set point weightings on the mass flow of 1 and 10 respectively. In both cases the set point weighting on the pressure is equal to 1. The results are presented in figure 6.9.

In both cases the controller tries to reach the desired operating points as close as possible, but they are never reached. In the case where the mass flow weighting is 1, the resulting deviation is distributed between the two variables, while in the case where the mass flow weighting is 10, the set point deviation disappears for the mass flow, at the expense of the expander pressure. Note that when the set point weighting on the mass flow is increased from 1 to 10, the contribution of this set point deviation to the total criterion is increased quadratically (100 times). Also recall that the absolute value of the model parameters in the controller criterion has been scaled to the original operating point (Appendix D.3).

From this experiment it can be concluded that the controller tries to get as close as possible to the operating point, but is stopped by one of the constraints which limit the operating area. In this experiment that constraint is the fully opened throttle valve. The resulting operating point is determined by the set point weightings. The higher the weighting on a certain set point relative to another, the closer the controller will try to reach that particular set point.

6.4 Transient response

Controller performance can also be approached from a dynamic point of view as how fast a new set point is reached or how well a dynamic trajectory can be followed. The speed by which a new set point can be reached, basically depends on the inputs (weightings and move constraints) and on the output constraints the controller encounters. In this section, first an illustration of a transient response is shown, after which the influence of the input weightings and of the output constraints is investigated.

6.4.1 Transients during set point change

Interesting transients are the mass flows through compressor and expander. When the mass flows are known, the resulting trajectory can be indicated in the (compressor) characteristic, possibly indicating dynamic problems such as temporarily exceeding the surge line. In the following simulation, the transient behaviour during a set point change is presented. In a simulation neither measurement noise nor model errors disturb a clear view of the transient. This holds especially since these mass flows cannot be measured directly.

As before, a new set point is specified in rotational speed and expander mass flow. In figure 6.10 the transient response of the mass flows through compressor and expander are compared by the different trajectories in the compressor map (left) and in a time plot (right).

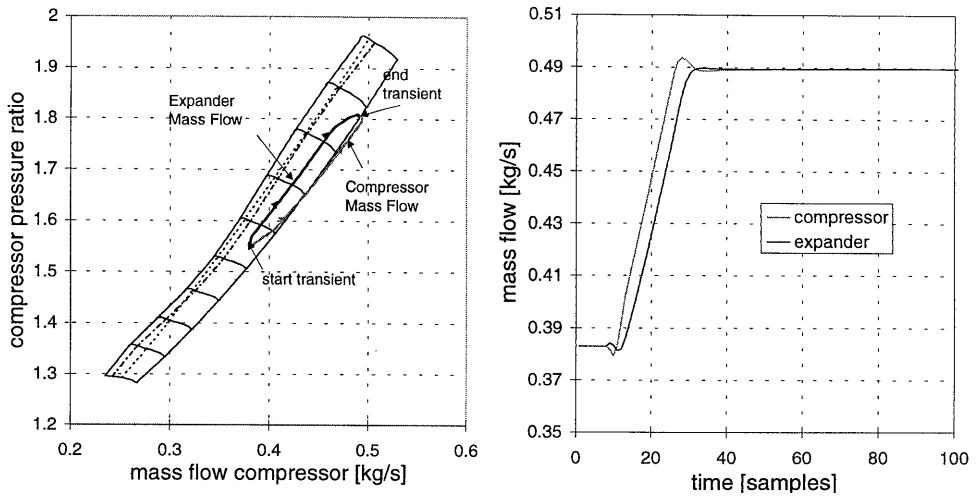


figure 6.10 : Transient response to a new set point specified in rotational speed and mass flow through the expander (obtained from simulation).

Interesting is the downward transient, that is, the transient back to the original operating point. This transient is shown in figure 6.11 in the compressor map. In figure 6.12 the surge ratios for both transients are shown. Typically, the surge constraint is much more involved in the downward transient. This means that for a gas turbine system like the laboratory installation, there is a potential danger of surge during fast “downwards” transients. A typical example is emergency shutdown. A dynamic model in the controller is able to anticipate to this problem.

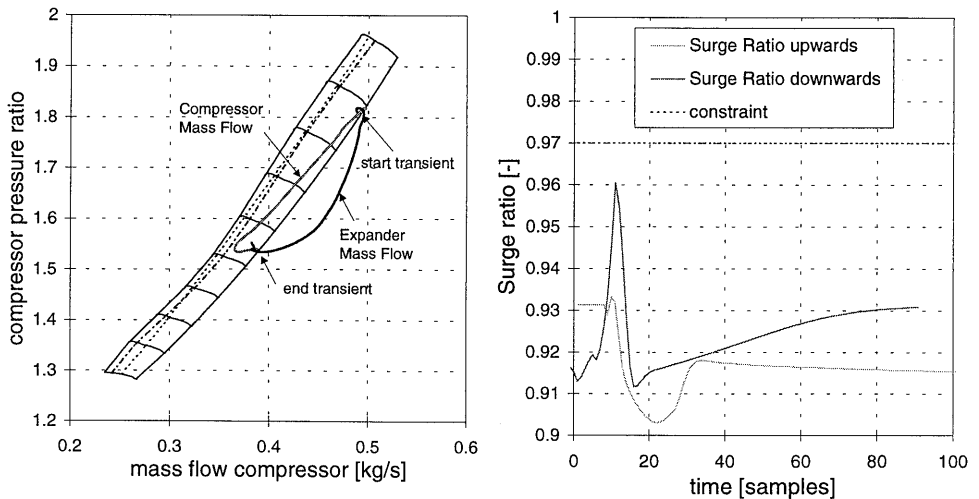


figure 6.11 : Transient response back to the original set point.

figure 6.12 : Surge ratio for both transients.

6.4.2 Influence of the input weightings

Of course, the input move constraints influence the dynamic system response. Completely determined by the maximum valve speed, they are, however, no tuning parameters. Only the input *weightings* can be changed. The system response is expected to slow down when the input weightings are increased. The influence of the input weightings is examined in three simulations (to avoid confusing measurement noise) for three different values of the input weighting on the fuel valve.

As a reference trajectory, at sample 20 a step in the rotational speed from 438 rev/s to 518 rev/s has been specified, as well as a corresponding step in the expander mass flow from 0.38 kg/s to 0.49 kg/s. At sample 170 a step back to the original operating point has been specified for both outputs. This simulation has been performed for a weighting of 30, 15, and 0 on the fuel valve position respectively. A zero weighting on the fuel valve implies that the moves of the fuel valve are not penalised. The results are shown in figure 6.13.

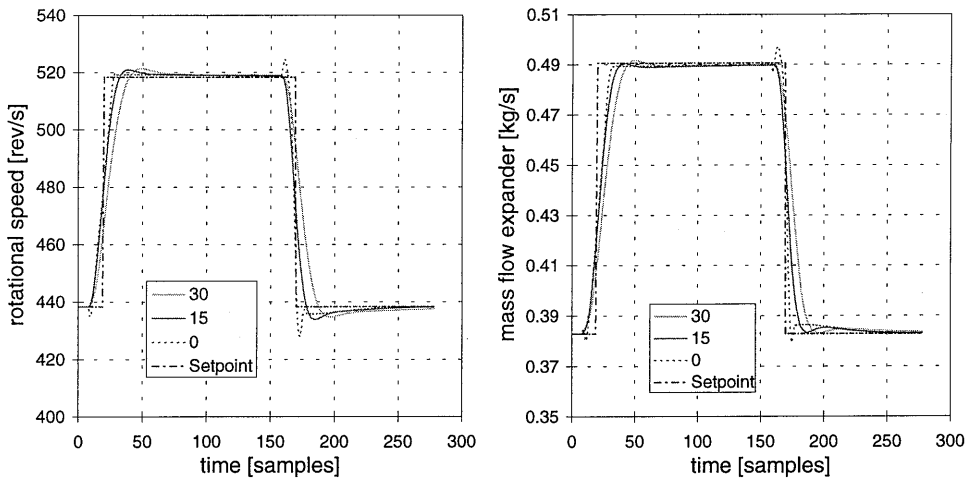


figure 6.13 : Simulated rotational speed and mass flow through the expander compared to the corresponding set points for different values of the input weightings.

The results agree with our expectations. The input weighting influences the speed of the controller. When the weighting on the fuel valve is 0, the fastest system response is obtained, while the slowest response holds for the input weighting is 30. There is, however, a significant difference between the step to a higher set point and the step to a lower set point. For instance, for an input weighting is 15, the response on the step to a higher set point is only slightly slower than weighting is 0, whereas the response on the step to a lower set point is significantly slower.

This result can be explained by the influence of the constraint on the expander temperature. The corresponding expander temperature is presented in figure 6.14, showing that for values 0 and 15 of the input weighting the temperature constraint is reached when a set point to the higher operating point is prescribed. In these cases the resulting speed of the system response is (partly) governed by the temperature constraint. Only in the case where the input weighting is 30, the penalty on a fuel valve move is so high that the temperature constraint is not reached anymore.

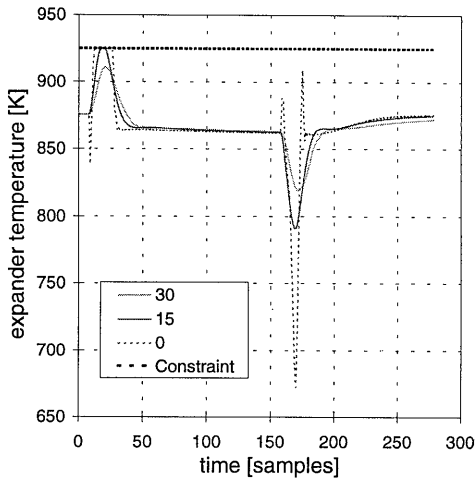


figure 6.14 : Expander temperature for different values of the input weightings.

When the system is set to a lower operating point, it is not slowed down by the temperature constraint at all. For a zero weighting on the fuel valve, the speed of the system response is governed by the maximum valve speed. Note the large temperature peak that results. For an input weighting of 15 or 30, the speed of the system response is only governed by the input weighting, and the system response becomes comparatively slower.

The “normal” weighting factor on the inputs, used in all other experiments and simulations in this chapter is 1.0.

6.4.3 Influence of temperature constraint

In the previous section the influence of the temperature constraint on the closed-loop system dynamics is already indicated. Now, this influence is examined in experiments. Again, consider a new set point for the rotational speed and the expander mass flow. At sample 20 a step in the rotational speed from 438 rev/s to 518 rev/s and a corresponding step in the expander mass flow from 0.38 kg/s to 0.49 kg/s are prescribed with at sample 170 a step back to the original operating point. This experiment has been performed for three different values of the temperature constraint: 880 K, 900 K, and 925 K. Results are presented in figure 6.15.

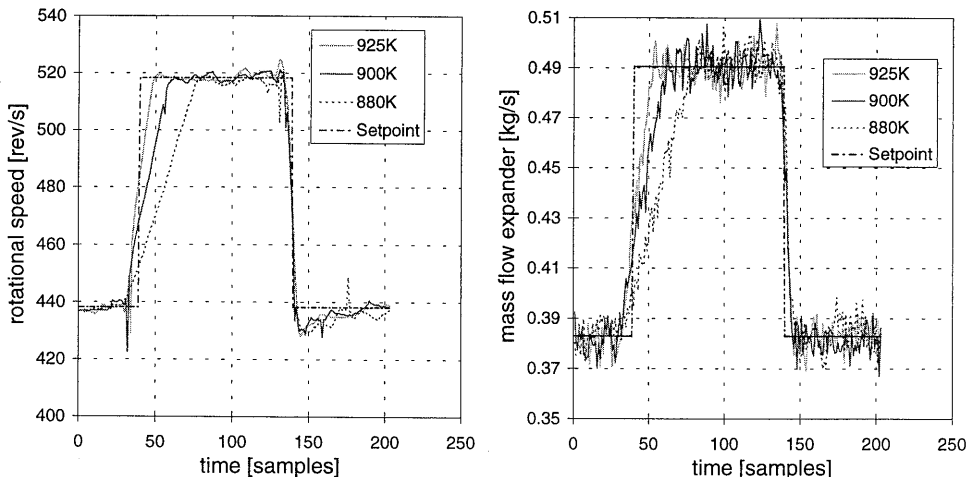


figure 6.15 : Measured response to a new set point specified in rotational speed and mass flow through the expander for different values of the maximum allowed expander temperature.

Lowering the maximum allowable expander temperature results in a slower system response. As the temperature may not exceed its constraint, while the system should accelerate as fast as possible, the allowed increase of the fuel flow per sample (or equivalently, the allowed input move) has to be reduced when the temperature constraint is lowered. As expected, the temperature constraint does not influence the response to a lower set point. In fact, these responses are approximately equal.

Figure 6.16 shows the corresponding expander temperature and the momentary value of the overall criterion for the three experiments. The criterion value is defined by

$$\text{criterion}(k) = \sum_{\text{setpoints}} \left[\Gamma^y (\text{measurement}(k) - \text{setpoint}(k)) \right]^2 + \sum_{\text{inputs}} \left[\Gamma^u (\text{input}(k) - \text{input}(k-1)) \right]^2 \quad (6.14)$$

and supports the previous result in a quantitative way. A lower setting of the temperature constraints corresponds to higher values of the criterion. Also the maximum criterion value shifts to a higher sample number.

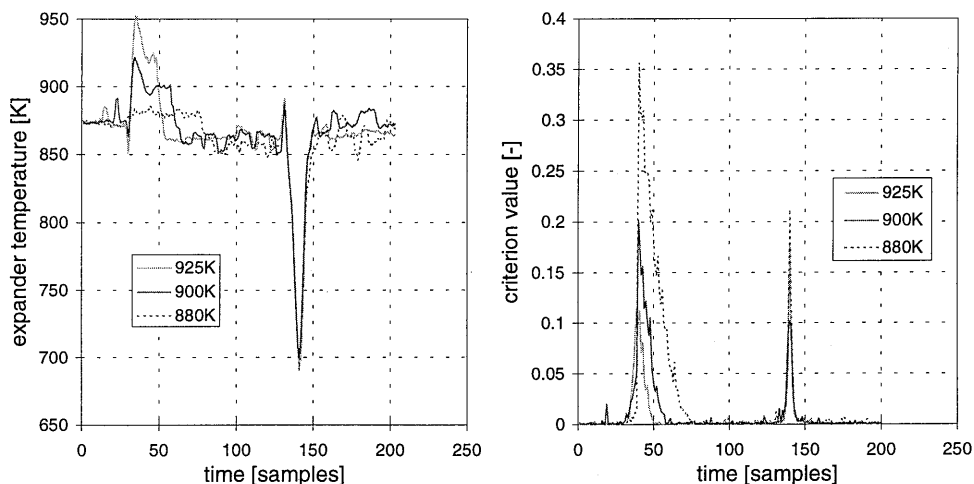


figure 6.16 : Expander temperature and overall criterion value during transient to a new set point for different values of the maximum allowed expander temperature

Clearly, however, the measured values of the expander temperature in figure 6.16 considerably exceed the constraint level. Indeed, the controller is capable of keeping the temperature within the constraints, but only for the (filtered) internal model predictions (not shown). The same phenomenon was already encountered in section 6.3.1 and displayed in figure 6.5.

This means that the controller is able for the constraint violation that is observed by the filter. During the transient, however, the mismatch between process measurement and internal prediction becomes so large that the filter is not able to correct it fast enough. This model mismatch has already been seen in Chapter 4 (see section 4.2.3). It appears hard to predict the expander temperature during transients. This is probably caused by an inadequate description of the (dynamic) combustion efficiency. In the present model, only steady state relations for the combustion efficiency as a function of fuel-air ratio are applied.

When we want to avoid the constraint violations, we can increase the filter gain for the temperature signal. This would be very effective, but also increase unwanted actions on measurement noise. Second, a faster MPC sampling would benefit the performance. Finally, the dynamic interaction between fuel valve changes and momentary temperature rise could be improved in the model. Still, a conclusion of this section is that the controller is capable of keeping the constraint reasonably well.

6.4.4 Trajectory control: sine response

This experiment illustrates the capabilities of the controller to track a periodic trajectory. A sinusoidal trajectory for the rotational speed (period 75 s, amplitude 80 rev/s, mean 438 rev/s) is specified while the throttle valve serves as a measured disturbance on the installation (sine with half frequency: period 150 s, amplitude 0.3, mean 0.7). In figure 6.17 both the sine of the trajectory and the disturbance are presented. Figure 6.18 shows the tracking result over a time interval of one full period of the disturbance in a steady state response, that is, after the switch-on phenomena.

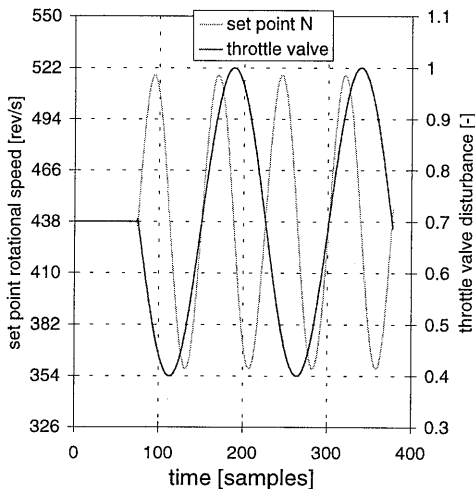


figure 6.17 : Sinusoidal trajectory for the rotational speed and the periodic (sine with half frequency) disturbance of the throttle valve.

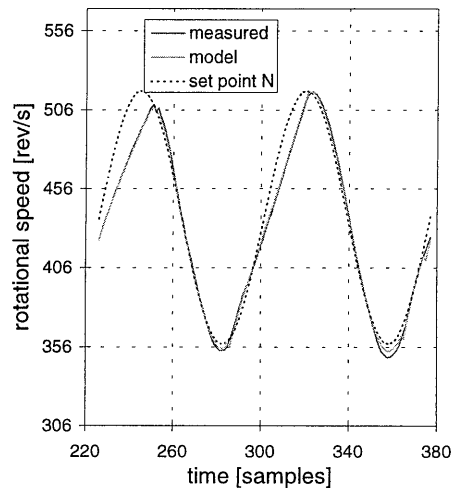


figure 6.18 : Measured and model response of the rotational speed (over the last two periods) compared to its set point.

Figure 6.18 shows that the controller is able to follow the trajectory on the rotational speed, except for the two rising flanks of the sine function. For these flanks, the temperature constraint is reached, as can be seen in figure 6.19, which displays the expander temperature over the same time interval. Moreover, a difference can be seen between the deviation at the first rising and at the second rising flank. This difference is caused by the opposite influence of the throttle valve disturbance in these two situations. At the first flank, the throttle valve is being closed from its mean position. At the second flank, the throttle valve is being opened from its mean position (see figure 6.17). The more the throttle valve is closed, the further to the left the operating point is on the compressor characteristic. This means that the mass flow through the system is smaller. So, at the first flank, the mass flow is smaller and tends to decrease further

which implies that the temperature constraint is reached earlier and less fuel can be added to accelerate the gas turbine. The deviation is therefore larger at the first flank.

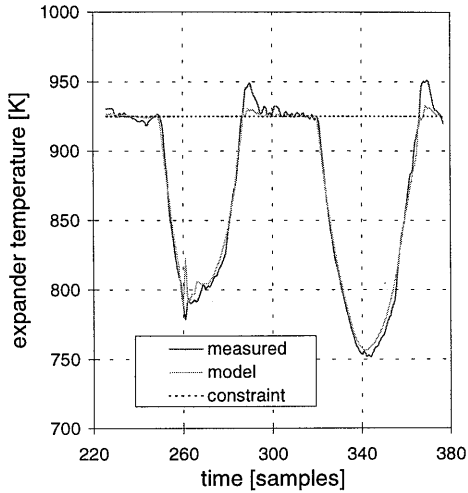


figure 6.19 : Corresponding expander temperature.

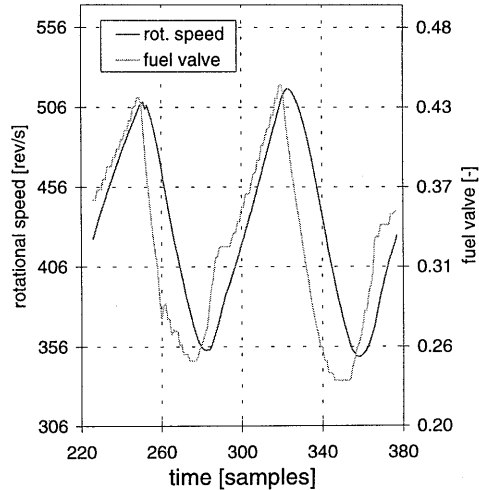


figure 6.20 : Comparison between the rotational speed and the fuel valve input.

Figure 6.19 shows that the controller indeed manages to keep the temperature within the constraints (although the measured temperature temporarily exceeds the constraints as we have discussed in the previous section). Finally, in figure 6.20, the realised rotational speed is compared to the input signal of the fuel valve. This graph illustrates the anticipative behaviour of the controller. Already 10-12 samples (one prediction horizon) before a change in sign of the derivative of the rotational speed, the fuel valve changes direction. The anticipative behaviour will be discussed in detail in section 6.6.

6.5 Robust performance

In this section the robust performance of the controller is investigated by means of presenting and analysing different real-time experiments and simulations. We do not seek to investigate theoretical criteria of robust performance for the gas turbine and its models. Robust performance implies the performance of the controller when disturbances or model errors are applied to the system.

We start this investigation with a treatment on the influence of different internal models in MPC on the performance. A different model may be regarded as a model error. With regard to disturbances, the most straightforward disturbance is the injection of compressed air from the utility network into the installation. Compressed air is an unmodelled, relatively large, disturbance. Another disturbance is the variation of the throttle valve when it is not used as an input to the system. In this case both feedforward (when the position of the valve is on-line available and the model predictions react on it) or feedback (when its position is unknown and only feedback information from changing process outputs is available) configurations can be tested. In the latter case additional model errors are introduced.

6.5.1 Different model combinations

Preliminary simulations with the different model combinations of table 5.1 (equal to table 5.1) on the gas turbine installation in [Vroemen, 1998] show the advantage of non-linear MPC methods. A non-linear model serves to simulate the gas turbine installation. These simulations are performed with a slightly different model of the laboratory gas turbine, in which the parameters were not yet validated. It contains no mass flow correction, constant efficiencies and a constant expander inlet cooling.

	Type of Model Predictive Control	Internal Observation Model	Internal Prediction Model	Internal Optimisation Model
1	Linear MPC (1xlin)	linearised once	linearised once	linearised once
2	Successive linearisation (sl)	non-linear	linearised successively	linearised successively
3	Non-linear prediction (nlp)	non-linear	non-linear	linearised once
4	Non-linear prediction and successive linearisation (nlp+sl)	non-linear	non-linear	linearised successively

table 6.6 : Combinations of models in non-linear MPC.

The results are presented in figure 6.21 and figure 6.22. Figure 6.21 displays a set point change at $t=20$ s in the compressor pressure and mass flow for four different model combinations. All approaches give satisfactory results, although the pressure response of linear MPC displays some overshoot. The temperature constraint is violated by linear MPC only. (Again, by the simulated process variable and not by the internal model value.) Figure 6.22 shows a set point change in the compressor mass flow that cannot be realised, because this operating point would result in both surge and temperature constraint violations.

The three non-linear methods all outperform linear MPC. The non-linear methods, however, do not outperform one another, although they take different execution times (see table 6.5). Especially the two methods (**sl** and **nlp+sl**) which incorporate successive linearisation in the optimisation model yield results very much alike, despite the very time consuming non-linear prediction model of method 4 (**nlp+sl**). Method 3 (**nlp**) gives only slightly different results as the other non-linear methods.

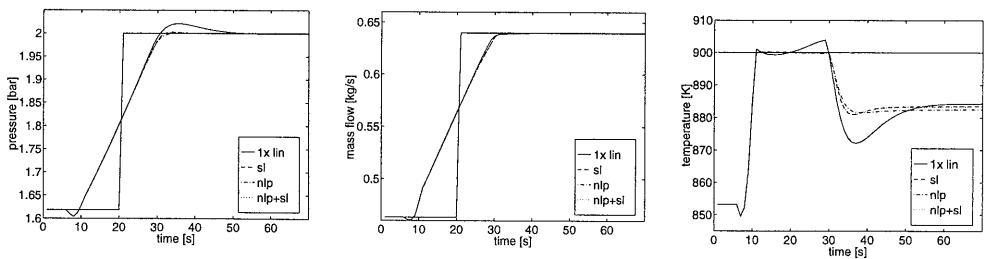


figure 6.21 : Compressor pressure, compressor mass flow, and expander temperature responses to a set point change in pressure and mass flow.

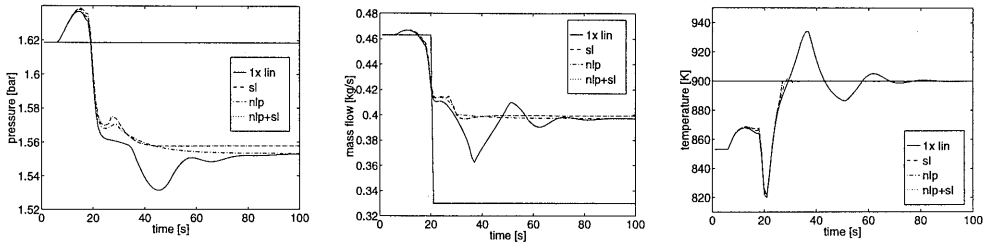


figure 6.22 : Compressor pressure, compressor mass flow, and expander temperature responses to an unreachable set point change in mass flow.

These results suggest that it is important to predict outputs by using some “semi” non-linear model. Furthermore, if successive linearisation is used to update the optimisation model, results are hardly dependent on the method of prediction: successive linearisation (method 2) or non-linear (method 4). Of course, computation times are considerably larger for the non-linear prediction. Both methods are implemented and tested on the laboratory installation. In some experiments in this chapter, linear MPC (method 1) is used as a comparison with successive linearisation. Method 3 has not been considered in practice, while method 4 takes too much time to be real-time implemented.

6.5.2 Model combinations and throttle valve disturbance

When the throttle valve is used as a disturbance, it is eliminated as a manipulable input for the controller. The throttle valve can be used as a measured or as an unmeasured disturbance. As a *measured disturbance*, its known position is used (as an additional “disturbance input”) in the internal models. In case of non-linear or successively linearised models, this also means that the model dynamics are adapted to the changing valve position. When the throttle valve is used as an *unmeasured disturbance*, one constant value is assumed for the throttle valve position in the internal models. The controller observes only indirectly, by means of the filter, the results of the changes in the throttle valve position. This situation can be compared with the case of a wrong parameter in the model.

In this section, three experiments examine the influence of a throttle valve disturbance on different model combinations. The experiments are indicated in table 6.7. Two non-linear experiments are compared with linear MPC. Linear MPC with measured disturbances uses a once linearised model in which changes in the dynamics of the system are not incorporated. Only the change in operating point is considered.

Experiment n ^o	model combination	throttle valve disturbance
1	linear MPC	measured disturbance
2	non-linear MPC: successive linearisation	measured disturbance
3	non-linear MPC: successive linearisation	unmeasured disturbance

table 6.7 : Experiments with three different model combinations and throttle valve disturbances.

For all experiments, the reference trajectory is defined as a series of ramps in the rotational speed. First from 438 rev/s to the minimum rotational speed constraint (325 rev/s), then to the maximum rotational speed constraint (550 rev/s) and finally back to the initial rotational speed. Before each experiment, the throttle valve is closed from 0.5 to 0.4, to introduce the disturbance.

We expect the system response to slow down when the throttle valve is closed. The operating point shifts towards the surge line and the temperature constraint is earlier reached. In the unmeasured disturbance case, the controller supposes that the valve is in its original position. The controller does not adapt its fuel flow and the system accelerates too fast, resulting in temperature constraint violations. Only the filter causes the system to slow down again. On the other hand, we expect that when the internal models know about the changed valve position, the controller will show the fastest response without temperature constraint violations.

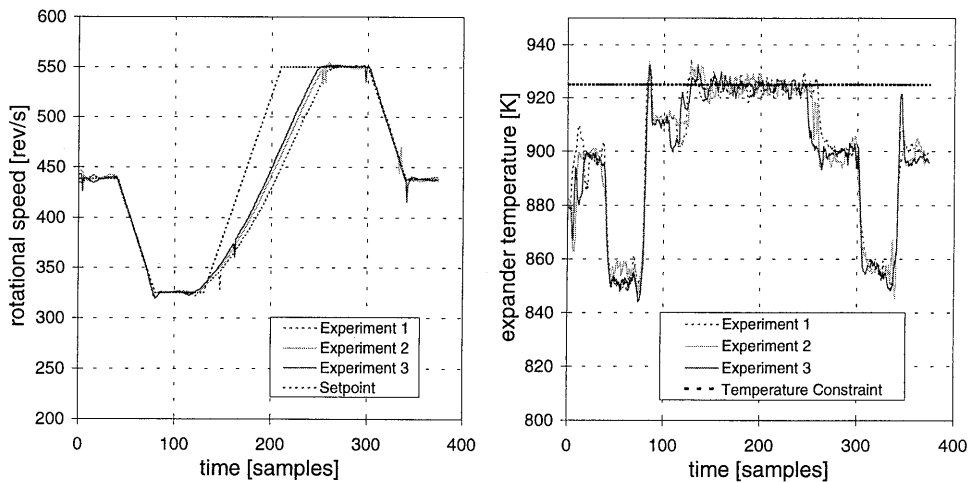


figure 6.23 : Responses of rotational speed and expander temperature for three different model combinations.

Results are presented in figure 6.23. This figure compares the rotational speed response for all experiments with the prescribed set point and also shows the corresponding expander temperature. Clearly, in the first tens of samples, the filter initialises the response to the throttle valve disturbance. During the ramp to a lower set point, the trajectory is perfectly followed by all three experiments. During the subsequent ramp to a higher rotational speed the measured rotational speed starts to deviate from the set point trajectory. The responses of the three experiments differ only slightly from each other.

In all experiments the temperature constraint rules the system response in the upward ramp. Already at the start of the ramp, the constraint is reached, see figure 6.23. This means that the filter corrections overrule possibly different predictions of the different experiments. The resulting differences in responses are marginal and probably badly reproducible. It does, however, indicate the robustness of MPC for disturbances of this kind.

6.5.3 Compressed air disturbances

A rigorous way to apply a disturbance to the system is the injection of compressed air. The compressed air can be injected into the buffer tank by (manually) opening a valve. In the presented experiment the controller action and the system response to the unmodelled disturbance of compressed air are examined. The controller cannot anticipate to this unmodelled disturbance. The results are presented in figure 6.24.

Both the rotational speed (438 rev/s) and the expander pressure (1.46 bar) are specified as constant set points. The throttle valve and the fuel valve are the inputs. At sample 35 the compressed air valve is opened, while at sample 90 the valve is closed again. The injected mass flow of compressed air is approximately 0.05 kg/s (or 12 % of the expander mass flow).

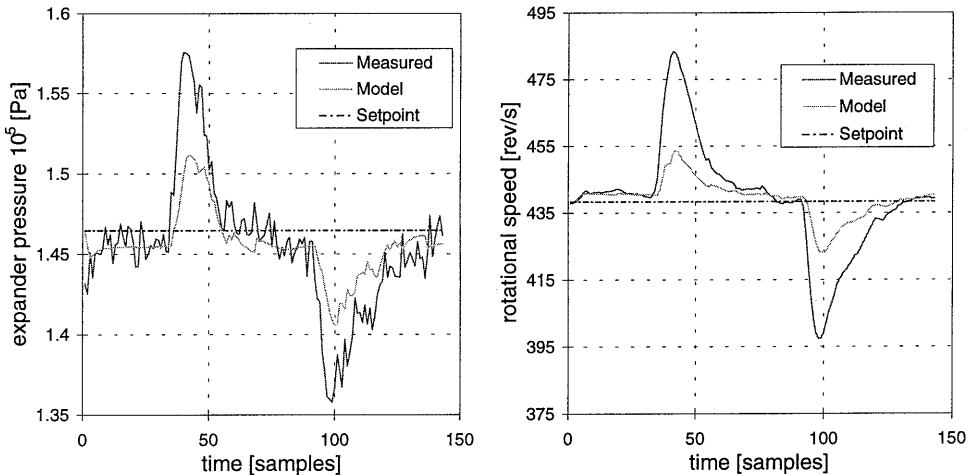


figure 6.24 : Measured expander pressure and rotational speed compared to internal model values (corrected by the filter) for a large disturbance of compressed air injection.

Indeed the controller manages to reach the original set points of both speed and pressure again. Note that the “steady-state” set point deviations are within the threshold range. The main effect of injecting compressed air is that extra power is added to the expander. This causes the gas turbine to accelerate. The rotational speed and expander inlet pressure increase. The controller closes the fuel valve, see the left graph of figure 6.25. This way the controller compensates for the extra power added by the compressed air. The opposite happens when the compressed air valve is closed again. This experiment shows that, although large filter corrections must be applied, the controller manages to respond correctly to the disturbances. The system is therefore robust for large disturbances.

In the two graphs on the right side of figure 6.25, we examine the mass flows through compressor and the surge ratio. The *unfiltered* internal model values are compared to the reconstructed (with measured rotational speed and measured pressure) values. This illustrates the model mismatches during the disturbance. Indeed, the model response is (initially, sample 40) quite opposite to the reconstructed mass flow and surge ratio. This, again, supports the reconstruction problems of the compressor mass flow and the fact that we cannot use the mass flow nor the surge ratio for closed loop control. The expander mass flow, which is not shown, does not display any irregularities.

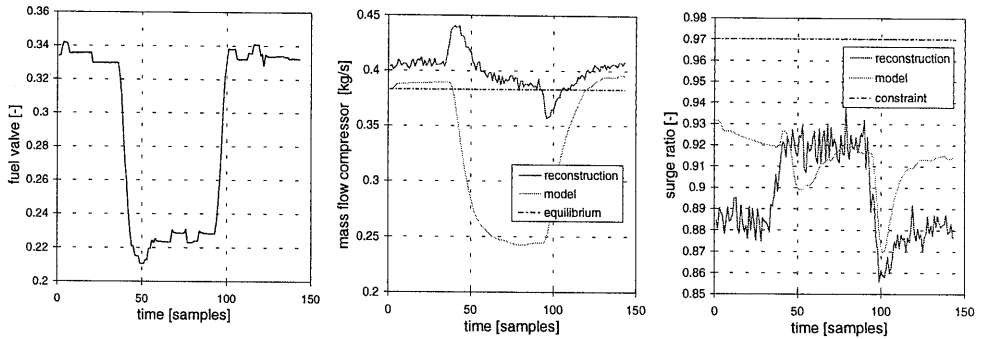


figure 6.25 : Corresponding fuel valve position and reconstructed values for the mass flows through compressor and expander.

6.6 Anticipation

In this section the anticipative behaviour of the Model Predictive Controller is examined. Although we already indicated the anticipation capabilities and noticed the “inverse controller response” in several experiments, now this behaviour is investigated in detail. First, the system response to a set point change with and without anticipation is compared in a simulation. Then, the influence of the size of the control horizon (relative to the prediction horizon) on the simulated performance is investigated.

For reasons of clarity a SISO set point control of the rotational speed with the fuel valve as only input is considered. No constraints on this output nor on the temperature are applied. The input weighting on the fuel valve has been lowered to 0.5, to prevent disturbing influence of input weightings on the results.

6.6.1 Set point change with and without anticipation

As a reference trajectory, at sample 20 a step in the rotational speed is specified from 438 rev/s to 463 rev/s. The throttle valve is not used as an input and is kept at the constant initial value. Figure 6.26 shows that when anticipation is used, the system starts responding to the future set point change, as soon as this change is observed in the prediction horizon. When no anticipation is used, the controller starts responding, when the set point change is activated. Note that because of the discrete character of the controller actually a bar chart of the inputs must be drawn. For reason of clarity this has not been done. Therefore it just looks like the controller without anticipation gives already a response before sample 20.

Remarkable is the inverse response that the system displays in the case with anticipation. First the fuel valve is closed and the rotational speed lowers, then the fuel valve opens again and the rotational speed rises to its new set point value. When no anticipation is used the response does not show this behaviour. The inverse response does not seem to be the optimal response on the set point change. It appears, for instance, already better when the “negative” control moves (in the first few samples) are suppressed. The inverse (controller) response is examined in more detail by investigating the influence of the size of the control horizon in the next section.

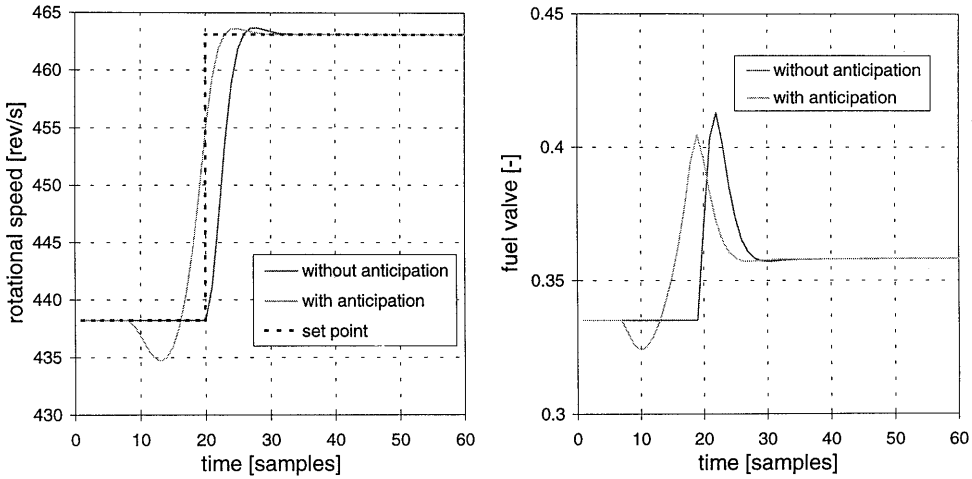


figure 6.26 : Simulated response of rotational speed to a set point change and the corresponding control input for two cases: with anticipation or without anticipation.

6.6.2 Anticipative behaviour for different sizes of the control horizon

Every sample, the controller determines the optimal control moves over the control horizon. Only the first of these computed control moves is implemented. The resulting input trajectory is therefore the result of a number of successive “sub-optimisations”. These sub-optimisations can be improved by increasing the control horizon relative to the prediction horizon. For this reason, it is expected that the controller will show an improved anticipative behaviour when the size of the control horizon is increased relative to the size of the prediction horizon.

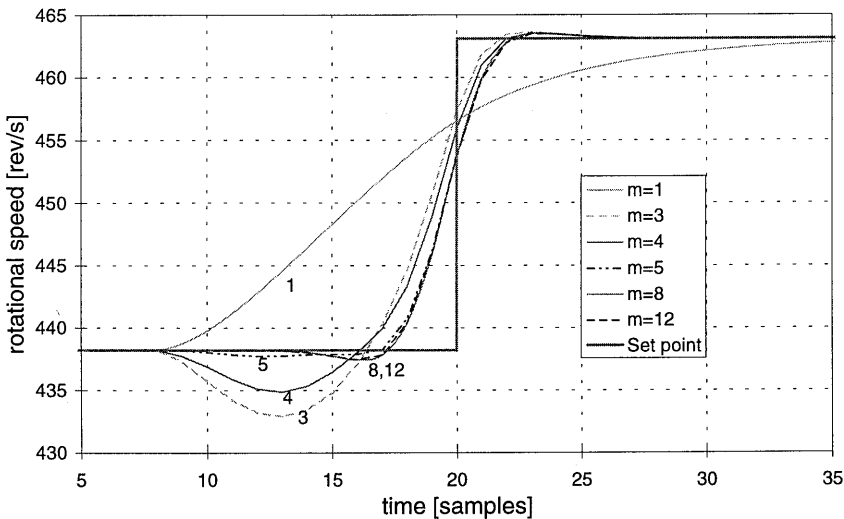


figure 6.27 : Response of rotational speed to a set point change for different settings of the control horizon.

Now consider the same simulation as in the previous section. The same reference trajectory is prescribed for six simulations that vary only in the size of the control horizon. The results are presented in figure 6.27.

For the special case of $m=1$, there is only one input that the controller can change every sample to optimise the response over the prediction horizon. Of course, this is also the value that is actually used. The figure shows that as soon as the set point step enters the prediction horizon, the controller can only optimise the trajectory over the prediction horizon, by opening the fuel valve a little.

When the control horizon consists of more than one sample, the controller has more degrees of freedom and has better opportunities to optimise the trajectory over the prediction horizon. The inverse controller response diminishes as the size of the control horizon increases. For $m = 8$ and $m = 12$ the responses are almost the same. Even in those cases still a (small) inverse response is present. This response, however, is likely to be the optimal solution as it may be balanced with the (equally sized) overshoot after the step.

The phenomenon of inverse response is studied in detail in Appendix E. The influence of the size of the control horizon is investigated by a visualisation of the full control and prediction horizon over successive samples during a transient set point change. A visualisation means that we examine and present for each sample the computed changes of the inputs over the control horizon and the corresponding predicted output responses over the prediction horizon. When we do this for several successive samples, a fair understanding of the MPC results can be obtained.

In the appendix, the control moves and corresponding rotational speed response are compared for the cases where $m = 4$ and $m = 12$. The essential difference follows from an analysis of the first few samples after the set point change enters the prediction horizon. In the case of $m = 4$, when the controller can only influence the input over the first four samples of the prediction horizon, the controller decides to close the fuel valve in the first two samples and then to open it in the last two samples of the control horizon. In this way a compromise is accomplished between the set point deviation before and after the step. As only the first of these control moves is actually used, this means that the controller closes the fuel valve. Because in the next sample only a slightly different optimisation problem is solved (the set point change is now two samples in the prediction horizon), this process is repeated, and the inverse controller response occurs.

In the case of $m = 12$, the controller postpones its control moves to the end of the control horizon, just before the set point step occurs. In the resulting trajectory the controller does nothing in the first samples, until a few samples before the step. Indeed, in this case the newly computed *first* input move of a sample equals the *second* input move of the previous sample. (See Appendix E.)

A conclusion is that the inverse controller response can be prevented by increasing the size of the control horizon relative to the prediction horizon. Increasing the control horizon, however, is not a very practical way to improve the anticipative behaviour of the controller. A larger control horizon requires excessive computation times. Because the robust performance of the closed loop system decreases with larger control horizons, the controller may also become too aggressive.

6.7 Discussion and conclusions

The main objective of this thesis is to assess the feasibility, the performance and the advantages of MPC on turbomachinery. In this chapter, MPC has been implemented and tested on the laboratory gas turbine. The following conclusions may be drawn.

Feasibility Within Primacs, we succeeded in a real-time implementation of MPC on the laboratory installation. The sample interval was limited to 1.5 seconds. Smaller intervals are possible when faster computers, more advanced algorithms and implementation, or further reduced models are applied. For most experiments that we carried out, the sample interval of 1.5 seconds sufficed. Only during fast transients, and especially for the expander temperature signal, a faster sampling may be required.

Within the applied sample interval, the only non-linear MPC approach that could be implemented is *successive linearisation*. This approach, however, is shown to be a useful and powerful extension to linear MPC. It allows a non-linear observation model in the filter, and an every sample updated linear model for prediction and optimisation. It is expected that other non-linear approaches (including the ultimate non-linear optimisation), will hardly contribute to an improved performance.

In the present real-time implementation, only the first order output disturbance filter has been tested. A problem in the (filter) implementation arises in the reconstruction of the mass flow through the compressor. For this reason, the compressor mass flow (and the accompanying quantities like compressor power and the distance to the surge line) are not used as a (closed-loop) controlled variable. It is recommended to improve this ill-conditioned reconstruction. Moreover, because of the problems that (steady state) model mismatches cause, it is highly recommended to implement and test the augmented Kalman filter.

Performance The performance of the presented MPC configuration is good. Both steady state set point variations and transient tracking of reference trajectories are performed well. Constraint limits are observed and hardly violated and the influence of tuning parameters like weighting factors and length of horizons is well understood. Also the robust performance, that is, the presence of model mismatches and disturbances, is handled correctly by the filter.

At this moment, we cannot present guidelines on how “good” the internal models of MPC need to be in order to obtain a good performance or to avoid feasibility problems. In this chapter, we found that the (considerable) steady state mismatches of the validated models did not impede a well performing controller. Apart from the reconstruction problems of the compressor mass flow, the only problem that is encountered with respect to the used models is the temporarily constraint violations of the expander temperature. During fast transients the expander temperature is not well predicted due to mismatches in the (dynamic) combustion efficiency.

We realise, however, that the presented experiments do not challenge the systems dynamics extensively at “higher frequencies”. The time scales of the system response are largely determined by the relatively slow inputs to the system (the control valves). For these time scales, the filter is powerful and fast enough to compensate for (dynamic) mismatches between model predictions and process measurements. Apart from the constraint violations of the expander temperature, we did not encounter any irregular or unstable behaviour. For the same reason (the well performing filter), we could hardly encounter differences between the implementa-

tion of different model combinations in MPC. Therefore, it is recommended to use faster inputs to the system in order to challenge the MPC configuration and the filter. Especially a fast and accurate blow-off valve would substantially influence the dynamic operation of the gas turbine configuration, as blow-off is a very effective, fast and highly non-linear input to the system. Also steam injection or (controlled) air injection are considered as new (and fast) inputs. When new inputs are introduced to the configuration, also different control objectives can be taken into account. It is expected that in these cases a smaller sample interval and an improved filter design are required. These requirements may exceed the present real-time capabilities of Primacs.

Advantages of MPC Constraint handling and anticipation appear to be realistic advantages of MPC for control of turbomachinery. For the gas turbine installation, surge and expander temperature constraints are reached frequently. Also the (move) constraints on the inputs strongly influence the controlled operation. It is emphasised that most “conventional” controllers cannot deal with constraints at all, especially not when constraints (like surge and expander temperature) are not on *controlled* outputs.

The surge constraint is implemented by the distance to the surge-line. Since there is no reliable measurement (reconstruction) of the compressor mass flow, the surge constraint can only be controlled in open-loop. This means that the location of the surge (control) line has to be specified by the compressor map and that the controller cannot anticipate to a possible wrong initial location or shifting of the surge line during operation. This corresponds, however, to existing industrial implementations of surge avoidance control (See also section 7.1).

As already stated, temperature constraint violations arise occasionally in the process measurement, and not in the internal model computations. This means that the violations are due to (dynamic) model mismatches and can be improved by faster sampling, higher filter gains, or enhanced models. When the constraint violations are large or last over a longer period, the filter can “pull” the internal model value across the constraint limit, causing unnecessary weighting of constraint violations in the optimisation criterion.

Anticipation has been studied in detail. Anticipative behaviour appears to be strongly related to the relative size of the control horizon with respect to the prediction horizon. Sub-optimal solutions are an inherent consequence of differences between these two horizons, leading to an “inverse” controller response.

Because, in general, the control horizon cannot be selected equal to the prediction horizon, the inverse controller response is an effect that cannot be avoided when the anticipative properties are desired or required. When this is unwanted, no anticipation must be used. Another solution is the introduction of a separate *anticipation horizon*. This anticipation horizon has the same size as the control horizon. Set point changes are no longer observed in the full prediction horizon, but only as they enter the anticipation horizon. This ad-hoc solution prevents the inverse controller response, but may lead to a degradation of the anticipative properties of the controller when the set point change is larger than the (maximum) change that can be reached within the anticipation horizon.

7 Compressor station control

Compressor stations are widely used in gas transportation and in compressed air utility networks. A compressor station comprises several compressors connected in parallel or in series. Parallel connections increase the throughput of the station and are realised by means of a common header. From this header a connection to the user is provided. The pressure in the header is the pressure that the user of the station experiences.

The basic control objective for industrial compressor applications is capacity, that is, the requested mass flow to the user, while the delivery pressure must be kept at either a constant level, above a minimum level or between a low and a high level. Disturbances like varying inlet conditions or leakage may influence the load and performance of the compressor station. Compressor stations are designed for a safe and reliable operation. Surge avoidance is a basic side condition that each separate compressor in the station must satisfy.

Modern compressor control systems are high performing, reliable and dedicated devices. In section 7.1 a brief survey on industrial compressor configurations and control is presented. For control of multiple compressors in a compressor station hierarchical methods are applied. Surge avoidance and capacity control are strictly separated.

The aim of this chapter is to present an investigation into the opportunities of advanced, model based, control strategies on complex turbomachinery installations. We do not try to implement existing (hierarchical) compressor controllers into the MPC concept. Instead, we implement MPC at an operational level as the primary controller. We do also not primarily attempt to improve the performance of existing industrial control systems. This would require extensive validation and tuning of both the model and the controller. In this thesis, we just want to sketch the opportunities of MPC for systems like a compressor station. The compressor station is an interesting application of the modular model approach and MPC tools that we developed in this thesis. Moreover, the compressor station case adds an essential property to the laboratory gas turbine: an optimisation of a surplus of degrees of freedom. Since we do not have the opportunity of real-time experiments, the analysis in this chapter is restricted to simulations.

The development of an MPC control system for a compressor station involves the selection of a control configuration, the determination of appropriate simulation and internal models, and the formulation of relevant control objectives. In several simulations in section 7.4, the properties and the performance of the MPC controller is investigated.

7.1 Industrial compressor control and opportunities for MPC

7.1.1 Configuration and control

Industrial compressor installations show almost always identical configurations [Nisenfel, 1982]. Figure 7.1 presents a typical configuration of two parallel compressors and a common header. A throttle valve and a recycle valve belong to the standard (control) equipment for each compressor. Separate compressors are powered by either an electric drive or by a (steam or gas) turbine. Turbines allow a variable speed.

The throttle valve is mainly used for capacity control and can be positioned before or behind the compressor. The effectiveness of a throttle valve is good in both positions but the energy efficiency of a discharge throttle valve is extremely bad.

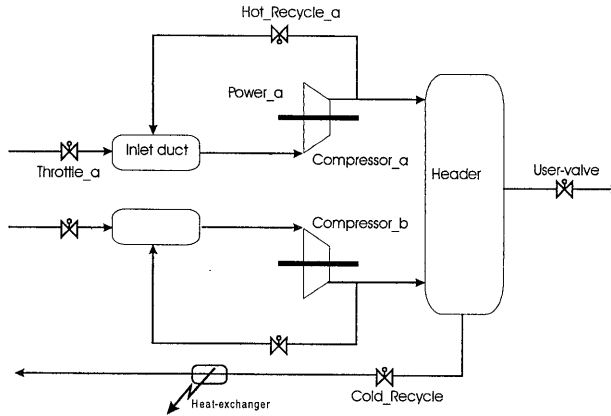


figure 7.1 : Industrial compressor configuration.

A recycle or a blow-off valve is mainly used for surge avoidance. When the compressor operating point tends to cross the surge line, the recycle valve is opened, increasing the mass flow through the compressor and avoiding surge¹. When a recycle is used without cooling, this is called a 'hot' recycle, as indicated in figure 7.1. A potential danger of a hot-recycle is heat buildup in the compressor system. To overcome this problem without using expensive heat-exchangers in every by-pass, one additional overall 'cold' recycle loop is applied in which a heat exchanger cools the compressed air. If sustained recycle becomes necessary it is routed through the cooled recycle line. For air systems, often blow-off configurations are applied rather than recycles. Blow-off avoids the temperature buildup problem.

Besides a throttle valve and a recycle valve, also one or more check valves or non-return valves are included in the standard configuration of a compressor. A check valve in the compressor discharge avoids flow reversal at transient operations like (emergency) shutdown.

The control problem of a single compressor has generally three inputs (power, throttle, recycle) versus only one output: the mass flow to the user. This control objective is subject to a number of constraints like surge avoidance and a prescribed boundary of delivery pressure. The problem is obviously indeterminate and can only be solved when additional criteria are proposed. Such criteria may be the minimisation of the power supply or the restriction that recycling may only be used to avoid surge, that is, to guarantee a minimum mass flow through the compressor, and not for capacity control.

The control problem of a compressor station that comprises multiple compressors, like the basic configuration of figure 7.1, is even more complex since all separate compressors have

¹ Often a "control line" is positioned in the compressor characteristic at the "safe" side of the surge line. Various anti-surge control systems differ in the way the control line is defined or in the way the location of the operating point with respect to the control line is defined [Botros, 1994b], [Nisenfel, 1982]. Most commonly applied is so-called flow- Δp control. For this strategy the mass flow through compressor and the pressure ratio over the compressor are measured and compared with the position of the surge-control line. Not only the distance itself, but also its rate of change determine the appropriate control action.

three inputs and still only one system output. The additional criterion required to solve this problem is called *load-balancing*: the balancing of the total station load over the separate compressors.

7.1.2 Conventional control of multiple compressors

Traditional load-balancing systems throttle back separate compressors one at a time, or apply equal inputs to all compressors allowing them to operate at the same operating points (even when the position of the surge line may not be the same for individual compressors). Both approaches suffer from serious disadvantages. When the load is not equivalently shared over all compressors, some may operate at low efficiencies and some compressors will be more liable to surge than others. Recycle on these compressors cannot be avoided, even though recycle over the whole installation is not necessary.

Modern load-balancing control systems maximise surge protection and process efficiency by operating multiple compressors in a station *equidistant* from their individual surge control lines [CCC, 1992], [Woodward, 1995]. A strict separation between surge and capacity control is implemented. One surge controller per compressor (or compression stage) is required, directly operating the recycle valve.

Capacity control is implemented by a hierarchical master-slave configuration. The function of the slave-loops, implemented on each compressor, is to keep all the compressors at the same distance from the surge line. An overall station controller (master) generates the set point of the distance to the surge line. The capacity controller is not allowed to use recycle. For compressors that operate at a constant rotational speed, only the throttle valve is a control input (SISO capacity control). Variable rotational speed (power as an extra control input) is often resolved by a split range control: set point changes are first anticipated by changes in rotational speed and outside the operation area of the input, by throttle valve actions. In case one or more compressors are recycling, load-balancing response is overruled by the surge controller, that is, the surge controller determines the distance to the surge line by means of recycle.

In practice, PID controllers are used for both master and slave loops as well as for the surge controller. Constraints are resolved by high/low selects. This means that different independent control loops (regulating the distance to the surge line, rotational speed, discharge pressure, temperature, etc.) propose values for a manipulated variable and only the value that satisfies the most restrictive criterion is selected [CCC, 1995]. Interactions between these control loops are not taken into account.

7.1.3 Opportunities for Model Predictive Control

Opportunities for MPC in compressor control are numerous. Using a dynamic model of the compressor station allows to consider much more than just the location of the surge line, including the (future) dynamic response of the installation as well as variations in inlet conditions and load patterns. Interactions between control inputs and controlled or constrained outputs are completely incorporated in MPC. Furthermore, an overall dynamic optimisation of control inputs to a certain criterion may benefit both the performance and the economical operation of a compressor station. In this respect also power inputs and the efficiencies of individual compressors can be taken into account.

In the MPC framework, advantages like constraint handling and anticipation to future set points and disturbances can be benefited from. It is possible to integrate trajectory tracking, load-balancing and constraints. Within MPC, surge and capacity control can be integrated into the station controller, allowing ‘optimal’ control even during recycle.

The standard MPC optimisation criterion (5.1) is in fact a load balancing criterion: the controller balances the total station load over all available compressors. MPC just minimises a criterion of weighted set point deviations versus weighted changes in inputs. The balancing criteria, however, are not unambiguous. The result depends not only on the weighting factors but also on the initial values of inputs and states. MPC provides the opportunity to implement load-balancing criteria like equal distance to the surge control line or other objectives like a minimisation of the overall power supply. When a “logic” optimisation (mixed integer problem, [Bemporad, 1998]) is included in the MPC criterion, it is also possible to include the scheduling of shut-down and start-up of separate compressors in a station.

7.2 Compressor station control case

7.2.1 System configuration

The model describes a generic compressor station. The configuration comprises two parallel compressors, each with its own (gas turbine) driver and is presented in figure 7.2. Both compressors are provided with a suction throttle valve and a hot recycle. An overall cold recycle is included as a blow-off. In the present version of the model, check valves are not included, since dynamic simulation of shut-down is not aimed at in this study. This feature is easily introduced in the non-linear model, but can hardly be included in a linear model.

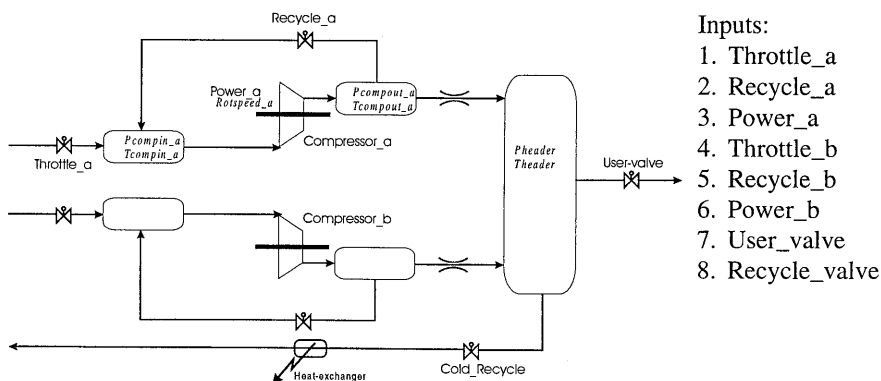


figure 7.2 : Compressor station MPC control configuration.

For each compressor we have three inputs: the position of the throttle valve, the position of the recycle valve and the power supply. Both compressors are connected by a common header. The overall cold recycle flow is controlled by the “cold-recycle” or “recycle-valve”. The mass flow to the user is determined by the position of the throttle valve in the pipeline from the header to the user. This “user-valve” is the eighth and final input to the system. The full set of non-linear model equations and parameter values is included in Appendix C.3.

7.2.2 Model assumptions

For our model of the generic compressor station the following six assumptions hold:

1. The compressor station is built from the lumped-model components developed in Chapter 3. Therefore, the components exhibit the same assumptions as before: ideal gas, adiabatic flow through valves, polytropic compression, no pressure drop over volume elements and static description of mass flows through compressors and valves.
For the volumes we apply the adiabatic, homogenous volume approach of section 3.2.2. Note that all volumes in the compressor station have more than one input and/or more than one output. The header, for instance, has two incoming mass flows and two outgoing mass flows. These extra mass flows can be easily introduced in our model description.
Valve dynamics and dead times are not included. Since the model is built from modules, the configuration is easily adapted to include more compressors (connected in parallel or in series), buffer tanks, or valves.
2. The compressor station is isolated from its environment. The installation does not exert upstream influence. This means that we assume a constant pressure and temperature supply to the compressor station (referred to as p_{amb} and T_{amb}). Of course, these inlet conditions can be varied, creating disturbances to the station. On the downstream side, the mass flow to the user only depends on the pressure and temperature in the header and on the user-valve position. This assumes a critical flow through the user-valve.
3. The compressor performance map can be scaled according to the general method of dimensionless parameters in Appendix A.3. This assumption is necessary to account for the influence of the inlet conditions on the compressor characteristic. (Temperature and pressure changes due to recycling). We assume a constant polytropic compression efficiency.
4. We selected two almost identical compressors. Both compressors obey the same characteristic but for **compressor_b** the mass flow scale is multiplied with a factor 1.1. Also a different efficiency has been assigned to both compressors. For **compressor_a** the efficiency is 0.70, while for **compressor_b** the efficiency is 0.60. This situation compares to a practical situation in which identical compressors are purchased that exhibit different behaviour.
5. A direct shaft power input to the compressor is assumed. In practice, a (gas) turbine will be used to power the compressor. The fuel rate and the inertia of gas turbine determines the available power during transients. In our model this inertia is neglected. Instead, a move rate on the power input is formulated.
6. We assume only one user of the compressor station. Multiple users can be simulated by superposition of load patterns.

The compressor characteristic we use in this chapter is the compressor of the BCC turbo-charger of the laboratory gas turbine. This is not a type of compressor that is likely to be used in industrial compressor stations. The capacity is too low and the compressor exhibits a narrow operation area. Also the other components like valves and volumes have been selected compared to the laboratory installation. We have made these selections because the relative dimensions of components has a large influence on the system behaviour and the components of the gas turbine are well known.

7.2.3 Control objectives

MPC control objectives for the generalised compressor station configuration involve integrated surge avoidance and capacity control. With capacity defined as the mass flow delivered to the user (the mass flow through the “user-valve”), we consider two control objectives:

1. A set point or trajectory on the mass flow to the user. This objective imposes a *reference load pattern* to the compressor station. The position of the “user-valve” (figure 7.2) is controlled by MPC.
2. Keep the pressure in the header within a minimum and maximum boundary constraint level while the position of the “user-valve” is influenced directly as an external disturbance. This control objective imposes an *actual load pattern* to the compressor station since, in general, the “user-valve” position determines the load of the station and cannot be used as a control input. The resulting mass flow to the user is evaluated as an output. In this control objective, an additional set point on the pressure in the header (at a value between the boundary limits) makes the system more deterrent. Otherwise, the header pressure depends on the history of the system and the mass flow to the user is not a unique function of the user-valve position.

Both objectives are subject to a number of constraints on outputs:

- Surge constraints on the separate compressor characteristics.
- Minimum and maximum rotational speeds for separate compressors.
- Maximum temperature in the compressor outlet plenum. (Temperature buildup due to hot-recycling.)
- Minimum and maximum pressure level in the header.

and on inputs:

- Minimum, maximum and move constraints on the power supply to the separate compressors and on the control valves positions.

7.3 MPC implementation

Besides the basic selection of a control objective (*reference* or *actual* load pattern) and the specification of constraints, in the MPC implementation some more aspects need to be specified. This section discusses the selection of model combinations and tuning parameters as well as the (control) options that can be encountered in the simulations.

Models for simulation and control We apply the non-linear model to simulate the compressor station. In most simulations, the same non-linear model is used as the internal observation model (IObM, **figure 5.3**), while a successively linearised model is applied for internal prediction and optimisation. This is the case of “perfect model” or “nominal” control. Model mismatches between the simulation model and the internal MPC observation model can be introduced to study **robustness**. Both parametric model mismatches (like different efficiency, inertia or static characteristic) as well as (external) unmodelled disturbances can be studied. Disturbances that act on the inlet conditions reflect upstream disturbances in the compressor network. Disturbances can be measured and forwarded to the controller or can be unknown to the internal model.

Tuning parameters Appropriate choices for the length of the prediction and of the control horizon need to be determined, as well as for the sample interval. Although these tuning parameters have a significant influence on the performance, they are fixed at reasonable values in our simulations: the sample interval is 1 second, $p = 30$ samples, and $m = 8$ samples.

More important is the selection of the weighting factors in the criterion. These factors reflect the relative importance of trajectory errors and control effort. The control effort is defined by input *moves*. Since only input *moves* are weighted, a (high) weighting factor avoids too much, undesired, movements of the control valves. On the other hand, a weighting factor of 0 allows arbitrary control moves (only limited by the constraints) and makes the system very “busy”. For our simulations we selected all input weighting factors constant and equal to 1, only the values of the set point weightings are varied. An inherent disadvantage of this input weighting is that (small) set point deviations may not be diminished because the decrease of the criterion value does not balance the control effort. Moreover, control valves may stay at rather arbitrary (and possibly) unwanted positions because the set points are already realised.

Anticipation Future set point changes and desired trajectories can be made available to the controller by means of anticipation. In our present Primacs implementation, unfortunately, the actual load pattern is defined as a prescribed trajectory of a valve position to which cannot be anticipated.

Recycle valve reset In conventional controllers, recycle valves are only activated by the dedicated surge controller. The integrated MPC controller, however, allows the use of recycle to minimise its criterion. It appears that recycle is frequently used because of its fast and effective response to drop pressure and mass flows during transients. Since only *changes* in inputs are weighted, MPC tends to leave the recycle valves open and to use other inputs (like power) to stabilise the new set point.

To overcome this unwanted effect, weighting of the absolute values of the input signals u instead of changes Δu in the optimisation criterion would benefit the performance. Within the framework of the current optimisation algorithm, this can be realised by a direct coupling of inputs to outputs and imposing reference values on these new “outputs”. For recycle, these references can be found in the optimal value of a closed valve or a corresponding set point of 0 [kg/s] on the recycle mass flows.

For other purposes, for instance the interesting criterion of minimum power input, such a natural reference may not be available. An interesting alternative is the introduction of a *dynamic reference*. This means that every sample a new reference value of minimum power input is computed according to momentary mass flows and pressure. The reference value changes along with the operating point of the compressor station.

Load balancing Two load-balancing criteria are evaluated in this thesis: an equal distance to the surge line for both compressors, and a minimum power input to the station. To be able to implement these two load balancing criteria, additional outputs are introduced in the model: The *distance to the surge line* and the *ideal power*. The latter is in fact the dynamic reference of minimum power mentioned above.

The *distance to the surge line* or *Devsurge* is available for each compressor of the station and is determined by the position of the operating point in the compressor map. The distance is computed in terms of mass flow over a constant rotational speed curve as

$$Devsurge = \frac{\text{mass flow at surge for the same rotational speed}}{\text{actual mass flow}} \quad (7.1)$$

We selected the ratio of mass flows instead of the difference since compressors with different size or capacity have incomparable distances to the surge line. Because the surge line is not a straight line, the ratio is not equivalent to the difference.

In the two compressor station, the difference of both *Devsurge* outputs can be used as a controlled output. A reference of 0 to the new output *Devdif* guarantees an equal distance to the surge line:

$$Devdif = Devsurge_a - Devsurge_b \quad (7.2)$$

The second load-balancing strategy uses the output *ideal power* as a dynamic reference to minimise power input to the compressor station. A new output of the compressor station can be defined as:

$$DevIdpow = \frac{\text{actual_power}}{\text{ideal_power}} = \frac{\text{Power_a} + \text{Power_b}}{\dot{m}_{\text{user}} Cp \left[T_{\text{amb}} \left(\frac{P_{\text{header}}}{P_{\text{amb}}} \right)^{\left(\frac{\gamma-1}{\gamma_{\text{ideal}}} \right)} - T_{\text{amb}} \right]} \quad (7.3)$$

The deviation ratio factor *DevIdpow* or *power ratio* between the actual and the ideal power can be minimised in the criterion versus reference value 1. The “ideal” efficiency or overall station efficiency is set at the arbitrary value of 0.5.

7.4 MPC simulation results

This section presents a number of simulations as an illustration of the opportunities of MPC for a parallel compressor station. For each simulation the most relevant inputs, outputs, set points and constraints are plotted and discussed. In this chapter, not all possible combinations of control options mentioned in section 7.3 will be studied in detail. Emphasis is on the two control objectives of *reference* and *actual* load pattern. For the reference load pattern, anticipation and model mismatches are investigated, while for the actual load pattern, the influence of an additional set point and of weighting factors is discussed. For both load patterns, two different load balancing strategies are compared: Equal distance to the surge line combined with weighted recycle versus minimisation of power input to the system. For the complete settings of all set points, constraints, weighting factors etc. please refer to Appendix F.

7.4.1 Reference load pattern with anticipation

In this first simulation a block pattern trajectory on the requested mass flow to the user is prescribed. This pattern is referred to as the *reference load pattern*. The following additional options are selected:

- The anticipation function is enabled.
- Reference values of 0 on all recycle flows (hot and cold) to minimise recycling.

- A surge constraint on $Devsurge$ at 0.95 for both compressors.
- A reference value of 0 on $Devdif$ to enforce an equal distance to the surge line for both compressors.
- A minimum constraint on the pressure in the header of 1.6 bar.
- The maximal power input is 100 kW per compressor.
- The rotational speed is limited between 420 - 460 rev/s.

Figure 7.3 displays the response of the mass flow to the user compared to the prescribed trajectory of the reference load pattern. The performance is good, the controller is able to track the trajectory closely. Anticipation to future set point changes can be recognised (response starts one full prediction horizon before the actual step). Differences in anticipation to a small or a large set point change can be observed. In figure 7.4 the surge avoidance behaviour of the controller during this simulation is shown. In the upper part of the figure the distance ratio ($Devsurge$) is drawn for both compressors. Both compressors reach the surge constraint at 0.95 during the period of low load. The difference ($Devdif$) between the two deviations to the surge line is very small. This difference is explicitly shown in the lower part of the figure (right side axis.) Indeed the controller is able to keep both compressor equidistant from the surge line.

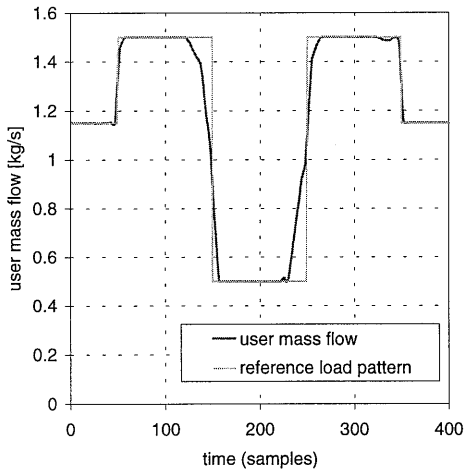


figure 7.3 : Mass flow to the user and reference load pattern trajectory.

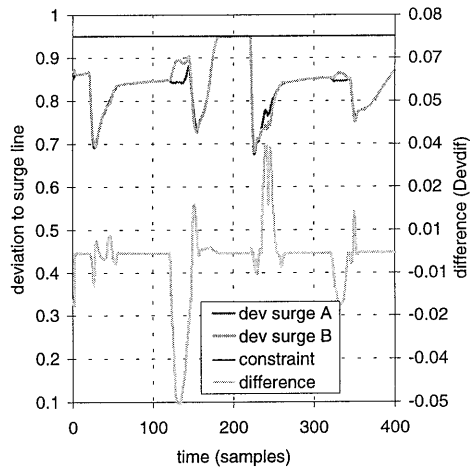


figure 7.4 : Surge avoidance behaviour.

In figure 7.5 the (control valve) inputs of the compressor station are presented. Different inputs for the two (different) compressors A and B are computed. As expected, the throttle valves (left figure) open and close with the requested capacity. The recycle valves (right figure) are very active. It appears that recycle is an effective mean to influence the behaviour of the station. Due to the zero reference of recycle flows in the control criterion, all recycle valves tend to almost completely closed position in steady state operation (apart from the period with sustained recycling when the surge constraints are reached). The activity of the control valves motivates the relatively strong weighting factors (1.0) on the inputs.

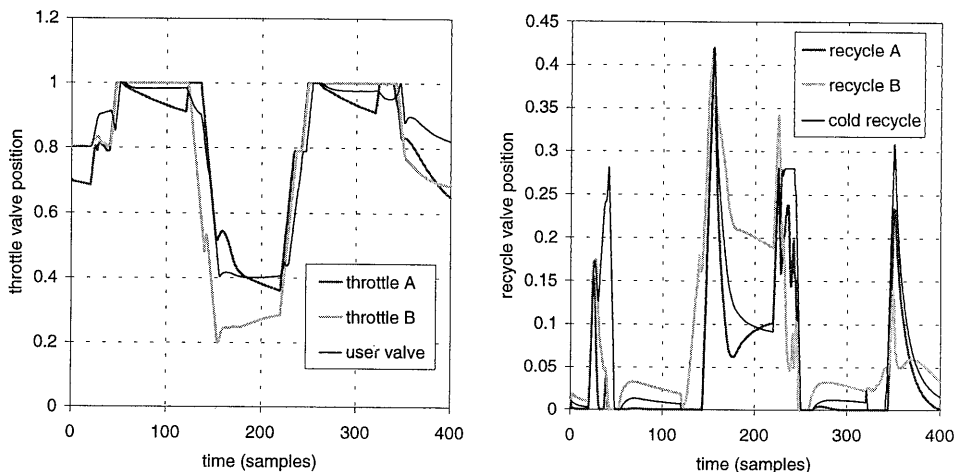


figure 7.5 : Corresponding (control valve) inputs to the compressor station. Left the positions of the throttle valves before compressor A and B together with the “user-valve” position. In the right side graph the recycle valve positions are shown, including the overall cold recycle valve.

In figure 7.6, the rotational speed, the power input, and the compressor outlet temperature are plotted. Compressor A reaches maximum rotational speed, while compressor B reaches maximum power input. Compressor B also reaches its constraint on the compressor outlet temperature. Indeed, as can be seen in figure 7.5, compressor B recycles more than compressor A. Recall that compressor A has a better efficiency and that compressor B delivers more mass flow at the same speed and pressure ratio.

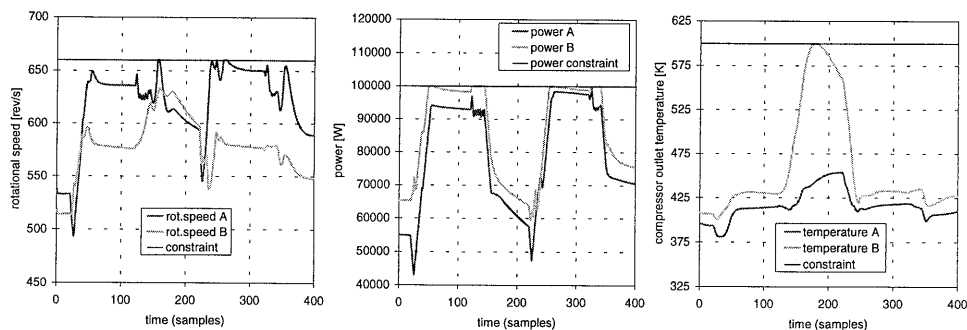


figure 7.6 : Rotational speed, power inputs, and compressor outlet temperature.

7.4.2 Reference load pattern without anticipation

In this section the previous simulation is repeated with disabled anticipation function. In figure 7.7 the mass flow and the computed control input of the user-valve are compared for the simulations with and without anticipation. Also in case without anticipation the tracking of the reference mass flow trajectory is good. As the response is not able to anticipate to set point changes, the new value is reached later. The response without anticipation shows the

inherent system inertia with respect to (large) set point changes. Inertia in the compressor station is mainly determined by the input move constraints, the volumes, and the acceleration of the compressors. The user-valve position shows very much the same signal, though slightly shifted in time.

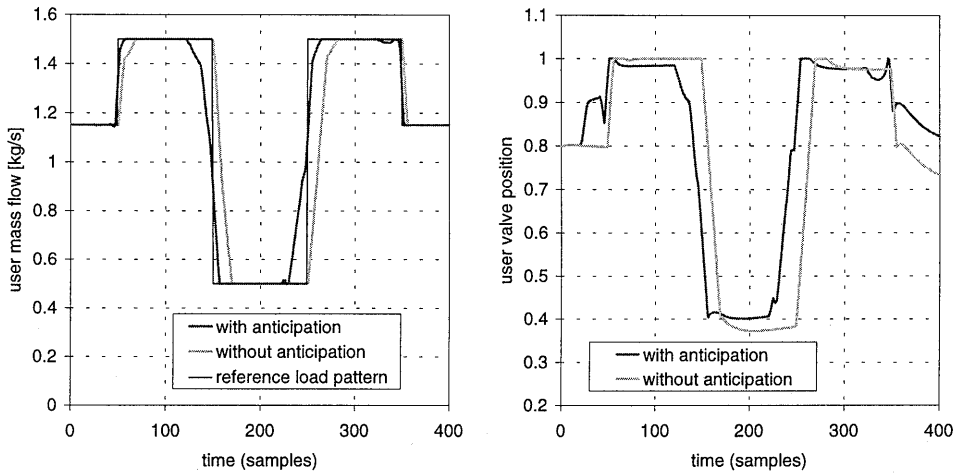


figure 7.7 : Response of user mass flow and user-valve control input of the same simulation with and without anticipation.

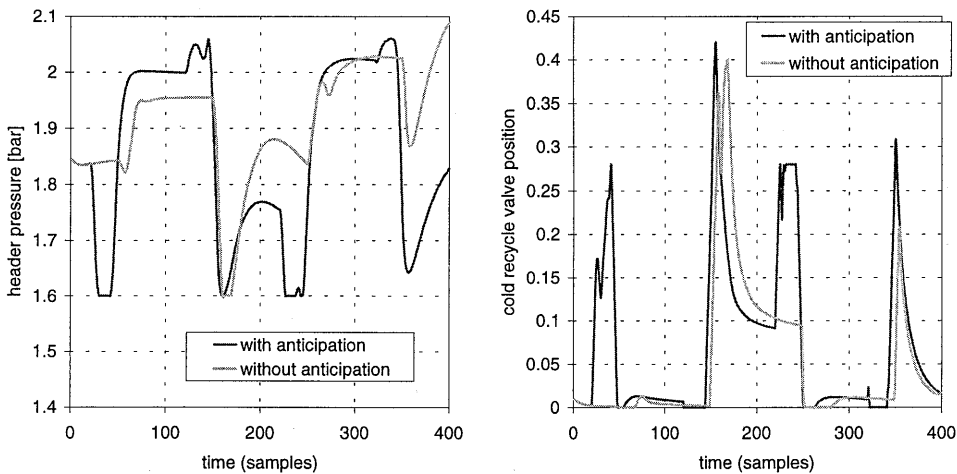


figure 7.8 : Header pressure and cold recycle valve input signal in case with and without anticipation.

The two responses of the pressure in the header, figure 7.8, show a remarkable difference. In case with anticipation, the pressure drops rapidly when a strong *increase* in the mass flow is encountered in the prediction horizon (see sample 20, sample 220). This pressure drop is mainly caused by the opening of the cold-recycle valve (figure 7.8), which is not opened in

case without anticipation. In anticipation to the coming mass flow step, the throttle valves are already opened (figure 7.5) and the power supply is already increased (figure 7.9), causing a temporary excess of air that needs to be recycled. This is not an efficient way, but since pressure and power are not weighted, it is effective to quickly increase the mass flow during the step.

The lower pressure constraint level at 1.6 bar is reached several times in both cases, but is not exceeded. Also note the difference in pressure levels at the end of the simulations with and without anticipation. Since pressure is not weighted and not fixed a certain set point, its value is determined (within constraint boundaries) by the “history” of the system, especially the momentary position of the control valves, because moves of the control valves are weighted. Because the history of both simulations differs, also the resulting pressure level does. If this is undesired, an additional set point on the pressure can be defined. This option will be investigated in other simulations.

Figure 7.9 compares the corresponding total (= summed) power input to both compressors and the power ratio in case with and without anticipation. As expected, the case with anticipation takes a little more power. This can be seen from the first period of the total power plot and from the power ratio, which is larger than in case without anticipation. Also, in the power ratio the two (recycle) peaks can be recognised at sample 50 and 220. For the last period, on the contrary, the total power is *higher* in case without anticipation. This is caused by the (too) high pressure level in case without anticipation. A set point on the pressure is expected to deal with this “free” pressure level.

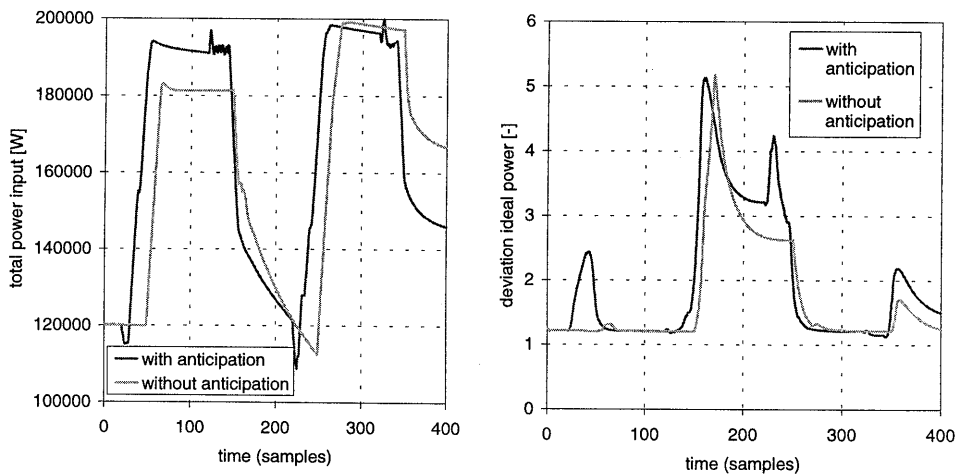


figure 7.9 : Total power input (to both compressors) and power ratio in case with and without anticipation

7.4.3 Reference load pattern and ideal power load balancing

In the simulations in this section again the reference load pattern trajectory on the requested mass flow to the user is prescribed. Instead of minimising the recycle flows and equal distance to the surge line, now the alternative load balancing criterion is activated, that is, minimisation

of the power input by means of the power ratio $DevI dpow$ (7.3). Summarising, the following options are selected for the simulations in this section:

- With anticipation.
- A reference value of 1.0 on the deviation ratio $DevI dpow$.
- A surge constraint on $Devsurge$ at 0.95 for both compressors.
- A minimum constraint on the pressure in the header of 1.6 bar.
- The maximal power input is 100 kW per compressor.
- The rotational speed is limited between 420 - 460 rev/s.

Two reference signals are prescribed, the mass flow and $DevI dpow$. In two simulations, different settings of the set point weightings are compared. The weighting factor on the mass flow is 1.0 in both simulations, while the factor for $DevI dpow$ is varied from 0.1 to 1.0. The weighting factors on the inputs are fixed at 1.0. The mass flow response and the controlled output $DevI dpow$ are plotted in figure 7.10. For reference, in this figure also the value of $DevI dpow$ for the simulation presented in section 7.4.1 is included in which $DevI dpow$ was an uncontrolled variable and the distance to the surge line is controlled instead. The corresponding power ratio is surprisingly large. We already concluded in section 7.4.2 that this was not an efficient control law. This data, however, is only indicated as a reference. Also in this case the power can be further minimised by different settings of the tuning parameters.

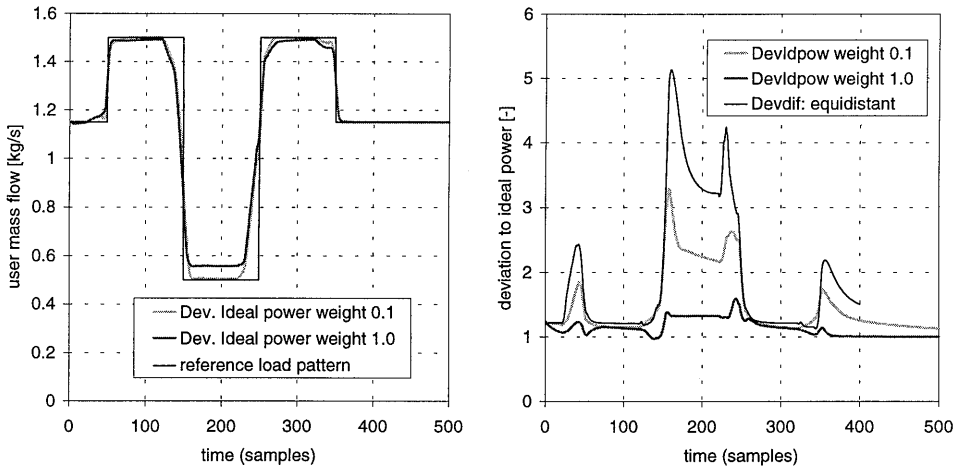


figure 7.10 : User mass flow and deviation to ideal power for two simulations with different weighting factor for $DevI dpow$, the power ratio.

As expected, the power ratio is considerably lower when the weight is 1.0 compared to 0.1. This means that the required power is only little higher than the “ideal” reference power. The lower power ratio indeed corresponds to a lower total power input to the system, as can be seen in figure 7.11. A consequence of the low power consumption, however, is that the reference trajectory on the mass flow is not completely reached for low mass flows.

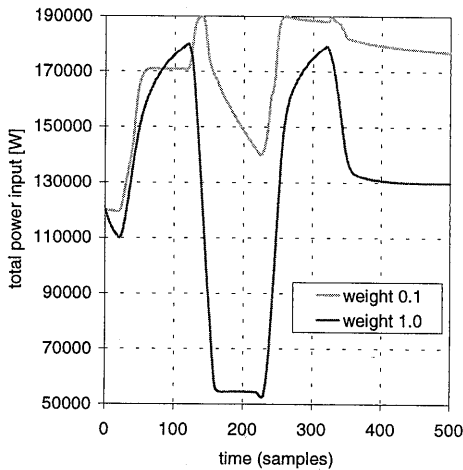


figure 7.11 : Total power input to the system for two simulations with different weighting factor for *DevIpow*.

Figure 7.12 shows the inputs to the control valves for the two simulations. These results provide insight in the control strategy that minimises the power ratio. To save power, capacity control is mostly realised by the user-valve. The throttle valves of the separate compressors are opened as much as possible, while all the recycle valves are closed as much as possible. In fact, recycle valves are less active (and more closed) in this control case than in the previous simulations where the recycle mass flows were minimised. In this respect the power minimisation load balancing strategy is successful.

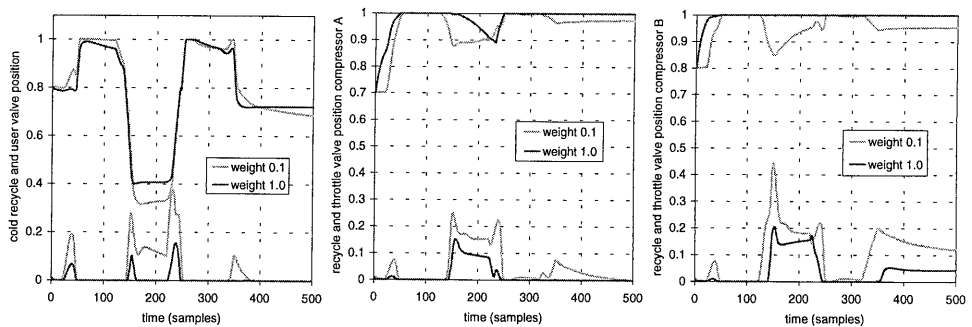


figure 7.12 : Inputs to the control valves for the two simulations with different weighting factor for *DevIpow*,

Finally, we show the effect of anticipation in this control setting. We apply a user mass flow weight of 1.0 and a (mean) power ratio weight of 0.5 to *DevIpow*, and repeat the above simulation with and without anticipation. Results are gathered in figure 7.13 and figure 7.14.

As expected, in case with anticipation, the mass flow reacts already before the set point changes and reaches its new steady value earlier. The deviation to the reference mass flow trajectory is lower. This takes, however, more power. We already discussed the blow-off action in anticipation to a future mass flow rise. Now we can also recognise the anticipation to a mass flow drop: At sample 150, the controller with anticipation does not need to close the throttle valves of the separate compressors as far as without anticipation. This has a positive effect on the power consumption. The large peak in the power ratio is avoided.

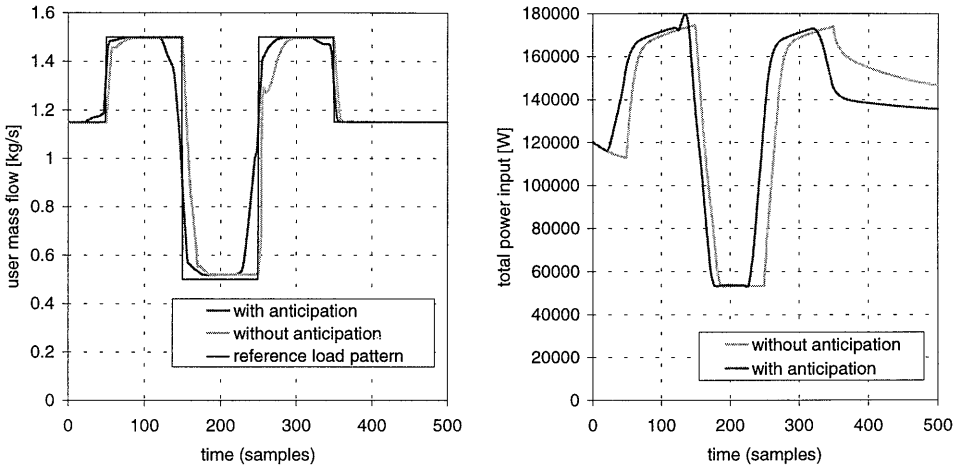


figure 7.13 : Mass flow to the user and total power input for simulations with and without anticipation.

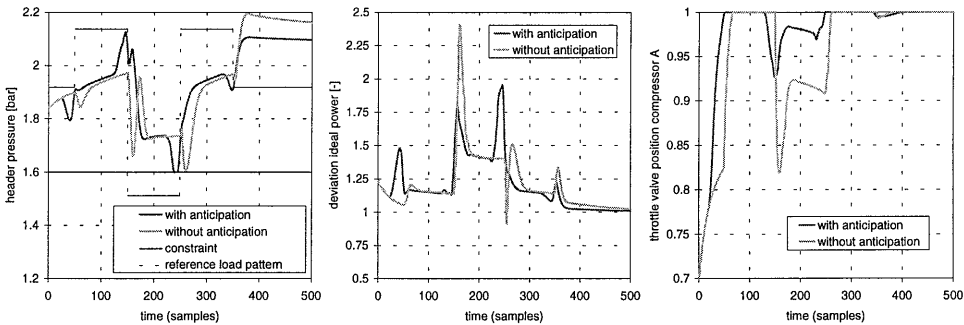


figure 7.14 : Header pressure, power ratio and throttle valve position of compressor A.

7.4.4 Actual load pattern with and without set point on header pressure

In the simulations of this section a block like pattern on the user-valve position is imposed to the system as an external disturbance. A ramp with maximum valve speed is selected, when faster disturbances are imposed, the system is not able to follow the reference because the recycle valves can not open quick enough. This load is referred to as the *actual load pattern*.

The user-valve is no longer an input to the system. The controller should keep the pressure in the header between 1.6 and 2.1 bar. Two different simulations are compared. One with an additional set point on the pressure in the header (at 1.85 bar, just in between the constraint limits) and one without this set point. Summarising, the options for the simulations are:

- Reference values of 0 on all recycle flows (hot and cold) to minimise recycling.
- A surge constraint on *Devsurge* at 0.95 for both compressors.

- A reference value of 0 on *Devdif* to enforce an equal distance to the surge line for both compressors.
- A minimum (1.6 bar) and maximum (2.1 bar) constraint on the pressure in the header.
- The maximal power input is 100 kW per compressor.
- The rotational speed is limited between 420 - 460 rev/s.
- Additional set point on the header pressure at 1.85 bar, weight 1.0.

Results are gathered in figure 7.15. The mass flow responses of both simulations are compared to the actual load pattern trajectory of the user-valve. In both simulations, the mass flow follows the position of the user valve well. In the case of a set point on the pressure, the mass flow settles a little quicker to a new valve position, that is, it follows the exact shape of the load pattern more closely, which is a desired property of the station. Also the mass flow range is larger in case with a set point. When no set point is defined, the pressure varies in between its limits but it does not violate the constraints.

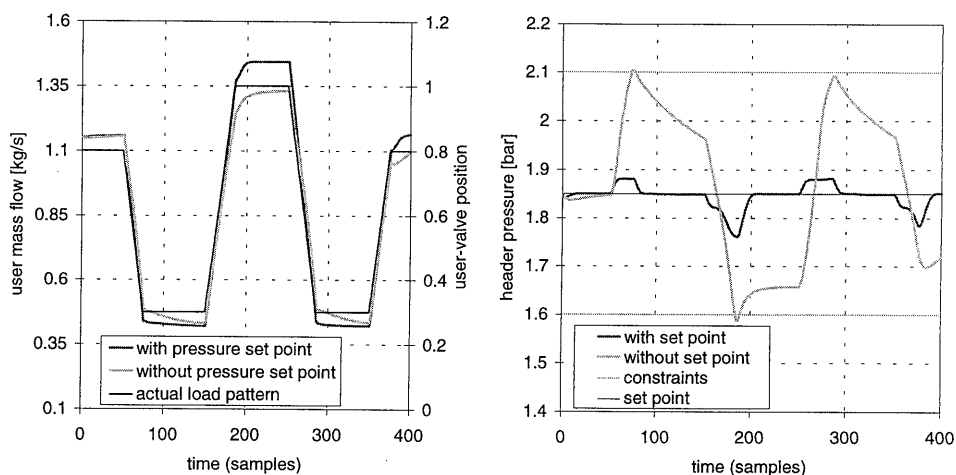


figure 7.15 : Actual load pattern simulations with surge distance load balancing. The load pattern of the user-valve position is shown with the responses of the mass flow to the user and the pressure in the header for simulations with and without a set point on the header pressure.

Apart from the differences in the mass flow response, it is difficult to determine which simulation performs better. In figure 7.16, the total power input (=summed power input of both compressors) and the (uncontrolled) power ratio are compared for the simulation with and without the additional set point. During low loads, the simulation with a set point takes less power, while during high mass flow loads the simulation without a set point takes considerably less power. (The corresponding mass flows are not always the same.) Surprisingly, the power ratio is approximately equal for both simulations. This is a consequence of the dependency of the power ratio from the header pressure. For different or non-referenced header pressures, the power ratio may not be compared.

More important, in figure 7.16 we also see that the total power tends to decrease over the entire simulation (especially in the case without set point). This is a consequence of the “free” pressure. In fact, the pressure tends to its lower limit when the simulation is carried out over a

longer period. Clearly, this is interesting for power saving, but it also withholds an important buffer function of the pressure in the header.

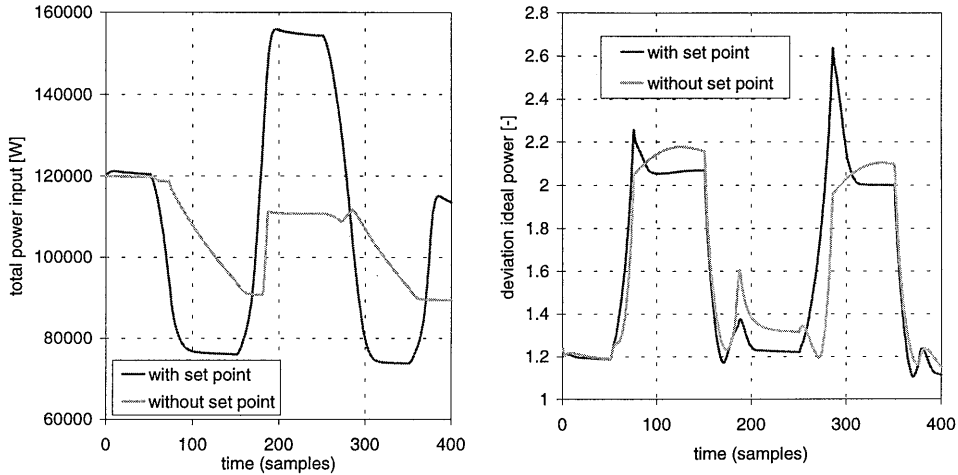


figure 7.16 : Total power input and power ratio for the simulations with and without a set point on the header pressure.

To conclude this section, figure 7.17 displays the distance to the surge line for compressor A and the corresponding control valves of this compressor (compressor B gives comparable results). Clearly, during low loads of the station a substantial recycling is required in both situations. To keep the header pressure at its set point, the throttle valves of the separate compressor are used. When no pressure set point is defined, these throttle valves have an arbitrary value. In the end they may go to the fully open position.

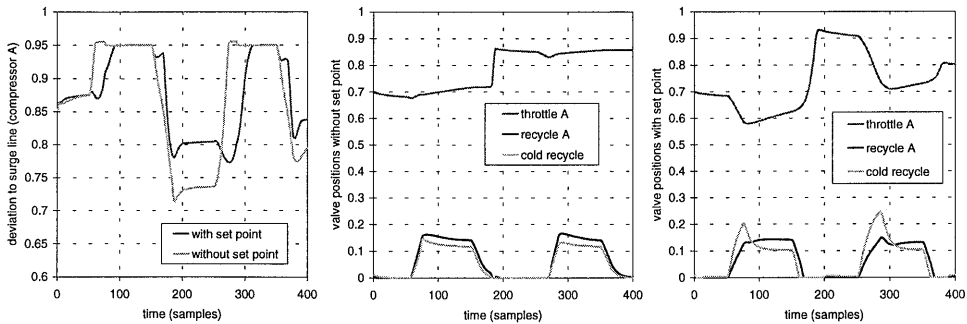


figure 7.17 : The distance to the surge line for compressor A and the corresponding control valves of this compressor in case with and without a set point on the header pressure.

7.4.5 Actual load pattern and ideal power load balancing

In the simulations in this section again the actual load pattern trajectory on the user-valve is prescribed. Now, the alternative load balancing power ratio criterion $DevIdpow$ is activated. Again, simulations with and without a set point on the header pressure will be compared. Summarising, the following options are selected for the simulations in this section:

- A reference value of 1.0 on the deviation ratio $DevIdpow$ with a set point weight of 0.1.
- A surge constraint on $Devsurge$ at 0.95 for both compressors.
- A minimum (1.6 bar) and maximum (2.1 bar) constraint on the pressure in the header.
- The maximal power input is 100 kW per compressor.
- The rotational speed is limited between 420 - 460 rev/s.
- Additional set point on the header pressure at 1.85 bar, weight 0.1.

Results are gathered in figure 7.18 and figure 7.19. The effect of the additional set point on the pressure is not large (Note that the weighting on the pressure set point has been decreased from 1.0 to 0.1 for the simulations in this section.) The major difference (and advantage) is that the pressure always returns to its fixed set point and is not indeterminate.

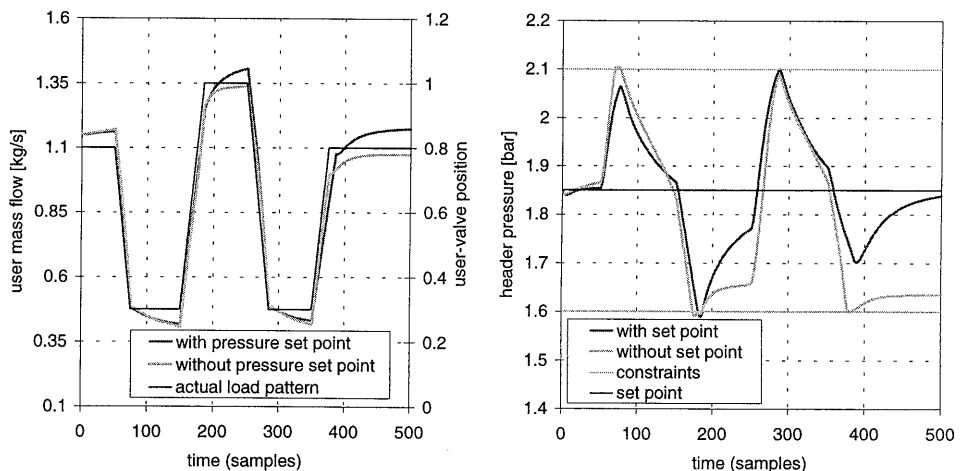


figure 7.18 : Actual load pattern simulations with ideal power load balancing. The responses of the mass flow to the user and the pressure in the header are shown for simulations with and without an additional set point on the header pressure.

Clearly, this fixed pressure level takes a little more power (figure 7.19), but is expected to give the station some buffering. The power ratio of both simulations is approximately the same. Comparing these simulations with the simulations of the previous section (where the distance to the surge line was controlled instead of the power ratio), shows that the power ratio is a little improved, especially for the simulation with a set point. This is probably caused by the lower set point weight.

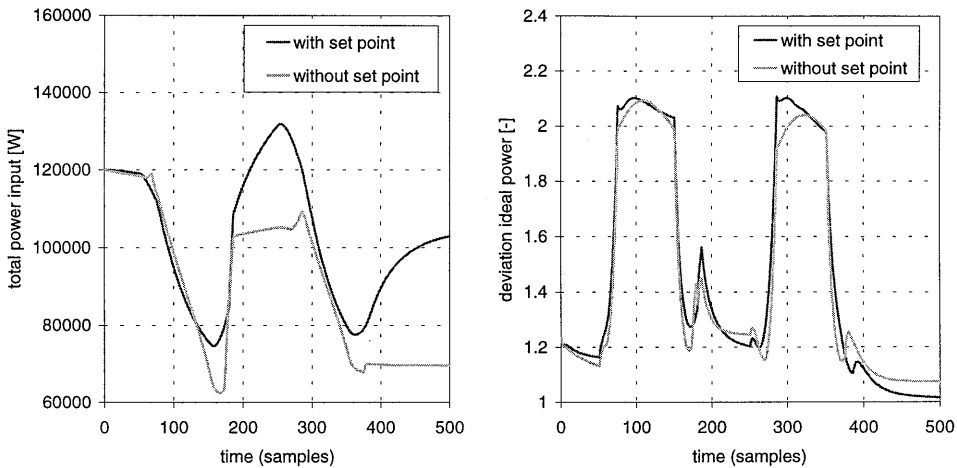


figure 7.19 : Total power input and power ratio for the simulations with and without a set point on the header pressure.

7.4.6 Reference load pattern and model mismatches

In this final simulation section, very briefly, the influence of model mismatches between the simulation model and the internal MPC observation model is investigated. In this chapter we will not put emphasis on robustness issues.

The simulation of section 7.4.1 is repeated, but now some parameters of the simulation model have been altered by approximately 10%. We also assume that all outputs can be measured and can be used for feedback.

- The ambient pressure p_{amb} has changed from 1.2 bar to 1.3 bar.
- The efficiency of both compressors is raised by 0.05.
- The filter constant for all controlled outputs (and constraints) is set at 0.3.

The remaining control options are the same as in section 7.4.1, but an extra set point on the header pressure has been added. Results of the mass flow response are shown in figure 7.20 and of the pressure response in figure 7.21.

Apart from the first tens of samples, when the filter initialises, hardly any difference between the model values and the process values can be seen, not even in a zoomed plot (right graph). This holds for both the mass flow and the pressure (as well as the other, not shown, outputs). This means that the filter is perfectly capable to compensate for the imposed errors. Of course, since we assume that all outputs can be measured, no reconstruction problems arise. This will be different in a real-time environment.

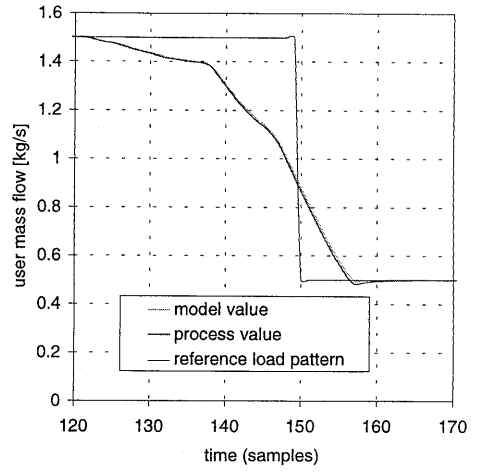
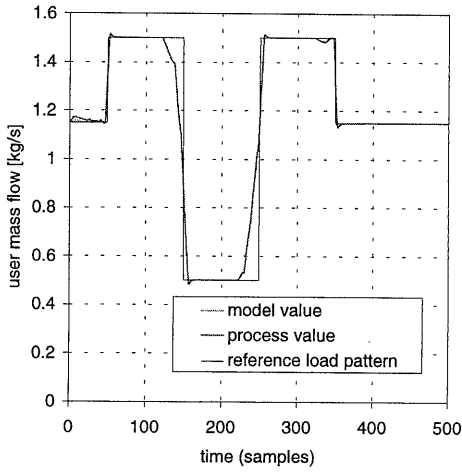


figure 7.20 : Mass flow response of the closed-loop response.

Figure 7.21 also compares the pressure response of this closed-loop simulation to the previous simulation in section 7.4.1. Apart from the model errors, also the pressure set point has been added. The effect of this set point is clearly seen in the figure. The main function of the set point is to fix the “average” working point of the installation.

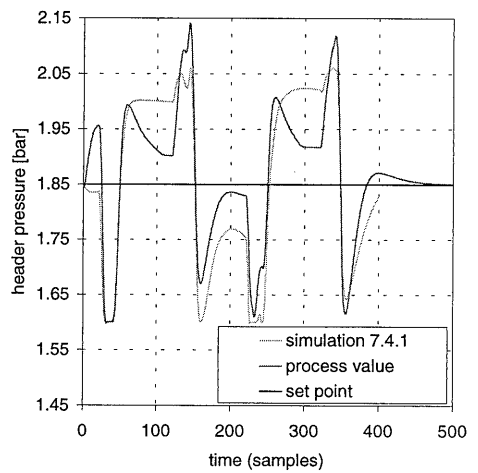
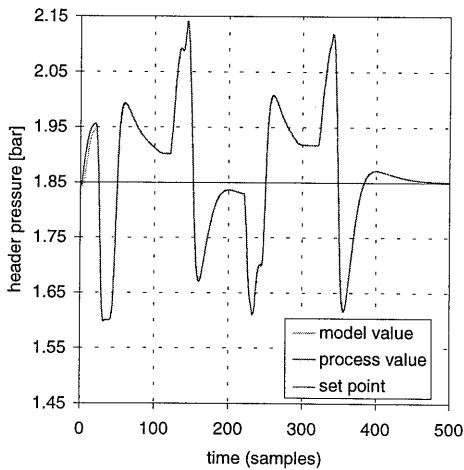


figure 7.21 : Header pressure in the closed-loop simulation. Both model and process values are plotted. The process values are compared to the previous simulation of section 7.4.1.

7.5 Discussion and conclusions

In this chapter, the analysis of compressor station control with MPC has been limited to rather straightforward simulation models and control objectives. Still, we have touched upon the profound opportunities that MPC offers for this control problem. Especially interaction between all control inputs and controlled outputs in combination with perfect constraint handling and dynamic optimisation is shown to benefit the performance of the station. Moreover, MPC offers opportunities for anticipation to future set point changes or disturbances and the application of relevant optimisation criteria like power minimisation.

The basic control objective of a compressor station is to deliver an amount of compressed air within certain constraint limits. Constraints are basically on surge avoidance and minimal header pressure. In our MPC configuration we have integrated surge and capacity control. In the simulations of this chapter we have shown that the performance of the MPC controller strongly depends on the selected control options and tuning parameters.

In the first place, we have compared two different load patterns of the station: The actual load pattern versus the reference load pattern. The performance for both load patterns is good. The applicable load pattern depends on the usage of a compressor station. The actual load pattern corresponds to the common case of a “user” that manipulates a valve or downstream process equipment. Model based control, however, offers the opportunity of a reference load pattern. The delivered amount of compressed air can be automatically adjusted to follow a prescribed, optimal, trajectory. The reference load pattern may be referred to as “air-by-wire”, as an operator can simply adjust the amount of air instead of a valve position.

In the second place, we have compared two different load balancing strategies: equidistant operation of both compressors to the surge line versus power minimisation with respect to an ideal dynamic reference. The, in industrial controllers commonly applied, equidistant-to-surge load balancing controller can well be implemented in MPC. Inherent to the applied optimisation criterion, we had to add an additional weight on recycling to avoid unnecessary recycle. As expected, this control option does not lead to minimal power usage. Model based controllers offer more sophisticated opportunities to minimise power usage. We have implemented a power minimising load balancing strategy by means of a dynamic minimum power input. This objective, indeed, succeeds in reducing the power input to the system compared to the equal-distance-to-surge criterion. Also the performance is good. Still, the ideal-power criterion it is not yet optimal. The definition of ideal power may be refined, especially during transients. Also, the dependence of the (actual) header pressure may be replaced by a fixed (set point) value of the pressure that the user experiences.

In some control cases we showed that the “average” operating point was not fixed when only the load of the station and the constraints were imposed. Indeed, the operating point of the compressor station is not unambiguous. Because of the large number of inputs, any operating point can be obtained with a number of different input combinations. In these cases, the operating point of the installation tends to drift towards a constraint. As we tried to minimise power input (or at least the input movements) this constraint is often the minimum pressure constraint. In general, this situation is not robust enough to guarantee a proper operation of the station under all conditions. An indicated solution is to fix the average operating point by means of an additional set point on the header pressure. This holds for both load patterns (actual and reference) of the compressor station. We showed that a fixed pressure level benefits the performance of the station. An additional pressure set point, however, appears to re-

quire more power. On the other hand, because of the higher (average) pressure level, it provides some important "buffer" during operation. Moreover, also a low value of the set point weighting already determines the (average) operating point and does not require excessive power.

The problem of an ambiguous operating point touches to an inherent problem of the compressor station: the optimal operating point. Indeed, a dynamic optimisation offers opportunities to increase the dynamic performance (transients between operating points and disturbance rejection). It appears, however, that the optimal operating point (for instance defined by minimal power input) can hardly be obtained from a dynamic optimisation (using criterion (5.1)) starting from an arbitrary operating point. The momentary performance strongly depends on the "history" of the system. The dynamic optimisation, therefore, should be supported by a "steady state optimisation" that determines the optimal operating point of the station. In present industrial implementations of non-linear MPC [Qin, 1998] such a separation between a local steady state optimisation followed by a dynamic optimisation is already available. Optimal steady state targets are computed for each input and output. These are then passed to a dynamic optimisation to compute the optimal input sequence that is required to move towards these targets.

A conclusion is that MPC is a challenging, new control strategy for compressor stations. We recommend additional research leading to real-time implementation and testing. First, our modelling needs to be validated on actual compressor installations. Therefore, a relevant industrial configuration needs to be modelled. All relevant information (geometry, component characteristics, etc.) needs to be available. Off-line experimental data can be used to validate the model. Prior to real-time implementation, in simulations, tuning guidelines with respect to input and set point weightings as well as the sample interval and the lengths of horizons should be determined.

Second, the most appropriate optimisation criterion must be determined. A selection of control objectives and additional options like load-balancing and set points need to be made in which also influences from outside the compressor station (like upstream influences or expected user patterns, etc.) can be included.

Finally, the MPC tools may need to be updated. We already mentioned the extension with a steady state optimisation. Another extension of the optimisation routine that would greatly improve the opportunities of MPC for a compressor station is the inclusion of a mixed integer problem in the optimisation [Bemporad, 1998]. A discrete optimisation in the controller allows to include a scheduling of switch on / switch off of compressors in the station. Last but not least, the consequences of an implementation of MPC as a hierarchical controller that generates set points from local controllers needs to be investigated.

8 Conclusions and recommendations

The aim of this study is to investigate the dynamic behaviour and control of turbomachinery installations. We focus on the development of physical models and the application of Model Predictive Control (MPC) as a model based control strategy. A derived aim of the study is to investigate the feasibility of MPC for use on turbomachinery. In this study, we have followed a three step methodology. First, we have developed general purpose dynamic simulation models. Second, we derived (non-linear) model-based control configurations based on Model Predictive Control. Third, we have applied these MPC configurations to representative configurations of compressor/expander systems.

In this study, we have realised a small, custom built, laboratory gas turbine set-up. This installation serves for experimental validation of the models and to test real-time (MPC) control implementations. The laboratory installation offers the opportunity to monitor and to influence the dynamic operation of a gas turbine. Industrial configurations are not available yet for these experiments. Indeed, the laboratory set-up is a fair representation of a gas turbine installation. The non-linearities, dynamics and constraints as well as the properties of the composing components show correspondence to industrial systems. Relevant time scales, however, differ considerably. In this study, emphasis is on the time scales encountered in the laboratory installation. A characteristic time scale for changes in operating point of the laboratory set-up is in the order of 15 seconds. For industrial systems this time scale is usually (much) larger.

Besides the laboratory gas turbine installation, we also considered a generalised compressor station for implementation of MPC. This compressor station comprises two compressors connected in parallel to a common header. The components of the station are chosen at the same scale as the gas turbine set-up. The dynamics of the station, therefore, exhibits approximately the same time scales.

8.1 Model development

The first step in our methodology is the development of dynamic simulation models of turbomachinery. Two types of models have been derived: the physical flow model and the lumped parameter model. Both models are non-linear and based on (vendor supplied) stationary component characteristics and instationary conservation laws over the volumes that connect successive components. The physical flow model also includes general conservation laws for compressible fluid flow through pipes. The physical basis and the modular approach ensure the flexible applicability to a large class of turbomachinery. The component modelling approach is limited to available component maps. The performance of the models depends on the quality of the maps. An extensive validation of model parameters is required.

For the models of the laboratory installation, a systematic validation of the parameters has been performed involving the mass flows through components, the efficiencies of compression, expansion, and combustion, the pressure drops over components, and the inertia parameters. Two problems were encountered during the validation. First, and unexpected, it was required to modify the compressor performance map (available from the original manufacturer) to have the model agree with the experimental results. It appeared, however, not uncommon to modify the composing component maps when an overall system is simulated. In

literature another example of this problem is encountered. [Owen, 1998] reports a state-of-the-art aeroengine simulation problem, in which the available compressor map from the original manufacturer had to be modified to match the experimental results. In the same study, problems were encountered in the determination of the combustion efficiency. Reasons for the component mismatch are not fully understood but may be in the interaction between components in an overall installation and in the methods by which the maps of separate components are determined.

The second problem in the parameter validation was the determination of the efficiencies of expansion and combustion. The modelled expander efficiency does not fully compare to the (expected) physical efficiency. This is caused by the (lumped) influence of the expander cooling system and the (neglected) temperature dependency of the heat capacity. With respect to the combustion efficiency, it appears difficult to model its dynamic behaviour. In the present models, the combustion efficiency is a static function of the fuel-air ratio. This leads, however, to significant (dynamic) model mismatches in the expander inlet temperature during fast transients.

In general, the performance of the validated models is good. Both steady state and transient simulations agree well with experimental results. This holds for the lumped model and for the physical flow model, although not all parameters of the last model have been validated. Differences between both model types are in the smallest time scale of phenomena they describe and in the required simulation times. Apparently, the cut-off frequency of the lumped parameter model for the laboratory set-up is estimated between 0.2 and 2 Hz, which is mainly determined by the large size of the buffer tank in the installation. When faster transients need to be modelled or controlled, the lumped model may fail. Then the physical flow model is required, since its cut-off frequency is approximately between 20 and 300 Hz for the laboratory installation. This is, however, at the expense of a considerably larger simulation time (factor larger than 10). Moreover, even the physical flow model fails to describe the (dynamic) combustion efficiency. Therefore smaller time scales cannot be simulated yet.

Our conclusion is that the non-linear lumped parameter model of the laboratory gas turbine set-up is suitable for transient simulations of the gas turbine. The lumped model is, therefore, suited for application in a model-based controller that controls the operating point. Only when fast transients, for instance due to sudden steam injection, need to be modelled or controlled, the full order physical flow model will be required. Then the parameter validation and the modelling of the combustion efficiency may need to be improved.

8.2 Model based control

The second step in our methodology is to develop a configuration for model predictive control that is suitable for turbomachinery and uses the lumped parameter models. For our MPC configuration we have used Primacs, a package for real-time model based control that is being developed by TNO-TPD (Delft, The Netherlands).

The concept of MPC is that a model of the system to be controlled is included in the controller to predict the systems response over a future horizon and to optimise the future input. Standard linear MPC uses one and the same (linear) model for these tasks. Because strong nonlinearities, displayed by turbomachinery and the large operating areas of most installations (for instance at start-up) cannot always adequately be handled by linear MPC, one of the goals of

this study is to implement certain approaches to non-linear MPC which are, however, still based on linear optimisation.

Although Primacs was originally designed for linear MPC, the flexible, modular structure allowed us to implement our own models and MPC configuration. We implemented two concepts: *non-linear prediction* and *successive linearisation*. Within successive linearisation, a non-linear model is used to provide every sample an updated linear model that can be used for prediction and optimisation. Non-linear prediction means that a non-linear model is used for prediction over the prediction horizon that is combined with a linear model to optimise the future inputs. Of course, in the latter case, both approaches can be combined when the linear model is successively linearised. The controller models for prediction and optimisation are referred to as the *internal prediction model* and the *internal optimisation model* respectively.

A third non-linear approach that we made available, is to use a successively linearised model for prediction and optimisation, while the original non-linear model serves to predict the model outputs only one-sample-ahead. This latter model we refer to as the *internal observation model*. This observation model plays an important role in the filter. It is especially this third approach that we have investigated.

Because of inevitable model mismatches and measurement noise or errors, a *filter* is required to correct the prediction of the internal model towards the actual process measurements. In our implementation we tested the first order integrating (output disturbance) filter. In this filter, a number of extra state elements track the offset between process measurements and model predictions. The non-linear one-sample-ahead observation model avoids that linearisation errors need to be included in the correction.

The first order filter performs well as long as all controlled outputs can be measured (or accurately reconstructed by other measurements) as well. When this reconstruction fails, the first order filter cannot correct the model predictions accurately and the controller performances degrades. A special reconstruction problem arises when an unmeasured output is a static function of (measured) states and this function is only valid for the originally values of these states and not for the corresponding measured process values. For this case an augmented Kalman filter, that updates the model states instead of the outputs, could be used.

8.3 Application of MPC on turbomachinery

We applied the MPC configuration to the laboratory gas turbine and to the generic compressor station. For the gas turbine set-up the emphasis is on real-time implementation. Compressor station control is quite complementary because of the surplus of degrees of freedom that parallel connected compressors possess. The MPC results for the compressor station are restricted to simulations. In both cases, we defined rather straightforward control objectives as set point and trajectory control, combined with constraints on inputs and outputs.

Laboratory gas turbine We succeeded in a real-time implementation of MPC on the laboratory installation. The sample interval was limited to 1.5 seconds. Within the applied sample interval, the *successive linearisation* approach could be implemented. This approach is shown to be a useful and powerful extension to linear MPC. It is expected that other non-linear approaches (besides non-linear prediction also the ultimate non-linear optimisation) will hardly contribute to an improved performance.

The performance of the presented MPC configuration is good. Both steady state set point variations and transient tracking of reference trajectories are performed well. Constraint limits are observed and hardly violated and the influence of tuning parameters like weighting factors and length of horizons is well understood. The presence of model mismatches and disturbances is handled correctly by the filter.

Constraint handling appears to be a realistic advantage of MPC for control of turbomachinery. It is emphasised that most “conventional” controllers cannot deal with constraints at all, especially not when constraints (like surge and expander temperature) are not on *controlled* outputs. For the gas turbine installation, surge and expander temperature constraints are reached frequently. Also (move) constraints on the inputs strongly influence the controlled operation.

Anticipation has been studied in detail. Anticipative behaviour appears to be strongly related to the relative size of the control horizon with respect to the prediction horizon. Sub-optimal solutions are an inherent consequence of differences between these two horizons and cause an “inverse” controller response.

Two remarks on the performance can be made. First, the reconstruction of mass flow through the compressor from *measured* data fails easily due to model errors or (systematic) measurement errors. Indeed, this mass flow is a static function of the model states rotational speed and pressure (ratio). This reconstruction problem enforced us to control the compressor mass flow (and therefore the distance to the surge line) in open-loop, that is, by the internal model value only. We did not yet solve this reconstruction problem. Solutions may be found in modifying the reconstruction of the mass flow, actually measure the mass flow or improve the filter design. The second performance problem is a temporary constraint violation of the measured (process) expander inlet temperature during fast transients. As the controller is able to keep the internal (filtered) model value within the constraint value, this appears to be a filter problem. The filter is not fast enough to compensate the mismatch of the expander temperature. Indicated solutions are in a higher filter gain for this output, a faster MPC sampling time, and, of course, in an improved modelling of the (dynamic) combustion efficiency.

Compressor station The application of MPC on the compressor station indicates the profound opportunities that MPC offers for this control problem. Especially, the dealing with interaction between all control inputs and controlled outputs in combination with perfect constraint handling and dynamic optimisation is shown to potentially improve the performance of the station. Moreover, MPC offers opportunities for anticipation to future set point changes or disturbances and the application of relevant optimisation criteria like power minimisation.

In our MPC configuration we have integrated surge and capacity control. In simulations we showed that the performance of the MPC controller strongly depends on the selected control options and tuning parameters. We have compared two different load patterns of the station and two different load balancing strategies. The applicable load pattern depends on the usage of a compressor station. The, in industrial control commonly applied, equidistant-to-surge load balancing controller can be implemented, but other load balancing strategies provide opportunities to minimise power input to the station. Several control options like recycle flow minimisation, dynamic minimum power reference, and an additional set point on the pressure in the header are investigated. In a preliminary conclusion, a dynamic minimum power reference, combined with a low-weighted set point on the header pressure gives promising results.

Constraint handling is one of the outstanding advantages of MPC for compressor station control. It is shown that surge can be avoided and that boundary limits on the pressure in the header or on the rotational speed can be guaranteed. Also input (move) constraints can be successfully taken into account. Anticipation appears especially useful for compressor stations when future load changes or disturbances can be predicted. Future research on compressor and gas supply networks need to be done to take the “environment” of the compressor station into account.

An inherent problem of the compressor station is that the optimal operating point cannot be determined from a dynamic optimisation starting from an arbitrary operating point. We recommend, therefore, that the dynamic optimisation is supported by a “steady state optimisation” that determines the optimal operating point of the station prior to a dynamic optimisation towards the new optimal operating point. Another useful extension of MPC is a discrete optimisation in the controller. A hybrid optimisation allows to include a scheduling of switch on / switch off of compressors within the dynamic optimisation of the operating point.

8.4 Consequences for industrial systems

In this thesis, MPC has been tested by a real-time implementation on the laboratory installation and by simulations on a generic compressor station. Both tests have been restricted to the particular geometry and response times of the laboratory set-up.

The consequences for industrial control systems are not immediately clear. Most industrial configurations and control objectives, including electrical generators and their load patterns, can be easily introduced into our modelling. The same type of dynamics and constraints hold. Surge is a potential danger for all compressors and also the expander temperature is constrained¹ for tripping and lifespan conditions. Also relevant optimisation criteria can be included in the MPC controller configuration. Indeed, the geometry and the response times of industrial systems may be different, which may cause problems in available computation times when large or complex models need to be included in the controller. Likely, however, the time constants of the dynamics of large scale installations are lower, so very small sample intervals may not be required. Moreover, a promising concept may be in a hierarchical controller implementation. Then, MPC is not used as the primary controller, but only computes the set points for local controllers. The sample interval of the MPC controller may be larger, allowing more complex models and optimisation criteria.

8.5 Recommendations

We find that MPC is a challenging, new control strategy both for gas turbine installations and for compressor stations. We conclude that MPC serves well on turbomachinery and is promising for industrial applications. More research, both in simulations and in experiments, leading to real-time implementation of MPC to (industrial) turbomachinery configurations is recommended. The following suggestions for future research are made:

¹ In industrial gas turbines and aero-engines, the expander inlet temperature constraint is often replaced by a constraint on the expander outlet temperature. Because of the extremely high inlet temperatures, the outlet temperature is better measurable.

First, we recommend to investigate some particular problems we encountered in this study that are not completely solved. These include the search for opportunities to improve the reconstruction of the mass flow through the compressor or to avoid this reconstruction, the interaction between components and the influence of this interaction on the (original) characteristics, the modelling of the dynamic combustion efficiency, and the proper determination of the components (polytropic) efficiencies.

Second, we recommend to extend the laboratory installation with fast and accurate control valves, especially on the blow-off, and with steam injection. Combined with appropriate model extensions and renewed validation, dynamic experiments and fast control experiments that challenge the dynamics of the system and the filter should be performed.

Third, we recommend to investigate the use of further reduced models. Some (physical) redundant states may be eliminated or black-box parts may be included. Also mathematical model reduction techniques may be taken into account. Reduced models may further reduce computation times and therefore aid to decrease the MPC sample interval and increase the controller performance. Reduced models may also ease model validation as not all physical parameters (redundant in mass flow, efficiency, pressure drop etc.) need to be determined but only a fixed number of “structure” parameters.

Fourth, we recommend some extensions to MPC. In the first place it is worthwhile to implement the augmented Kalman filter to study its performance on the laboratory installation. Further we mentioned the inclusion of a mixed integer optimisation problem and the introduction of a steady state optimisation in the compressor station case.

Finally, we recommend to study the opportunities of model based *active* surge control. In this thesis, we focused on surge *avoidance*, as surge was regarded a static instability. In closed-loop control, however, it is possible to modify the dynamic behaviour of the compressor and to *prevent* surge (and to enlarge the operating area of the compressor) by means of (dynamic) inputs to the system. This approach is referred to as active surge control.

References

- Badmus, O.O.; Chowdhury, S.; Eveker K.M.; Nett C.N.; Control-oriented high-frequency turbomachinery modelling: single-stage compression system one-dimensional model, *Journal of Turbomachinery*, Vol. 117, p. 47-61, 1995a.
- Badmus, O.O.; Eveker K.M.; Nett C.N.; Control-oriented high-frequency turbomachinery modelling: general one-dimensional model development, *Journal of Turbomachinery*, Vol. 117, p. 320-335, 1995b.
- Badmus, O.O.; Chowdhury, S.; Nett C.N.; Nonlinear control of surge in axial compression systems, *Automatica*, Vol. 32, p. 59-70, 1996.
- Bemporad, Alberto; Morari, Manfred; Predictive control of constrained hybrid systems, *International symposium on nonlinear model predictive control: Assessment and future directions*, Ascona, Switzerland, 1998.
- Bequette, B. Wayne; Nonlinear control of chemical processes: a review, *Industrial Engineering Chemistry Research*, Vol. 30, p. 1391-1413, 1991.
- Bird, R. Byron; Steward, Warren E.; Lightfoot, Edwin N.; *Transport phenomena*, Wiley, 1960.
- Bitmead, R.R.; Gevers, M.; Wertz, V.; *Adaptive optimal control: the thinking man's GPC*, Prentice Hall, 1990.
- Botros, K.K.; Campbell, P.J.; Mah, D.B.; Dynamic simulation of compressor station operation including centrifugal compressor and gas turbine, *Journal of Engineering for Gas Turbines and Power*, Vol. 113, p. 300-311, 1991.
- Botros, K.K.; Transient phenomena in compressor stations during surge, *Journal of Engineering for Gas Turbines and Power*, Vol. 116, p. 133-142, 1994a.
- Botros, K.K.; Henderson, J.F.; Developments in centrifugal compressor control—a technology assessment, *Journal of Turbomachinery*, Vol. 116, p. 240-249, 1994b.
- Botros, K.K.; Richards, D.J.; Roorda, O.; Effects of check valve dynamics on the sizing of recycle systems for centrifugal compressors, *ASME paper 96-GT-94*, 1996.
- Brengel, David. D.; Seider, Warren D.; Multistep nonlinear Predictive Controller, *Industrial Engineering Chemistry Research*, Vol.28, p.1812-1822, 1989.
- CCC, Application Note AN21, Compressor Controls Corporation, 1992.
- CCC, publication PB4104, Compressor Controls Corporation, 1995.
- Clarke, D.W.; Mohtadi, C.; Tuffs, P.S.; Generalised predictive control-part 1 the basic algorithm, *Automatica*, Vol. 23, p.137-148, 1987.
- Clarke, D.W.; Scattolini, R.; Constrained receding-horizon predictive control, *IEEE Proc. Pt. D.*, Vol. 138, p.347-354, 1991.
- Cohen, H.; Rogers, G.F.C.; Saravanamuttoo, H.I.H.; *Gas turbine theory*, 3rd edition, Longman, 1987.
- Cumpsty, N.A.; *Compressor aerodynamics*, Longman, 1989.
- Cutler, C.R.; Ramaker, B.L.; Dynamic matrix control - A computer control algorithm, *Proc. Joint American Control Conf.*, 1980.

- De Nicolao, G.; Magni, L.; Scattolini, R.; Stability and robustness of nonlinear receding horizon control, International symposium on nonlinear model predictive control: Assessment and future directions, Ascona, Switzerland, 1998.
- Eaton, John W.; Rawlings, James B.; Model predictive control of chemical processes, Chemical Engineering Science, Vol. 47, p. 705-720, 1992.
- Econosto, Technical product documentation, Econosto BV, 1992.
- Edgar, T.F.; Himmelblau, D.M.; Optimization of chemical processes, McGraw-Hill, 1988.
- Ffows Williams, J.E.; Harper, M.F.L.; Allwright, D.J.; Active stabilization of compressor instability and surge in a working engine, Journal of Turbomachinery, Vol. 115, p. 68-75, 1993.
- Fink, D.A.; Cumpsty, N.A.; Greitzer, E.M.; Surge dynamics in a free-spool centrifugal compressor, Journal of Turbomachinery, Vol. 114, p. 321-332, 1992.
- Garcia, Carlos E.; Quadratic dynamic matrix control of nonlinear processes, AIChE Annual Meeting, San Francisco, 1984.
- Garcia, Carlos E.; Morshedi, A.M.; Quadratic programming solution of dynamic matrix control (QDMC), Chemical Engineering Communications, Vol. 46, p. 73-87, 1986.
- Garcia, C.E.; Prett, D.M.; Morari, M.; Model predictive control: theory and practice - a survey, Automatica, Vol.25, p.335-348, 1989.
- Garrard, Doug; ATEC: The aerodynamic turbine engine code for the analysis of transient and dynamic gasturbine engine system operations, part 1: Model development, ASME paper 96-GT-193, 1996; Part 2: Numerical simulations, ASME paper 96-GT-194, 1996.
- Gasunie, Physical properties of natural gases, Nederlandse Gasunie, 1987.
- Gattu, Gangadhar; Zafiriou, Evangelos; Nonlinear quadratic dynamic matrix control with state estimation, Industrial Engineering Chemistry Research, Vol. 31, p. 1096-1104, 1992.
- GAVO-1987: Voorschriften voor aardgas installaties, part 1 NEN 1078, 4th edition (in Dutch); part 2 NEN 2078, Nederlands Normalisatie Instituut, 1987.
- Greitzer, E.M.; Surge and rotating stall in axial flow compressors, part 1 Theoretical compression system model, part 2 Experimental results and comparison with theory, Journal of Engineering for Power, Vol. 98, p. 190-217, 1976.
- Greitzer, E.M.; Moore, F.K.; A theory of post-stall transients in axial compression systems: part 2 Application, Journal of Engineering for Gas Turbines and Power, Vol. 108, p. 231-239, 1986.
- Gysling, D.L.; Greitzer, E.M.; Dynamic control of rotating stall in axial flow compressors using aeromechanical feedback, Journal of Turbomachinery, Vol. 117, p. 307-319, 1995.
- Janna, William S.; Engineering heat transfer, SI Edition, Van Nostrand Reinhold, 1988.
- Kuznetsov, A.G.; Constrained predictive control: a brief survey, Journal A, Vol.37, No. 2, p. 3-8, 1996.
- Kwakernaak, H.; Sivan, R.; Linear optimal control systems, Wiley, 1972.
- Lee, Jay H.; Ricker, N. Lawrence; Extended kalman filter based nonlinear model predictive control, Proceedings of the American Control Conference, p. 1895-1899, 1993.
- Lee, J.H.; Yu, Z.H.; Tuning of model predictive control for robust performance, Computers Chem. Engng., Vol.18, p.15-37, 1994.

- Lefebvre, Arthur W.; Gas turbine combustion, McGraw-Hill, 1983.
- Li, W.C.; Biegler, L.T.; Multistep, Newton type control strategies for constrained nonlinear processes, Chem Eng Res Des, Vol. 67, p.562-577, 1989.
- Magni, L.; Nijmeijer, H., Van der Schaft, A.; A receding horizon approach to the nonlinear H_∞ control problem, submitted to Automatica, 1998.
- Mehra, R.K. *et al*; Model algorithmic control: review and recent development, Engineering foundation conference on chemical process control, 1982.
- Moore, F.K.; Greitzer, E.M.; A theory of post-stall transients in axial compression systems: Part I — Development of equations, Journal of Engineering for Gas Turbines and Power, Vol. 108, p. 68-76, 1986.
- Morari, M.; Garcia, C.E.; Lee, J.H.; Pretz, D.M.; Model predictive control, Prentice Hall, preprint, 1993a.
- Morari, M.; Ricker, N.L.; Model predictive control toolbox, Matlab functions for the analysis and design of Model Predictive Control systems, The MathWorks, 1993b.
- Mosca, E.; Zhang, J.; Stable redesign of predictive control, Automatica, Vol. 28, p.1229-1233, 1992.
- Muske, Kenneth R.; Rawlings, James B.; Model predictive control with linear models, AIChE Journal, Vol. 39, p. 262-286, 1993.
- NEN 3005, Het meten van het debiet van vloeistof- en gasstromen in gesloten leidingen door middel van meetschijven (In Dutch), Nederlands Normalisatie Instituut (NNI), 1972.
- Nisenfel, A. Eli; Centrifugal compressors, Monograph series/Instrument Society of America, no. 3, 1982.
- Oliveira, Numo M.C. de; Biegler, Lorenz T.; Constraint handling and stability properties of model-predictive control, AIChE Journal, Vol. 40, p. 1138-1155, 1994.
- Oliveira, Numo M.C. de; Biegler, Lorenz T.; An extension of Newton-type algorithms for nonlinear process control, Automatica, Vol. 31, p. 281-286, 1995.
- Patwardhan, Asutosh A.; Rawlings, James B.; Edgar, Thomas F.; Nonlinear model predictive control, Chemical Engineering Communications, Vol. 87, p. 123-141, 1990.
- Profit report, Supervisory Model Based Control, Deliverable D.2.4, Esprit II project 5352, 1992.
- Qin, S. Joe; Badgewell, Thomas A.; An overview of nonlinear model predictive control applications, International symposium on nonlinear model predictive control: Assessment and future directions, Ascona, Switzerland, 1998.
- Press, W.H.; Teukolsky, S.A.; Vetterling, W.T.; Flannery, B.P.; Numerical recipes in FORTRAN, 2nd edition, Cambridge University Press, 1992.
- Patankar, Suhas V.; Numerical heat transfer and fluid flow, Hemisphere Publishing Corporation, 1980.
- Parr, E.A.; Industrial control handbook, volume I, Collins, 1985.
- Pinsley, J.E.; Guenette, G.R.; Epstein, A.H.; Greitzer, E.M.; Active stabilization of centrifugal compressor surge, Journal of Turbomachinery, Vol. 113, p. 723-732, 1991.
- Rawlings, J.B.; Muske, K.R.; The stability of constraint receding horizon control, IEEE Transactions on Automatic control, Vol.38, p.1512-1516, 1993.

- Richalet, J.; Rault, A.; Testud, J.L.; Papon, J.; Model predictive heuristic control: Application to industrial processes, *Automatica*, Vol. 14, p. 413-428, 1978.
- Rogers, G.F.C.; Mayhew, Y.R.; *Engineering thermodynamics*, 4th edition, Longman, 1992.
- Schobeiri, M.T.; Attia, M.; Lippke, C.; GETRAN: A generic, modularly structured computer code for simulation of dynamic behavior of aero- and power generation gas turbine engines, *Journal of Engineering for Gas Turbines and Power*, Vol. 116, p. 483-494, 1994.
- Schobeiri, M.T.; Attia, M.; Advances in nonlinear dynamic engine simulation with an example: dynamic performance behaviour of a gas turbine with one reheat turbine stage and two combustion chambers, ASME paper 96-GT-392, 1996.
- Simon, J.S.; Valavani, L.; Epstein, A.H.; Greitzer, E.M.; Evaluation of approaches to active compressor surge stabilization, *Journal of Turbomachinery*, Vol. 115, p. 57-67, 1993.
- Sistu, Phani B.; Bequette, B.Wayne; Nonlinear predictive control of uncertain processes: application to a CSTR, *AIChE Journal*, Vol. 37, p. 1711-1723, 1991.
- Sistu, P.B.; Gopinath, R.S.; Bequette, B.W.; Computational issues in nonlinear predictive control, *Computers and Chemical Engineering*, Vol. 17, p. 361-366, 1993.
- Streeter, Victor L.; Wylie, K. Benjamin; *Fluid mechanics*, McGraw-Hill, 1985.
- Van Essen, H. A.; Design of a laboratory gas turbine installation, Stan Ackermans Institute, Eindhoven University of Technology, ISBN 90-5282-452-5, 1995.
- Vroemen, B.G.; Van Essen, H.A.; Kok, J.J.; Van Steenhoven, A.A.; Nonlinear model predictive control of a laboratory gas turbine installation, ASME paper 98-GT-100, 1998.
- Woodward, Technical product information, Woodward Governor Company, 1995.
- Zheng, Alex; Morari, Manfred; Stability of model predictive control with mixed constraints, *IEEE Transactions on Automatic Control*, Vol. 40, p 1818- 1823, 1995.

A Component Characteristics

A.1 Gas turbine preliminaries

Compression and expansion in a gas turbine are partly irreversible processes. Figure A.1 presents a T-s diagram of a simple gas turbine cycle which include non-isentropic compressor and expansion. The *ideal* or *isentropic* temperatures are marked with an accent. In the same figure the influence of a pressure drop ($p_2 - p_3$) between compressor outlet and expander inlet is included. The temperatures without pressure drop are marked with an asterisk. From this diagram the isentropic efficiency of compressor and expander can be defined as:

$$\eta_{c,isen} = \frac{T_2' - T_1}{T_2 - T_1} \quad \text{and} \quad \eta_{t,isen} = \frac{T_3 - T_4}{T_3 - T_4'} \quad \text{re-}$$

spectively. From these definitions the actual temperature difference over the compressor and the expander can be computed from:

$$T_2 - T_1 = \frac{T_1}{\eta_{c,isen}} \left(\left(\frac{p_2}{p_1} \right)^{\frac{\gamma-1}{\gamma}} - 1 \right) \quad \text{and}$$

$$T_3 - T_4 = \eta_{t,isen} T_3 \left(1 - \left(\frac{p_4}{p_3} \right)^{\frac{\gamma-1}{\gamma}} \right).$$

For turbomachinery often a polytropic definition of efficiency instead of the isentropic definition is applied. The reason for this is that one constant efficiency can be determined for a compression or expansion process even when this process consists of multiple stages over which the isentropic (stage) efficiency will not be constant. A polytropic state transformation is defined by:

$$\frac{T}{p^{\frac{\gamma-1}{\eta}} \left(\frac{\gamma}{\gamma} \right)} = \text{constant} \quad (\text{A.1})$$

with η the polytropic efficiency. According to this definition, the actual temperature ratios over the compressor and the expander can be determined as

$$\left(\frac{T_2}{T_1} \right) = \left(\frac{p_2}{p_1} \right)^{\left(\frac{\gamma-1}{\gamma \eta_c} \right)} \quad \text{and} \quad \left(\frac{T_3}{T_4} \right) = \left(\frac{p_3}{p_4} \right)^{\left(\frac{\eta_t (\gamma-1)}{\gamma} \right)} \quad (\text{A.2})$$

respectively. The corresponding polytropic efficiencies of compressor and expander are

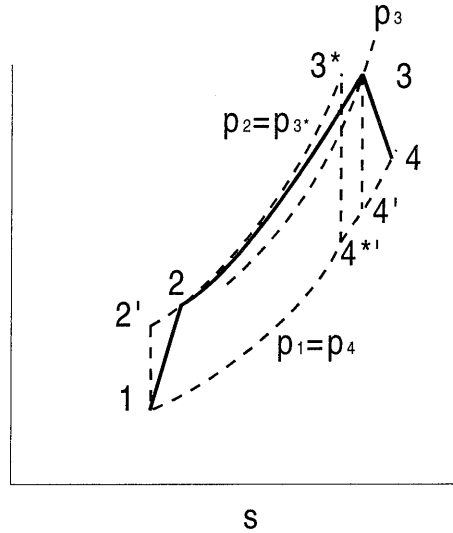


figure A.1 : T-s diagram of a simple gas turbine cycle including non-isentropic compression and expansion and a pressure drop between compressor outlet and expander inlet.

$$\eta_c = \frac{\gamma - 1}{\gamma} \frac{\ln\left(\frac{p_2}{p_1}\right)}{\ln\left(\frac{T_2}{T_1}\right)} \quad \text{and} \quad \eta_t = \frac{\gamma}{\gamma - 1} \frac{\ln\left(\frac{T_3}{T_4}\right)}{\ln\left(\frac{p_3}{p_4}\right)} \quad (\text{A.3})$$

The corresponding power required by a compression process is determined by

$$P_c = \dot{m}_c C_{p,c} (T_2 - T_1) = \dot{m}_c C_{p,c} T_1 \left(\left(\frac{p_2}{p_1} \right)^{\frac{\gamma-1}{\eta_c}} - 1 \right) \quad (\text{A.4})$$

while, analogous, the power delivered by an expansion process is determined by

$$P_t = \dot{m}_t C_{p,t} (T_3 - T_4) = \dot{m}_t C_{p,t} T_3 \left(1 - \left(\frac{p_4}{p_3} \right)^{\frac{\eta_t(\gamma-1)}{\gamma}} \right) \quad (\text{A.5})$$

A.2 Compressor characteristic

Figure A.2 presents the original compressor characteristic of the BBC VTR160 turbocharger according to the graphical representation provided by the manufacturer. The compressor

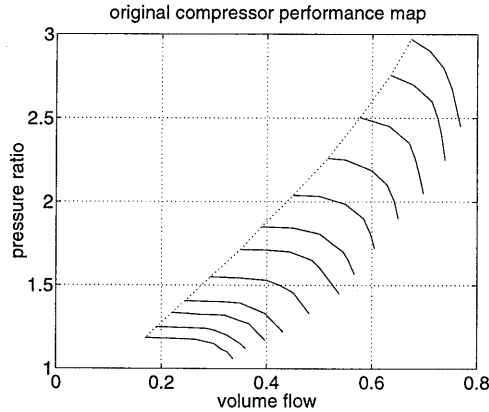


figure A.2 : Original compressor performance map.

(total) pressure ratio $Prat$ (-) is plotted versus the volume flow \dot{V} (m^3/s) through the compressor for various values of the rotational speed N (rev/min). In the original map, the pressure ratio and the volume flow are both referenced to air of a temperature of 288 (K), and a pressure of 1.0 (bar). The normalised density of air at this pressure and temperature is 1.2 (kg/m^3).

Figure A.3 compares our mathematical fit of the compressor characteristic to the data from the manufacturer. The fit is based on a second order polynomial fit:

$$Prat = \frac{p_2}{p_1} = A(N) \dot{V}^2 + B(N) \dot{V} + C(N) \quad (\text{A.6})$$

for any rotational speed within a range from 15000 to 42000 rev/min. The extremes of the parabolas are fixed on the surge line. The coefficients $A(N)$, $B(N)$, and $C(N)$ are determined by sixth order polynomial fits over the complete range of rotational speeds. This approach leads to a satisfactory description of the compressor performance map. In figure A.3 points obtained from the original graphical representation of the performance map at a constant rotational speed are plotted in crosses '+', while the mathematical fit of the corresponding rotational speed curve is drawn in solid lines. The dashed line shows the actual surge line according to the manufacturer, while the solid "surge line" shows the surge line according to the fit as the linked maximums of all curves of rotational speed.

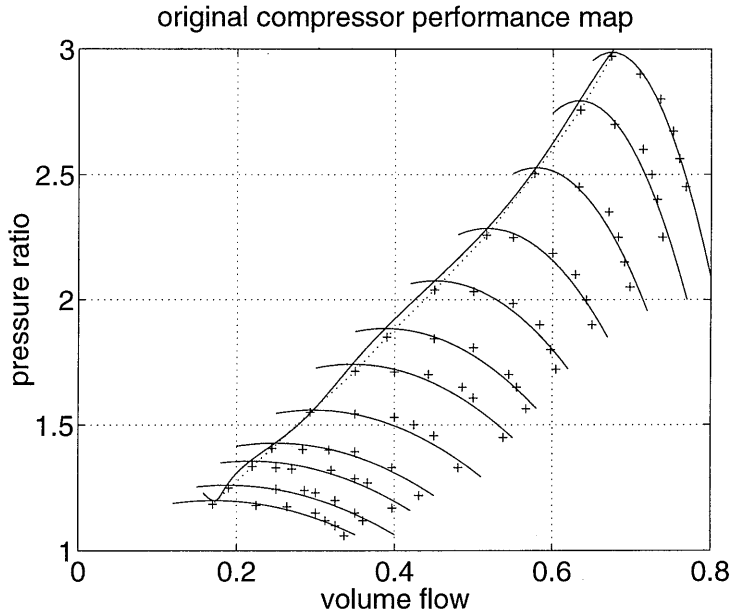


figure A.3 : Mathematical fit of the compressor performance map.

Within the operating range of the compressor, the accuracy of the fit is rather good. The fit is limited for high (42000 rev/min) and low values (15000 rev/min) of the rotational speed. The parabolic shape of the rotational speed curves does not match the choking behaviour of the compressor characteristic: in the real map, the pressure gradient at higher mass flow becomes very steep due to break-away of flow and dropping efficiencies. The parabolic shape cannot represent this behaviour. This does not compromise the use of the fit since operating in the choking area of the compressor is excluded in normal operation of the gas turbine. The expander is more likely to choke and due to the reverse pressure gradient in the expander this does not influence the pressure gradient or efficiency of the expander. The parabolic shape can also not follow the almost flat lines of constant rotational speed near the surge line leading to small deviations in the fit over the whole curve. Although these deviations are rather small, their influence is significant because of the ill-conditioning of the characteristic.

The maximum allowable rotating speed of the turbocharger has been limited to 35000 rev/min. This speed corresponds to a pressure ratio of about 2.25.

	A(N)	B(N)	C(N)
1	2.77309428403675e+001	-1.45197329098387e+002	7.25717433841597e+001
N	-1.15180363512399e-002	+4.04918186433896e-002	-1.86190895383627e-002
N^2	+1.57304616982506e-006	-4.52872638270511e-006	+1.95883720952405e-006
N^3	-1.058110041784e-010	+2.60954693821889e-010	-1.06175287530094e-010
N^4	+3.72374699463208e-015	-8.11642530137263e-015	+3.10922060166141e-015
N^5	-6.51912048495668e-020	+1.28243058048326e-019	-4.61132963429711e-020
N^6	+4.36553159400385e-025	-7.88466994246646e-025	+2.63995234246694e-025

table A.1 : coefficients for the parabolic curves

A.3 Scaling compressor characteristic

In general, three dimensionless numbers are used to represent the flow and the rotational speed in the compressor characteristic. Besides the obvious dimensionless parameter p_2 / p_1

these are a dimensionless mass flow $\frac{\dot{m}\sqrt{RT_1}}{D^2 p_1}$ and rotational speed $\frac{ND}{\sqrt{T_1}R}$.

For a constant characteristic diameter D and a gas constant R , that is always the same compressor and the same fluid composition, these dimensionless numbers can be simplified to the

following semi-dimensionless parameters $\frac{\dot{m}\sqrt{T_1}}{p_1}$ and $\frac{N}{\sqrt{T_1}}$ respectively.

Scaled to a fixed reference temperature (of 288 K) and pressure (of 1.0 bar) they may be written like normalised numbers:

$$\tilde{m} = \frac{\dot{m}\sqrt{\frac{T_1}{288}}}{\frac{p_1}{1.0}} \quad \text{and} \quad \tilde{N} = \frac{N}{\sqrt{\frac{T_1}{288}}} \quad (\text{A.7})$$

These numbers can be used to transform the real or actually measured properties to properties that can be compared with those used in the original characteristic. Consider the following definitions:

	<i>normalised</i>	<i>actual</i>	<i>original characteristic</i>
Mass flow	\tilde{m} [-]	\dot{m} [kg/s]	\dot{V} [m ³ /s]
Rotational speed	\tilde{N} [-]	ω [rev/s]	N [rev/min]
Pressure ratio	$\frac{p_2}{p_1}$ [-]	$\frac{p_2}{p_1}$ [-]	$Prat$ [-]

table A.2 : Scaling notation.

Note that \dot{V} is the volume flow according to the original characteristic, that is, fixed to the reference conditions, it is *not* equivalent to the actual mass flow. We assume that the actual mass flow \dot{m} (kg/s) is the original characteristic volume flow \dot{V} multiplied with a scale factor:

$$\dot{m} = \dot{V} \frac{p_1}{\sqrt{\frac{T_1}{288}}} 1.2 \quad (\text{A.8})$$

The pressure p_1 is in [bar] and therefore the reference pressure of 1.0 bar vanishes. The normal density of air is 1.2 kg/m^3 . Furthermore, the actual rotational speed ω [rev/s] is assumed to equal the rotational speed N multiplied with a scale factor:

$$\omega = N \sqrt{\frac{T_1}{288}} \frac{1}{60} \quad (\text{A.9})$$

This scaling implies that at a higher value of the inlet temperature T_1 the same mass flow corresponds to a higher volume flow in the characteristic and a correction to a higher rotational speed. This is in line with a decreased density at a higher value of the inlet temperature, to cope with the higher volume flow. Both mass flow and rotational speed are corrected by the square root of the temperature. The inlet pressure has similar effects though opposite to the inlet temperature since an increase of inlet pressure corresponds to a higher inlet density.

The compressor *mass flow* characteristic is presented in figure A.4 for different ambient conditions when the scaling rules are applied to the original volume flow of the compressor map.

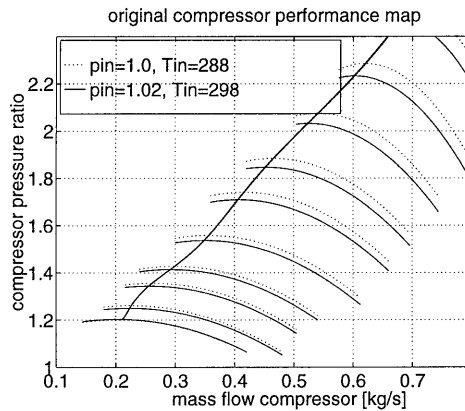


figure A.4 : Influence of scaling parameters on the compressor performance map.

Mass flow from pressure and rotational speed When the actual compressor mass flow is computed from the actual pressure p_2 over the compressor and the actual rotational speed ω of the turbine shaft, this implies that the following steps are executed:

1. The actual compressor outlet pressure is corrected to match the pressure ratio of the original characteristic:

$$Prat = \frac{p_2}{p_{amb}} \quad (\text{A.10})$$

2. The actual rotational speed is corrected to match the original characteristic:

$$N = \omega 60 \sqrt{\frac{288}{T_{amb}}} \quad (\text{A.11})$$

3. The volume flow according to the original characteristic is computed from the mathematical fit using $Prat$ and N :

$$\dot{V} = \frac{-B(N) - \sqrt{B(N)B(N) - 4A(N)[C(N) - Prat]}{2A(N)} \quad (\text{A.12})$$

4. This volume flow is corrected to the actual mass flow according to:

$$\dot{m} = \dot{V} \frac{P_{amb}}{\sqrt{\frac{T_{amb}}{288}}} 1.2 \quad (\text{A.13})$$

The almost flat rotational speed curves near the surge line cause an ill-conditioned characteristic. It is difficult to reconstruct the mass flow from (measured) pressure and rotational speed.

Pressure ratio from mass flow and rotational speed The inverse computation of the actual pressure ratio from measured (actual) mass flow and rotational speed is used to present and compare measured and simulated results. This procedure does not reflect conditioning problems. The following scaling steps are required:

1. The actual rotational speed is corrected to match the original characteristic:

$$N = \omega 60 \sqrt{\frac{288}{T_{amb}}} \quad (\text{A.14})$$

2. The actual mass flow is corrected to the volume flow of the original characteristic:

$$\dot{V} = \frac{\dot{m}}{\frac{P_{amb}}{\sqrt{\frac{T_{amb}}{288}}} 1.2} \quad (\text{A.15})$$

3. The pressure ratio according to the original characteristic is computed from the fit:

$$Prat = A(N)\dot{V}^2 + B(N)\dot{V} + C(N) \quad (\text{A.16})$$

4. The actual pressure ratio or the actual compressor outlet pressure is computed:

$$\frac{P_2}{P_1} = Prat \frac{P_{amb}}{P_1} \quad (\text{A.17})$$

A.4 Expander characteristic

The original expander performance map in figure A.5 presents the dimensionless flow coefficient α_t versus the pressure ratio over the expander.

$$\alpha_t = 0.082815 + 1.167342 \left(\frac{P_{03}}{P_4} \right) - 0.476851 \left(\frac{P_{03}}{P_4} \right)^2 + 0.088298 \left(\frac{P_{03}}{P_4} \right)^3 - 0.006181 \left(\frac{P_{03}}{P_4} \right)^4 \quad (\text{A.18})$$

This pressure ratio is actually defined as the total pressure before the expander over the static pressure after the expander. The flow coefficient is a dimensionless mass flow. In figure A.5 the fourth order polynomial fit (A.18) of the original graphical map is presented. According to the manufacturer, the actual mass flow is related to the flow coefficient by formula (A.19)

in which α_t is the flow coefficient and S_{resT} is the area measure of expander and nozzle ring with a fixed value of 21.1 cm². The performance map in which the explicit mass flow is plotted versus the pressure ratio is presented in figure A.6. The expander inlet temperature then becomes an additional parameter for the characteristic.

$$\dot{m} = \alpha_t S_{resT} P_{03} 10 \sqrt{\frac{2\gamma}{\gamma-1} \left[\left(\frac{P_{03}}{P_4} \right)^{-\frac{2}{\gamma}} - \left(\frac{P_{03}}{P_4} \right)^{-\frac{\gamma+1}{\gamma}} \right]} RT_3 \quad (A.19)$$

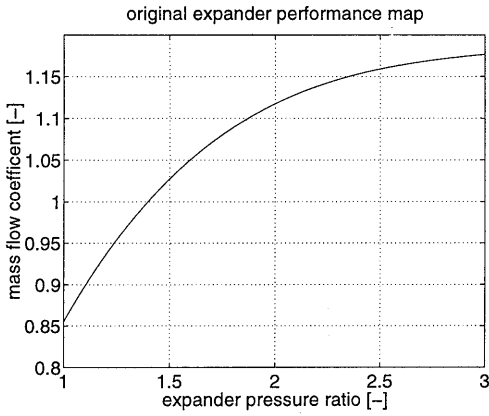


figure A.5 : Original expander performance map

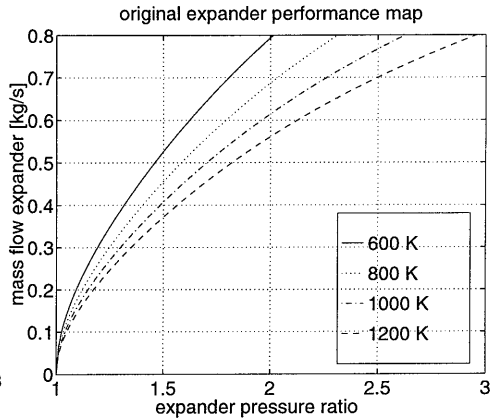


figure A.6 : Expander mass flow characteristic

A.5 Mass flow corrections compressor and expander

In Chapter 4 the mass flow correction for the compressor and expander are discussed. A correction appears necessary since the mass flows through both components should be equal in a stationary operating point. Both mass flows are corrected towards the actually measured mass flow through the orifice. In this section the procedure by which the correction factors are obtained is discussed. The procedure uses a data set of 20 stationary operating points scattered over the whole working area. This data set has been introduced in chapter 4.

Compressor correction The mass flow through the compressor is determined by the fit of the compressor characteristic. This fit consists of parabolic curves for constant rotational speed (A.6) for which the top has been fixed to the surge line. The mass flow is computed according to (A.12) and (A.13) as

$$\dot{m}_c = f(N, p_2, p_1, T_1) \quad (A.20)$$

The compressor characteristic *fit* is corrected. The correction consists of two parts (note that these two correction steps are additional to the already applied scaling correction for the ambient conditions).

1. The effective rotational speed is decreased, so that the corresponding mass flow for the same input rotational speed and pressures are lowered. This is accomplished by multiplying

the actual rotational speed N with a scale factor N_{scale} before the parabolic coefficients $A_{org}(N)$, $B_{org}(N)$, and $C_{org}(N)$ are computed from the original values of table A.1.

2. The resulting coefficients A_{org} and B_{org} are multiplied by a factor ab_corr that adapts the steepness of the parabola. In order to keep the top of the parabola on the (original) surge line the coefficient C_{org} is multiplied with the factor

$$c_corr = \frac{B_{org}^2}{4A_{org}C_{org}}(ab_corr - 1) + 1 \tag{A.21}$$

The correction factors N_{scale} and ab_corr are determined from a fit procedure. Since both factors are closely related and the problem is badly conditioned, we have tried the following procedure: We started with $ab_corr = 1.0$, that is, no correction. For each stationary point in the data set an optimal value of the factor N_{scale} can be found. These values are presented in figure A.7 as N_{scale_start} . We correlated these correction factors to a (preliminary) quadratic fit of the actual rotational speed (not shown). Then, applying this fit of N_{scale} we did the same for ab_corr . The optimal values for each operating point are presented as ab_corr_start in figure A.8. Clearly, these values are hard to correlate to the rotational speed. Moreover, inherent to the correction principle, this factor is extremely bad scaled near the surge line. Therefore we choose to find a constant ab_corr . Finally, using the indicated starting values, we have optimised the quadratic coefficients of N_{scale} along with the constant value of ab_corr over all data points resulting in the final factors N_{scale} and ab_corr that are indicated in figure A.7 and figure A.8. The result of the compressor mass flow correction is presented in figure A.9.

$$N_{scale} = ((142.064 * N - 130.10838) * N + 10.3207083) * N + 0.755338013 \tag{A.22}$$

$$ab_corr = 3.697263364 \tag{A.23}$$

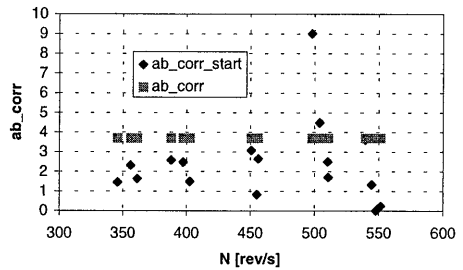
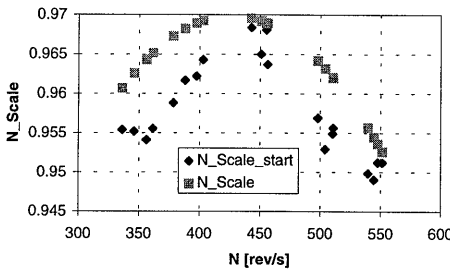


figure A.7 : Compressor map correction factor N_{scale} . figure A.8 : Compressor map correction factor ab_corr .

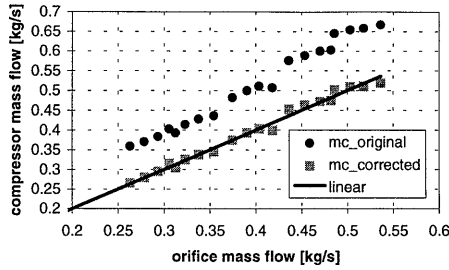


figure A.9 : Compressor map mass flow correction.

Expander correction The mass flow correction of the expander mass flow to the orifice mass flow is very straightforward by a correction factor that is a function in the rotational speed divided by the square root of the (uncooled) expander inlet temperature. This correlation is presented in figure A.10.

$$mt_factor_fit = 0.00018103 * \left(\frac{N}{\sqrt{T_3}} \right)^2 - 0.013827948 \frac{N}{\sqrt{T_3}} + 1.144389627 \quad (A.24)$$

The result of the expander mass flow correction is presented in figure A.11. Since the correction is a function of both rotational speed and expander inlet temperature, the performance map is now also a function of both:

$$\dot{m}_t = f(p_3, p_4, T_3, N) \quad (A.25)$$

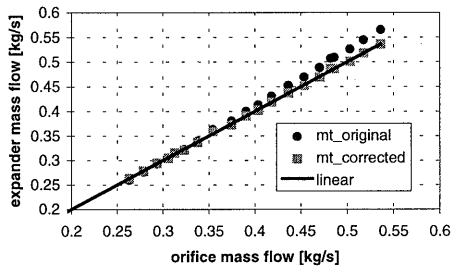
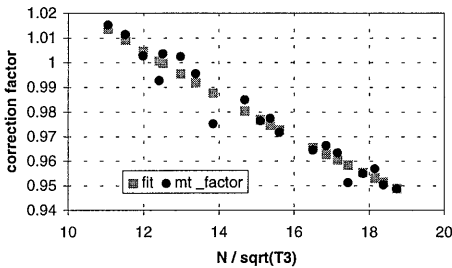


figure A.10 : Expander map mass flow correction factor.

figure A.11 : Expander map mass flow correction.

A.6 Compressor and expander polytropic efficiencies

The compressor and expander (polytropic) efficiencies must agree with the power balance between compressor and expander. The experimental data gathered in experiments is analysed in a spreadsheet. We use the same data set as in the previous section. Apart from the efficiencies, also the cooling system plays an important role in the power balance. In this section we presume that an explicit, algebraic, function of the cooled expander inlet temperature is avail-

able in terms of the mass flow through the turbine, the expander inlet pressure and inlet temperature.

$$T_3^* = f(\dot{m}_t, p_3, T_3, \text{heatfact}) \quad (\text{A.26})$$

The additional parameter *heatfact* can be freely chosen as a heat exchanging surface correction factor. A correction factor is very well acceptable since the geometry of the cooler is only roughly estimated.

Polytropic compressor efficiency We assume that the polytropic compressor efficiency can be reconstructed from the measured temperature T_2 . For purpose in the simulation models, a mathematical correlation between this temperature and the pressure ratio over the compressor has been derived and depicted in figure A.12.

$$\eta_c = f(\text{prat}_c) \quad (\text{A.27})$$

In figure A.12 the relatively large scattering between fitted and measured efficiencies is emphasised, while in figure A.13 the causing temperature differences appear to be very small: the compressor efficiency is a very sensitive parameter that can hardly be reconstructed from a single temperature measurement.

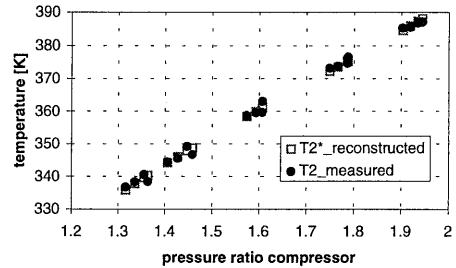
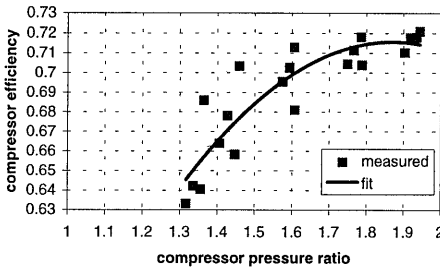


figure A.12 : Measured compressor efficiency and fit. figure A.13 : Measured and reconstructed compressor outlet temperature.

Polytropic expander efficiency The isentropic expander efficiency is given in the original characteristic and well described by the following polynomial in the pressure ratio over the expander:

$$\eta_{t,isen} = ((-0.00048 \text{ prat}_t - 0.003704) \text{ prat}_t - 0.009924) \text{ prat}_t + 0.788052 \quad (\text{A.28})$$

We adapt this efficiency into our analysis as a starting point for the actual expander efficiency. First the isentropic efficiency must be corrected towards the polytropic efficiency by the following conversion. The resulting *original* efficiency is plotted in figure A.14 together with the *measured* efficiency that is computed from the measured temperatures T_3 and T_4 .

In stationary operating points, a specific power balance equation must hold

$$C_{p,c} T_1 \left(\left(\frac{p_2}{p_1} \right)^{\left(\frac{\gamma-1}{\gamma} \right)} - 1 \right) = C_{p,t} T_3^* \left(1 - \left(\frac{p_4}{p_3} \right)^{\left(\frac{\eta_t(\gamma-1)}{\gamma} \right)} \right) \quad (\text{A.29})$$

In this equation, the mass flows and the polytropic efficiencies for the compressor and the expander are already determined by the previous assumptions. The parameter *heatfact* (and the resulting temperature T_3^*) is still undetermined. This parameter can now be chosen a constant value by optimising equation (A.29). The value of this parameter is 2.0.

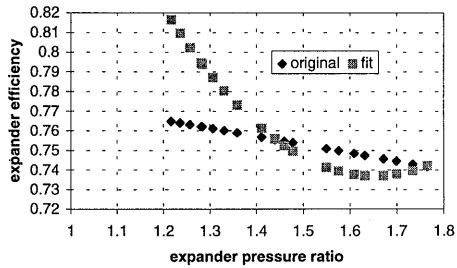
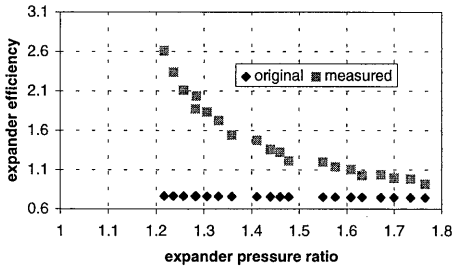


figure A.14 : Original and measured expander efficiency.

figure A.15 : Original and fitted expander efficiency.

Finally, the polytropic efficiency over the expander is corrected by applying a new correlation to equation (A.29) in which the constant value for *heatfact* has been substituted. The resulting efficiency *fit* (A.30) is plotted versus the *original* efficiency in figure A.15.

$$\eta_t = f(\text{prat}_t) \tag{ A.30 }$$

We have chosen to adapt the polytropic efficiency as a function of the operation area rather than the parameter *heatfact*. Several arguments can be employed to support this choice. First, it is physically more correct to apply a constant parameter *heatfact* since it is meant to be an area correction factor: Influences over the operation area are already modelled in the cooling system by the appropriate Reynolds and Nusselt relations. Second, when the parameter *heatfact* is varied over the operation area, its value varies from -1 to 4, which is not acceptable. A final argument can be found in the resulting polytropic efficiency, which shows a remarkable correspondence to the efficiency that is determined by the measured temperatures. The resulting value of 2.0 for *heatfact* is physically acceptable since it corresponds to an area correction factor.

A.7 Matching of compressor and expander

Stable operating points of the turbocharger in the laboratory installation can be found from a matching procedure of the characteristics. This procedure can be summarised by:

1. Select an operating point in the compressor characteristic as an initial point.
2. Determine (or otherwise estimate) the polytropic compressor efficiency from the basic correlation $\eta_c = f(\text{prat}_c)$ (A.27).
3. Compute the temperature rise in the compressor and the power required for the compressor to operate in the initial working point:

$$T_2^* = T_1 \left(\frac{p_2}{p_1} \right)^{\frac{(\gamma-1)}{\gamma \eta_c}} \text{ and } P_c = \dot{m}_c C_{p,c} (T_2^* - T_1) \tag{ A.31 }$$

4. Estimate the pressure losses in the system (and in the flue gas duct) and determine the pressure ratio p_3/p_4 over the expander.
5. Determine the corresponding flow coefficient in the expander characteristic and compute the required expander inlet temperature T_3^* and mass flow through the expander to fulfil this coefficient.
6. Determine (or otherwise estimate) the polytropic compressor efficiency from the basic correlation $\eta_t = f(\text{pr}_{at_t})$ (A.30).
7. Compute the expander outlet temperature T_4 and the power developed in the expander:

$$T_4^* = T_3^* \left(\frac{p_4}{p_3} \right)^{\frac{(\gamma_t - 1)\eta_t}{\gamma_t}} \quad \text{and} \quad P_t = \dot{m}_t C_{p,t} (T_3^* - T_4^*) \quad (\text{A.32})$$

8. A power balance holds. Compare the amounts of power required by the compressor and delivered by the expander. In any case these are not (about) equal, in step 1. another working point (for instance another pressure ratio and mass flow on the same constant speed curve) must be selected and the procedure must be repeated.

Obviously a dynamic simulation model converges to a stationary operating point for a prescribed power input and included pressure drop relations. The difference between the actual combustion chamber outlet temperature and the expander inlet temperature is then included by the expander cooling.

A.8 Control valve characteristics

In general two types of control valves are used, valves with a linear and valves with an exponential or logarithmic characteristic. For a linear characteristic the K_v value is proportional to the valve (seat) position S and obtains its maximum value at fully opened position: $K_v = cS$. For a logarithmic characteristic, the value is proportional to its derivative to the valve position: $K_v = c \frac{dK_v}{dS}$. Logarithmic characteristic offers improved control performance at small valve positions. For this reason, the fuel valve has been selected logarithmic, while the blow-off valve and the throttle valve have linear characteristics.

Note that because of the empirical character, the K_v -relation is not exactly equivalent to a Bernoulli equation. The K_v -relation can be written as a frequently used semi-dimensionless mass flow [Econosto, 1992]:

$$\frac{\dot{m} \sqrt{T_{in}}}{p_{in}} = \frac{K_v}{7} \sqrt{\rho_n \frac{p_{out}}{p_{in}} \left(1 - \frac{p_{out}}{p_{in}} \right)} \quad (\text{A.33})$$

The resulting mass flow through the control valve is shown in figure A.17 as a function of the actual K_v value and the pressure ration over the valve. Clearly, the transition from subcritical to super critical flow at a pressure ratio of 0.5 can be seen.

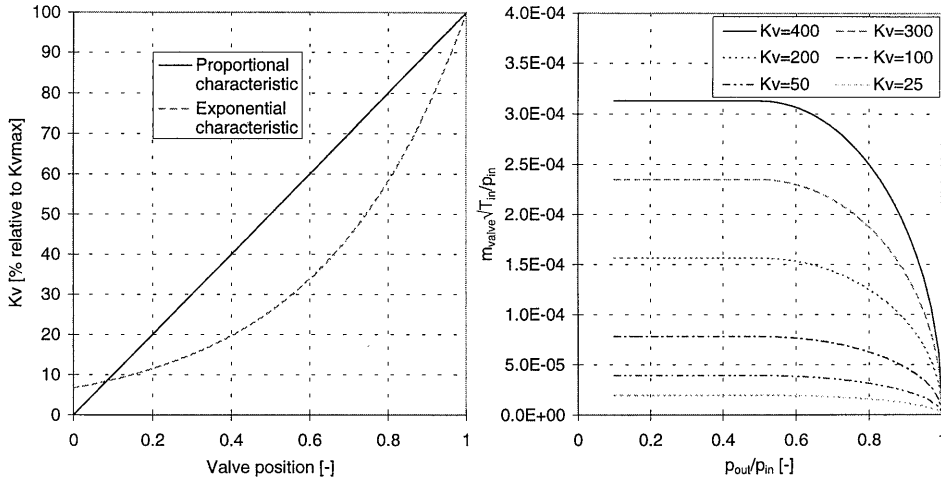


figure A.16 : Control valve characteristics. figure A.17 : Semi-dimensionless mass flow as a function of the actual K_v value and the pressure ratio over the valve.

A.9 Orifice characteristic

An orifice causes a pressure drop in a pipe line due to an acceleration of fluid at a sudden constriction (the orifice). This pressure drop is a measure for the volume flow of the fluid through the orifice. When the local density of the fluid is measured, also the mass flow is available. For the design specifications of the orifice in the laboratory set-up, please refer to [Essen, 1995]. Since the design is according to [NEN3005, 1972], the mass flow through the orifice can be expressed by

$$\dot{m} = \alpha \varepsilon \frac{\pi}{4} d^2 \sqrt{2 \Delta p \rho} \tag{A.34}$$

- \dot{m} mass flow through the orifice [kg/s]
- α flow coefficient [-]
- ε expansion factor [-]
- d diameter orifice [m]
- Δp pressure drop [Pa]
- ρ inlet fluid density [kg/m³]

According to [NEN3005, 1972], the expansion factor ε and the flow coefficient α are determined by empirical relations as a function of the orifice geometry and the appropriate Reynolds number:

$$\varepsilon = 1 - \left(0.41 + 0.35 \beta^4 \right) \frac{\Delta p}{\kappa p_{\text{in}}} \tag{A.35}$$

$$\alpha = A(\beta, D) + \frac{B(\beta, D)}{Re_d} \tag{A.36}$$

in which D is the diameter of the pipe in which the orifice is mounted, β is the diameter ratio d/D , κ is the pipe's average surface roughness, p_{in} is the pressure in the pipe before the orifice, and Re_D is defined as (with η is the dynamic viscosity [$N \cdot s / m^2$]):

$$Re_D = \frac{\rho UD}{\eta} = \frac{4 \dot{m}}{\pi D \eta} \quad (\text{A.37})$$

For the design geometry ($d = 0.0789$ m, $D = 0.1615$ m, $\beta = 0.49$, $\eta = 2.3 \cdot 10^{-5}$, $\kappa = 0.05$), $A = 0.6208$ and $B = 243.8$, both under the mild condition that $5.5 \cdot 10^4 < Re_D < 10^7$. Although the determination of the expansion factor ϵ and the flow coefficient α is an iterative procedure, the variations with Reynolds are so small that constant values can be used in the mass flow computations. In this thesis the following values have been used: For the flow coefficient $\alpha = 0.622$, and for the expansion factor $\epsilon = 0.9877$.

In figure A.18 an illustration of the pressure drop vs. mass flow relation over the orifice is presented. This curve has been created by different amounts of compressed air (with a constant temperature of 288 K). Of course, when the inlet temperature changes significantly, this curve does no longer reflect the actual mass flow/pressure drop relation.

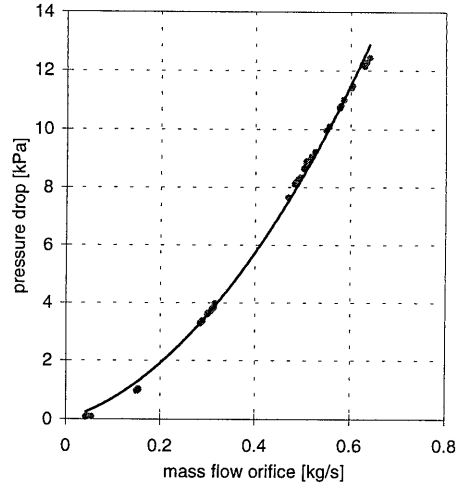


figure A.18 : Pressure drop vs. mass flow relation for the orifice examined at different rates of compressed air flows with a constant temperature (288 K).

It is interesting to determine the accumulated (measurement) error in the mass flow computation. In [NEN3005, 1972], the following formula is used:

$$\frac{\sigma_{\dot{m}}}{\dot{m}} = \sqrt{\left(\frac{\sigma_{\alpha}}{\alpha}\right)^2 + \left(\frac{\sigma_{\epsilon}}{\epsilon}\right)^2 + 4\left(\frac{\beta^4}{\alpha}\right)\left(\frac{\sigma_D}{D}\right)^2 + 4\left(1 + \frac{\beta^4}{\alpha}\right)\left(\frac{\sigma_d}{d}\right)^2 + \frac{1}{4}\left(\frac{\sigma_{\Delta p}}{\Delta p}\right)^2 + \frac{1}{4}\left(\frac{\sigma_{\rho}}{\rho}\right)^2} \quad (\text{A.38})$$

With $\frac{\sigma_{\alpha}}{\alpha} = 0.003$, $\frac{\sigma_D}{D} = \frac{0.05 \text{ mm}}{D \text{ mm}} = 0.0003$, and $\frac{\sigma_d}{d} = \frac{0.05 \text{ mm}}{d \text{ mm}} = 0.0006$, suppose the accuracy of the measurement instruments is 1 %.

Then $\frac{\sigma_{\Delta p}}{\Delta p} = 0.01$, $\frac{\sigma_p}{p} = 0.01$, $\frac{\sigma_T}{T} = 0.01$, and

$$\text{(approximately)} \quad \frac{\sigma_{\rho}}{\rho} = \sqrt{\left(\frac{\sigma_p}{p}\right)^2 + \left(\frac{\sigma_T}{T}\right)^2} = 0.011, \text{ and } \frac{\sigma_{\epsilon}}{\epsilon} = \sqrt{2\left[\left(\frac{\sigma_p}{p}\right)^2 + \left(\frac{\sigma_{\Delta p}}{\Delta p}\right)^2\right]},$$

With these data, (A.38) gives a measurement error $\tau_{\dot{m}}$ of approximately 5% on the mass flow according to

$$\tau_{\dot{m}} = \left(2 \frac{\sigma_{\dot{m}}}{\dot{m}} + \tau_{add} \right) \tag{A.39}$$

in which an additional tolerance τ_{add} of 0.25 % is added due to design restrictions. When however, the accuracy of the measurement instruments drops to 5% (for instance due to low mass flows and low pressure drops), the measurement error in the mass flow rises quickly to 20 %.

A.10 Fuel supply characteristic

In figure A.19 the measured pulse frequency of the natural gas flow meter is presented. Although the fuel control valve has an exponential characteristic, the valve appears to be linear within the used operating area (an opening between 0.2 -0.4). From these pulses a straightforward conversion to mass flow of natural gas is made by

$$\dot{m}_{fuel} = 0.833 \frac{freq}{250} \tag{A.40}$$

in which 0.833 is the, assumed constant, density of the natural gas and 250 is the conversion factor from frequency to volume flow. In figure A.19 also this mass flow is presented. A fit of the Kv value of the linear characteristic has been derived:

$$Kv_{fuel} = 0.04 + 1.80 S_{fuel} \tag{A.41}$$

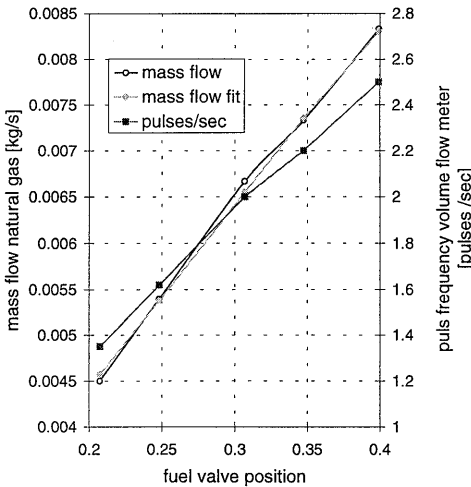


figure A.19 : Measured pulse frequency and mass flow fuel and derived fuel flow fit.

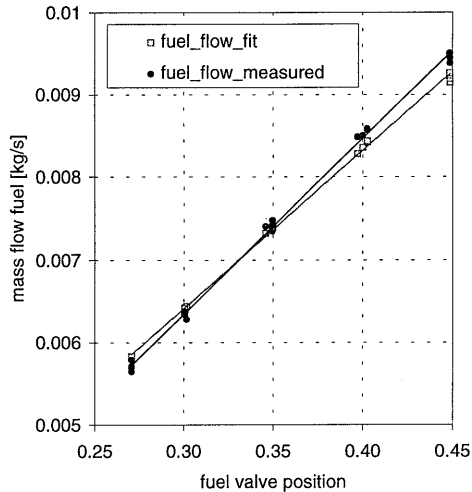


figure A.20 : Measured fuel flow compared with fuel flow fit for the “validation” data set of Chapter 4.

The corresponding mass flow fit is shown in figure A.19 according to the Kv relations:

$$\dot{m} = \frac{K_v \text{ fuel}}{7.0 \cdot 10^5} \sqrt{\frac{\rho_n p_{out}}{T_{in}} (p_{in} - p_{out})} \text{ for subcritical flow, i.e. } \left(\frac{p_{out}}{p_{in}} \right) \geq 0.5 \quad (\text{A.42})$$

$$\dot{m} = \frac{K_v \text{ fuel}}{14.0 \cdot 10^5} p_{in} \sqrt{\frac{\rho_n}{T_{in}}} \text{ for supercritical flow, i.e. } \left(\frac{p_{out}}{p_{in}} \right) < 0.5 \quad (\text{A.43})$$

with fixed values of $T_{in} = 313 \text{ K}$, $p_{in} = 3.0 \cdot 10^5 \text{ Pa}$ and $\rho_n = 0.833 \text{ kg/m}^3$

Figure A.20 shows the same result on a completely different data set, that is, the data set used in Chapter 4 to validate the model parameters.

B Expander Cooling Modelling

The cooling water circuitry is designed to protect the turbocharger. An side effect is the cooling of the expander inlet flow. The temperature of this inlet flow is measured as the outlet temperature of the combustion chamber. It appears to be impossible to measure the temperature after cooling since this temperature may be fictive: it is the temperature that the turbine experiences and that determines the power that the expander develops. Moreover, no physical position can be pointed out where this temperature rules. The most reliable position is just before the expander rotor but high velocities and possibly inhomogeneous distributions do not allow the temperature to be measured straightforward.

It is possible to model the cooling system and to estimate the temperature after cooling. This estimation can be validated from the power balance in experimental results. The first step in modelling the cooling system is to transform the complex geometry of the turbine heat exchanger to a standard double pipe heat exchanger. Then the heat transfer coefficient that applies to this situation must be determined. Finally the cooled power and the temperature after cooling can be computed.

B.1 Geometry of the turbine cooling system

The cooling system is located around the expander volute and can be recognised in the right side of figure B.1. The cooling water is indicated by a set of black dotted lines.

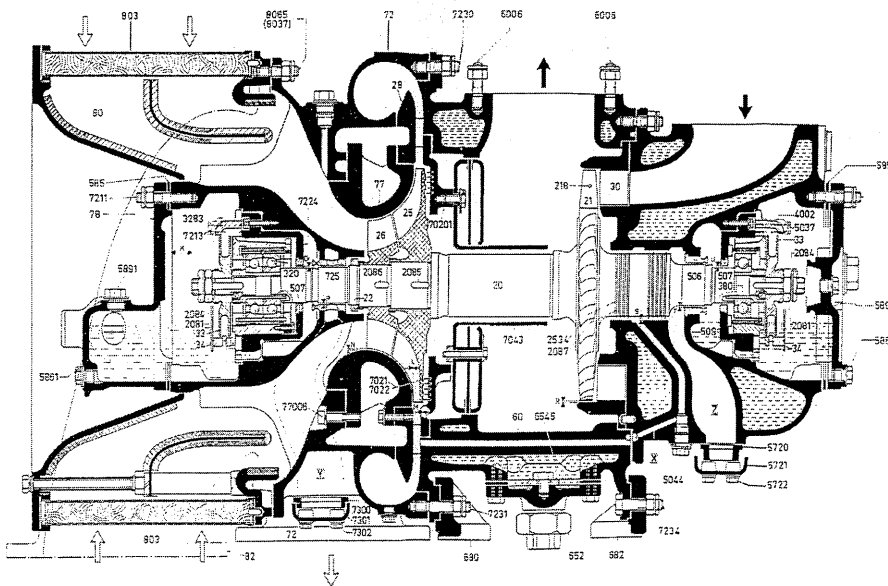


figure B.1 : Geometry of the cooling system of the turbocharger.

The complex geometry of the actual cooling shell is represented like a volute with the following dimensions:

r	(effective) radius expander volute shell	0.200 m
R	outline expander shell	0.250 m
s	wall thickness between gas and water	0.0080 m
S	average thickness annulus	0.010 m

Which results in the corresponding geometry of a double pipe heat exchanger that is sketched in the following two figures. In figure B.3, the cross-section of the double pipe heat-exchanger is shown with the annulus concentric around the pipe and a wall thickness of s . In figure B.2, the length of the configuration is represented.

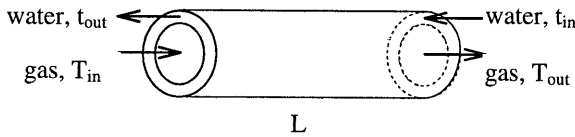


figure B.2 : Double pipe heat exchanger.

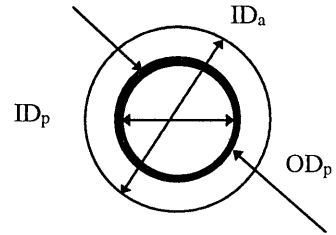


figure B.3 : Cross-section pipe and annulus.

L	length	$2\pi r$	1.257 m
OD _p	outer diameter pipe (combustion gas)	R/π	0.080 m
ID _p	inner diameter pipe (combustion gas)	$R/\pi - 2s$	0.064 m
ID _a	inner diameter annulus (cooling water)	$R/\pi + 2S$	0.100 m

B.2 Determination of the heat exchanger coefficient

From the assumed geometry, the Reynolds numbers are for the gas flow in the pipe (index p) and for the cooling water flow in the annulus (index a)

$$Re_p = \frac{\dot{m}_p}{\rho_p A_p} \frac{ID_p}{v_p} \quad \text{and} \quad Re_a = \frac{\dot{m}_a}{\rho_a A_a} \frac{D_e}{v_a} \quad \text{respectively,} \quad (\text{B.1})$$

$$\text{with } D_e = \frac{ID_a^2 - OD_p^2}{OD_p^2} \quad \text{the equivalent diameter of the annulus and} \quad (\text{B.2})$$

$$A_p = \frac{\pi}{4} ID_p^2 \quad \text{and} \quad A_a = \frac{\pi}{4} (ID_a^2 - OD_p^2) \quad \text{are the appropriate flow areas.} \quad (\text{B.3})$$

The corresponding Nusselt numbers are

$$Nu_p = \frac{h_i \cdot ID_p}{k_p} = 0.023 \cdot Re_p^{4/5} \cdot Pr_p^{3/10} \quad \text{and} \quad Nu_a = \frac{h_o \cdot D_e}{k_a} = 0.023 \cdot Re_a^{4/5} \cdot Pr_a^{4/10} \quad (\text{B.4})$$

for the gas flow being cooled and for the water flow being heated respectively.

From these equations the convection coefficients h_i and h_o can be determined and the heat exchanger coefficient

$$\frac{1}{U} = \frac{1}{h_{io}} + \frac{1}{h_o} \quad (\text{with } h_{io} = h_i \frac{ID_p}{OD_p}) \quad (\text{B.5})$$

resulting in:

$$U = \frac{OD_p}{Nu_p k_p} + \frac{D_e}{Nu_a k_a}. \quad (\text{B.6})$$

B.3 Temperature after cooling and cooled power

Under the assumption of counter flow, the cooled power for the double pipe heat exchanger is equal to [Janna, 1988] $Q = U \cdot A \cdot \text{LMTD}$ with $A = L\pi OD_p$ the overall heat exchanging surface and

$$\text{LMTD} = \frac{(T_{in} - t_{out}) - (T_{out} - t_{in})}{\ln\left(\frac{T_{in} - t_{out}}{T_{out} - t_{in}}\right)} \quad (\text{B.7})$$

the logarithmic mean temperature difference. This cooling power equals

$$Q = \dot{m}_p C_{p,p} (T_{out} - T_{in}) = \dot{m}_a C_{p,a} (t_{in} - t_{out}). \quad (\text{B.8})$$

When the mass flows, the heat capacities, and the inlet temperatures of both cooling water and gas being cooled are known, analytic expressions for the outlet temperatures and for the cooling power Q can be derived. With $P = \frac{\dot{m}_a C_{p,a}}{\dot{m}_p C_{p,p}}$ and $K = \frac{U \cdot A \cdot (P-1)}{\dot{m}_a C_{p,a}}$ an analytic expression

for the cooled temperature is:

$$T_{out} = \frac{T_{in}(P-1) - Pt_{in}(1 - \exp(K))}{P \exp(K) - 1}. \quad (\text{B.9})$$

This expression can be written as an explicit function of $T_{out} = f(\dot{m}_p, U, T_{in})$ for constant values of \dot{m}_a , t_{in} and the heat capacities.

The geometry of this double pipe configuration has been roughly estimated from the complex turbocharger geometry. In the simulation therefore a correction factor may be applied. We apply a constant factor *heafact* to the overall heat exchanging surface A . The value of this factor should be determined from experimental results. The analysis is discussed in section B.5.

The same approach is valid when not the temperature after the heat exchanger but the inlet temperature is unknown when the outlet temperature is measured. This is the case for the expander outlet temperature. The exhaust temperature is measured and this is in fact the cooled

temperature of the temperature just after the expander rotor. Under the same assumptions an analytic expression for the temperature before cooling is:

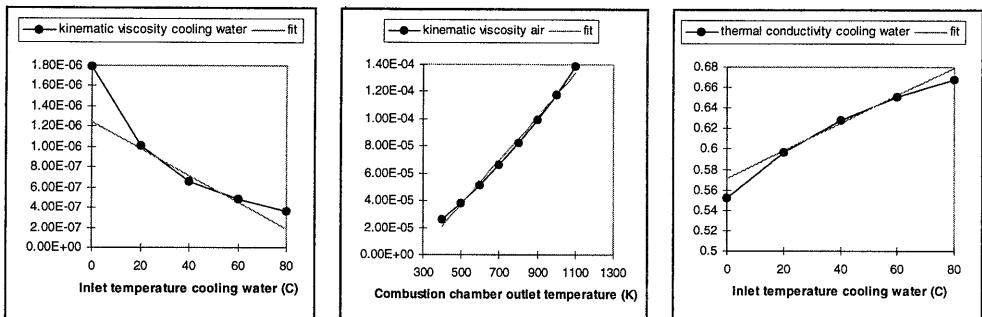
$$T_{in} = \frac{T_{out}(P \exp(K) - 1) + P t_{in}(1 - \exp(K))}{P - 1} \quad (\text{B.10})$$

For reasons of simplicity, the same geometry is proposed for this heat exchanger. Strictly, it is not possible to model the expander outlet cooling as a double pipe heat exchanger like the inlet cooler. The estimated cooling cannot be accurate enough to predict the expander's polytropic efficiency and the corresponding power developed by the expander. Therefore, we will not apply a cooling after the expander in the model. Instead, we will prescribe the expander efficiency from the original characteristic and correct the power developed by the expander by the inlet cooling only. This means that the measured outlet temperature of the expander (the exhaust temperature) will be neglected.

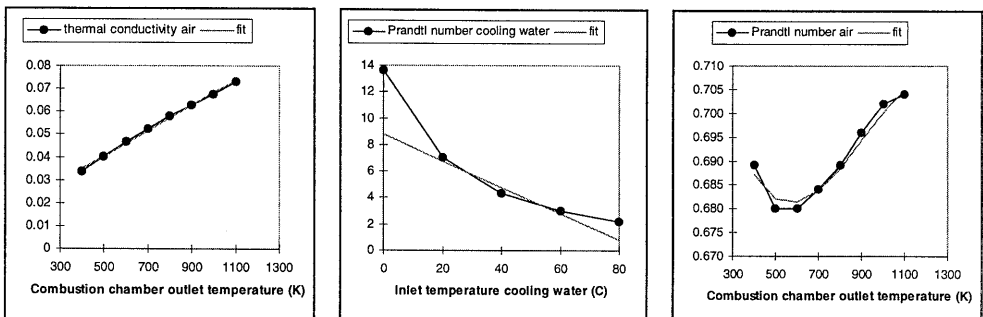
B.4 Thermodynamic data

In the computer code basic linear and polynomial fits for the thermodynamic properties are used. The data is from [Janna, 1988]. The purpose of the fits is to account for some variance in conditions and does not need to be very accurate. The composition of the combustion gasses for instance is neglected and the data for air at standard pressure is used.

In the following six graphs, the kinematic viscosity, the thermal conductivity and the Prandtl numbers of cooling water and combustion gasses are shown. The fits used in the computer code are presented below.



$$v_a = (1.242 - 0.0132 * (T_{coolwater,in} - 273.)) / 1.0E6; \quad v_p = (-42.9632 + 0.1605 * T_{t,in}) / 1.0E6;$$



$$k_a = 0.5713 + 0.00135 \cdot (T_{coolwater,in} - 273.);$$

$$k_p = 0.0126132142857144 + 5.55523809523809E-5 \cdot T_{t,in};$$

$$Pr_a = 4.0 \quad \text{or} \quad Pr_a = 8.7733 - 0.1 \cdot (T_{coolwater,in} - 273.);$$

$$Pr_p = 0.685 \quad \text{or} \quad Pr_p = 0.7712 - 3.7324E-3 \cdot T_{t,in} + 4.78205E-7 \cdot T_{t,in}^2 - 1.7599E-10 \cdot T_{t,in}^3;$$

B.5 Parameter heatfact and temperature profile

An explicit function of the heat exchanger coefficient in terms of the mass flow through the expander, the expander inlet pressure and inlet temperature is derived according to (B.6) when geometry and thermodynamic relations are substituted and a constant mass flow of cooling water with a constant inlet temperature is chosen.

$$U = f(\dot{m}_t, p_3, T_3) \tag{B.11}$$

The temperature after cooling is computed from the proposed double pipe heat exchanger configuration (B.9) with the additional parameter *heatfact* to be freely chosen as an heat exchanging surface correction factor. A correction factor is very well acceptable since the geometry of the cooler is only roughly estimated.

$$T_{cool} = f(\dot{m}_t, p_3, U \cdot \text{heatfact}) \tag{B.12}$$

In stationary operating points, this cooled temperature is equal to the expander inlet temperature T_3^* . During transients, however, the inertia of the heat exchanger should be taken into account. In the lumped model this is done by a basic first order lag on the expander inlet temperature with a time constant of τ_q , described by the following ordinary differential equation:

$$\frac{dT_3^*}{dt} = \frac{1}{\tau_q} (T_{cool} - T_3^*). \tag{B.13}$$

The value of the parameter *heatfact* has been determined from a data set of stationary operating points by the optimisation of the power balance along with the determination of the polytropic compressor and expander efficiencies. Its optimal value appears to be 2.0 which is physically acceptable because it is an area correction factor. All errors (geometry, heat transfer rates etc. are lumped into this correction factor).

The parameter *heatfact* determines the temperature profile over the expander:

$$T_{t,in} > T_{t,in}^* > T_{t,out}^* > T_{t,out} \quad \text{or} \quad T_3 > T_3^* > T_4^* > T_4 \tag{B.14}$$

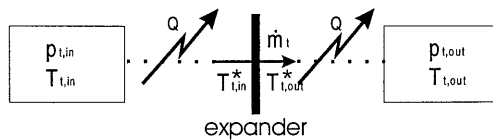


figure B.4 : Temperature profile over the expander.

C Model Equations

This appendix presents the lumped parameter dynamic simulation models used in this thesis. In the first section, the governing conservation equations for a homogeneous, ideally stirred, adiabatic volume are derived. The resulting set of equations is applied all the models. In two subsequent sections the configuration, the full set of model equations, and the parameter list for both the laboratory gas turbine installation and the generalised compressor station are presented. The appendix closes with a section on an alternative (instationary) momentum equation that may replace the static mass flow relations in both models.

C.1 Conservation equations for a homogeneous volume

The derivation starts with a formulation of the general energy conservation law [Bird, 1960], stated in terms of enthalpy:

$$\frac{\partial \rho H}{\partial t} = -(\nabla \cdot \rho H v) - (\nabla \cdot q) - (\tau : \nabla v) + \frac{Dp}{Dt} \quad (\text{C.1})$$

In which

$$\frac{Dp}{Dt} = \frac{\partial p}{\partial t} + v \frac{\partial p}{\partial x} \quad (\text{C.2})$$

Under the assumptions that is gravitation is neglected, no heat is added or distracted and viscous dissipation is neglected this relation equals

$$\frac{\partial \rho H}{\partial t} = -\frac{\partial \rho v H}{\partial x} + \frac{Dp}{Dt} \quad \text{or even} \quad \frac{DH}{Dt} = \frac{1}{\rho} \frac{Dp}{Dt} \quad (\text{C.3})$$

when the continuity equation is substituted. When, however, a power flux q [W/m^2] through the surface of the volume is included it is possible to account for heat losses or the addition of combustion energy.

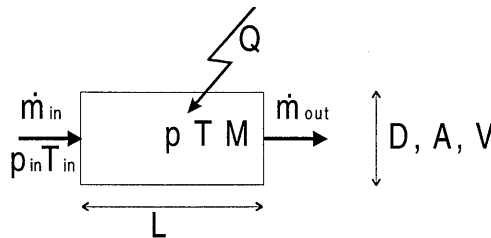


figure C.1 : Homogeneous volume.

An ideally stirred volume is assumed as schematically drawn in figure C.1. This implies that the pressure and temperature and, if relevant, the composition and heat capacity of the fluid, are homogeneous within the volume. The outlet values of pressure and temperature are equal to those within the volume, while the input temperature, pressure or composition may vary. The input pressure, however, is accounted for in the incoming mass flow (one may regard this as a momentum equation) so, consequently, the term $\partial p / \partial x$ is neglected over the volume. Then, under the assumption of an ideal gas, with $H = C_p T$, the energy equation reduces to

$$\rho C_p \frac{\partial T}{\partial t} = -\rho C_p v \frac{\partial T}{\partial x} - \frac{\partial q}{\partial x} + \frac{\partial p}{\partial t} \quad (\text{C.4})$$

which may be rewritten as

$$\rho C_p \frac{\partial T}{\partial t} = -C_p \frac{\dot{m}}{A} \frac{\partial T}{\partial x} - \frac{\partial q}{\partial x} + \frac{\partial p}{\partial t} \quad (\text{C.5})$$

Integrated over the (control) volume V this equation becomes (with $\frac{\partial M}{\partial t} = \dot{m}_{in} - \dot{m}_{uit}$, $\frac{\partial T}{\partial x} = \frac{T - T_{in}}{L}$, and $\frac{\partial q}{\partial x} = \frac{q}{L} = \frac{-Q}{V}$ in which $Q = q \frac{V}{L} = qA$ [W] is the added (positive sign) or extracted (negative sign) power over the whole volume)

$$\frac{\partial T}{\partial t} = \frac{RT}{p} \left(\frac{\dot{m}_{in}}{V} (T_{in} - T) + \frac{Q}{C_p V} + \frac{1}{C_p} \frac{\partial p}{\partial t} \right) \quad (\text{C.6})$$

Since the ideal gas law $pV = MRT$ holds over the volume, this again results in a coupled set of partial differential equations:

$$\frac{\partial p}{\partial t} = \frac{RT}{V} \frac{\partial M}{\partial t} + \frac{p}{T} \frac{\partial T}{\partial t} \quad (\text{C.7})$$

This system can be explicitly rewritten towards the following set of straightforward equations:

$$\frac{\partial T}{\partial t} = \frac{RT}{pV} \left[\gamma \left(\dot{m}_{in} T_{in} - \dot{m}_{uit} T + \frac{Q}{C_p} \right) - T (\dot{m}_{in} - \dot{m}_{uit}) \right] \quad (\text{C.8})$$

$$\frac{\partial p}{\partial t} = \frac{\gamma R}{V} \left(\dot{m}_{in} T_{in} - \dot{m}_{uit} T + \frac{Q}{C_p} \right) \quad (\text{C.9})$$

The added heat may be generated by a combustion process within the volume. Especially in this situation, differences in values between input and output heat capacity $C_{p,in}$ and C_p should be taken into account. Assume the value of heat capacity of the incoming flow is denoted $C_{p,in}$ and C_p , R , and γ correspond to the thermodynamic state T and p within the volume. Then the same equations change to:

$$\frac{\partial T}{\partial t} = \frac{RT}{pV} \left[\gamma \left(\dot{m}_{in} \frac{C_{p,in}}{C_p} T_{in} - \dot{m}_{uit} T + \frac{Q}{C_p} \right) - T (\dot{m}_{in} - \dot{m}_{uit}) \right] \quad (\text{C.10})$$

$$\frac{\partial p}{\partial t} = \frac{\gamma R}{V} \left(\dot{m}_{in} \frac{C_{p,in}}{C_p} T_{in} - \dot{m}_{uit} T + \frac{Q}{C_p} \right) \quad (\text{C.11})$$

Note that also the additional mass of the injected fuel should be taken into account. Additional mass can be described by adding an input: two mass flows in and only one out. Both mass flows may have different temperatures and heat capacities. The mass flow fuel, however, is often negligible compared to the main mass flow of air.

C.2 Lumped parameter gas turbine model

The lumped parameter gas turbine model describes a full gas turbine. The component characteristics are included in the model by a set of quasi-steady algebraic equations. These flow- Δp relationships are used to determine the mass flow through the components. The dynamic behaviour is lumped into three separate volumes. These volumes represent the size of the compressor duct, the plenum, and the combustion chamber respectively. In the volumes a mass and energy conservation equation is solved.

Figure C.2 presents the model configuration schematically. The following components are included: compressor, compressor duct volume, blow-off valve, buffer tank volume, throttle valve, combustion chamber volume, expander.

Compressor and expander are coupled by a power balance in the form of an ODE in the rotational speed. *Power* is the external supply of combustion heat into in terms of power [W], equivalent to an amount of natural gas and a combustion efficiency. *Cooling* indicates the expander cooling system. The temperature T_{cool} is the resulting steady state expander inlet temperature. Cooling inertia is introduced by a first order time lag.

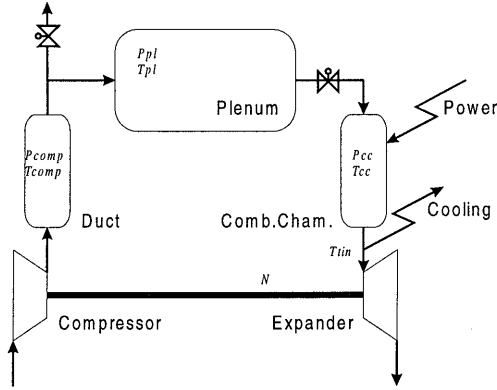


figure C.2 : Lumped parameter configuration.

The overall model consists of eight state variables as indicates in *italic* in figure C.2 and ten algebraic equations. The inlet conditions are constant and indicated as p_{amb} , T_{amb} .

steady state compressor characteristic

$$\dot{m}_c = f(N, p_{comp}, p_{amb}, T_{amb}) \quad (C.12)$$

pressure drop piping and buffer-tank

$$\dot{m}_{pl} = \sqrt{\frac{2p_{comp}}{RT_{comp}\xi}} A_C^2 (p_{comp} - p_{pl}) \quad (C.13)$$

steady state blow-off valve characteristic

$$\dot{m}_{bl} = \frac{S_{bl} K_{v_{bl}}}{7.0} \sqrt{\frac{\rho_n p_{amb} (p_{pl} - p_{amb})}{T_{pl}}} \quad (C.14)$$

steady state throttle valve characteristic

$$\dot{m}_{th} = \frac{S_{th} K_{v_{th}}}{7.0} \sqrt{\frac{\rho_n p_{cc} (p_{pl} - p_{cc})}{T_{pl}}} \quad (C.15)$$

expander outlet pressure

$$p_{t,out} = 1.02 p_{amb} \quad (C.16)$$

steady state expander characteristic

$$\dot{m}_t = f(p_{cc}, T_{cc}, p_{t,out}) \quad (C.17)$$

the polytropic compressor efficiency

$$T_{c,out} = T_{amb} \left(\frac{p_{pl}}{p_{amb}} \right)^{\frac{(\gamma-1)}{\gamma \eta_c}} \quad (C.18)$$

the polytropic expander efficiency

$$T_{t,out} = T_{cc} \left(\frac{p_{t,out}}{p_{cc}} \right)^{\frac{(\gamma-1) \eta_T}{\gamma}} \quad (C.19)$$

steady state cooled expander temperature

$$T_{cool} = f(\dot{m}_t, T_{cc}, p_{cc}, \text{heatfact}) \quad (C.20)$$

thermal input power

$$Power = f(S_{fuel}, p_{cc}, \eta_{comb}) \quad (C.21)$$

$$\frac{dp_{comp}}{dt} = \frac{\gamma R}{V_{comp}} \left(\dot{m}_c T_{c,out} - (\dot{m}_{pl} + \dot{m}_{bl}) T_{comp} \right) \quad (C.22)$$

$$\frac{dT_{comp}}{dt} = \frac{RT_{comp}}{p_{comp} V_{comp}} \left(\gamma \left(\dot{m}_c T_{c,out} - (\dot{m}_{pl} + \dot{m}_{bl}) T_{comp} \right) - T_{comp} \left(\dot{m}_c - (\dot{m}_{pl} + \dot{m}_{bl}) \right) \right)$$

$$\frac{dp_{pl}}{dt} = \frac{\gamma R}{V_{pl}} \left(\dot{m}_{pl} T_{comp} - \dot{m}_{th} T_{pl} \right) \quad (C.23)$$

$$\frac{dT_{pl}}{dt} = \frac{RT_{pl}}{p_{pl} V_{pl}} \left(\gamma \left(\dot{m}_{pl} T_{comp} - \dot{m}_{th} T_{pl} \right) - T_{pl} \left(\dot{m}_{pl} - \dot{m}_{th} \right) \right)$$

$$\frac{dp_{cc}}{dt} = \frac{\gamma_t R_t}{V_{cc}} \left(\dot{m}_{th} \frac{C_p}{C_{p,t}} T_{pl} - \dot{m}_t T_{cc} + \frac{Power}{C_{p,t}} \right) \quad (C.24)$$

$$\frac{dT_{cc}}{dt} = \frac{R_t T_{cc}}{p_{cc} V_{cc}} \left(\gamma_t \left(\dot{m}_{th} \frac{C_p}{C_{p,t}} T_{pl} - \dot{m}_t T_{cc} + \frac{Power}{C_{p,t}} \right) - T_{cc} \left(\dot{m}_{th} - \dot{m}_t \right) \right)$$

$$\frac{dN}{dt} = \frac{\dot{m}_t C_{p,t} (T_{t,in} - T_{t,out}) - \dot{m}_c C_p (T_{c,out} - T_{amb})}{I N} \quad (C.25)$$

$$\frac{dT_{t,in}}{dt} = \frac{1}{\tau_q} (T_{cool} - T_{t,in}) \quad (C.26)$$

Parameter list lumped parameter model**thermodynamic properties:**

$\gamma = 1.4$	$C_p = 1010.$	$R = 287.0$	$\rho_n = 1.2$
$\gamma_t = 1.375$	$C_{p,t} = 1060.$	$R_t = 289.2$	

geometry and inertia:

$A_C = 0.018$	$V_{comp} = 0.5$	$I = 0.01$	$\tau_q = 1.0$
$KV_{bl} = 100$	$V_{pl} = 2.5$		
$KV_{th.} = .430$	$V_{cc} = 1.5$		

additional parameters:

$\xi = 96.72900158 * m_t^2 - 93.19533131 * m_t + 73.52140519$
$heatfact = 2.0$
$\eta_T = 0.418858271 * pr_{at}^2 - 1.384121427 * pr_{at} + 1.880420315$
$\eta_C = 0.85858975 * pr_{at} - 0.229627525 * pr_{at}^2 - 0.086976076$
$\eta_{comb} = -10.81538674 * m_{fuel} / m_t + 0.9950247$

C.3 Lumped parameter compressor station model

The compressor station model describes a generalised configuration of a compressor station. It is comprised of two compressors connected in parallel by a common discharge header. The configuration is shown in figure C.3. The inlet conditions (pressure, temperature, and composition) of the station are assumed constant but can be freely chosen.

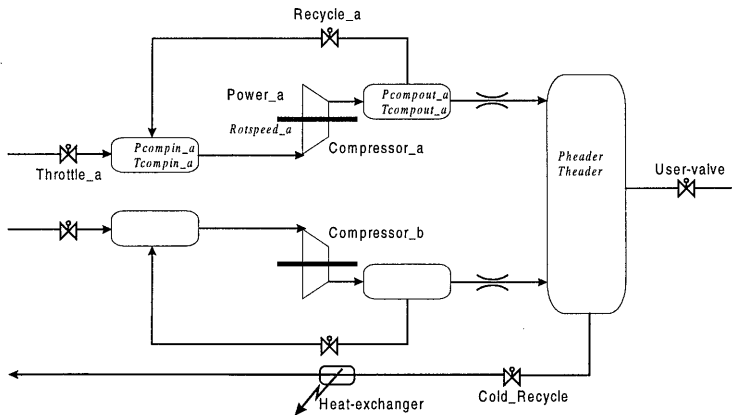


figure C.3: Compressor station configuration.

The two compressors have an identical input and output structure. Each compressor has three inputs: the power input to the compressor, the recycle valve and the suction throttle valve. The combined header supplies two extra inputs to the system: the position of the (throttle) valve mounted between the header and the user and the cold recycle or overall station recycle valve. The output of the station is the mass flow required by the user and/or the pressure that is experienced by the user.

The overall model consists of twelve state variable (that is, twelve differential equations) and ten algebraic equations. The inlet conditions are constant and indicated p_{amb} , T_{amb} .

steady state throttle valve characteristic A.

$$\dot{m}_{throt,a} = \frac{S_{throt,a} K_{v_{throt,a}}}{7.0} \sqrt{\frac{\rho_n P_{compin,a} (P_{amb} - P_{compin,a})}{T_{amb}}} \quad (C.27)$$

steady state compressor characteristic A.

$$\dot{m}_{comp,a} = f(N, P_{compout,a}, P_{compin,a}, T_{compin,a}) \quad (C.28)$$

steady state recycle valve characteristic A.

$$\dot{m}_{recl,a} = \frac{S_{recl,a} K_{v_{recl,a}}}{7.0} \sqrt{\frac{\rho_n P_{compin,a} (P_{compout,a} - P_{compin,a})}{T_{compout,a}}} \quad (C.29)$$

steady state header mass flow A.

$$\dot{m}_{head,a} = \sqrt{\frac{2P_{compout,a}}{RT_{compout,a} \xi}} A_C^2 (P_{compout,a} - P_{header}) \quad (C.30)$$

the polytropic compressor efficiency A.

$$T_{c,out,a} = T_{compin,a} \left(\frac{P_{compout,a}}{P_{compin,a}} \right)^{\frac{(\gamma-1)}{\gamma \eta_{C,a}}} \quad (C.31)$$

$$\begin{aligned} \frac{dp_{compin,a}}{dt} &= \frac{\gamma R}{V_{compin,a}} (\dot{m}_{throt,a} T_{amb} + \dot{m}_{recl,a} T_{compout,a} - \dot{m}_{comp,a} T_{compin,a}) \\ \frac{dT_{compin,a}}{dt} &= \frac{RT_{compin,a}}{P_{compin,a} V_{compin,a}} \left(\gamma (\dot{m}_{throt,a} T_{amb} + \dot{m}_{recl,a} T_{compout,a} - \dot{m}_{comp,a} T_{compin,a}) \right. \\ &\quad \left. - T_{compin,a} (\dot{m}_{throt,a} + \dot{m}_{recl,a} - \dot{m}_{comp,a}) \right) \end{aligned} \quad (C.32)$$

$$\begin{aligned} \frac{dp_{compout,a}}{dt} &= \frac{\gamma R}{V_{compout,a}} (\dot{m}_{comp,a} T_{c,out,a} - (\dot{m}_{head,a} + \dot{m}_{recl,a}) T_{compout,a}) \\ \frac{dT_{compout,a}}{dt} &= \frac{RT_{compout,a}}{P_{compout,a} V_{compout,a}} \left(\gamma (\dot{m}_{comp,a} T_{c,out,a} - (\dot{m}_{head,a} + \dot{m}_{recl,a}) T_{compout,a}) \right. \\ &\quad \left. - T_{compin,a} (\dot{m}_{comp,a} - (\dot{m}_{head,a} + \dot{m}_{recl,a})) \right) \end{aligned} \quad (C.33)$$

$$\frac{dN_a}{dt} = \frac{Power_a - \dot{m}_{comp,a} C_p (T_{c,out,a} - T_{compin,a})}{I N_a 2\pi^2} \quad (C.34)$$

The same set of five static equations and five ordinary differential equations holds for compressor B. All indices a are replaced by index b . For the header the following equations hold:

steady state overall cold recycle valve characteristic.

$$\dot{m}_{recl} = \frac{S_{recl} K_{v_{recl}}}{14.0 \cdot 10^5} P_{header} \sqrt{\frac{\rho_n}{T_{header}}} \quad (C.35)$$

steady state user valve characteristic.

$$\dot{m}_{user} = \frac{S_{user} K_{v_{user}}}{14.0 \cdot 10^5} P_{header} \sqrt{\frac{\rho_n}{T_{header}}} \quad (C.36)$$

$$\begin{aligned} \frac{dp_{header}}{dt} &= \frac{\gamma R}{V_{header}} \left(\dot{m}_{head,a} T_{compout,a} + \dot{m}_{head,b} T_{compout,b} - (\dot{m}_{user} + \dot{m}_{recl}) T_{header} \right) \\ \frac{dT_{header}}{dt} &= \frac{RT_{header}}{P_{header} V_{header}} \left(\gamma \left(\dot{m}_{head,a} T_{compout,a} + \dot{m}_{head,b} T_{compout,b} - (\dot{m}_{user} + \dot{m}_{recl}) T_{header} \right) \right. \\ &\quad \left. - T_{compin,a} (\dot{m}_{head,a} + \dot{m}_{head,b} - \dot{m}_{user} - \dot{m}_{recl}) \right) \end{aligned} \quad (C.37)$$

Parameter list lumped parameter compressor station model:

thermodynamic properties:

$$\gamma = 1.4 \quad C_p = 1010. \quad R = 287.0 \quad \rho_n = 1.2$$

geometry:

$$\begin{aligned} A_c = 0.018 \quad V_{compin} = 2.0 \quad I = 0.01 \quad K_{vtrott} = 200 \\ V_{compout} = 2.0 \quad K_{v_{recl}} = 160 \\ V_{header} = 10.0 \end{aligned}$$

additional parameters:

$$\begin{aligned} \xi = 30.0 \\ \eta_{c,a} = 0.70 \\ \eta_{c,b} = 0.60 \end{aligned}$$

C.4 Alternative mass flow equations

In order to add inertia or dead time to the flow through a valve or a compressor, the static mass flow relations of the characteristics can be extended to ordinary differential equations. Although the physical background of these equations is not solid, the additional inertia may benefit the dynamic model performance. The differential equation provides some flexibility in the characteristic during transients. Only in stationary operation the exact working point is prescribed by the characteristic. The formulation of these equations is of importance for the numerical condition of the set of equations. The new differential equations corresponding with the mass flows appear to have very small time scales while the pressure and temperature equations have larger time scales. This difference introduces stiffness to the system of equations which is likely to complicate the solution.

The mass flow through the compressor can be formulated as an ordinary differential equation:

$$\frac{d\dot{m}_c}{dt} = \frac{A_c}{L_c} \left(\text{prat}_{ss} - \frac{P_{comp}}{P_{amb}} \right) P_{amb} \quad (\text{C.38})$$

in which P_{comp}/P_{amb} is the actual pressure ratio over the compressor and prat_{ss} is the steady state pressure ratio determined from the compressor characteristic as a function of \dot{m}_c , and the inlet conditions T_{amb} and P_{amb} . The mass flow through valves may be formulated as

$$\frac{d\dot{m}}{dt} = \frac{A}{L} (\Delta p_{ss} - \Delta p) \quad (\text{C.39})$$

in which Δp_{ss} is the steady state pressure drop over the control valve, determined from the flow/ Δp characteristic.

The derivation of these equations from the original momentum equation start with the assumption of a constant surface A . When only pressure forces act on the volume, the general momentum equation

$$\frac{\partial v}{\partial t} = -v \frac{\partial v}{\partial x} - \frac{1}{\rho} \frac{\partial p}{\partial x} \quad (\text{C.40})$$

may be integrated over a control volume to V to

$$\frac{V}{A} \frac{d\dot{m}}{dt} + [(\dot{m}v)_{in} - (\dot{m}v)_{out}] + A(P_{in} - P_{out}) = 0 \quad (\text{C.41})$$

With $\frac{V}{A} = L$ and with the steady state assumption

$$[(\dot{m}v)_{in} - (\dot{m}v)_{out}] = A(P_{ss} - P_{in}) \quad (\text{C.42})$$

the momentum equation becomes

$$\frac{d\dot{m}}{dt} = \frac{A}{L} (P_{ss} - P_{out}) \quad (\text{C.43})$$

which can easily be transformed to describe the pressure ratio of a compressor (C.38) or pressure drop to denote flow through a control valve (C.39). Note that this derivation implies that the instationary convection term $v \frac{\partial v}{\partial x}$ in the momentum equation (C.40) can be assumed to be in steady state at all times.

C.5 Sensitivity analysis

As not all the outputs of the model used by the controller can be measured in the laboratory set-up, a number of outputs must be reconstructed from the measurement data. The following outputs are measured directly: $p_2 = P_{comp}$, $T_2 = T_{comp}$, $p_3 = P_{cc}$, $T_3 = T_{cc}$, N . The following outputs cannot be measured directly: the mass flows through compressor \dot{m}_c and expander \dot{m}_t , the power required by the compressor P_{comp} and delivered by the expander P_{urb} , and finally, the surge ratio R_{surge} . The accuracy of the reconstruction depends on the sensitivity of the static equations for errors in the measured outputs which are used in the reconstruction. The

sensitivity can be assessed by computing the condition number. This condition number relates relative errors in the arguments of a function to a relative error in the function value.

For a function $f = f(x, y, z)$ a relative error $\left| \frac{\Delta x}{x} \right|, \left| \frac{\Delta y}{y} \right|, \left| \frac{\Delta z}{z} \right|$ in one of the variables x, y, z , leads to a relative error in f of $\left| \frac{\Delta f}{f} \right|$. Using a second order Taylor approximation yields :

$$\left| \frac{\Delta f}{f(x, y, z)} \right| = \left| \frac{df}{dx} \Big|_{x, y, z} \frac{x}{f(x, y, z)} \right| \left| \frac{\Delta x}{x} \right| + \left| \frac{df}{dy} \Big|_{x, y, z} \frac{y}{f(x, y, z)} \right| \left| \frac{\Delta y}{y} \right| + \left| \frac{df}{dz} \Big|_{x, y, z} \frac{z}{f(x, y, z)} \right| \left| \frac{\Delta z}{z} \right|. \tag{C.44}$$

When $\left| \frac{\Delta x}{x} \right| \leq \epsilon, \left| \frac{\Delta y}{y} \right| \leq \epsilon, \left| \frac{\Delta z}{z} \right| \leq \epsilon$, then the following relation for the maximal relative error in f can be derived:

$$\left| \frac{\Delta f}{f(x, y, z)} \right| \leq \left(\left| \frac{df}{dx} \Big|_{x, y, z} \frac{x}{f(x, y, z)} \right| + \left| \frac{df}{dy} \Big|_{x, y, z} \frac{y}{f(x, y, z)} \right| + \left| \frac{df}{dz} \Big|_{x, y, z} \frac{z}{f(x, y, z)} \right| \right) \epsilon = c(x, y, z) \epsilon \tag{C.45}$$

in which $c(x, y, z)$ is the condition number for errors in x, y and z . A high condition number means that a small error in one of the arguments of the function can lead to a large relative error in f . In that case the problem is ill-conditioned. When the condition number has an order of magnitude of 1, a small relative error ϵ , does not lead to a large relative error in f . In that case the problem is well-conditioned.

Figure C.6 shows the condition number for the compressor mass flow as a function of p_{comp}/p_{surge} over the operating area near the surge line. This *surge pressure ratio* is a *pressure* measure of the distance from the surge line over a constant rotational speed line. In fact, this measure is equivalent to the *mass flow* measure of the surge ratio R_{surge} , see figure C.4. The conversion factor is indicated in figure C.5 as a function of rotational speed.

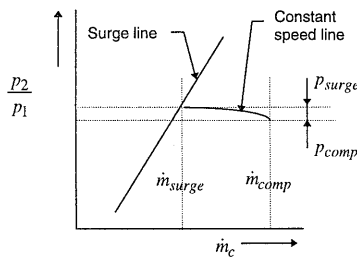


figure C.4 : Equivalence between pressure and mass flow measures of the distance to the surge line.

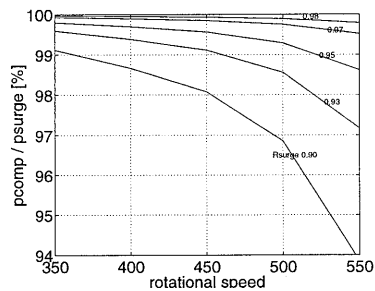


figure C.5 : Conversion between surge pressure and surge mass flow ratio.

For operating points near the surge line (for $p_{comp}/p_{surge} \rightarrow 100\%$), the condition number increases exponentially. This is caused by the fact that the parabolic constant rotational speed lines have their top at the surge line. Small changes in p_{comp} cause large changes in the compressor mass flow near this top. In fact, the condition number is rather high over the whole operating area, the reconstruction problem is ill-conditioned.

The real problem with this reconstruction, however, are possible measurement errors. Both measurement noise and systematic measurement errors like drift of transducers strongly influence the surge pressure ratio. p_{surge} is determined by the measured rotational speed only, while p_{comp} is a function of both speed and pressure. Due to measurement errors, the fatal limit $p_{comp}/p_{surge} \rightarrow 100\%$ is easily reached and even exceeded.

The condition number for the surge ratio R_{surge} is shown in figure C.7. The curves for this condition number closely resemble the curves for the condition number of the compressor mass flow. The ill-conditioned reconstruction of the compressor mass flow determines the condition of the surge ratio. Of course, the same remarks with regard to measurement errors hold.

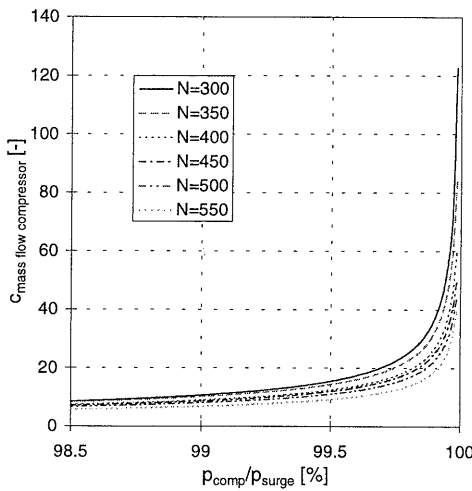


figure C.6 : Condition number for the compressor mass flow, as a function of p_{comp}/p_{surge} for different values of the rotational speed N .

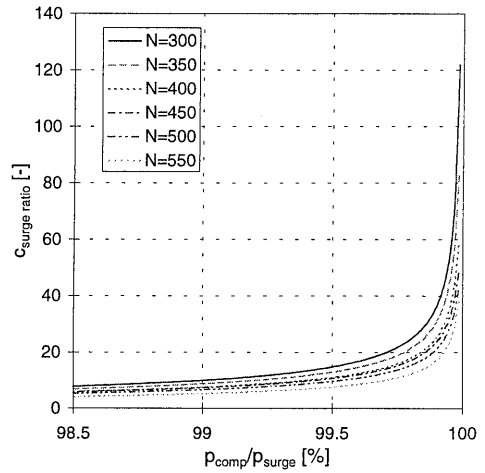


figure C.7 : Condition number for R_{surges} as a function of p_{comp}/p_{surge} for different values of the rotational speed N .

Figure C.8 and figure C.9 show the condition number for the expander mass flow. This condition number is almost independent of N and T_{cc} , (the rotational speed and the expander temperature). This is caused by the fact that these variables only translate the expander mass flow curve and do not alter the shape of the curve. Over the whole operating area, however, the condition number is not large and the reconstruction problem is well-conditioned. Moreover, the critical limit of 1 in the pressure ratio is never reached, not even in the case of measurement errors.

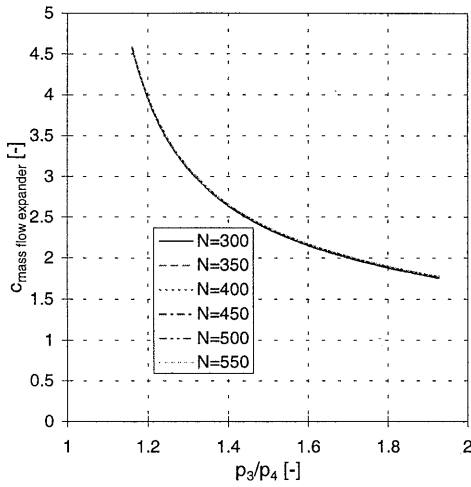


figure C.8 : Condition number for the expander mass flow, as a function of the expander pressure ratio for different values of the rotational speed and $T_{cc}=837.5$ K

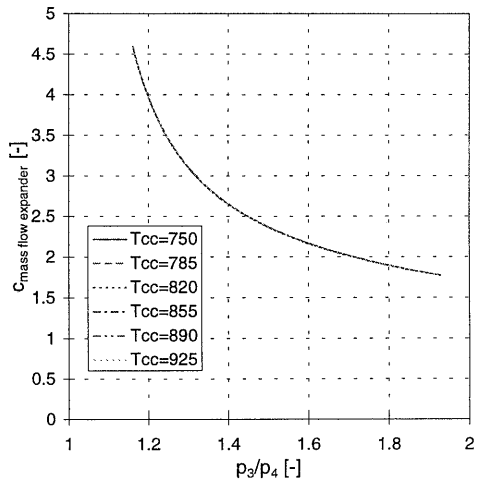


figure C.9 : Condition number for the expander mass flow, as a function of the expander pressure ratio for different values of the expander temperature and $N=425$ rev/s.

Figure C.10 shows the condition number for the (required) compressor power. For operating points near the surge line, the condition number increases exponentially. This is caused by the close coupling to the compressor mass flow. Therefore, the same remarks with regard to measurement errors hold for this reconstruction. The condition number for the (delivered) expander power, finally, is presented in figure C.11. This reconstruction problem is well-conditioned and no problems with measurement error are expected.

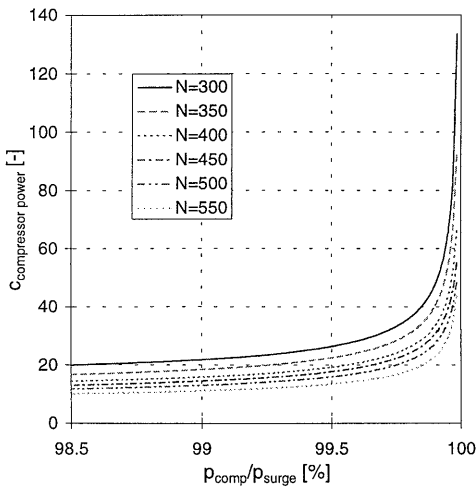


figure C.10 : Condition number for the compressor power, as a function of p_{comp}/p_{surge} for different values of N .

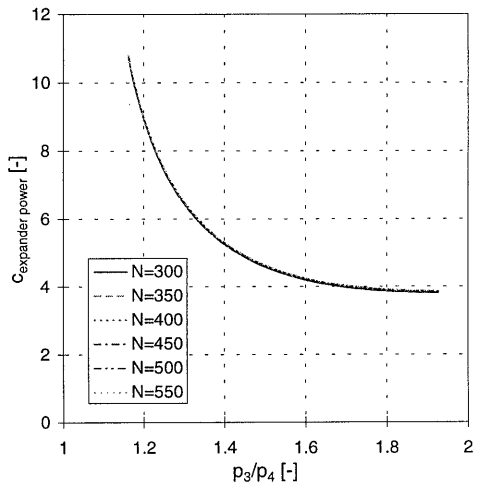


figure C.11 : Condition number for the expander power, as a function of pressure ratio for different values of N and $T_{cc}=837.5$ K.

D Instrumentation and Control

D.1 LabVIEW data-acquisition system

LabVIEW is a graphical programming environment for data-acquisition and control, data analysis and data presentation. A LabVIEW program is assembled from objects called Virtual Instruments. In the graphical programming language, all functions (like operations on data) are depicted as block-modules, while the data being transferred between the functions is depicted as lines. The data-acquisition program is written in LabVIEW 4.0 and uses the following National Instruments hardware: AT-MIO-64F-5, PC-DIO24.

The program is a flexible low-speed data-acquisition system. It is capable to acquire, display and store a few dozen analogue channels at speeds up to 10 Hz. The data-acquisition part has been extended with the valve positioning control system (see Appendix D.2) and the DDE coupling to the Primacs computer. The limited capacity of the program is determined by the use of software timers. The main loop of the program runs at the rate determined by the prescribed *sample interval*. Every sample, an adjustable (usually 70) measurements of each channel are acquired and the average value is computed as the sample result. At adjustable multiples of sample interval, the displays are updated and data is transferred to hard disk. This software timer induces some variability in the cycle of the main loop. In our case this is not a problem. A solution can be found in hardware timed I/O. The block diagram of the LabVIEW data-acquisition program is presented in figure D.1.

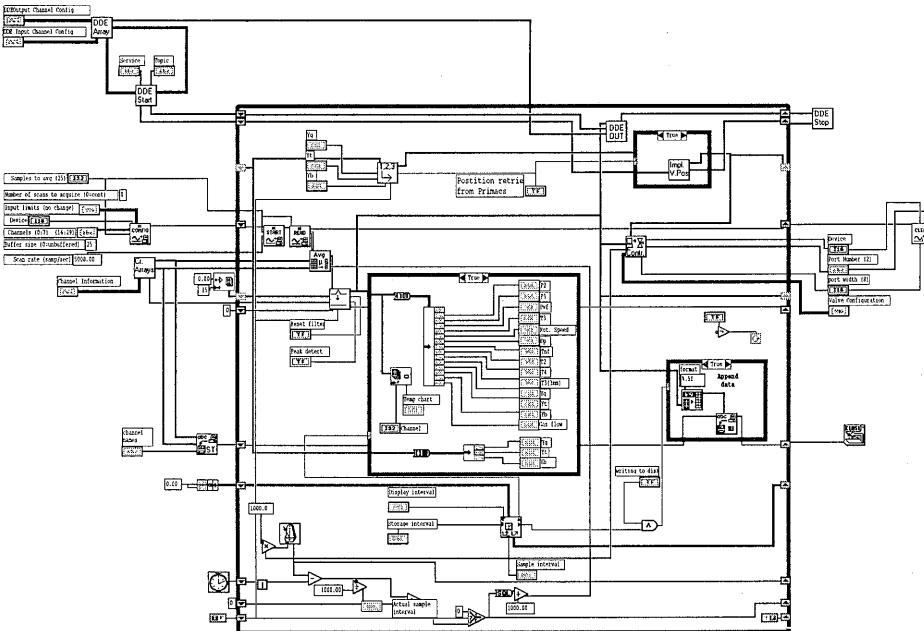


figure D.1 : LabVIEW block diagram of the data-acquisition system.

D.2 LabVIEW valve positioning control system

The three electrically powered valves are equipped with an electrical motor. The motor drives a spindle. Since the motor can only be turned on and off (in both directions), the valves are opened and closed at a constant speed. This speed is different for each of the valves. The valve motors are powered by relays that are controlled by the valve positioning system.

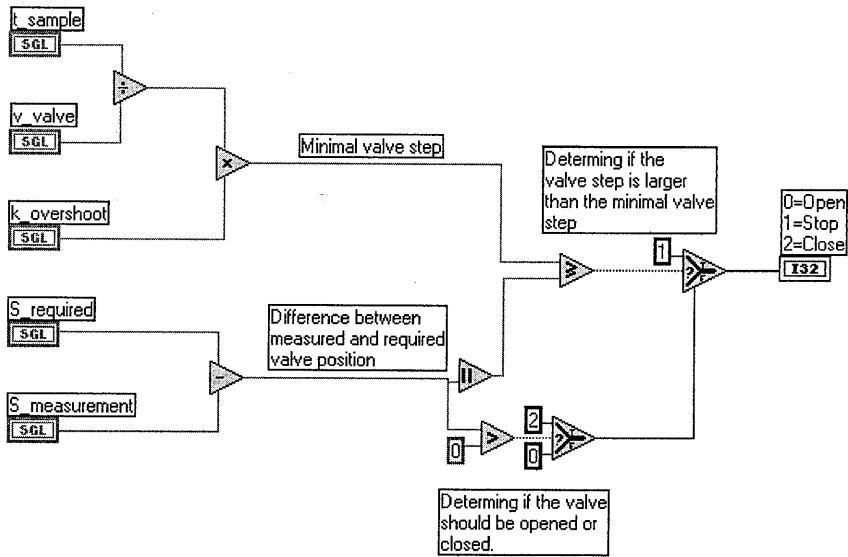


figure D.2 : Valve positioning system

The valve positioning system has been programmed within the data acquisition system. The graphical “source code” in figure D.2 gives a schematic overview of the operation of the valve positioning system. The following functions can be seen:

1. The system computes the difference between the measured and required valve position. If the absolute value of this difference is smaller than the smallest step the valve can make in one sample time, the system will decide to stop the valve.
2. If the difference is larger than the smallest step the system will determine whether the required position is greater than the measured position. If this is the case, the system will decide to open the valve.
3. If the required position is smaller than the measured position, the system decides to close the valve.

The smallest step the valve can make in one sample depends theoretically on the sample time of the valve positioning system and on the valve speed:

$$\Delta S_{\min, \text{theor}} = v_{\text{valve}} \cdot t_{\text{sample}} \quad (\text{D.1})$$

with t_{sample} [s] is the data acquisition sample time and v_{valve} [1/s] is the (relative) valve speed, defined by the actual speed divided by the full stroke. In the laboratory set up $t_{\text{sample}}=0.10$ sec is used.

In practice, the actual smallest step that can be implemented is larger, because the valve displays some backlash and some overshoot occurs. To account for these effects, an empirically determined overshoot factor $k_{overshoot}$ is applied:

$$\Delta S_{\min} = v_{\text{valve}} \cdot t_{\text{sample}} \cdot k_{\text{overshoot}} \quad (\text{D.2})$$

The minimal step which can be implemented on the actual valves is thus determined by the sample time, the valve speed and the overshoot factor. For each of the valves this results in the minimal step which is presented in table D.1:

Valve	$v_{\text{valve}} [\text{s}^{-1}]$	$k_{\text{overshoot}} [-]$	$\Delta S_{\min} [-]$ (for $t_{\text{sample}}=0.1 \text{ sec}$)
Blow-off	0.014837	3.00	0.0044511
Throttle	0.009091	2.50	0.0022727
Fuel	0.022883	1.60	0.0036613

table D.1: Minimal valve step per sample for all control valves.

D.3 Threshold and Scaling

In Primacs, all signals are scaled to improve the numerical condition of the involved (matrix) computations and to ensure that all signals and weighting factors are comparable in the MPC criterion. The scaling rule is simple, the scaled value X_{scaled} of the original signal X is

$$X_{\text{scaled}} = \frac{X - x_{\text{offset}}}{x_{\text{amplitude}}} \quad (\text{D.3})$$

in which x_{offset} and $x_{\text{amplitude}}$ are the offset value of the signal X and the expected amplitude variation of the signal X respectively. For all signals, constant offset and amplitude factors are determined. For the gas turbine the following scaling factors are gathered in table D.2.

Model name	internal Primacs name	offset value	amplitude value	threshold value
blow-off valve	VALVEBlow	0.0	1.0	-
throttle valve	VALVETHrot	0.5	0.5	-
fuel valve	VALVEGas	0.335	0.665	-
compressor pressure	PRESComp	1.57268e5	42732	650
compressor temperature	TEMPComp	356.698	56.698	0
plenum pressure	PRESPlenum	1.49605e5	50395	0
plenum temperature	TEMPPlenum	356.698	56.698	0
expander pressure	PRESCch	1.46450e5	53550	2000
expander temperature	TEMPCch	875.362	375.362	2
rotational speed	Rotspeed	438.216	161.784	1.5
cooled expander temperature	TEMPTurbin	808.671	308.671	0
compressor mass flow	FLOWComp	0.382935	0.217065	0
expander mass flow	FLOWTurb	0.382935	0.217065	0.01
compressor power	POWComp	22895.55	22104.4	0
expander power	POWTurb	22895.55	22104.4	1000
combustion power	POWComb	217361.14	132638.9	0
surge ratio	SURGERat	0.931348	0.111348	0

table D.2 : Primacs scaling factors gas turbine model.

The threshold values for each filtered signal in Primacs, introduced in Chapter 6, are determined from an analysis of both the variance in measurement noise and the sensitivity of minimum valve position changes on the signals. The threshold values are defined as percentages of the corresponding signals and are presented in absolute values in table D.2.

For the compressor station model the Primacs scaling factors are presented in table D.3:

Model name	internal Primacs name	offset value	amplitude value
inputs			
throttle valve A	VALVETHrota	0.70	0.5
recycle valve A	VALVEBlowa	0.01	0.6
power A	Powera	55000	35000
throttle valve B	VALVETHrotb	0.80	0.6
recycle valve B	VALVEBlowb	0.01	0.6
power B	Powerb	65000	35000
user-valve	VALVEHeader	0.80	0.6
cold recycle-valve	VALVERecycle	0.01	0.6
states			
inlet temperature A	TEMPCompina	302.00157	302.00157
inlet pressure A	PRESCompina	99688.88186	24922.220
outlet temperature A	TEMPCompouta	395.67336	395.67336
outlet pressure A	PRESCompouta	193241.03758	96620.518
rotational speed A	Rotspeeda	537.25954	134.31488
inlet temperature B	TEMPCompinb	302.12851	302.12851
inlet pressure B	PRESCompinb	103528.63210	25882.158
outlet temperature B	TEMPCompoutb	407.80650	407.80650
outlet pressure B	PRESCompoutb	194362.10566	97181.052
rotational speed B	Rotspeedb	518.12524	129.53131
header temperature	TEMPHeader	401.88446	200.94223
header pressure	PRESHeader	184427.17774	92213.588
(extra) outputs			
mass flow A	FLOWCompa	0.581343	0.290671
mass flow B	FLOWCompb	0.608986	0.304493
cold recycle flow	FLOWRecycle	0.014396	0.80
user mass flow	FLOWHeader	1.151746	1.151746
recycle flow A	FLOWBlowa	0.012162	0.80
recycle flow B	FLOWBlowb	0.012023	0.80
distance to surge A	DEVSurgea	0.851281	0.15
distance to surge B	DEVSurgeb	0.867141	0.15
difference in distance to surge A-B	DEVdif	-0.0158601	0.1
power ratio	DEVidpow	1.23530	4.0

table D.3 : Primacs scaling factors compressor station model.

D.4 Primacs

Primacs is a computer package for real-time process control. Primacs is being developed by TNO-TPD from Delft. It is written in C++ and available on the PC platform under Windows NT. Due to the object oriented programming, Primacs has a modular structure that facilitate a flexible usage. Primacs consist of separate functional modules. Besides Primacs "system" modules, the modules that are relevant for a user are the modules in which the applied models, the controller configuration and the filter are defined. These can be developed completely independent from the system modules. In Primacs, modules are defined by their inputs and outputs. Modules are coupled by assigning outputs of one module to inputs of another module.

Module types are

- User definable model modules:
 - Define model equations, inputs and outputs, sample interval, integration routines.

In our real-time application, the three internal models (for controller prediction, optimisation and one step ahead observation), the filter (including reconstruction), and the process simulation models are developed in user defined modules.

- MPC controller module:
 - Sophisticated Model Predictive Control algorithms.
- Primacs kernel module:
 - User interface for developing MPC configurations (coupling of modules).
 - User interface for real-time control parameters and set-points.
 - User interface for data storage, data monitoring and presentation

D.5 Linear optimisation algorithms

In this section the MPC optimisation problem is reformulated towards standard linear optimisation algorithms used in Primacs: Least Squares for unconstrained optimisation and Quadratic Programming for constrained optimisation. This derivation is discussed extensively in the specification of the source code of a preliminary Primacs version [Profit,1992]. For a description on the algorithms themselves a reference is made to standard textbooks on optimisations, for instance [Edgar, 1988].

Consider the following linear, discrete time model:

$$\begin{aligned} x(k+1) &= \Phi x(k) + \Gamma u(k) \\ y(k+1) &= Cx(k+1) + Du(k) \end{aligned} \quad (\text{D.4})$$

Suppose we can formulate the evolution of the states over the whole prediction horizon (of p samples) by the following summation of a constant input term and a term due to momentary changes in the inputs:

$$x^n(k+1) = \begin{bmatrix} x(k+1 | k) \\ \vdots \\ x(k+p | k) \end{bmatrix} = x_{\Delta u=0}^n(k+1) + x_{\Delta u}^n(k) \quad (\text{D.5})$$

Then also the outputs can be written as

$$y^n(k+1) = \begin{bmatrix} y(k+1|k) \\ \dots \\ y(k+p|k) \end{bmatrix} = y_{\Delta u=0}^n(k+1) + y_{\Delta u}^n(k+1) \quad (\text{D.6})$$

according to

$$y_{\Delta u=0}^n(k+1) = \mathbf{C}^n x_{\Delta u=0}^n(k+1) + \mathbf{D}^n u(k) \quad (\text{D.7})$$

$$y_{\Delta u}^n(k+1) = \mathbf{C}^n x_{\Delta u}^n(k+1) + \mathbf{D}^n \Delta u^m(k) \quad (\text{D.8})$$

With $x_{\Delta u}^n(k+1) = \mathbf{S} \Delta u^m(k)$ equation (D.8) can be written as

$$y_{\Delta u}^n(k+1) = (\mathbf{C}^n \mathbf{S} + \mathbf{D}^n) \Delta u^m(k) = \mathbf{A} \Delta u^m(k) \quad (\text{D.10})$$

Finally, we introduce the tracking error e as

$$e^n(k) = y^n(k) - r^n(k) \quad (\text{D.11})$$

and when we define

$$e_{\Delta u=0}^n(k) = y_{\Delta u=0}^n(k) - r^n(k) \quad (\text{D.12})$$

we can state the following quadratic optimisation criterion for the **constrained optimisation**:

$$\min_{\Delta u^m} J = \left(e_{\Delta u=0}^n + \mathbf{A} \Delta u^m \right)^T \mathbf{Q}^n \left(e_{\Delta u=0}^n + \mathbf{A} \Delta u^m \right) + \left(\Delta u^m \right)^T \mathbf{P}^m \left(\Delta u^m \right) \quad (\text{D.13})$$

Which, after convenient reformulating, can be transformed into a standard QP problem

$$\min_{\Delta u^m} J = \frac{1}{2} \left(\Delta u^m \right)^T \left[\mathbf{A}^T \mathbf{Q}^n \mathbf{A} + \mathbf{P}^m \right] \left(\Delta u^m \right) + \left(e_{\Delta u=0}^n \mathbf{Q}^n \mathbf{A} \right) \Delta u^m \quad (\text{D.14})$$

because, the standard QP problem is formulated with a Hessian \mathbf{H} and a gradient \mathbf{G} like:

$$\min_x f(x) = \frac{1}{2} x^T \mathbf{H} x + \mathbf{G}^T x \quad (\text{D.15})$$

In the standard QP problem, constraints are formulated as

$$\mathbf{C} x \geq \mathbf{c} \quad (\text{D.16})$$

Constraints on the outputs, inputs and move constraints can be straightforward written in the above notation according to

$$\begin{aligned} y_{\min}^n &\leq y_{\Delta u=0}^n + y_{\Delta u}^n = y_{\Delta u=0}^n + \mathbf{A} \Delta u^m \leq y_{\max}^n \\ u_{\min}^m &\leq u^m + \Delta u^m \leq u_{\max}^m \\ -\Delta u_{\max}^m &\leq \Delta u^m \leq \Delta u_{\max}^m \end{aligned} \quad (\text{D.17})$$

respectively. In matrix notation corresponding to (D.16) these constraints become

$$\begin{bmatrix} \mathbf{A} \\ \mathbf{A} \\ \mathbf{I} \\ -\mathbf{I} \\ \mathbf{I} \\ -\mathbf{I} \end{bmatrix} \Delta u^m \geq \begin{bmatrix} y_{\Delta u=0}^n - y_{\max}^n \\ y_{\min}^n - y_{\Delta u=0}^n \\ u_{\min}^m - u^m \\ u^m - u_{\max}^m \\ -\Delta u_{\max}^m \\ \Delta u_{\max}^m \end{bmatrix} \quad (\text{D.18})$$

Finally, in the same notation, the solution for the **unconstrained optimisation** problem is

$$\Delta u^m = \left[\mathbf{A}^T \mathbf{Q}^n \mathbf{A} + \mathbf{P}^m \right]^{-1} \mathbf{A}^T \mathbf{Q}^n e_{\Delta u=0}^n = \mathbf{K}_{\text{MPC}} e_{\Delta u=0}^n \quad (\text{D.19})$$

D.6 Controller computation times

Computation times are crucial for the feasibility of MPC. When computation times become too large, and the corresponding controller sample interval needs to be adapted, model predictions cannot be updated fast enough and possibly important events within one sample time are not predicted by the controller. In this appendix the computation time of the controller is determined for several cases. From this, a selection is made for the sample time.

The computation time is influenced by the sample time, the type of model which is used and the constraints the controller deals with:

- For fixed sizes of the prediction (20 seconds) and control horizon (6 seconds), table D.1 lists the different sample times for which the computation time is determined.

Sample Time [s]	Prediction horizon [samples]	Control horizon [samples]
2	10	3
1.5	13	4
1.2	17	5
1	20	6

table D.4 : Size of the prediction and control horizon for different sample times.

- Also the type of model which is used for the IOBM, IPM and IOM influences the computation time, as the different types of models require different computational effort.
- Finally the constraints which are imposed on the controller influence the computation time. When the controller does not violate any constraint, only the unconstrained problem has to be solved. When the controller needs to account for constraints, the unconstrained as well as the constrained problem has to be solved. This results in higher computation times. The worst case situation however is reached when the controller has to weight constraints violations: in this case the unconstrained, constrained as well as the soft constrained problem have to be solved.

For the three combinations of models which are used in the research the computation times have been determined as a function of the sample time, in the situation when one constraint is reached, as well as in the situation when a constraint is exceeded and the controller uses soft

constraints. The results are presented in figure D.1 and figure D.2. These figures show that the sample time, the use of different models and the constraint situation have indeed the effect which is described above.

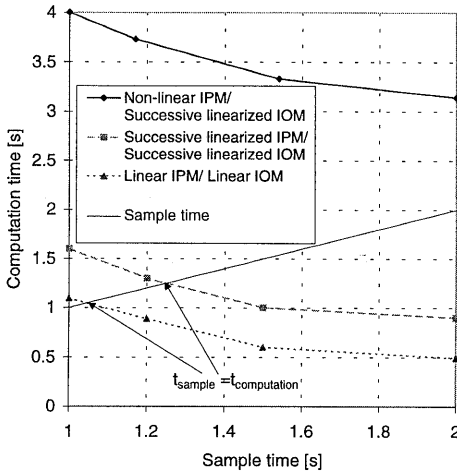


figure D.3 : Computation time as a function of the sample time in the situation when one constraint has been exceeded.

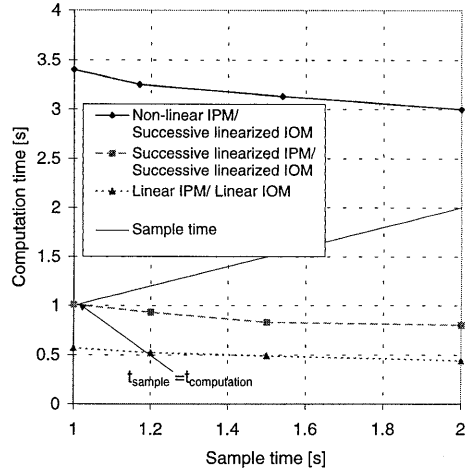


figure D.4 : Computation time as a function of the sample time when one constraint has been reached, but a solution within the constraints has been found.

The sample interval for which the computation time equals the sample interval can be regarded as a minimum value for the sample interval. This must be investigated in the case where the controller encounters “soft constraints”, that is, one or more constraint violations cannot be avoided, as this is the worst case situation. The minimal sample interval can then be obtained from figure D.3, for each of the model combinations, by considering the computation time which equals the sample time. For the different model combinations this minimum sample interval is presented in table D.5.

	Model combination	Minimum sample interval [s]
1	Linear MPC: Linear models for prediction and optimisation.	1.05
2	Non-linear MPC: Non-linear model for observation, successively linearised models for prediction and optimisation.	1.25
3	Non-linear MPC: Non-linear model for observation and prediction, successively linearised model for optimisation.	>3

table D.5 : Minimum required MPC sample interval for different internal model combinations.

According to this table a sample interval of 1.05 s can be realised for linear MPC and 1.25s when successive linearisation is applied. However, to leave computation “space”, for other processes on the computer system (like monitoring and hard disk storage) a computation time of 1.5 s has been chosen in both cases.

D.7 Resolution of valves and minimal input move

In the following experiments the application of a threshold range on a constant set point is examined. As an initial disturbance, a small step to the set points of rotational speed and expander mass flow have been specified. From sample 40 on a constant rotational speed of 463 rev/s and a constant mass flow of 0.42 kg/s are requested. The experiment is performed with and without threshold on the set points.

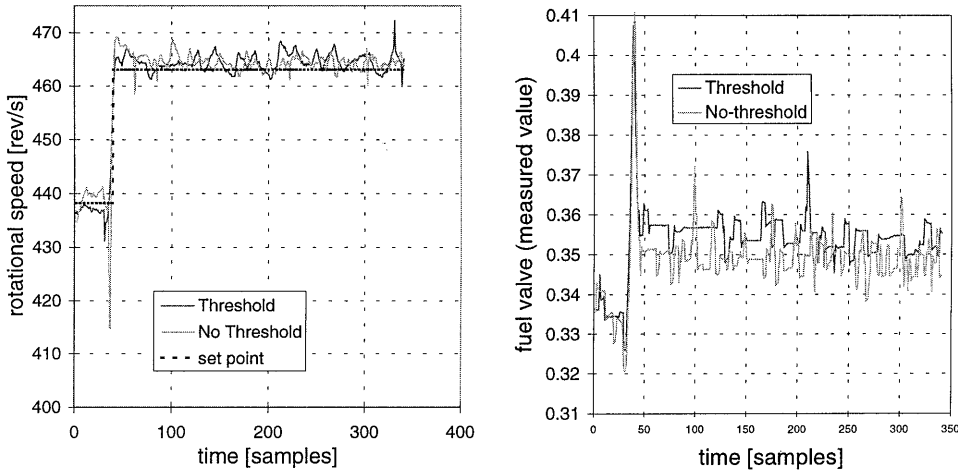


figure D.5 : Measured rotational speed and corresponding input signal of the fuel valve compared in experiments with and without a threshold.

The results, presented in figure D.5, show that the set point of the rotational speed is easily reached in both cases. Also the expander mass flow set point is easily reached (not shown). Clearly, more peaks are present in the measured rotational speed signal when no threshold is applied. This is expected, because these peaks are related to the high voltage switching of the relays of the inputs. With a threshold, less control moves are expected. Indeed, the corresponding input signal (fuel valve) shows significantly less moves.

We can attempt to put this in a more quantitative way. In each sample during the experiment, the momentary value of the optimisation criterion can be computed according to:

$$criterion(k) = \sum_{setpoints} \left[\Gamma^y (measurement(k) - setpoint(k)) \right]^2 + \sum_{inputs} \left[\Gamma^u (input(k) - input(k-1)) \right]^2 \quad (D.20)$$

When the criterion values of each sample are added up over a transient, the total criterion value C is obtained, which expresses the controller performance over this transient:

$$C = \sum_{setpoints} \sum_{k=k_{start}}^{k=k_{end}} \left[\Gamma^y (measurement(k) - setpoint(k)) \right]^2 + \sum_{inputs} \sum_{k=k_{start}}^{k=k_{end}} \left[\Gamma^u (input(k) - input(k-1)) \right]^2 \quad (D.21)$$

Each term of the criterion can be computed separately. Comparing the same experiment with and without the threshold, table D.6 presents the contribution to the total criterion value for

each of the controlled set points as well as the contribution of all inputs. To be able to compare different outputs and inputs with each other, the outputs and inputs have been scaled before the criterion value have been computed, such that their value is between -1 and 1. In this way quantitative measures are obtained.

	Contribution of each of the set points to the total criterion value (x 100)		Contribution of each of the inputs to the total criterion value (x 100)	
	N	\dot{m}_t	fuel valve	throttle valve
Threshold	0.99	8.47	3.04	2.44
No threshold	1.52	8.71	6.46	2.64

table D.6 : Criterion values for set points and inputs in case with and without threshold.

These results show that the contribution of the inputs to the total criterion value decreases when a threshold is applied, implicating that less control actions are required by the controller when a threshold is applied. This is according to what we expected. The constant value for the throttle valve is caused by its slow opening from start value 0.5 to 1.0 during the transient (not shown). The contribution of the expander mass flow to the total criterion value does not change and is mainly caused by measurement noise. The contribution of the rotational speed set point decreases when a threshold is applied. This is not according to what we expected: in principle a threshold would increase the criterion value. The decrease is probably caused by the reduced number of control actions.

D.8 Filter gain

In three experiments we examined the influence of the filter gain on the controller response to unmeasured disturbances in the process. The controller should keep the rotational speed at a constant set point of 438 rev/s. The disturbance is introduced by a moving throttle valve. The internal models keep a constant throttle valve position, while the actual (disturbance) trajectory is shown in figure D.6.

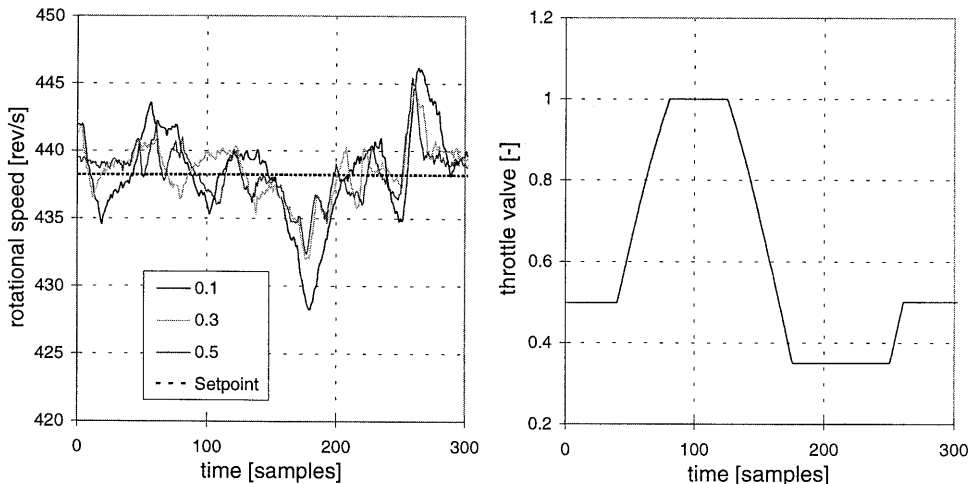


figure D.6 : Measured rotational speed for different values of the filter gain and for a constant set point. The only input used is the fuel valve, the throttle valve has been used to apply disturbances according to the right side figure.

For the controlled outputs (measured rotational speed) and for the manipulated inputs (computed fuel valve position), the contribution to the total criterion value is computed. This way a quantitative measure is obtained to evaluate the filter gain. The results are presented in table D.7 which show that when the filter gain increases, the contribution of the set point deviation to the total criterion value decreases while the contribution of the input increases. This means that when a higher filter gain is applied, the set point is closer (and faster) reached on account of larger input moves.

Filter gain	Contribution of the set point to the total criterion value (x 1000)	Contribution of the input to the total criterion value (x1000)	Total Criterion Value (x 1000)
0.1	19	0.5	19.5
0.3	7.4	3.7	11.1
0.5	5.9	5.6	11.5

table D.7 : Criterion values for different settings of the filter gain.

As the contribution of the set points decreases and the contribution of the inputs increases, a minimum total criterion value can be expected. In these experiments, the total criterion value indeed is minimal for a gain of 0.3. The criterion value, however, depends strongly on scaling and weighting of inputs and set points. In the presented case, the weighting of both is equal to 1, and both signals are scaled to the set point. When the inputs weightings (or scaling) would be (made) larger, the contribution of the inputs would outweigh the contribution of the outputs and thus decrease the optimal value for the total criterion. The experiments presented here are not aimed to tune the filter. This would require more experiments. The filter gain of 0.3, however, performs well and is used in most experiments.

E Visualisation of Anticipative Behaviour

In Chapter 6, the anticipative behaviour of the MPC controller has been treated. It has been discovered that the controller exhibits an inverse controller response: when the set point is supposed to rise, the initial control actions cause the output to lower first. In Chapter 6 we showed that the inverse controller response diminishes when the size of the control horizon is increased relative to the prediction horizon. This phenomena is studied in detail in this appendix. We discuss the influence of the size of control horizon by a visualisation of the full control and prediction horizon during successive samples of a transient set point change.

A visualisation means that we examine and present the computed changes of the inputs over the control horizon and the corresponding predicted output responses over the prediction horizon for a number of samples. For reasons of clarity a SISO set point control of the rotational speed with the fuel valve as input is considered. Also no constraints are applied.

Simulations for two different lengths of the control horizon are compared. First, we present the case where the control horizon is 4 samples (related to the prediction horizon of 13 samples) and after that the case where the control horizon is 12 samples. In fact this is the maximum length since at sample k the value of the control input for sample $k+1$ is computed.

In both cases, the control moves in the control horizon and the response of the rotational speed in the prediction horizon are displayed for each sample from the moment the set point step enters the prediction horizon up to 4 samples after the actual step. Results are displayed in the figures E.1 to E.4. The x-axis indicates the number of samples relative to the step: at sample 0 the actual set point step takes place. Note that every indicated sample value describes the value on the *coming* interval; the indicated value at sample -1, for example, holds *between* sample -1 and sample 0. These line-diagrams are only used (instead of more appropriate bar charts) for a clear graphical presentation.

Figure E.1 and figure E.3 show the computed control moves over the control horizon for a control horizon of 4 and 12 samples respectively. In figure E.1 therefore 17 “lines” of four elements are displayed: one for each sample starting 12 samples before the actual set point change up to 4 samples afterwards. To interpret this result, the corresponding control moves of all successive samples are connected by lines. Remark that the connecting line of all first samples represents the values that are actually used by the controller. Equivalent, figure E.3 displays 17 “lines” of twelve elements. For reasons of clarity, now not all lines that connect corresponding samples are shown but only the first, second, seventh and twelfth.

Figure E.2 and figure E.4 show the response of the rotational speed over the prediction horizon (13 samples) for a control horizon of 4 and 12 samples respectively.

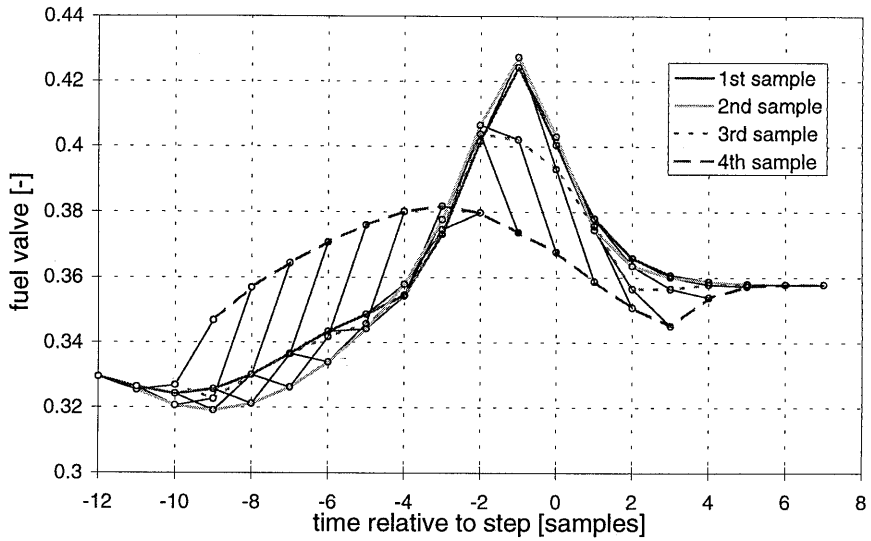


figure E.1 : Computed control moves of the fuel valve over the control horizon of four samples, displayed 17 times: starting 12 samples before the actual set point step up to 4 samples afterwards. The indicated lines connect the corresponding elements of the control horizon of successive samples.

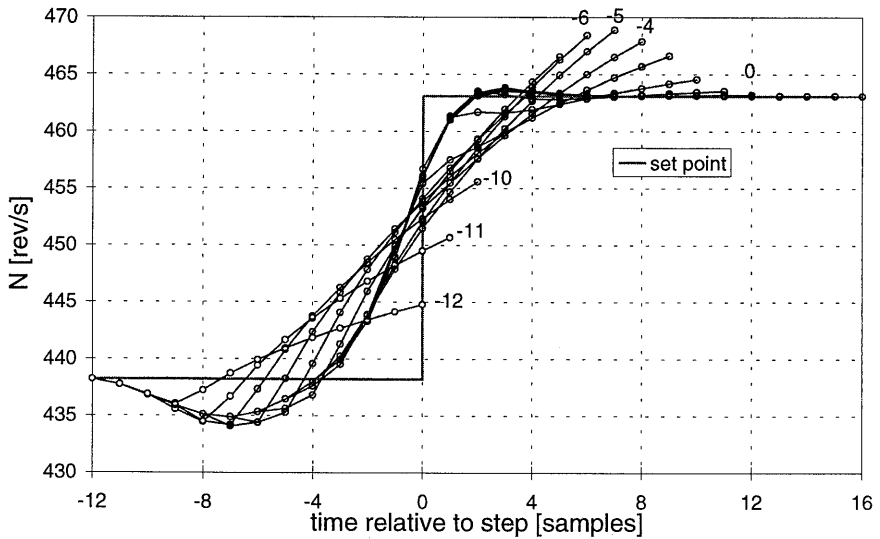


figure E.2 : Predicted (output) response of the rotational speed over the prediction horizon. Displayed 17 times, starting 12 samples before the actual set point change up to 4 samples afterwards. The end-points of the predictions of -12, -11, and -10, as well as -6, -5, -4, and 0 are marked.

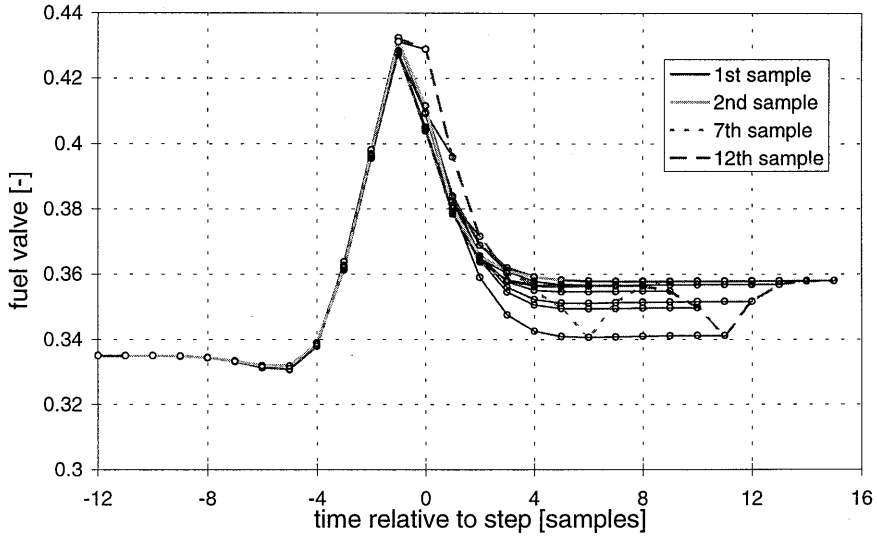


figure E.3 : Computed control moves of the fuel valve over the control horizon of twelve samples, displayed 17 times: starting 12 samples before the actual set point step up to 4 samples afterwards. The indicated lines connect the corresponding elements of the control horizon of successive samples.

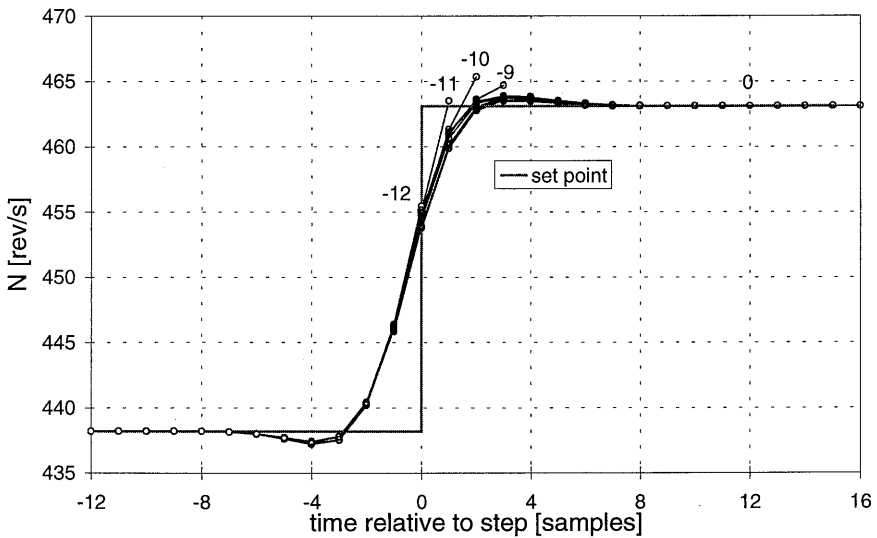


figure E.4 : Predicted (output) response of the rotational speed over the prediction horizon for a control horizon of twelve samples. Displayed 17 times, starting 12 samples before the actual set point change up to 4 samples afterwards. The end-points of the predictions of -12 to -9 and 0 are marked.

Figure E.4 shows that the controller is almost perfectly capable to follow the prescribed set point step in the predictions over the horizon. This holds already from the moment the step enters the prediction horizon. This response is realised by the corresponding input moves shown in figure E.3. The successively computed input moves over the whole control horizon closely correspond to each other. This means in particular that the newly computed *first* input move of a sample equals the *second* input move of the previous sample. The controller is indeed *overall* optimal. In detail, these "optimal" control actions consist of three samples in which the valve is fast opened (samples -3, -2, -1) followed three samples of fast closing of the valve (samples 0, 1, 2). Because of the large number of degrees of freedom within the twelve samples control horizon this optimal solution is computed for all samples.

Clearly the same performance cannot be reached for the four sample control horizon. The first samples after which the future set point step enters the prediction horizon show the most striking results. In figure E.1 and figure E.2 we see for these first samples that the future set point can hardly be effectuated by only changing the available four input moves of the control horizon. The newly computed *first* input move does not correspond to the *second* input move of the previous sample. During the first few samples after the moment that the step has entered the prediction horizon, the controller closes the fuel valve in the first two samples of the control horizon and opens it for the remaining two samples. This way a compromise is found between the set point deviation before the step, and the set point deviation after the step. Only the first input move of the control horizon is implemented and due to this effect the inverse controller response is explained.

In the case where the control horizon is 12 samples, the controller postpones the control moves to three samples before the step. When the control horizon is 4 samples, the controller cannot do this and is forced to compute sub-optimal control moves.

F Controller Settings in Experiments and Simulations

In this appendix the settings of the controller of all the experiments and simulations in Chapter 6 and Chapter 7 are listed. The following Primacs notation has been adopted for the set point and throttle valve trajectories:

- $\text{step}(kstep)$ A step from 0 to 1 at sample $kstep$,
- $\text{ramp}(kbegin, duration)$ A ramp from 0 to 1 beginning at sample $kbegin$ and ending at $kbegin + duration$,
- $\text{sin}(ksample / a)$ A sine-wave with zero mean and period $a * 2\pi$.

F.1 Settings of the experiment in section 4.7

The settings used in this open-loop experiment are presented in table F.1.

PRIMACS experiment number: nr0100							
Set points							
	Weighting	Filter Gain	Threshold	Trajectory			
N	3	-	-	438.216+step(50)*80.048 518.264-step(130)*80.048			
\dot{m}_b	3	-	-	0.382935+step(50)*0.107513 0.490448-step(130)*0.107513			
Disturbance							
				No disturbance			
Constraints						MPC	
	Weighting	Filter Gain	Threshold	Low	High	Parameter	Value
T_{cc}	99	-	-	-	925	p	10
N	99	-	-	325	550	m	3
R_{surge}	99	-	-	-	0.97	sample time	2 s
Inputs						Model	
	Weighting	Low	High	Move C.	Combination		
S_{fuel}	1	0	1	0.045766	Successive linearisation		
S_{thr}	1	0	1	0.018182			

Table F.1: Settings of open-loop experiment section 4.7.

F.2 Settings of experiments in section 6.3.1

In section 6.3.1 an experiment presents the response to a new set point within the operation area. The settings used in this experiments are presented in table F.2.

PRIMACS experiment number: nr0101				
Set points				
	Weighting	Filter Gain	Threshold	Trajectory
N	3	0.1	-	438.216+step(50)*80.048 518.264-step(130)*80.048
\dot{m}_b	3	0.1	-	0.382935+step(50)*0.107513 0.490448-step(130)*0.107513
Disturbance				
				No disturbance

Constraints						MPC	
	Weighting	Filter Gain	Threshold	Low	High	Parameter	Value
T_{cc}	99	0.1	-	-	925	p	10
N	99	0.1	-	325	550	m	3
R_{surge}	99	0.1	-	-	0.97	sample time	2 s
Inputs						Model	
	Weighting	Low	High	Move C.		Combination	
S_{fuel}	1	0	1	0.045766		Successive linearisation	
S_{thr}	1	0	1	0.018182			

Table F.2: Settings of experiment to a new set point within the operation area.

F.3 Settings of experiments in section 6.3.2

In section 6.3.2, two experiments are presented, in which an unreachable operating point in the surge area has been prescribed by set points on the rotational speed and the expander mass flow. The experiment is performed for two different values of the rotational speed. The settings used in these experiments are presented in table F.3 and table F.4.

PRIMACS experiment number: nr0435							
Set points							
	Weighting	Filter Gain	Threshold	Trajectory			
N	1	0.3	1.5	438.216			
\dot{m}_b	1	0.3	0.01	0.382935-ramp(70,80)*0.10			
Disturbance							
				No disturbance			
Constraints						MPC	
	Weighting	Filter Gain	Threshold	Low	High	Parameter	Value
T_{cc}	99	0.3	2	-	925	p	13
N	99	0.3	1.5	325	550	m	4
R_{surge}	99	0	-	-	0.97	sample time	1.5 s
Inputs						Model	
	Weighting	Low	High	Move C.		Combination	
S_{fuel}	1	0	1	0.0343245		Successive linearisation	
S_{thr}	1	0	1	0.0136365			

Table F.3 : Settings of the experiment at 438 rev/s.

PRIMACS experiment number: nr0438							
Set points							
	Weighting	Filter Gain	Threshold	Trajectory			
N	1	0.3	1.5	350			
\dot{m}_b	1	0.3	0.01	0.29-ramp(70,80)*0.10			
Disturbance							
				No disturbance			
Constraints						MPC	
	Weighting	Filter Gain	Threshold	Low	High	Parameter	Value
T_{cc}	99	0.3	2	-	925	p	13
N	99	0.3	1.5	325	550	m	4
R_{surge}	99	0	-	-	0.97	sample time	1.5 s
Inputs						Model	
	Weighting	Low	High	Move C.		Combination	
S_{fuel}	1	0	1	0.0343245		Successive linearisation	
S_{thr}	1	0	1	0.0136365			

Table F.4 : Settings of the experiment at 350 rev/s.

F.4 Settings of experiments in section 6.3.3

In section 6.3.3, two experiments are presented, in which an unreachable operating point has been defined by two set points for different values of the weighting of the set points. The settings used in these experiments are presented in table F.5.

PRIMACS experiment numbers: nr0431/nr0430							
Set points							
	Weighting	Filter Gain	Threshold	Trajectory			
p_{cc}	1	0.3	2000	146450			
\dot{m}_{lb}	1, 10	0.3	0.01	0.382935+step(40)*0.10			
Disturbance							
				No disturbance			
Constraints						MPC	
	Weighting	Filter Gain	Threshold	Low	High	Parameter	Value
T_{cc}	99	0.3	2	-	925	p	13
N	99	0.3	1.5	325	550	m	4
R_{surge}	99	0	-	-	0.97	sample time	1.5 s
Inputs						Model	
	Weighting	Low	High	Move C.		Combination	
S_{fuel}	1	0	1	0.0343245		Successive linearisation	
S_{thr}	1	0	1	0.0136365			

Table F.5 : Settings of the two experiments with set point weighting 1.0 and 10.0.

F.5 Settings of simulations in section 6.4.1

In section 6.4.1 a transient simulation is presented. The settings used in this simulation are presented in table F.6.

PRIMACS experiment numbers: nr0464							
Set points							
	Weighting	Filter Gain	Threshold	Trajectory			
N	1	0.3	1.5	438.216+step(20)*80.048 518.264-step(120)*80.048			
\dot{m}_{lb}	1	0.3	0.01	0.382935+step(20)*0.107513 0.490448-step(120)*0.107513			
Disturbance							
				no disturbance			
Constraints						MPC	
	Weighting	Filter Gain	Threshold	Low	High	Parameter	Value
T_{cc}	99	0.3	2	-	925	p	13
N	99	0.3	1.5	325	550	m	4
R_{surge}	99	0	-	-	0.97	sample time	1.5 s
Inputs						Model	
	Weighting	Low	High	Move C.		Combination	
S_{fuel}	1	0	1	0.0343245		Successive linearisation	
S_{thr}	1	0	1	0.0136365			

Table F.6 : Settings of the transient simulation

F.6 Settings of simulations in section 6.4.2

In section 6.4.2, three simulations are presented, in which the same set point trajectory has been used for three different values of the weighting on the fuel valve input. The settings used in these experiments are presented in table F.7.

PRIMACS experiment numbers: nr0452, nr0453, nr0454							
Set points							
	Weighting	Filter Gain	Threshold	Trajectory			
N	1	0.3	1.5	438.216+step(20)*80.048 518.264-step(170)*80.048			
\dot{m}_{tb}	1	0.3	0.01	0.382935+step(20)*0.107513 0.490448-step(170)*0.107513			
Disturbance							
				No disturbance			
Constraints						MPC	
	Weighting	Filter Gain	Threshold	Low	High	Parameter	Value
T_{cc}	99	0.3	2	-	925	p	13
N	99	0.3	1.5	325	550	m	4
R_{surge}	99	0	-	-	0.97	sample time	1.5 s
Inputs						Model	
	Weighting	Low	High	Move C.		Combination	
S_{fuel}	30, 15, 0	0	1	0.0343245		Successive linearisation	
S_{thr}	1	0	1	0.0136365			

Table F.7 : Settings of the three experiments with set point weightings 30, 15 and 0.

F.7 Settings of experiments in section 6.4.3

In section 6.4.3, three experiments are presented, in which the same set point trajectory has been used for three different values of the constraint on the expander inlet temperature. The settings used in these experiments are presented in table F.8.

PRIMACS experiment numbers: nr0344, nr0345, nr0346							
Set points							
	Weighting	Filter Gain	Threshold	Trajectory			
N	1	0.3	1.5	438.216+step(20)*80.048 518.264-step(170)*80.048			
\dot{m}_{tb}	1	0.3	0.01	0.382935+step(20)*0.107513 0.490448-step(170)*0.107513			
Disturbance							
				No disturbance			
Constraints						MPC	
	Weighting	Filter Gain	Threshold	Low	High	Parameter	Value
T_{cc}	99	0.3	2	-	880, 900, 925	p	13
N	99	0.3	1.5	325	550	m	4
R_{surge}	99	0	-	-	0.97	sample time	1.5 s
Inputs						Model	
	Weighting	Low	High	Move C.		Combination	
S_{fuel}	1	0	1	0.0343245		Successive linearisation	
S_{thr}	1	0	1	0.0136365			

Table F.8 : Settings of the three experiments with constraint on T_{cc} of 880, 900 and 925 K.

F.8 Settings of the experiment in section 6.4.4

In section 6.4.4, an experiment is presented, in which a sine-wave reference trajectory on the rotational speed as well as a sine-wave trajectory on the throttle valve disturbance has been used. The settings used in this experiment is presented in table F.9.

Experiment: "Sine-wave" / PRIMACS experiment number: nr0024							
Set points							
	Weighting	Filter Gain	Threshold	Trajectory			
N	1	0.3	1.5	438+sin(k/12)*step(75)			
Disturbance							
	Measured?			Trajectory			
Throttle valve	measured			0.7+0.3*sin(k/sample/24)*step(75)			
Constraints						MPC	
	Weighting	Filter Gain	Threshold	Low	High	Parameter	Value
T _{cc}	99	0.3	2	-	925	p	13
N	99	0.3	1.5	325	550	m	4
R _{surge}	99	0	-	-	0.97	sample time	1.5 s
Inputs						Model	
	Weighting	Low	High	Move C.		Combination	
S _{fuel}	0.5	0	1	0.0343245		Successive linearisation	

Table F.9 : Settings of the sine response experiment in section 6.4.4.

F.9 Settings of experiments in section 6.5.2

In section 6.5.2, three experiments are presented, in which the same set point trajectory has been used for three different types of model errors. The settings used in these experiments are presented in the tables F.11-F.13:

PRIMACS experiment number: nr0032							
Set points							
	Weighting	Filter Gain	Threshold	Trajectory			
N	1	0.3	1.5	438.216-ramp(40,40)*113.216 325+ramp(130,80)*225 550-ramp(300,40)*111.784			
Disturbance							
	Measured?			Trajectory			
Throttle Valve	measured			0.5→0.4			
Constraints						MPC	
	Weighting	Filter Gain	Threshold	Low	High	Parameter	Value
T _{cc}	99	0.3	2	-	925	p	13
N	99	0.3	1.5	325	550	m	4
R _{surge}	99	0	-	-	0.97	sample time	1.5 s
Inputs						Model	
	Weighting	Low	High	Move C.		Combination	
S _{fuel}	1	0	1	0.0343245		Linear MPC	

Table F.11 : Settings of experiment 1.

PRIMACS experiment number: nr0031							
Set points							
	Weighting	Filter Gain	Threshold	Trajectory			
N	1	0.3	1.5	438.216-ramp(40,40)*113.216 325+ramp(130,80)*225 550-ramp(300,40)*111.784			
Disturbance							
	Measured?			Trajectory			
Throttle Valve	measured			0.5→0.4			

Constraints						MPC	
	Weighting	Filter Gain	Threshold	Low	High	Parameter	Value
T _{cc}	99	0.3	2	-	925	p	13
N	99	0.3	1.5	325	550	m	4
R _{surge}	99	0	-	-	0.97	sample time	1.5 s
Inputs						Model	
	Weighting	Low	High	Move C.		Combination	
S _{fuel}	1	0	1	0.0343245		Successive linearisation	

Table F.12 : Settings of experiment 2.

PRIMACS experiment number: nr0034							
Set points							
	Weighting	Filter Gain	Threshold	Trajectory			
N	1	0.3	1.5	438.216-ramp(40,40)*113.216 325+ramp(130,80)*225 550-ramp(300,40)*111.784			
Disturbance							
	Measured?			Trajectory			
Throttle Valve	unmeasured			0.5→0.4			
Constraints						MPC	
	Weighting	Filter Gain	Threshold	Low	High	Parameter	Value
T _{cc}	99	0.3	2	-	925	p	13
N	99	0.3	1.5	325	550	m	4
R _{surge}	99	0	-	-	0.97	sample time	1.5 s
Inputs						Model	
	Weighting	Low	High	Move C.		Combination	
S _{fuel}	1	0	1	0.0343245		Successive linearisation	

Table F.13 : Settings of experiment 3.

F.10 Settings of the experiment in section 6.5.3

In section 6.5.3, a disturbance to the system has been applied by means of compressed air. The settings used in these experiments are presented in the tables F.14.

PRIMACS experiment number: nr0434							
Set points							
	Weighting	Filter Gain	Threshold	Trajectory			
p _{cc}	1	0.3	2000	146450			
N	1	0.3	1.5	438.216			
Disturbance							
	Measured?			Trajectory			
Compressed air	unmeasured			Compressed air valve opened at k=35, Compressed air valve closed at k=90			
Constraints						MPC	
	Weighting	Filter Gain	Threshold	Low	High	Parameter	Value
T _{cc}	99	0.3	2	-	925	p	13
N	99	0.3	1.5	325	550	m	4
R _{surge}	99	0	-	-	0.97	sample time	1.5 s
Inputs						Model	
	Weighting	Low	High	Move C.		Combination	
S _{fuel}	1	0	1	0.0343245		Successive linearisation	
S _{thr}	1	0	1	0.0136365			

Table F.14 : Settings of the compressed air experiment.

F.11 Settings of simulations in section 6.6.1

In section 6.6.1, two simulations are presented, in which the same set point trajectory has been used with anticipation and without. The settings used in these experiments are presented in table F.15.

PRIMACS experiment numbers: nr0086, nr0087							
Set points							
	Weighting	Filter Gain	Threshold	Trajectory			
N	1	0.3	1.5	438.216+step(20)*24.881 (without anticipation and with anticipation)			
Disturbance							
	Measured?			Trajectory			
Throttle valve	measured			0.5			
Constraints						MPC	
	Weighting	Filter Gain	Threshold	Low	High	Parameter	Value
T _{cc}	99	0.3	2	-	1200	p	13
N	99	0.3	1.5	325	550	m	4
R _{surge}	99	0	-	-	0.97	sample time	1.5 s
Inputs						Model	
	Weighting	Low	High	Move C.		Combination	
S _{fuel}	0.5	0	1	0.0343245		Successive linearisation	

Table F.15 : Settings of the two experiments with anticipation and without.

F.12 Settings of simulations in section 6.6.2

In section 6.6.2, six simulations are presented, in which the same set point trajectory has been used for different values of the control horizon. The settings used in these experiments are presented in table F.16.

PRIMACS experiment numbers: nr0039, nr0043, nr0044, nr0045, nr0046 and nr0048							
Set points							
	Weighting	Filter Gain	Threshold	Trajectory			
N	1	0.3	1.5	438.216+step(20)*24.881			
Disturbance							
	Measured?			Trajectory			
Throttle valve	measured			0.5			
Constraints						MPC	
	Weighting	Filter Gain	Threshold	Low	High	Parameter	Value
T _{cc}	99	0.3	2	-	1200	p	13
N	99	0.3	1.5	325	550	m	1,2,3,4,8,12
R _{surge}	99	0	-	-	0.97	sample time	1.5 s
Inputs						Model	
	Weighting	Low	High	Move C.		Combination	
S _{fuel}	0.5	0	1	0.0343245		Successive linearisation	

Table F.16 : Settings of the eight experiments with m=1,3,4,5,8,12.

F.13 Settings of the simulation in section 7.4.1

In section 7.4.1, a simulation is presented with a reference load pattern, that is, the mass flow to the user is prescribed by a reference trajectory and the “user-valve”(or ValveHeader) is a manipulated variable of the control system. The settings used in this simulation are presented in table F.17.

PRIMACS experiment number: nr040							
Set points							
	Weighting	Filter Gain	Trajectory				
\dot{m}_{user}	10		1.15 + 0.35*step(50) - step(150) + step(250) - 0.35*step(350)				
FlowRecycle	0.1		0				
FlowRecycleA	0.1		0				
FlowRecycleB	0.1		0				
Load-balancing (equal distance to the surge line)							
DevDif	1		0				
Disturbances							
			No disturbance				
Constraints outputs						MPC settings	
	Weighting	Filter Gain	Low	High		Parameter	Value
RotspeedA	1		420	660		p	30
RotspeedB	1		420	660		m	8
PresHeader	10		160000	300000		sample time	1 s
TempCompA	1			600			
TempCompB	1			600		blocking	---
DevsurgeA	10			0.95			
DevsurgeB	10			0.95			
Constraints Inputs					Model Combination and remarks		
	Weighting	Low	High	Move	<ul style="list-style-type: none"> • Non-linear (open-loop) simulation without model mismatches. • Successive linearisation for prediction and optimisation. • reference load pattern • equal distance to surge line • with anticipation 		
ValveThrotA	1	0.2	1	0.03			
ValveBlowA	1	0	0.8	0.04			
PowerA	1	10000	100000	2000			
ValveThrotB	1	0.2	1	0.03			
ValveBlowB	1	0	0.8	0.04			
PowerB	1	10000	100000	2000			
ValveHeader	1	0.2	1	0.03			
ValveRecycle	1	0	0.8	0.04			

Table F.17: Settings of compressor station simulation with reference load pattern, anticipation and equal distance to the surge line load balancing.

F.14 Settings of the simulation in section 7.4.2

In section 7.4.2, the previous simulation is repeated **without** anticipation. The remaining settings are the same as the previous table (F.17). **PRIMACS experiment number nr041.**

F.15 Settings of the simulation in section 7.4.3

In section 7.4.3, a simulation is presented with a reference load pattern. Now the alternative load balancing strategy of minimisation of power is applied. Simulations are carried out for different values of the set point weighting factor on *DevIdpow* and with or without anticipation. The settings used in this simulation are presented in table F.18.

PRIMACS experiment number: nr047 (DevIdpow weight 0.1, with anticipation), nr0051 (DevIdpow weight 1.0, with anticipation), nr0056 (DevIdpow weight 0.5, with anticipation), nr0057 (DevIdpow weight 0.5, without anticipation)							
Set points							
	Weighting	Filter Gain	Trajectory				
\dot{m}_{user}	1		1.15 + 0.35*step(50) - step(150) + step(250) - 0.35*step(350)				
Load-balancing (power minimisation)							
DevIdpow	0.1 0.5 1.0		0				

Disturbances						
			No disturbance			
Constraints outputs					MPC settings	
	Weighting	Filter Gain	Low	High	Parameter	Value
RotspeedA	1		420	660	p	30
RotspeedB	1		420	660	m	8
PresHeader	10		160000	300000	sample time	1 s
TempCompA	1			600		
TempCompB	1			600	blocking	---
DevsurgeA	10			0.95		
DevsurgeB	10			0.95		
Constraints Inputs					Model Combination and remarks	
	Weighting	Low	High	Move	<ul style="list-style-type: none"> • Non-linear (open-loop) simulation without model mismatches. • Successive linearisation for prediction and optimisation. • Reference load pattern • Power minimisation • With or without anticipation see header for experiment number. 	
ValveThrotA	1	0.2	1	0.03		
ValveBlowA	1	0	0.8	0.04		
PowerA	1	10000	100000	2000		
ValveThrotB	1	0.2	1	0.03		
ValveBlowB	1	0	0.8	0.04		
PowerB	1	10000	100000	2000		
ValveHeader	1	0.2	1	0.03		
ValveRecycle	1	0	0.8	0.04		

Table F.18 : Settings of compressor station simulation with reference load pattern, anticipation and power minimisation load balancing.

F.16 Settings of the simulation in section 7.4.4

In section 7.4.4 a simulation is presented with the actual load pattern, that is, the user-valve (“ValveHeader”) is not a control input but an external disturbance to the system. Two experiments are carried out: with and without an additional set point on the header pressure (“PresHeader”). The settings used in this simulation are presented in table F.19.

PRIMACS experiment number: (disturbance database) nr0033 (with pressure set point), nr0034 (without pressure set point),						
Set points						
	Weighting	Filter Gain	Trajectory			
PresHeader	1		185000 (optional)			
FlowRecycle	0.1		0			
FlowRecycleA	0.1		0			
FlowRecycleB	0.1		0			
Load-balancing (equal distance to the surge line)						
DevDif	1		0			
Disturbances						
			Trajectory			
ValveHeader			0.8 - 0.5*ramp(50,25) + 0.7*ramp(150,35) - 0.7*ramp(250,35) + 0.5*ramp(350,25)			
Constraints outputs					MPC settings	
	Weighting	Filter Gain	Low	High	Parameter	Value
RotspeedA	1		420	660	p	30
RotspeedB	1		420	660	m	8
PresHeader	10		160000	210000	sample time	1 s
TempCompA	1			600		
TempCompB	1			600	blocking	---
DevsurgeA	10			0.95		
DevsurgeB	10			0.95		

Constraints Inputs					Model Combination and remarks
	Weighting	Low	High	Move	
ValveThrotA	1	0.2	1	0.03	<ul style="list-style-type: none"> • Non-linear (open-loop) simulation without model mismatches. • Successive linearisation for prediction and optimisation • Optional set point header pressure • Actual load pattern • Equal distance to surge line • Without anticipation
ValveBlowA	1	0	0.8	0.04	
PowerA	1	10000	100000	2000	
ValveThrotB	1	0.2	1	0.03	
ValveBlowB	1	0	0.8	0.04	
PowerB	1	10000	100000	2000	
ValveRecycle	1	0	0.8	0.04	

Table F.19 : Settings of compressor station simulation.

F.17 Settings of the simulation in section 7.4.5

In section 7.4.4 a simulation is presented with the actual load pattern, now the alternative load balancing criterion of power minimisation is applied. Two experiments are carried out: with and without an additional set point on the header pressure (“PresHeader”). The settings used in this simulation are presented in table F.20.

PRIMACS experiment number: (disturbance database) nr0046 (DevIdpow weight 0.1, with pressure set point), nr0051 (DevIdpow weight 0.2, without pressure set point)							
Set points							
	Weighting	Filter Gain	Trajectory				
PresHeader	0.1		185000 (optional)				
Load-balancing (power minimisation)							
DevIdpow	0.2	0.1	0				
Disturbances							
			Trajectory				
ValveHeader			0.8 - 0.5*ramp(50,25) + 0.7*ramp(150,35) - 0.7*ramp(250,35) + 0.5*ramp(350,25)				
Constraints outputs						MPC settings	
	Weighting	Filter Gain	Low	High		Parameter	Value
RotspeedA	1		420	660		p	30
RotspeedB	1		420	660		m	8
PresHeader	10		160000	210000		sample time	1 s
TempCompA	1			600			
TempCompB	1			600		blocking	---
DevsurgeA	100			0.95			
DevsurgeB	100			0.95			
Constraints Inputs					Model Combination and remarks		
	Weighting	Low	High	Move	<ul style="list-style-type: none"> • Non-linear (open-loop) simulation without model mismatches. • Successive linearisation for prediction and optimisation • Optional set point header pressure • Actual load pattern • Power minimisation • Without anticipation 		
ValveThrotA	1	0.2	1	0.03			
ValveBlowA	1	0	0.8	0.04			
PowerA	1	10000	100000	2000			
ValveThrotB	1	0.2	1	0.03			
ValveBlowB	1	0	0.8	0.04			
PowerB	1	10000	100000	2000			
ValveRecycle	1	0	0.8	0.04			

Table F.19 : Settings of compressor station simulation.

F.18 Settings of the simulation in section 7.4.6

In section 7.4.6, a closed-loop simulation is presented with a reference load pattern, that is, the mass flow to the user is prescribed by a reference trajectory. Now, model mismatches between

the non-linear simulation model and the internal observation and prediction model are applied. The settings used in this simulation are presented in table F.20. Model differences: ambient pressure 1.3 in stead of 1.2 bar, efficiency of compressor A 0.75 instead of 0.7, and efficiency of compressor B 0.65 instead of 0.6.

PRIMACS experiment number: nr077							
Set points							
	Weighting	Filter Gain	Trajectory				
\dot{m}_{user}	1.0	0.3	1.15 + 0.35*step(50) - step(150) + step(250) - 0.35*step(350)				
PresHeader	0.1	0.3	185000				
FlowRecycle	0.1	0.3	0				
FlowRecycleA	0.1	0.3	0				
FlowRecycleB	0.1	0.3	0				
Load-balancing (equal distance to the surge line)							
DevDif	1.0		0				
Disturbances							
			Trajectory				
			No disturbance				
Constraints outputs						MPC settings	
	Weighting	Filter Gain	Low	High		Parameter	Value
RotspeedA	1	0.3	420	660		p	30
RotspeedB	1	0.3	420	660		m	8
PresHeader	10	0.3	160000	300000		sample time	1 s
TempCompA	1	0.3		600			
TempCompB	1	0.3		600		blocking	---
DevsurgeA	10	0.3		0.95			
DevsurgeB	10	0.3		0.95			
Constraints Inputs					Model Combination and remarks		
	Weighting	Low	High	Move	<ul style="list-style-type: none"> • Non-linear (closed-loop) simulation with model mismatches. • Successive linearisation for prediction and optimisation. • reference load pattern • equal distance to surge line • with anticipation 		
ValveThrotA	1	0.2	1	0.03			
ValveBlowA	1	0	0.8	0.04			
PowerA	1	10000	100000	2000			
ValveThrotB	1	0.2	1	0.03			
ValveBlowB	1	0	0.8	0.04			
PowerB	1	10000	100000	2000			
ValveHeader	1	0.2	1	0.03			
ValveRecycle	1	0	0.8	0.04			

Table F.20 : Settings of compressor station closed-loop simulation with reference load pattern, anticipation and equal distance to the surge line load balancing.

F.19 Settings of experiments in Appendix D.7

In Appendix D.7, two experiments are presented, one with a threshold range and one without. The settings used in these experiments are presented in the tables F.21 and F.22.

PRIMACS experiment number: nr0427				
Set points				
	Weighting	Filter Gain	Threshold	Trajectory
N	1	0.3	1.5	438.216+step(40)*24.881
\dot{m}_b	1	0.3	0.01	0.382935+step(40)*0.036105
Disturbance				
				No disturbance

Constraints						MPC	
	Weighting	Filter Gain	Threshold	Low	High	Parameter	Value
T _{cc}	99	0.3	2	-	925	p	13
N	99	0.3	1.5	325	550	m	4
R _{surge}	99	0	-	-	0.97	sample time	1.5 s
Inputs						Model	
	Weighting	Low	High	Move C.		Combination	
S _{fuel}	1	0	1	0.0343245		Successive linearisation	
S _{thr}	1	0	1	0.0136365			

Table F.21 : Settings of experiment with threshold.

PRIMACS experiment number: nr0428							
Set points							
	Weighting	Filter Gain	Threshold	Trajectory			
N	1	0.3	-	438.216+step(40)*24.881			
m _{nb}	1	0.3	-	0.382935+step(40)*0.036105			
Disturbance							
				No disturbance			
Constraints						MPC	
	Weighting	Filter Gain	Threshold	Low	High	Parameter	Value
T _{cc}	99	0.3	-	-	925	p	13
N	99	0.3	-	325	550	m	4
R _{surge}	99	0	-	-	0.97	sample time	1.5 s
Inputs						Model	
	Weighting	Low	High	Move C.		Combination	
S _{fuel}	1	0	1	0.0343245		Successive linearisation	
S _{thr}	1	0	1	0.0136365			

Table F.22 : Settings of experiment without threshold.

F.20 Settings of experiments in Appendix D.8

In Appendix D.8, three experiments are presented, in which the same reference trajectory and disturbance has been used for three different values of the filter gain. The settings used in these experiments are presented in table F.23.

PRIMACS experiment numbers: nr0027, nr0028, nr0029							
Set points							
	Weighting	Filter Gain	Threshold	Trajectory			
N	1	0.1, 0.3, 0.5	1.5	438.216			
Disturbance							
	Measured?			Trajectory			
Throttle Valve	unmeasured			0.5+step(40)*0.5 1.0-step(125)*0.65 0.35+step(250)*0.15			
Constraints						MPC	
	Weighting	Filter Gain	Threshold	Low	High	Parameter	Value
T _{cc}	99	0.1, 0.3, 0.5	-	-	925	p	13
N	99	0.1, 0.3, 0.5	-	325	550	m	4
R _{surge}	99	0	-	-	0.97	sample time	1.5 s
Inputs						Model	
	Weighting	Low	High	Move C.		Combination	
S _{fuel}	1	0	1	0.0343245		Successive linearisation	

Table F.23 : Settings of the three experiments with filter gains 0.1, 0.3 and 0.5.

Summary

The aim of this study is to investigate the dynamic behaviour and control of turbomachinery. Turbomachinery refers to installations that consist of rotary devices like compressors and expanders or turbines. Turbomachines, for example gas turbines, are commonly applied in aero-engines and in power generation. Knowledge of the dynamic behaviour and control can improve the performance of these systems. In this study, we have followed a three step methodology: the development of dynamic simulation models of turbomachines, the development of model-based control configurations, and the application of these configurations to representative installations. We focus on the development of physical models and the application of Model Predictive Control (MPC) as a model based control strategy. A derived aim is to investigate the feasibility of MPC for use on turbomachinery.

In the first part of this thesis, two different types of non-linear dynamic simulation models are derived: the *physical flow model* and the *lumped parameter model*. Both models are based on (vendor supplied) steady component characteristics and unsteady conservation laws over the volumes that connect successive components. The physical flow model also includes general conservation laws for compressible fluid flow through pipes. The physical basis and the modular approach ensure the flexible applicability to a large class of turbomachines. The model validity is determined by experiments on a custom-built laboratory gas turbine installation. The installation, realised during this study in the laboratory, offers the opportunity to monitor and to influence the dynamic operation of a gas turbine. The performance of the validated models is good. Both steady state and transient responses of the models agree well with experimental results.

In the second part of this thesis, we develop configurations for Model Predictive Control. Especially, the handling of constraints (for instance minimum or maximum values on the inputs or outputs) and interactions (between inputs and outputs) form the basis for selecting this particular controller type. For our MPC development we have used Primacs, a package for real-time model based control that is being developed by TNO-TPD (Delft, The Netherlands). The concept of MPC is to include a model of the system to be controlled in the controller to predict the systems response over a future horizon and to optimise the future inputs. Standard linear MPC uses one linear model for prediction and optimisation. Strong non-linearities, displayed by turbomachinery, and the large operating area of most installations (for instance at start-up) cannot always be adequately handled by linear MPC. In this study certain non-linear approaches (based on successive linearisation and non-linear prediction) which are still based on linear optimisation are studied and applied.

The final step is to apply the MPC configurations to representative installations. Our feasibility study concerns system performance, robustness for external disturbances and for model mismatches and the required computation time. We succeeded in real-time implementation of MPC on the laboratory installation. Within the applied sample interval, the *successive linearisation* approach could be implemented. This approach is shown to be a useful and powerful extension to linear MPC. Indeed, the advantages of MPC, constraint and interactions handling, give excellent results. Special attention has been paid to filtering and anticipation to future set-point changes.

Besides the laboratory installation, we also considered a generalised compressor station for implementation of MPC. This compressor station comprises two compressors connected in parallel to a common header. The MPC results for the compressor station are restricted to simulations. Compressor station control is quite complementary to the gas turbine problem because of the surplus of degrees of freedom (inputs) that parallel connected compressors possess. The application of MPC to the compressor station indicates the profound opportunities that MPC offers for this control problem. Especially, dealing with interaction between all control inputs and controlled outputs in combination with perfect constraint handling and dynamic optimisation is shown to potentially improve the performance of the station. New control objectives like power minimisation become feasible.

Samenvatting

Het onderwerp van deze studie betreft het bestuderen van het dynamisch gedrag en de regeling van turbomachines. De algemene term turbomachines verwijst naar installaties waarin roterende stromingsmachines zoals compressoren of turbines voorkomen. Turbomachines, bijvoorbeeld gasturbines, worden veel gebruikt in vliegtuigmotoren en electriciteitscentrales. Meer kennis over het dynamisch gedrag en de regeling kan de prestaties van deze systemen verbeteren. Deze studie wordt in drie stappen uitgevoerd: het ontwikkelen van dynamische simulatie modellen voor turbomachines, het ontwikkelen van modelgebaseerde regelstrategieën en tenslotte, de toepassing van deze strategieën op representatieve installaties. We richten ons op het ontwikkelen van fysische modellen en de toepassing van *Model Predictive Control* (MPC) als modelgebaseerde regelstrategie. Een afgeleide doelstelling is het onderzoeken van de haalbaarheid van MPC voor toepassing op turbomachines.

In het eerste deel van dit proefschrift worden twee verschillende niet-lineaire dynamische simulatie modellen afgeleid: het fysische stromingsmodel (*physical flow model*) en het geconcentreerde-parameter model (*lumped parameter model*). Beide modellen zijn gebaseerd op de stationaire componentkarakteristieken (beschikbaar gesteld door de fabrikanten) en op instationaire behoudswetten voor de volumes die opeenvolgende componenten verbinden. Het *physical flow model* beschrijft daarnaast ook de instationaire behoudswetten voor samendrukbare stroming door pijpen. De fysische basis en de modulaire structuur verzekeren een flexibele toepassing van de modellen op een grote klasse van turbomachines. De validiteit van de modellen is vastgesteld door middel van experimenten op een speciaal ontworpen gasturbine-installatie. Deze installatie, die tijdens deze studie ontworpen en gebouwd is in het laboratorium, biedt de mogelijkheid om het dynamisch gedrag van een gasturbine te bestuderen en te beïnvloeden. De resultaten van de modellen zijn goed. Zowel de stationaire als de dynamische responsies van de modellen komen goed overeen met de verkregen experimentele resultaten.

In het tweede deel van dit proefschrift worden strategieën voor Model Predictive Control ontwikkeld. Vooral de goede mogelijkheden om beperkende randvoorwaarden (bijvoorbeeld minimum of maximum waarden op de ingangen of op de uitgangen) en interacties tussen ingangen en uitgangen mee te nemen in de regelalgoritmes hebben geleid tot de keuze voor MPC. Voor de implementatie van MPC hebben we gebruik gemaakt van *Primacs*, een pakket voor *real-time* modelgebaseerd regelen dat wordt ontwikkeld door TNO-TPD (Delft, Nederland). De basis idee van MPC is dat een model van het te regelen systeem gebruikt wordt om het toekomstige gedrag van het systeem te voorspellen en de toekomstige ingangen van het systeem te optimaliseren met betrekking tot een gekozen criterium. Standaard (lineaire) MPC gebruikt hetzelfde lineaire model voor voorspelling en optimalisatie. Het niet-lineaire gedrag en het grote werkgebied van de meeste turbomachines (denk bijvoorbeeld aan het opstarten) kunnen echter niet goed worden aangepakt met lineaire MPC. In deze studie zijn daarom niet-lineaire methoden (gebaseerd op herhaalde linearisatie en niet-lineaire voorspelling) beschikbaar onderzocht en toegepast. Deze methoden zijn nog steeds gebaseerd op lineaire optimalisatie.

Tenslotte worden de ontwikkelde MPC strategieën toegepast op representatieve installaties. In deze haalbaarheidsstudie van MPC bestuderen we de prestaties van het geregelde systeem, de robuustheid voor externe verstoringen en modelfouten en de noodzakelijke rekentijd voor

voorspelling en optimalisatie. Op de laboratorium-installatie is het gelukt om een *real-time* MPC configuratie te implementeren. Binnen de minimaal haalbare tijdstep kon de strategie van herhaald lineariseren worden toegepast. Deze methode vormt een nuttige en krachtige uitbreiding van lineaire MPC. De voordelen van MPC, te weten rekening houden met beperkingen en interacties, komen uitstekend tot hun recht. Speciale aandacht is geschonken aan filteren en anticipatie: het rekening houden met toekomstige veranderingen in bijvoorbeeld het referentie-sigitaal.

Naast de laboratorium-installatie hebben we ook een generiek compressorstation gekozen om MPC toe te passen. Dit compressorstation bestaat uit twee parallelgeschakelde compressoren die uitmonden in een gemeenschappelijk drukvat. De resultaten met MPC voor het compressorstation zijn beperkt tot simulaties. Het regelprobleem van het compressorstation is een uitbreiding op dat van de gasturbine vanwege het grote aantal vrijheidsgraden (ingangen) van de parallel geschakelde compressoren. Simulatieresultaten laten de mogelijkheden van MPC voor dit regelprobleem zien. Vooral de mogelijkheid om, in een dynamische optimalisatie, interacties tussen en beperkingen op de ingangen en de uitgangen mee te nemen, toont de potentiële mogelijkheden voor het verbeteren van de prestaties van een compressorstation aan. Nieuwe regeldoelstellingen zoals het minimaliseren van het benodigde vermogen zijn mogelijk.

Nawoord

Na het succesvol afronden van mijn studie Werktuigbouwkunde begon ik in maart 1993 aan de ontwerpersopleiding "Proces- en Productontwerp" van het Stan Ackermans Instituut. Mijn ontwerpopdracht zou ik uitvoeren binnen de sectie Werktuigkundige Energietechnologie (WET) van de faculteit Werktuigbouwkunde. Ik voelde me al snel zeer thuis in deze sectie en samen met mijn begeleider Rick de Lange en enkele enthousiaste studenten werd met het ontwerp van een gasturbine-opstelling in het laboratorium begonnen. Deze opstelling zou dienen voor het onderzoeken van het dynamische gedrag van gasturbines tijdens snelle transiënten, waarbij vooral werd gedacht aan stoominjectie (STIG systemen). Twee jaar later ronde ik de ontwerpersopleiding af. De installatie was gebouwd maar nog niet volledig operationeel. Met financiële steun van TNO kreeg ik rond die tijd de mogelijkheid mijn werk voort te zetten in het kader van een promotieonderzoek met als onderwerp het modelleren en regelen van turbomachines. De laboratorium-opstelling zou vanzelfsprekend dienen als validatie- en testopstelling. Het resultaat van mijn promotieonderzoek is nu vastgelegd in dit proefschrift.

Op deze plaats wil ik iedereen bedanken die een bijdrage geleverd heeft aan het tot stand komen van mijn proefschrift. In de eerste plaats noem ik mijn copromotor Rick de Lange en mijn promotoren Anton van Steenhoven en Jan Kok voor hun inspirerende en ondersteunende begeleiding. Verder bedank ik een aantal studenten die middels hun afstudeerwerk bijgedragen hebben tot het resultaat. Eric Scholten en Stef Verhagen werkten aan het ontwerp en de bouw van de laboratorium-installatie. Anton Aarts en Gino Lambert werkten aan de eerste aanzet tot de modellen. Tido van der Meulen, Willem van Aaken en Edwin Loenen hielpen met de meetinstrumenten en het data-acquisitiesysteem. Tenslotte werkten Inge Satter, Gert Leenheers, Bas Vroemen en Edwin Loenen aan de implementatie van Model Predictive Control in Primacs.

Het softwarepakket Primacs werd ter beschikking gesteld door TNO-TPD. Daarnaast heb ik ondersteuning gehad van de TNO'ers Ruud van der Linden, Jan Smeulers en vooral van Wim Bouman en Walter Renes, waarvoor mijn hartelijke dank.

Ik heb het heel erg gewaardeerd dat de sfeer en de samenwerking in de groep WET altijd zeer prettig is geweest (en nog steeds is). Hiervoor bedank ik alle medewerkers en medewerksters van de sectie en al mijn kamergenoten van de afgelopen jaren. In het bijzonder wil ik Frits van Veghel bedanken die altijd voor me klaar stond in het laboratorium. Vooral zijn assistentie tijdens de vele lawaaierige "buiten werktijd" meetsessies en zijn vermogen om praktische problemen op te lossen zijn voor mij erg belangrijk geweest.

Tenslotte bedank ik mijn "nieuwe" collega's Jan, Henk, Frans, Bram, Jos, René en Niels voor de kans die zij mij boden om als docent op de universiteit te blijven werken en voor de "ruimte" die ik kreeg om mijn proefschrift af te kunnen maken.

Bedankt !



Utrecht, 17 September 1998.

Curriculum Vitae

- 11 maart 1968 Geboren te Tiel.
- 1980 - 1986 Ongedeeld VWO, Koningin Wilhelmina College, Culemborg.
- 1986 - 1992 Werktuigbouwkunde, Technische Universiteit Eindhoven. Met lof afgestudeerd binnen de sectie Systeem- en Regeltechniek met als afstudeerverslag "*Symbols speak louder than Numbers: Analysis and Design of Non-linear Control Systems with the Symbolic Computation System MAPLE*". Winnaar "*Regeltechniekprijs 1992*" van het Koninklijk Instituut van Ingenieurs.
- 1993 - 1995 Ontwerpersopleiding "Proces- en Productontwerp", Stan Ackermans Instituut, Technische Universiteit Eindhoven. Ontwerpopdracht "*Design of a laboratory gas turbine installation*" uitgevoerd als twee-jarige assistent in opleiding (TWAIO) binnen de sectie Werktuigkundige Energietechnologie, faculteit Werktuigbouwkunde, Technische Universiteit Eindhoven.
- 1995 - 1997 Promotieonderzoek, uitgevoerd als assistent in opleiding (AIO) binnen de sectie Werktuigkundige Energietechnologie, faculteit Werktuigbouwkunde, Technische Universiteit Eindhoven.
- 1 december 1997 Universitair Docent, sectie Systeem- en Regeltechniek, faculteit Werktuigbouwkunde, Technische Universiteit Eindhoven.

